3-7-2016 12:00 AM

Click And Bioorthogonal Chemistry For The Chemical Modification Of Nanomaterials

Pierangelo Gobbo
The University of Western Ontario

Supervisor
Prof. Mark S. Workentin
The University of Western Ontario

Graduate Program in Chemistry
A thesis submitted in partial fulfillment of the requirements for the degree in Doctor of Philosophy

Abstract

The goal of this Ph.D. thesis work is the development of novel reactive nanomaterial templates that can be chemically modified in a facile and robust (*i.e.*, formation of covalent bonds) way for the further modification of the nanomaterial's physical-chemical properties by the reaction partner molecular system. This type of technology was employed to further expand the application of nanomaterials in nanomedicine, chemical biology and materials science.

In order to reach this goal, as a proof of concept, small (ϕ = 3nm) gold nanoparticles (AuNPs) and carbon nanotubes (CNT) were used as the nanomaterial substrates. Innovative synthetic strategies for the introduction of click and bioorthogonal functional groups onto the surface of these nanomaterials were developed. These functional groups include a maleimide that can undergo three click reactions with different functional groups (*i.e.*, Michael addition with nucleophiles, Diels-Alder cycloaddition with dienes, dipolar cycloadditions with dipolar molecules), strained alkynes for bioorthogonal strain-promoted cycloaddition reactions with azides and nitrones, and methyl-2-(diphenylphosphino)benzoate moieties for the bioorthogonal Staudinger-Bertozzi ligation with azides.

In order to study and characterize these clickable and bioorthogonal nanomaterial templates, methodologies for the determination of the amount of reactive functionalities introduced onto the nanomaterial's surface and the evaluation of their proper reactivity were also developed. ^{1}H NMR spectroscopy, transmission electron microscopy, and thermogravimetric analysis, were methodically used for the quantification of the interfacial reactive functionalities. ^{1}H NMR spectroscopy was also employed to follow the correct interfacial reactivity of the nanomaterial template. Finally, in collaboration with Surface Science Western, the use of X-ray photoelectron spectroscopy (XPS) was developed as a method to independently confirm all the previously obtained results and, more specifically, quantitate the amount of interfacial reactive molecules that were introduced, track the interfacial organic chemistry of the nanomaterial template, and determine interfacial reaction yields. In all cases the clickable and bioorthogonal nanomaterial templates were found to react quickly, efficiently and chemoselectively with their *chemical reporter* through a simple pour-and-mix type of

chemistry. The utility of these clickable and bioorthogonal nanomaterial templates was finally showcased in bioconjugation, for the synthesis of fluorogenic biosensors, nanomaterial hybrids and nanomaterial-based MRI contrast agents.

Keywords

Gold Nanoparticle, Carbon Nanotube, Functional Nanomaterial, Click Chemistry, Bioorthogonal Chemistry, Michael-Type Addition, Diels-Alder Cycloaddition, Strain-Promoted Alkyne-Azide Cycloaddition, Staudinger-Bertozzi Ligation.

Co-Authorship Statement

Chapter 1: I wrote the drafts of the manuscript, with input and final edit by my supervisor, Prof. M. S. Workentin.

Chapter 2: I performed all the experimental work and I wrote the drafts of the manuscript, with input and final edit by my supervisor, Prof. M. S. Workentin.

Chapter 3: M. Milne, supervised by Prof. Hudson, and I contributed equally to the work. M. Milne synthesized and characterized the DO3A contrast agent. N. McVicar, supervised by Prof. R. Bartha, performed the MRI experiments. I synthesized and characterized the Maleimide-AuNP and the Gd-AuNP. M. Milne and I wrote the draft of the manuscript with input and minor edits from the other co-authors and final edit by Prof. R. H. E. Hudson and Prof. M.S. Workentin.

Chapter 4: Weissman and Winger were two undergraduate students under my direct co-supervision, along with my supervisor, Prof. M. S. Workentin. I mentored Weissman during the synthesis and characterization of the rhodamine B-MPA fluorophore and the performance and analysis of the fluorescence experiments. I mentored Winger during the performance and analysis of the ^{1}H NMR kinetic experiments. Ghiassian synthesized some Maleimide-AuNP starting material. I wrote the draft of the manuscript with final edit by my supervisor, Prof. M. S. Workentin.

Chapter 5: Dr. M. Biesinger performed the XPS measurements and assisted in the discussion of the results. I performed the synthesis and characterization of the nanomaterial hybrid. I wrote the drafts of the manuscript, with input and minor edits from the other co-author and final edit by my supervisor, Prof. M. S. Workentin.

Chapter 6: I wrote the drafts of the manuscript, with input and final edit by my supervisor, Prof. M. S. Workentin.

Chapter 7: X. Wang, supervised by Prof. R. H. E. Hudson, and I contributed equally to the work. Wang synthesized and characterized the peptides employed in this work. M. Suchy synthesized the DBCO linker. I synthesized and characterized the azide-AuNP and the

peptide-AuNP. R. Wang and I wrote the drafts of the manuscript, with input and minor edits from the other co-author and final edit by Prof. R. H. E. Hudson and Prof. M. S. Workentin.

Chapter 8: Z. Mossman and A. Niaux were two undergraduate students under my direct co-supervision, along with my supervisor, Prof. M. S. Workentin. Z. Mossman and A. Niaux helped with the synthesis and characterization of the compounds reported in this work. A. Nazemi, under the supervision of Prof. E. Gillies, prepared the azide-functionalized vesicles. I wrote the draft of the manuscript, with input and minor edits from the other co-authors and final edit by my supervisor, Prof. M. S. Workentin.

Chapter 9: W. Luo and Dr. S. J. Cho helped with the synthesis and characterization of the thiolated ligand. Wang synthesized and characterized the peptide. Dr. M. Biesinger performed the XPS experiments and assisted in the discussion of the XPS results. I synthesized and characterized the Staudinger-AuNP and investigated their interfacial reactivity. I wrote the drafts of the manuscript, with input and minor edits from the other co-authors and final edit by my supervisor, Prof. M. S. Workentin.

Chapter 10: S. Novoa was an undergraduate summer student under my direct co-supervision, along with my supervisor, Prof. M. S. Workentin. S. Novoa helped with the synthesis and characterization of the azide-terminated thiolated ligand. Dr. M. Biesinger performed the XPS experiments and assisted in the discussion of the XPS results. I wrote the drafts of the manuscript, with input and minor edits from the other co-authors and final edit by my supervisor, Prof. M. S. Workentin.

Acknowledgments

I am deeply thankful to the Government of Canada and to Research Western for a Vanier Scholarship and funding my research.

A special thanks to my thesis examiners for taking the time out of their busy schedule to be on my defense committee.

I would like to express my gratitude to Mark Workentin for his unmatchable and contagious enthusiasm, patience, and support. I would like to thank him for these marvellous 5 years of research together and for everything he taught me inside and outside the lab. I am really grateful to him for the fantastic, countless career and networking opportunities he constantly presented me throughout my stay at Western. *Grazie!*

I would also particularly like to acknowledge Robert Hudson for his constant support and advice, for writing me reference letters and, of course, for the numerous scientific discussions we had over a "caffettino".

I would then like to thank the following faculty members that I had the chance to learn from or collaborate with over the past years: Professor Paul Ragogna, Professor Michael Kerr, Professor James Wisner, Professor Elizabeth Gillies, Professor François Lagugné-Labarthet, Professor Joe Gilroy, Professor Len Luyt, Professor Tito Scaiano, Professor Vladimir Popik, Professor Robert Bartha, and Professor Maria Drangova. A special thank also to Dr. Mark Biesinger (Surface Science Western) for his invaluable help with the XPS characterization.

I wish to express my gratitude to all the staff of the Department of Chemistry for the constant, always-ready and high-quality support. A particular thanks to Mathew *"Matteo"* Willans, Yves Rambour, Doug Hairsine, Paul Boyle, John Vanstone and John Aukema *"J&J"*, Barakat Misk, Monica Chirigel, Marylou Hart, Darlene McDonald.

I wish to thank the past and present members of the Workentin Group and all the students I had the fortune to work with and learn from: Dr. Hossain Ismaili, Dr. Sara Ghiassian, Dr. Mahdi Hesari, Dr. Sung Ju *"Giuseppe"* Cho, Dr. Mia Biondi, Wilson *"Willy"* Luo, Mariachiara *"MC"* Zuin, Tommaso *"Mr BJ"* Romagnoli, Praveen *"Mr. G"* Gunawardene,

Vaishnavi *"Vaish"* Somasundaram, Ziyan *"Leila"* Zhu, Zack Mossman, Aurelia Niaux, Jennifer *"Jen"* Keir, Samantha *"Samantella"* Novoa, Max *"Maxy"* Weissman, Kathleen Winger, Alexis *"Alex"* Prestwich, Alexander "*The Hoser"* Van Belois, Becky *"Bambi"* Wright, Melanie *"Mel"* Lui, Dr. Mark *"Milny"* Milne, Dr. Nevin McVicar, Xiaoxiao (Rachael) Wang, Dr. Mojmir Suchy, Dr. Ali Nazemi, Stephanie *"Steph"* Barbon, Dr. Jacquelyn *"Jackie"* Price, Eleanor *"Pupona"* Magdzinski, Gregory *"Greg"* Wallace, Dr. Mohammedali Tabatabaei, Dr. Nastaran Kazemi-Zanjani, Dr. Kevin Stamplecoskie.

A last big *Grazie!* goes to my family, girlfriend, and closer friends, whose persistent love and encouragement overcame countries, oceans and cultures. Without your love and support I would have never reached my personal goals.

Table of Contents

List of Tables

List of Figures

List of Schemes

List of Appendices

List of Abbreviations and Symbols

(FP)Maleimdie-AuNP or (Pt)Maleimide-AuNP	Furan-protected maleimide-functionalized AuNP
atm	Atmosphere
AuNP	Gold nanoparticle
Azide-AuNP	Azide-functionalized AuNP
C_{12}-AuNP	1-Dodecanthiol-functionalized gold nanoparticle
CA	Contrast agent
CD_2Cl_2	Deuterated dichloromethane
CD_3Cl	Deuterated chloroform
CD_3CN	Deuterated acetonitrile
CH_2Cl_2 or DCM	Dichloromethane
CH_3Cl	Chloroform
CH_3CN or ACN	Acetonitrile
cm^{-1}	Wavenumber
CNT	Carbon nanotube
D_2O	Deuterated water
DBCO	Dibenzocyclooctyne
DBCO-AuNP	DBCO-functionalized AuNP
DIPEA	N,N-Diisopropylethylamine

DMF	Dimethylformamide
DMSO	Dimethyl sulfoxide
EDC	1-Ethyl-3-(3-dimethylaminopropyl)carbodiimide
ESI	Electronic supporting information
ESI-MS	Electrospray ionization-mass spectrometry
EtOH	Ethanol
eV	Electronvolt
g	Gram
GSH or GS	Glutathione
h	Hours
H_2O	Water
HBTU	(1H-Benzotriazol-1-yloxy)(dimethylamino)-N,N-dimethylmethaniminium hexafluorophosphate
HOMO	Highest occupied molecular orbital
HPLC	High performance liquid chromatography
I-SBL	Interfacial Staudinger-Bertozzi ligation (reaction)
I-SPAAC	Interfacial Strain-promoted alkyne-azide cycloaddition (reaction)
ICP-OES	Inductively coupled plasma-optical emission spectrometry
IR	Infrared
kDa	Kilodalton

LUMO	Lowest unoccupied molecular orbital
M	Molar
Maleimide-AuNP	Maleimide-functionalized AuNP
MeOH or CH_3OH	Methanol
MHz	Megahertz
min	Minutes
mM	Millimolar
mol	Mole
MPA	4-Mercaptophenylacetic acid
MRI	Magnetic resonance imaging
MWCO	Molecular weight cut-off
NHS	N-Hydroxysuccinimide
nm	Nanometer
NMR	Nuclear magnetic resonance spectroscopy
ºC	Degree Celsius
PBS	Phosphate buffer solution
ppm	Parts-per-million
rpm	Revolutions per minute
s	second
SPAAC	Strain-promoted alkyne-azide cycloaddition (reaction)

SPAAC-PAD	Strain-promoted alkyne-azide cycloaddition-post assembly deprotection (strategy)
SPR	Surface plasmon resonance
Staudinger-AuNP	Methyl-2-(diphenylphosphino)benzoate-functionalized AuNP
SWCNT	Single-walled carbon nanotube
T	Tesla
TEG-AuNP or MeO-EG_3-AuNP	Triethylene glycol gold nanoparticle
TEM	Transmission electron microscopy
TES	Triethylsilane
TFA	Trifluoroacetic acid
TGA	Thermogravimetric analysis
THF	Tetrahydrofuran
uL	Microliter
UPLC	Ultra performance liquid chromatography
UV-Vis	Ultraviolet-visible
XPS	X-ray photoelectron spectroscopy
ϕ	Diameter

Preface

The present thesis is divided in two parts: **Part I**, which includes *Chapters 1-5*, and **Part II**, which includes *Chapters 6-10*.

Part I

Part I describes the synthesis, characterization and applications of small, water-soluble maleimide-functionalized AuNPs. *Chapter 1* serves as an introduction to *Chapters 2-5* and introduces the reader to maleimide chemistry and to the methodologies developed in the Workentin group for the incorporation of maleimide functionalities at the interface of AuNPs. *Chapter 1* starts by illustrating the synthesis, characterization and reactivity of organic-solvent soluble Maleimide-AuNPs, and continues by describing the evolution of ideas that eventually brought to the synthesis of their water-soluble version. *Chapter 1* will be published as an account paper.

Chapter 2 describes the synthesis and characterization of small, water-soluble Maleimide-AuNP. It also describes the issues behind their successful synthesis, especially the hydrolysis of the interfacial maleimide moieties during the interfacial deprotection reaction.

Part I continues with *Chapter 3-5*, which show how maleimide chemistry further expands the scope AuNPs in nanomedicine, drug delivery and materials chemistry, respectively. In particular, *Chapter 4* shows how maleimide chemistry, despite its consolidate use in many different fields of chemical sciences, still reserves surprises in its reactivity and proper precautions must be taken when using the maleimide group. This chapter demonstrates that the Michael-type addition reaction at the interface of Maleimide-AuNPs can be reversible, impacting the use of the nanomaterial template as a drug carrier and for bioconjugation. It also shows that the retro Michael-type addition reaction can be exploited for the delivery of a molecular cargo, thus expanding the scope of the water-soluble Maleimide-AuNPs.

Part II

Part II introduces the concept of bioorthogonally reactive nanomaterials templates. It describes our methodologies to introduce bioorthogonal functionalities onto the surface of AuNPs, determine the number of bioorthogonal functionalities that have been introduced,

and obtain proof of successful interfacial bioorthogonal chemistry. *Chapter 6* serves as an introduction and outlook to *Chapters 7-10* and will be published as an account paper.

Chapters 7-8 describe the challenges that we had to overcome for synthesizing small water-soluble gold nanoparticles able to react through the interfacial strain-promoted alkyne-azide cycloaddition reaction. These two chapters (and especially *Chapter 7*) highlight the importance of developing synthetic methodologies for the introduction of *bioorthogonal groups*, rather than *chemical reporters*, at the nanomaterial's interface. *Chapter 9* describes the synthesis, characterization and reactivity of small AuNPs displaying interfacial methyl-2-(diphenylphosphino)benzoate moieties for Staudinger-Bertozzi ligation. This chapter demonstrates the utility of the resulting Staudinger-AuNPs in bioconjugation, due to their high chemoselectivity towards the azide *chemical reporter*, and ease of following their interfacial reactivity. Finally, *Chapter 10* further extends the concept of bioorthogonal nanomaterial template to other nanomaterials, which describes the synthesis, characterization and reactivity of strained alkyne-modified single-walled carbon nanotubes.

Chapter 1

1 Maleimide-Modified Gold Nanoparticle (AuNP): a Versatile Platform for Interfacial Click Reactions Leading to Chemically Modified AuNPs

Chapter 1 will be published as an account paper.

I wrote the drafts of the manuscript, with input and final edit by my supervisor, Prof. M. S. Workentin.

ABSTRACT: The maleimide moiety can undergo a wide variety of organic reactions, including Diels-Alder reactions, dipolar cycloadditions and Michael-type additions, making them a suitable moiety for further elaboration of the functionality at the interface of AuNPs through key reactions useful in a host of applications. This account will cover 1) our approach to prepare Maleimide-AuNPs; 2) our survey of the scope of the reactivity of the Maleimide-AuNPs, which was very slow, impractical and required the development of high pressure techniques in AuNP chemistry yielding dramatic results, and 3) the extension of these ideas to prepare water-soluble small AuNPs expanding the scope of the organic transformation to aqueous environments. Within each of these sections there were problems and issues that had to be overcome, and we will describe the evolution of the ideas so that readers can get a glimpse of our thinking and problem solving as we proceeded.

1.1 Introduction

Our main research interest is directed towards the investigation of fundamental aspects of interfacial organic reactions on 2D and 3D surfaces and the demonstration of their potential applications. While organic reactions in solution are described by well-defined and intuitive physical-organic chemistry rules, organic reactions that take place at material interfaces sometimes behave in very different ways. A complete understanding of the factors that cause these reactivity changes is essential for rational design and control of any functional material and nanomaterial.

A preferred 3D surface that we use as a template for our investigations are monolayer protected gold nanoparticles (AuNPs). This particular nanosystem attracted our attention because of its properties that make them a desirable material for all sorts of applications. These range from molecular and biomolecular electronics, to catalysis, sensing and drug delivery. In fact, AuNPs can be made chemically stable, are easy to synthesize, and have size dependent Coulomb charging effects that make them ideal for the preparation of transistors and non-volatile memory devices.[1-4] The AuNP's size plays a fundamental role also in catalysis, where the catalytic activity is inversely proportional to the nanoparticle size. Some typical reactions catalyzed by AuNPs are oxidation of alcohols, reduction of nitro-groups, and oxidation of carbon monoxide.[5] Furthermore, pseudo-spherical AuNPs with a gold core diameter larger than 5 nm display a surface plasmon resonance (SPR) when the gold core's conduction electrons enter in resonance with incident photons, conditions that is satisfied by the visible light (typically 500 to 550 nm). Because of this property, AuNPs display size-dependent colors ranging from brown to blue that are commonly used for the creation of colorimetric (bio)sensors.[6-9] Another advantage of monolayer protected AuNPs is that they are a robust system due to the presence of an organic corona strongly bound to the gold core through a gold-sulfur bond (126 kJ mol^{-1}).[10] These nanoparticles can be readily dried and redispersed in different solvents with little to no aggregation, and can be exposed to drastic reactions conditions (like high temperatures and very high pressure, and preserve their physical chemical properties. Furthermore, functional groups can be easily introduced onto the AuNP's organic corona through a ligand exchange reaction with an appropriately functionalized

thiolated ligand. These characteristics make the monolayer-protected AuNPs an ideal template for the investigation of interfacial organic chemistry reactions by using a pure traditional organic analytical approach. Furthermore, these properties merged with the virtually limitless potential of interfacial organic chemistry provide novel routes towards the synthesis of functional nanomaterials.

One of the most attractive functional groups that we successfully introduced onto the AuNP's organic corona is the maleimide group. The maleimide moiety finds application in the most diverse areas of chemistry. For example, it has been used in material chemistry for the synthesis of polymers[11-19], hydrogels[20, 21] and biomaterials[22], and for the functionalization of surfaces and the preparation of sensors.[23-26] Applications in biochemistry instead involve biolabeling[27-30], pharmaceutics[31, 32], and preparation of biosensors that involve attachment of biomolecules to surfaces.[33-37]

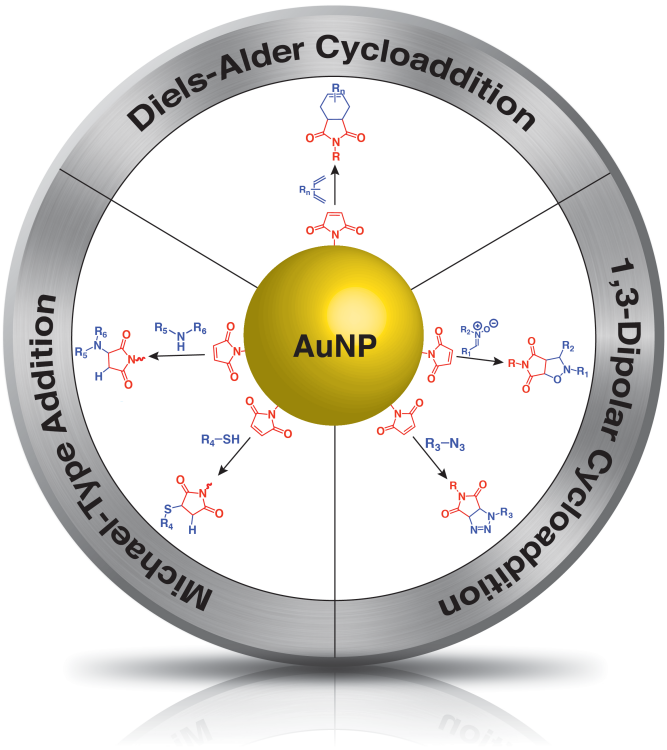

Figure 1.1: Representation of the reactivity of the maleimide group at the interface of a AuNP. The maleimide can undergo Diels-Alder cycloaddition with dienes, Michael-type additions with thiols and amines (nucleophiles), and 1,3-dipolar cycloadditions with nitrones and azides.

The reason why this molecular unit attracts so much interest is because it is small, symmetrical, stable, biocompatible, and can be easily functionalized through its nucleophilic nitrogen to form the corresponding *N*-substituted derivatives. Furthermore, maleimides can undergo three different click reactions: Michael-type addition with nucleophiles, 1,3-dipolar cycloadditions with nitrones and azides, and Diels-Alder cycloadditions with dienes (see Figure 1.1). These three reactions are desirable because they form stable reaction products, the reaction conditions are generally mild due to the low activation energy required, and they can all occur in water media. Another important characteristic of this interesting functional group is its tendency to hydrolyze. Maleimide undergoes a mono-hydrolysis at both basic and acidic pH to form maleamic acid.[38, 39] Additionally, as shown by our research group (*vide infra*), under more drastic reaction conditions *N*-substituted maleimide undergoes a double hydrolysis to form maleic acid and the corresponding *N*-substituted primary amine.[40] However, it was shown that *N*-substituted maleimides are generally stable and do not hydrolyze at pH ranging from 6.5 to 7.5, and that their stability is related to the substituent at the nitrogen.[41] This ability to hydrolyze can represent an advantage or a disadvantage, depending on the application. If the maleimide hydrolyzes before having the chance to react with the clickable partner molecule, the efficiency of the reaction would decrease notably, as the maleamic acid is much less reactive towards Michael-type additions, 1,3-dipolar cycloadditions and Diels-Alder cycloadditions. Alternatively, if the hydrolysis takes place after the maleimide has reacted with the target molecular system, then possible retro-reactions, like the retro-Diels-Alder cycloaddition and the retro Michael-type addition, would also be hindered.[41, 42] This is desirable for those applications that rely on the formation of a stable and robust link between the molecular system of interest and a substrate formed through maleimide chemistry. It is clear that the introduction of such a functional group onto AuNPs can lead to the development of novel functional nanomaterials and further expand the scope of AuNPs in materials chemistry, chemical biology and nanomedicine.

In this account we aim to describe our challenges in the development of a synthetic approach to the preparation of organic solvent-soluble Maleimide-AuNPs, where we had to be mindful of the high reactivity of maleimide with thiols. We will also go through our survey of the reactivity of the Maleimide-AuNP, which tend to react very slowly

because of the conditions under which the AuNP are stable, and required the development of high-pressure techniques in AuNP chemistry with dramatic results. Finally we will describe the extension of our work towards the preparation of water-soluble Maleimide-AuNP, expanding the scope of the organic transformations to aqueous environments.

1.2 Maleimide-AuNP: the synthetic strategy

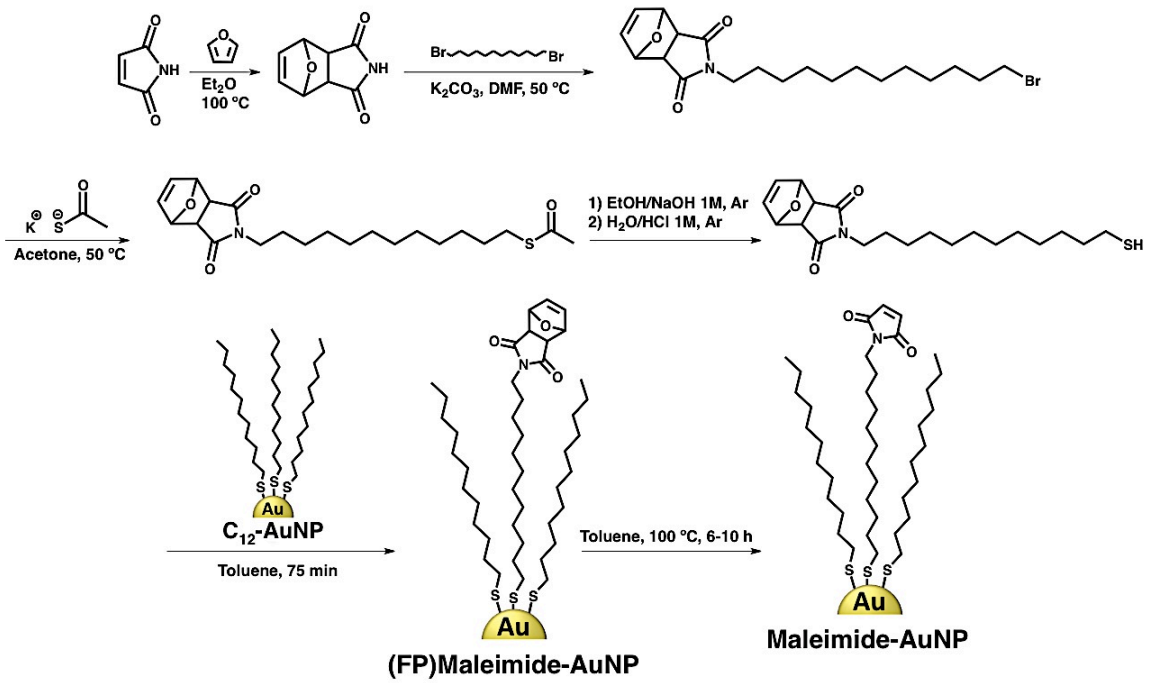

Scheme 1.1: Synthesis of organic solvent-soluble Maleimide-AuNP.

The first 3D platform that we used for the investigation of interfacial organic reactions is the dodecanethiol-AuNP (C_{12}-AuNP). C_{12}-AuNP initially attracted our attention because of their thermal stability and ability to be dried and redissolved in the majority of organic solvents. C_{12}-AuNP can be easily prepared through the Brust-Schiffrin method, which involves the controlled reduction of the $HAuCl_4$ with $NaBH_4$ in presence of dodecanethiol. This synthetic method is versatile because it makes it possible to easily vary the size of the nanoparticle's gold core from 2 to 10 nm simply by changing the Au:S ratio.[43] For these reasons C_{12}-AuNP have been selected for our studies providing a robust nanomaterial substrate for our investigations.[44]

The subsequent step was the synthesis of a thiolated ligand that contains a maleimide in the ω position. As mentioned before, the maleimide is highly reactive towards nucleophiles, therefore such a maleimide-thiolated ligand would rapidly self-react. Therefore, the maleimide moiety needs to be protected. Scheme 1.1 describes our synthetic strategy leading to organic solvent-soluble Maleimide-AuNPs. The first step involves the protection of the maleimide with furan through a Diels-Alder reaction. The furan-protected maleimide is then attached to one extremity of a 1,12-dibromododecane spacer. This molecular spacer has a similar molecular structure to the C_{12}-AuNP ligands, so that it ensures a good packing of the monolayer around the gold core and preservation of a robust organic corona. Finally, the other extremity of the spacer is transformed into thiol. The resulting furan-protected maleimide-thiolated ligand can then be introduced onto the AuNP's organic corona through a ligand exchange reaction by simply mixing the newly synthesized ligand with the C_{12}-AuNP substrate in toluene for 75 min. Subsequently, the furan-protected maleimide AuNP ((FP)Maleimide-AuNP) undergoes a very careful process of purification in order to remove any unbound thiol before the deprotection reaction. This process involves repeatedly washing a AuNP thin film made inside a round bottom flask with 95% ethanol, which selectively dissolves unbound thiols. The final step involves the deprotection of the maleimide through a retro-Diels-Alder reaction by heating the (FP)Maleimide-AuNPs in toluene at 100 ºC for 6-10 hours. This retro-Diels-Alder strategy avoids the problem of the competitive Michael-type addition to the maleimide, leading to the Maleimide-AuNP template in a safe and efficient way. In the literature, AuNP have been reported to be sensitive to high temperatures. However, at 100 ºC only a negligible amount of thiolated ligands are cleaved off the gold core as disulfides, and only a slight broadening of the gold core size distribution is observed through TEM images. This indicates a good stability of the C_{12}-AuNP substrate under the retro-Diels-Alder reaction conditions.[44, 45]

The synthesis of Maleimide-AuNP can be easily followed by ^{1}H NMR spectroscopy (see to Figure 1.2). While the ^{1}H NMR spectrum of C_{12}-AuNP only shows the signals of aliphatic protons in the 0-2 ppm region, after the ligand exchange reaction the typical three peaks of the furan-protected maleimide thiolated ligand appear.

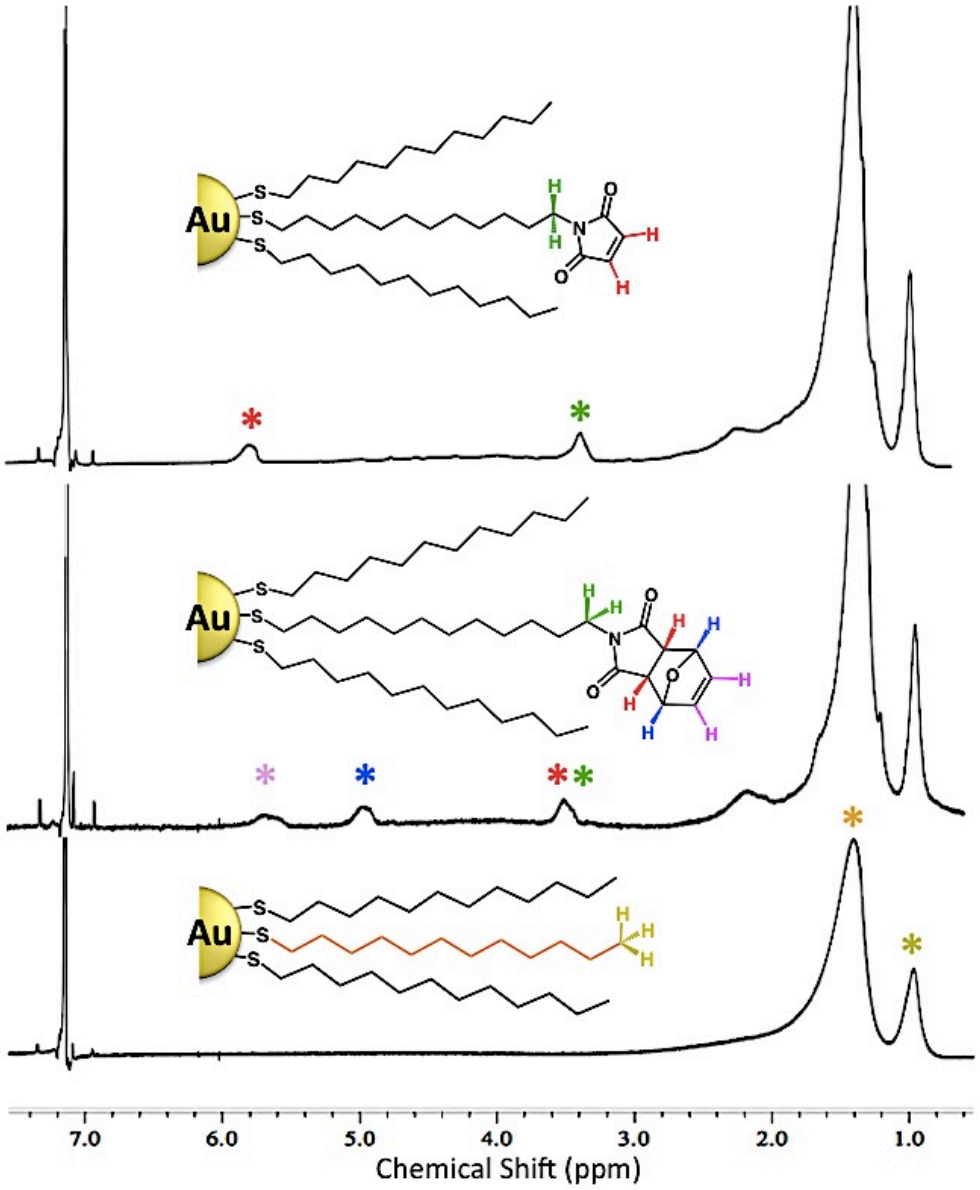

Figure 1.2: ^{1}H NMR characterization of C_{12}-AuNP (bottom), (FP)Maleimide-AuNP (center), Maleimide-AuNP (top). Spectra recorded in $CDCl_3$ and referenced to residual $CHCl_3$.

The peak at 3.50 ppm corresponds to the two protons alpha to the carbonyls of the furan-protected maleimide moiety. The peak at 4.95 ppm corresponds to the two protons next to the bridged oxygen, while the peak at 5.65 ppm corresponds the two alkene protons. After the retro-Diels-Alder reaction, because of the loss of furan, the peaks at 4.95 ppm and 5.65 ppm disappear and the signal at 3.50 ppm shifts to 5.80 ppm, upfield with

respect to the former alkene peak of the (FP)Maleimide-AuNPs. These organic solvent-soluble Maleimide-AuNP were found to be stable for months and the solubility of the precursor C_{12}-AuNP was retained.

Our synthetic strategy provides an easy and efficient route to the synthesis of AuNPs displaying an interfacial reactive maleimide moiety. The interfacial retro-Diels-Alder reaction is easy to perform, quantitative, and the generated furan can be easily removed, leading to a pure Maleimide-AuNP sample. Because of this, and since the introduction of the maleimide group exploits a direct ligand exchange reaction, the amount of maleimide at the AuNP's interface can be carefully tuned. This would not be possible if an interfacial coupling approach (*e.g.*, reaction between an alcohol- or amine-terminate AuNP with maleimidopropionic acid) was used.[44] The Maleimide-AuNPs synthesized through our retro-Diels-Alder method represents a very stable and robust nanomaterial template that allows us to investigate the interfacial Michael-type addition, 1,3-dipolar cycloaddition, and Diels-Alder cycloaddition reactions in great detail.

1.3 Reactivity of the organic solvent-soluble Maleimide-AuNP template

The organic solvent-soluble Maleimide-AuNPs could efficiently undergo several Diels-Alder/retro-Diels-Alder cycles. It was possible to re-protect the Maleimide-AuNPs by mixing them with furan at room temperature for 1 day to reform the (FP)Maleimide-AuNPs. The reaction could be monitored by ^{1}H NMR spectroscopy through the disappearance of the maleimide's alkene peak at 5.80 ppm and the reappearance of the peaks of the interfacial Diels-Alder adduct at 3.50, 4.96, and 5.65 ppm. It is worth noting that the forward-Diels-Alder performed at room temperature to re-protect the AuNP's maleimide moieties leads to a mixture of *endo*- and *exo*- products. Prolonged heating at 50 ºC converts the mixture of isomers exclusively to the *exo*-isomer, the most thermodynamically stable product. Subsequently, it was possible to re-deprotect the (FP)Maleimide-AuNP by heating again at 100 ºC. The repeated cycling for protecting and deprotecting the Maleimide-AuNP using high temperature was not found to affect the solubility and stability of the AuNPs. Most importantly, the increase of the gold core size

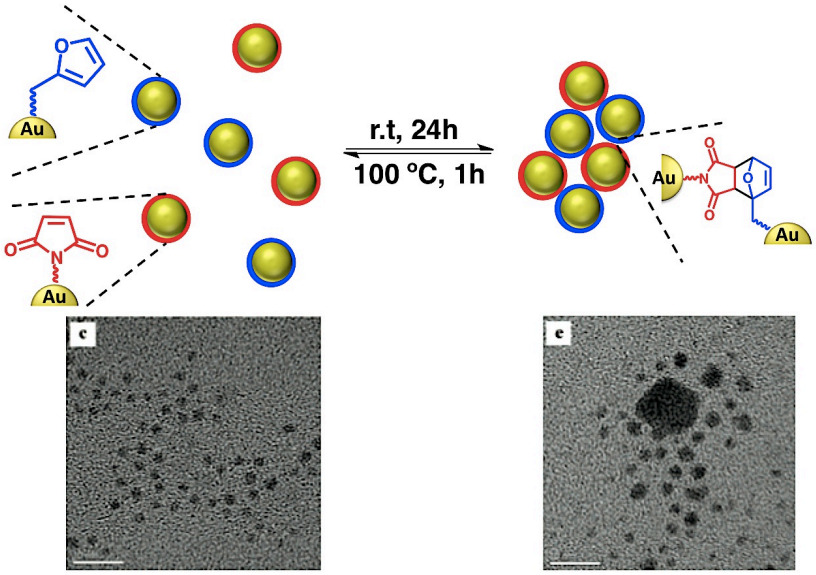

Figure 1.3: Representation of the Diels-Alder and retro-Diels-Alder reaction between maleimide-modified AuNPs and furan-modified AuNPs with the corresponding TEM images (scale bar 10 nm).

distribution due to the high temperature required for the retro-Diels-Alder to occur took place only in the first cycle.[44]

The organic solvent-soluble Maleimide-AuNPs could then reversibly form inter-particle macrostructures, reacting at room temperature with furan-modified AuNPs, see Figure 1.3. The resulting nanoparticle macrostructures were formed on the time scale of days, and slowly precipitated out of solution. Heating of the macrostructures at 100 ºC for 1h in toluene triggered the retro-Diels-Alder reaction that caused the disaggregation of the macrostructures and the re-dissolution of the two populations of AuNPs (*i.e.*, Maleimide-AuNPs and Furan-AuNPs). The reversible formation of the AuNP aggregates was completely reversible even after 30 Diels-Alder/retro-Diels-Alder cycles.[44]

The reactivity of the Maleimide-AuNPs through Diels-Alder reaction was then tested using a wide range of dienes, and it was compared to the same reaction carried out in solution using *N*-dodecylmaleimide as a model compound. The interfacial reactivity could be followed by the disappearance of the maleimide peak at 5.80 ppm and the appearance of the peaks of the interfacial cycloaddition product.

Table 1.1: Times for completion for the interfacial Diels-Alder cycloaddition, 1,3-dipolar cycloaddition and Michael-type addition reaction with different dienes, dipoles and amines, respectively. The model reaction involves use of *N*-dodecylmaleimide in place of Maleimide-AuNP. Reactions performed in CH_2Cl_2 and at room temperature.

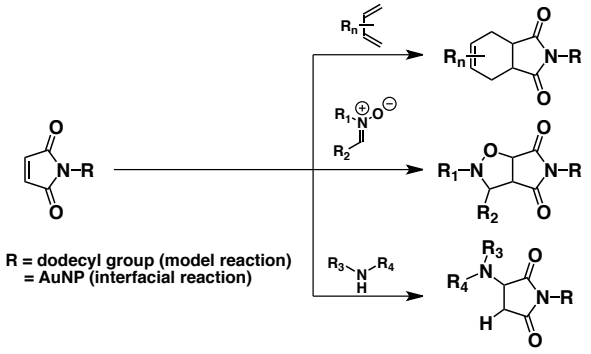

	Clickable Partner	Model Reaction	Interfacial Reaction	Interfacial Reaction (11,000 atm)
Diels-Alder cycloaddition	**a**	40 h	6 d	10 min
	b	24 h	6 d	10 min
	c	7 d	NR in 7 d	10 min
	d	3 d	60% in 7 d	10 min
1,3-dipolar cycloaddition	**e**	2 h	2 h	10 min
	f	10 h	1 d	10 min
	g	30 h	3 d	10 min
	h	3 d	7 d	10 min
Michael-type addition	**i**	30 h	72 h	30 min
	j	65 h	80 h	45 min
	k	56 h	80 h	45 min

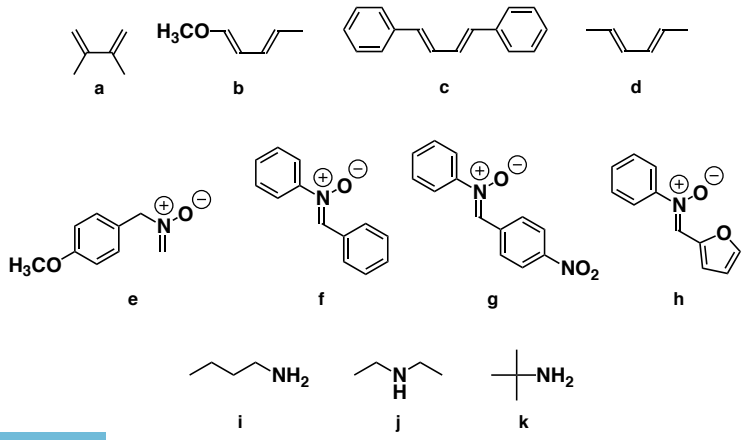

Due to the typical broad peaks of the ^{1}H NMR spectrum of a AuNP sample, proof of proper interfacial reactivity for each cycloaddition reaction was obtained by comparing the ^{1}H NMR spectrum of the interfacial reaction product with that of the corresponding model reaction in homogeneous solution. An excellent correspondence between the peak chemical shifts indicated successful interfacial reactivity. The data reported in Table 1.1 shows that, as expected, electron deficient dienes (*e.g.*, Table 1.1, entry **c**) or more sterically hindered dienes (*e.g.*, Table 1.1, entry **d**) reacted more sluggishly in both interfacial and model reactions. More interestingly, Table 1.1 also shows that the reaction at the AuNP interface is always slower than the corresponding reaction in solution, reaching completion in the time scale of days instead of hours. This is most likely due to the bulky character of the AuNP that imposes unique diffusional parameters and constraints to the orientation required for the reaction to occur.[46] On one hand, the Maleimide-AuNP template demonstrated versatility by reacting cleanly (as per ^{1}H NMR spectroscopy) with a range of dienes under standard conditions, however, on the other hand the long reaction times required for the reactions to reach completion (~ 1 week) can be impractical and hinder potential applications for this nanomaterial template.

This pushed us to explore the possibility of using very high pressure to increase the kinetics of the interfacial Diels-Alder reaction. This idea was supported by the fact that the Diels-Alder reaction has a negative volume of activation. The activation volume ($\Delta V^{\ddagger}$) is defined as the difference between the partial molar volume of the transition state and the sum of the partial molar volumes of the reactants. In other words, for the generic chemical reaction:

$$A + B \rightarrow [\ddagger] \rightarrow P$$

The activation volume is:

$$\Delta V^{\ddagger} = V^{\ddagger} - V_A - V_B$$

Because the activation volume is related to the reaction rate constant (k) by the equation:

$$\Delta V^{\ddagger} = -RT \left(\frac{\partial \ln k}{\partial P}\right)_T$$

it follows that the smaller the activation volume, the higher the rate constant is, and an increase of P is accompanied by an increase in k.[47, 48] In other words, in theory high pressure can be used to push the reactions forward. However, in order to have an appreciable change in the kinetic rate constant the pressure applied must be very high (>10000 atm).

While theory shows that the method would work, we had to face some practical challenges. First of all: will the AuNP substrate survive such drastic reaction conditions? To answer this question Maleimide-AuNPs were dissolved in CH_2Cl_2 and exposed to 11000 atm for 24 h. Surprisingly, TEM images recorded before and after exposing of the AuNPs to high pressure showed that the AuNP's size distribution did not undergo any change after the high pressure treatment, and that the Maleimide-AuNPs were perfectly stable and could be dried and readily redissolved in organic solvent with little to no aggregation.

Subsequently, the interfacial Diels-Alder cycloaddition was investigated under very high pressure conditions.[46] Results surpassed our expectations: all the interfacial reactions, which took days or weeks at atmospheric pressure, reached completion in the time scale of minutes. Table 1.1 summarizes our findings. Most importantly, the AuNP physical-chemical properties after the high-pressure reaction were well preserved: the functionalized AuNPs could be dried and readily redissolved in organic solvents with little to no aggregation, and TEM images confirmed that after the high-pressure reaction AuNPs retained their original size and shape.

We next investigated the 1,3-dipolar cycloaddition[49], and the Michael-type addition reaction[45] at the interface of the organic solvent-soluble Maleimide-AuNP template using a family of nitrones and amines, respectively. For the investigation of the Michael-type addition reaction, thiols were avoided because during the long reaction time in non-protic solvents ligand exchange reaction could occur, making the characterization of the product difficult or impossible. For these studies, we employed a similar methodology to that used for the Diels-Alder reaction, and the interfacial reaction was followed by ^{1}H NMR spectroscopy and compared to the corresponding model reaction carried out in solution

using *N*-dodecylmaleimide as the model molecule. Results are summarized in Table 1.1 and, similarly to the Diels-Alder reaction, show that the Maleimide-AuNPs gave the cycloaddition or the Michael-type addition products cleanly but on a longer time scale than the corresponding model reactions in homogeneous solution. This confirms our hypothesis that the AuNP environment must impose particular constraints to the reaction mechanisms.

Through the screening of differently substituted nitrones it was possible to evaluate steric and electronic effects for the interfacial 1,3-dipolar cycloaddition. In particular the inductive effect exerted by N-aryl substituted nitrones was found to favor the reactivity by enhancing the dipolar nature of the nitrone. The presence of electron-withdrawing substituents at the carbon or nitrogen terminus of the nitrone was found instead to decrease its reactivity (see Table 1.1, compare entries **f-g**). However, steric hindrance was found to play the major role. Because of the bulky character of the AuNP, sterically hindered nitrones were found to enhance the difference in the reaction rates between interfacial reaction and model reaction. If the C-terminus of the nitrone is not sterically hindered (non-substituted, see Table 1.1, entry **e**), the reaction at the AuNP interface can take place in the time scale of hours and is comparable to the rate of the model reaction. Finally, it is worth noting that a furan-substituted nitrone (see Table 1.1, entry **h**) has been found to react exclusively through the 1,3-dipolar cycloaddition rather than through Diels-Alder reaction. This could in part be due to a more negative activation and reaction volume for the dipolar cycloaddition than for the Diels-Alder cycloaddition reaction.[49]

Electronic and steric effects were also investigated for the interfacial Michael-type addition reaction by employing differently substituted amines. As expected, it was observed that the increased nucleophilic character of the amine resulted in faster reaction kinetic, and that the increased steric hindrance on the amine increased the reaction time (see Table 1.1). Furthermore, as observed for both the cycloaddition reactions, the interfacial reaction was always found to be slower than the corresponding reaction in solution.

Finally, because both 1,3-dipolar cycloaddition and the Michael-type addition also have negative activation volumes, the possibility of using very high pressure was investigated in an attempt to increase their reaction kinetics. Table 1.1 shows that for both reactions the corresponding products could be obtained in a few minutes, while under normal atmosphere the reactions would require hours or days. These results further show the generality of our high pressure methodology for increasing the reactivity of the Maleimide-AuNP and making it an excellent and versatile template for its further modification with potentially any molecular system of interest.

For the first time very high pressure was employed for the functionalization of AuNPs. The interfacial reactions that under normal conditions take a very long time, reach completion in a few minutes under very high pressure, without causing any alteration on the AuNP's core and therefore preserving the AuNP's size-dependent physical-chemical properties. This new high-pressure strategy opened new scenarios for the functionalization of AuNPs, making it possible to safely react interfacial groups that would show poor reactivity under normal condition.

1.4 Synthesis of the water-soluble Maleimide-AuNP template

The success achieved with the organic solvent-soluble Maleimide-AuNPs pushed us to expand their versatility even more. The Maleimide-AuNPs synthesized so far present the restriction that they can be readily redissolved exclusively in organic solvents, ranging from apolar solvents (*i.e.*, benzene, hexanes) to solvents with a low to medium polarity (*i.e.*, toluene, THF, CH_2Cl_2) that are known to disfavor the reactivity of the interfacial maleimide moieties. Attempts were made in order to try to push the reactivity of the organic solvent-soluble Maleimide-AuNP template by using protic solvents. For example, a catalytic amount of methanol was added to a solution of Maleimide-AuNPs and a nucleophile in CH_2Cl_2, but it failed to catalyze the Michael-type addition reaction because of the instantaneous precipitation of insoluble Maleimide-AuNPs. The strategy of using very high pressure solved this slow reaction kinetic issue. Carrying out the reactions at 11000 atm significantly decreased the reaction times and had no effect on the AuNPs, which could maintain their size-dependent physical-chemical properties.

However, the use of the very high pressure is not straightforward. It requires a specific apparatus and, most importantly, it cannot be employed with particularly delicate systems like biosystems or biomolecules, therefore restricting many potential applications of the Maleimide-AuNPs in chemical biology and medicine. Because of these reasons we were pushed to design a new Maleimide-AuNP that could display solubility in protic solvents and especially in water. These type of solvents are well known to catalyze the Michael-type addition, the 1,3-dipolar cycloaddition, and the Diels-Alder cycloaddition by lowering the energy level of the maleimide's LUMO and making the maleimide a better electrophile, dipolarophile and dienophile.[50-54]

Because the solubility properties are mainly related to the AuNP's organic corona, the first thing to change was the ligand that constitutes the template. We synthesized a new AuNP template using triethylene glycol-monomethylether-thiol (MeO-EG_3-SH) as the new ligand (see Scheme 1.2). The ethylene glycol framework has a double function: is confers the AuNP both water-solubility and solubility in polar organic solvents, and it is well known to be biocompatible and hinder protein adsorption. This can potentially prolong the AuNP's circulation half-life, and reduce the AuNP's immunogenicity, making the nanosystem suitable for many applications in both chemical biology and nanomedicine.[55-57] The solubility in organic solvents is very important because it allows us to perform the retro-Diels-Alder reaction to deprotect the maleimide under reaction conditions that avoid the hydrolysis of the maleimide. If a hydroxy-terminated thiolated ligand was used, the resulting AuNPs would have not been soluble in toluene where the maleimide deprotection reaction is most efficient (*vide infra*).

The desired TEG-AuNPs were synthesized using a modified one-phase synthesis method. Briefly, $HAuCl_4$ was mixed with MeO-EG_3-SH in a solvent mixture of methanol and acetic acid, and with a Au/S ratio of 1:3. Once the bright yellow color of the solution faded, an aqueous solution of $NaBH_4$ was slowly added to the reaction mixture. The success of AuNPs formation was confirmed by the typical rapid change of the solution's color from light yellow to dark brown, indicating formation of small (~3 nm) AuNPs (as per TEM images).[40]

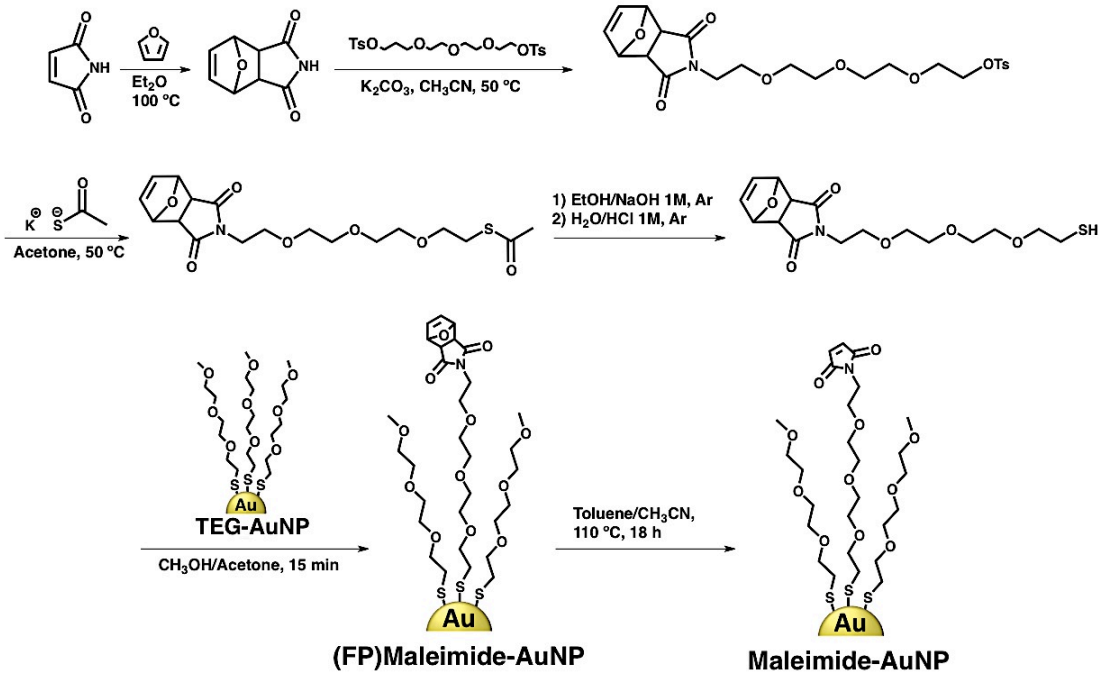

Scheme 1.2: Synthesis of water-soluble Maleimide-AuNP.

To obtain the water-soluble Maleimide-AuNPs we used a retro-Diels-Alder-based synthetic strategy similar to that described above. The required (FP)Maleimide thiolated ligand was synthesized using tetraethylene glycol as the starting material. The extra ethylene glycol unit has the function of minimizing the steric hindrance at the maleimide, making it more prone to undergo interfacial reactions. The synthetic path leading to the new water-soluble furan-protected-maleimide-thiol ((FP)Maleimide-EG_4-SH) is reported in Scheme 1.2. First, the maleimide is protected with furan. Subsequently, the furan-protected maleimide is attached to one extremity of the tetraethylene glycole spacer. Finally, the thiol is synthesized on the other extremity of the spacer. The (FP)Maleimide-EG_4-SH was then introduced onto the MeO-EG_3-AuNP organic corona through a ligand exchange reaction by using a mixture of methanol and acetone as the solvent. Similarly to their organic solvent-soluble counterparts, the (FP)Maleimide-AuNPs were thoroughly washed in order to remove any unreacted thiols before the deprotection of the maleimide group. To wash away the free thiols we employed trituration in hexanes (which selectively dissolves the thiols but not the (FP)Maleimide-AuNP), followed by dialysis.

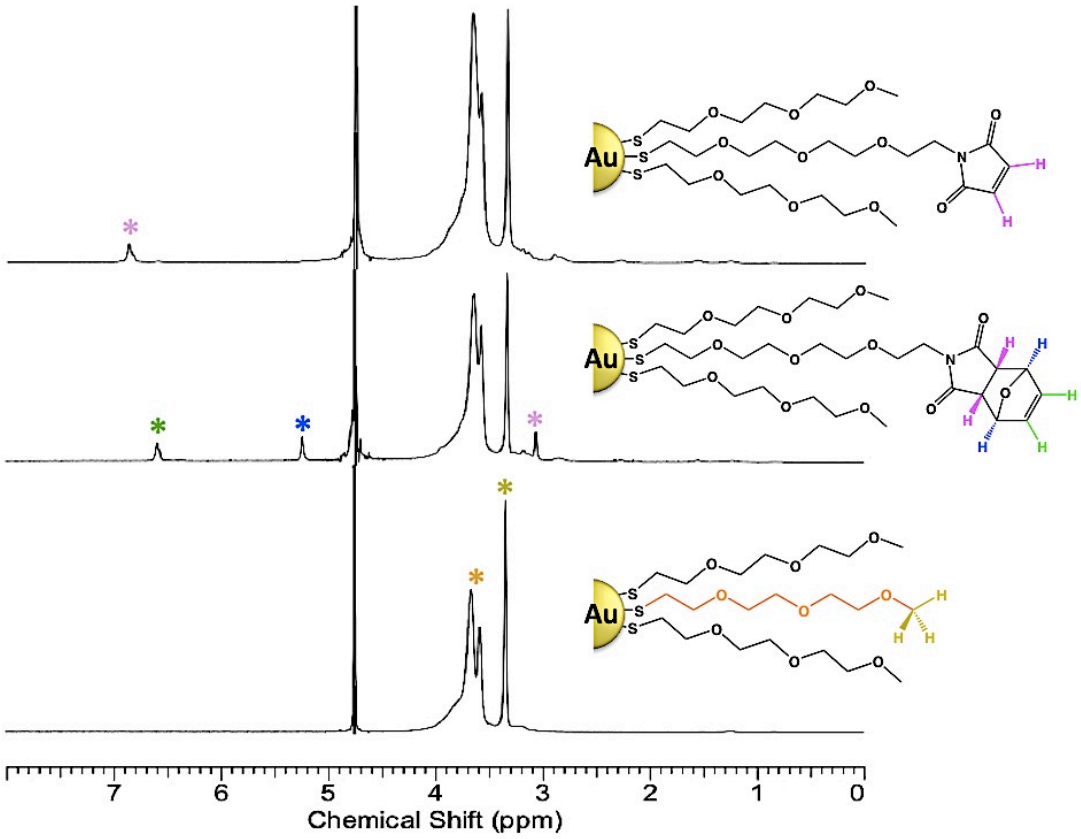

Figure 1.4: ^{1}H NMR characterization of TEG-AuNP (bottom), water-soluble (FP)Maleimide-AuNP (center), and water-soluble Maleimide-AuNP (top). Spectra recorded using D_2O as solvent and referenced to residual H_2O.

The retro-Diels-Alder reaction to deprotect the maleimide functionalities from the furan was carried out by dissolving the nanoparticles in a mixture of toluene and CH_3CN in a 10:1 ratio, and heating the system at 110 ºC for overnight. Also in this case, each synthetic step leading to the final water-soluble Maleimide-AuNPs could be easily monitored by ^{1}H NMR spectroscopy (refer to Figure 1.4). The ^{1}H NMR spectrum recorded in D_2O for the (FP)Maleimide-EG_4-AuNP shows the peak of the two maleimides alkene protons at 6.60 ppm, the peak of the two protons adjacent to the bridged oxygen at 5.25 ppm, and the peak of the two protons closer to the carbonyls at 3.07 ppm. After the deprotection reaction the peaks of the Diels-Alder adduct at 6.60, 5.25, and 3.07 ppm disappeard, and a new peak appears at 6.86 ppm, which corresponds to the alkene protons of the deprotected maleimide.

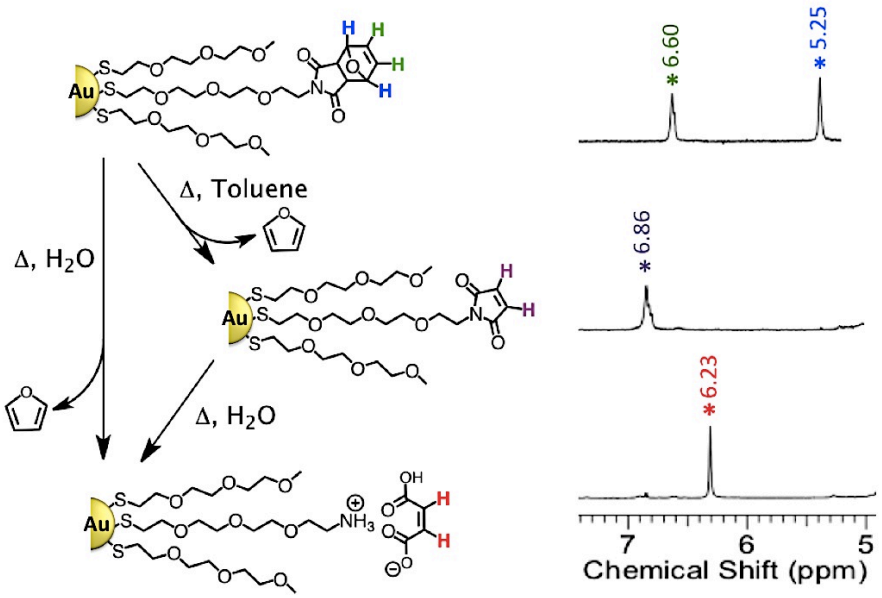

Figure 1.5: Reaction scheme and ^{1}H NMR spectra recorded in D_2O illustrating the result of the retro-Diels-Alder reaction carried out using water or toluene as solvents.

TEM images recorded before and after the retro-Diels-Alder reaction showed that the high temperature required for the deprotection reaction caused a slight increase of the AuNP's size from 2.0 ± 0.3 nm to 2.5 ± 0.5 nm, and a slight broadening of the AuNP's size distribution.[40]

The solvent employed to carry out the retro-Diels-Alder reaction and deprotect the interfacial maleimide functionalities has a key role in the synthetic procedure. The solvent must 1) have a high-enough boiling point in order to trigger the retro-Diels-Alder reaction, 2) be reasonably easy to remove, 3) be able to completely dissolve the (FP)Maleimide-AuNP and not cause any side reaction. The solvent initially employed was toluene.[40] However, after the ligand exchange reaction to introduce the furan-protected maleimide-thiolated ligands, the solubility of the (FP)Maleimide-AuNP in toluene is low, resulting in a poor yield for the retro-Diels-Alder reaction. Further improvement of the deprotection reaction found the best solvent to be a 10:1 toluene-acetonitrile mixture.[58] Different attempts have been made using different mixtures of organic solvents (*e.g.*, CH_3CN, acetone, CH_2Cl_2 and water), and all of them resulted in a

poor retro-Diels-Alder reaction yield or in AuNPs aggregation. The use of water as the solvent for the deprotection resulted in the most interesting outcome. After the deprotection reaction in water the ^{1}H NMR of the resulting AuNPs resulted to be very similar to that of the Maleimide-AuNPs (see Figure 1.5). A more careful analysis, however, showed that the alkene peak fell at 6.23 ppm (instead of 6.86 ppm), upfield with respect to the peak at 6.60 ppm related to the alkene protons of the furan-protected maleimide. Further investigations demonstrated that heating the furan-protected or deprotected Maleimide-AuNPs in water at 100 ºC causes a double hydrolysis of the maleimide moieties, leading to maleic acid (responsible for the peak at 6.23 ppm) and interfacial primary amines (see Figure 1.5).[40] This result would explain the lack of reactivity towards the Michael-type addition reaction of Maleimide-AuNPs prepared through a protocol that involves a prolonged heating in water.[59] It also showed that the retro-Diels-Alder reaction to deprotect the maleimide from the furan can only be successful if the (FP)Maleimide-AuNP retain their solubility in organic solvent, highlighting the importance of the methyl-terminated thiolated ligands that compose our TEG-AuNP staring material.

One of the greatest advantages of these water-soluble Maleimide-AuNP is that they are based on short tri- and tetraethylene glycol ligands. These small ligands, with a well-defined molecular structure ensure precise characterization of the AuNP allowing us to determine with good precision the average number of ligands and more importantly the average number of maleimide functionalities present at the AuNP's interface. This is very important, especially in anticipation of their potential use as drug carriers or labeling agents, where the number of interfacial drugs or biomolecules represents valuable information for therapeutic and quantitative purposes. Through the combination of TEM images, TGA data, and ^{1}H NMR spectra of the Maleimide-AuNP and assuming that the AuNP are spherical and perfectly monodispersed in size, it is possible to calculate a AuNP raw formula of Au_{500} (MeO-EG_3-S)$_{200}$ (Maleimide-EG_4-S)$_{80}$.[58]

1.5 Reactivity of the Water-Soluble Maleimide-AuNP Template

The water-soluble Maleimide-AuNPs have been tested towards the Michael-type addition, the 1,3-dipolar cycloaddition and the Diels-Alder cycloaddition reaction. As expected, the reaction times for the 1,3-dipolar cycloaddition and Diels-Alder cycloaddition performed in polar protic or aprotic organic solvent were found to be substantially shorter than in CH_2Cl_2 or $CHCl_3$. However, nitrones or dienes with bulky substituents were still found to react on the time scale of days, suggesting that for these two types of reactions steric restrictions represent the main rate-limiting factor.[60]

The major improvement was observed for the Michael-type addition reaction, whose reaction time in protic solvents decreased from days to minutes/hours. This opened a plethora of new possibilities and applications for the Maleimide-AuNP template. We showcased this by employing them for bioconjugation, drug delivery, medical imaging and the synthesis of nanomaterial hybrids.

In our first work we were able to conjugate cysteine on onto the AuNP through a Michael-type addition reaction that occurred in minutes in water media, and could be monitored through ^{1}H NMR spectroscopy by the disappearance of the maleimide peak at 6.89 ppm and the appearance of the thioether product peaks at 3.25 and 3.17 ppm.[40]

In a subsequent work we successfully employed the Michael-type addition reaction to conjugate a gadolinium-based contrast agent (DO3A-amine) onto the Maleimide-AuNPs. Because we can follow the AuNP's interfacial reactivity and fully characterize the resulting conjugate, we were able to determine the amount of contrast agents per particle with good precision. In particular, inductively coupled plasma-optical emission spectrometry (ICP-OES) showed that on average we had 56 gadolinium contrast agents per particle. This information was employed to perform *in vivo* MRI experiments, which showed good contrast on the kidneys (see Figure 1.6) and a prolonged circulation time for the contrast agent-nanocarrier system compared to the contrast agent alone.[58]

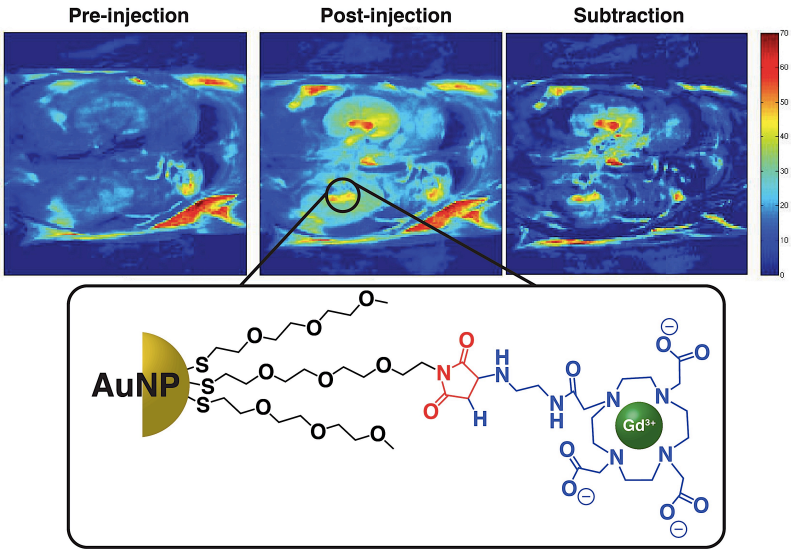

Figure 1.6: Top: MRI images showing the kidneys of a mouse. Bottom: schematic representation of the Maleimide-AuNP functionalized with the DO3A gadolinium-based contrast agent.

Recently, we investigated the occurrence of the glutathione-mediated retro Michael-type addition at the Maleimide-AuNP's interface. We demonstrated that if the Michael donor employed for conjugation has a low pK_a (*e.g.*, benzenethiol), then under physiological conditions (37 ºC, pH 7.4, 10-18 mM glutathione) an interfacial retro Michael-type addition readily occurs, causing the release of the thiol with low pK_a and the formation of the more thermodynamically stable glutathione-maleimide thioether adduct (see to Figure 1.7). This type of reactivity represents a threat for applications that require the molecular cargo to be permanently bound to the nanocarrier (*e.g.*, medical imaging, bioconjugation), because it would cause a gradual undesired release of the payload.

We also demonstrated that in the eventuality where it is not possible to select a thiol with high pK_a for the conjugation step, then the retro reaction can be blocked by hydrolyzing (or "locking") the interfacial maleimide-thioether adduct under reaction conditions where the AuNPs are stable. This methodology was shown to be very efficient in hindering the retro Michael-type addition reaction and lock the thioether adduct at the AuNP's interface.

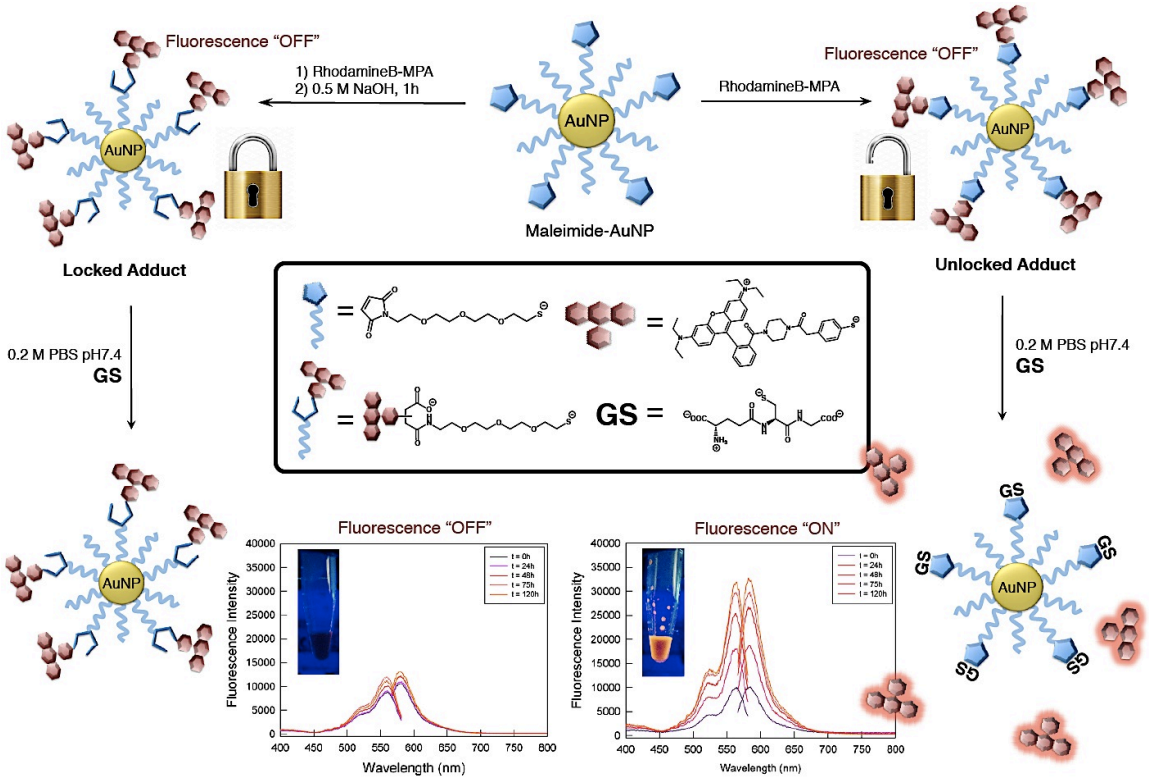

Figure 1.7: Cartoon representing the concept of "locked" or "unlocked" adduct on the fluorogenic AuNPs. When the fluorogenic AuNP are hydrolyzed and the rhodamine-maleimide adduct is "locked" (left path) there is no retro Michael-type addition reaction with glutathione (GS) and there is no turn-on of fluorescence. On the other hand, if the fluorogenic AuNP remains "unlocked" (right path), the retro Michael-type addition occurs and there is turn-on of fluorescence. Fluorescence data recorded over time in 0.2 M PBS pH 7.4, λ_{exc} = 556.6 nm, λ_{em} = 591.5 nm. The insets in the fluorescence data plots show pictures of the hydrolyzed fluorogenic AuNP (left) and fluorogenic AuNP contained in an eppendorf tube and exposed to a long wave lamp. ***Figure reproduced from reference 61 with permission of the American Chemical Society.***

In this same work we also showed that the retro Michael-type addition reaction expands the scope of the Maleimide-AuNP template, and allows its use for delivering a molecular payload. We showcased this by synthesizing a benzenethiol-functionalized rhodamine B fluorescent molecule that was conjugated onto the Maleimide-AuNP template through a rapid Michael addition reaction.

In this nanosystem, the fluorescence of rhodamine B was quenched by the gold core through a FRET mechanism, but upon exposure to biological concentrations of glutathione, rhodamine B was released in solution through the retro Michael-type addition reaction where its fluorescence was not quenched (see Figure 1.7).[61] This fluorogenic AuNP demonstrated that the retro Michael-type addition reaction can find potential use for the selective intracellular delivery of molecules of interest from a AuNP carrier by exploiting the biological distribution of glutathione. However, further fundamental investigations on the retro Michael-type addition reaction are still required in order to improve its yield and kinetics, and to make it an efficient tool for drug delivery.

Finally, we demonstrated how the Maleimide-AuNP template can create new opportunities in materials chemistry by synthesizing a AuNP-decorated carbon nanotube (CNT), a desirable hybrid material that can find diverse applications in catalysis, sensing and energy storage. [62] The synthesis of a AuNP-CNT hybrid material can be challenging because of the lack of synthetic techniques that allow a robust coating of the CNT's walls with AuNP. By employing an interfacial Michael-type addition reaction we were able to covalently bind our Maleimide-AuNPs onto thiol modified single-walled CNTs (SWCNT) through a simple "*pour and mix*" type of chemistry.

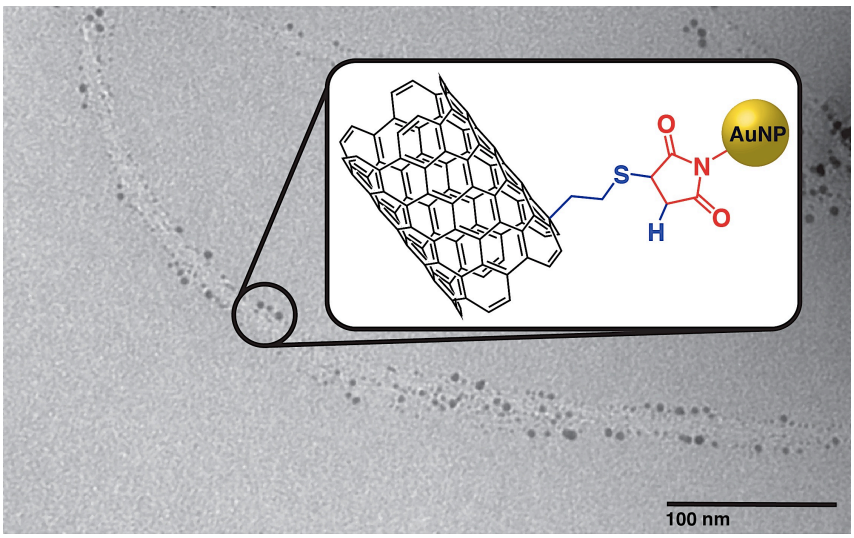

Figure 1.8: TEM image of SWCNT decorated with 3 nm Maleimide-AuNP through an interfacial Michael-type addition reaction.

Direct mixing of Maleimide-AuNPs with thiol modified SWCNTs in water media for 60 minutes lead to SWCNTs covered with ~3 nm AuNP as shown by TEM images (see Figure 1.8). Proof of successful interfacial Michael-type addition reaction was also confirmed by X-ray photoelectron spectroscopy, which showed the appearance of the components for newly formed C-S-C bonds in the S 2p core line.

This work demonstrated that interfacial click chemistry gives excellent opportunities in materials chemistry, allowing the synthesis of hybrid nanomaterials, in a facile, reliable, and robust way.

1.6 Concluding remarks

Both organic solvent-soluble and water-soluble small Maleimide-AuNP have been successfully synthesized through a retro-Diels-Alder strategy that preserves the integrity of the maleimide functionality at the AuNPs interface. Because of the small size of the gold core and thiol ligands, it was possible to fully characterize these nanoparticles and determine the amount of functionalities that were introduced onto the AuNP's organic corona. This information is of great utility for applications of the Maleimide-AuNP template in chemical biology and nanomedicine.

The reactivity of the organic solvent-soluble Maleimide-AuNPs has been thoroughly investigated towards the Michael-type addition reaction, the 1,3-dipolar cycloaddition, and the Diels-Alder cycloaddition reactions. These reactions at the AuNP's interface were found to be effective, but with a sluggish rate and dominated by steric effects. These issues could be solved with the use of very high pressure, by taking advantage of the negative activation volumes of the three different reactions. Results were excellent: besides notably decreasing the reaction times from days or weeks to minutes, Maleimide-AuNPs were found to be perfectly stable after the high-pressure treatment with no changes observed on the size and shape of the gold core.

A water-soluble version of these AuNPs was subsequently created, with the goal of expanding the applications of the Maleimide-AuNP template to the water media, and enhancing the reactivity of the three types of interfacial reactions through the use of

protic solvents. The reactivity of the Maleimide-AuNPs showed to be very efficient towards all three types of reaction, occurring at room temperature or under physiological conditions, and on a useful time scale. Furthermore, we were able to expand the scope of the Maleimide-AuNP template's chemistry and showcase its potential in bioconjugation, nanomedicine, and drug delivery.

The Maleimide-AuNPs find their role as a versatile template for applications in many fields of science. Their potential is highlighted by the possibility of making them soluble in any kind of solvent by switching from the C_{12}-AuNP to the MeO-EG_3-AuNP substrate, and by their ability to quickly undergo three different click reactions with different functional groups (*i.e.*, nucleophiles, azide, nitrones and dienes), while preserving their size-dependent properties. This ensures an effective, efficient, and safe way to create new hybrid nanomaterials and AuNP-bioconjugates, with a consequent great future impact in materials chemistry, chemical biology and nanomedicine.

1.7 References

1. Lee, J. S., Recent progress in gold nanoparticle-based non-volatile memory devices. *Gold Bull.* **2010,** *43*, 189-199.

2. Khondaker, S. I.; Luo, K.; Yao, Z., The fabrication of single-electron transistors using dielectrophoretic trapping of individual gold nanoparticles. *Nanotechnology* **2010,** *21*.

3. Kim, S. J.; Lee, J. S., Flexible Organic Transistor Memory Devices. *Nano Lett.* **2010,** *10*, 2884-2890.

4. Homberger, M.; Simon, U., On the application potential of gold nanoparticles in nanoelectronics and biomedicine. *Phil. Trans. R. Soc. A* **2010,** *368*, 1405-1453.

5. Mikami, Y.; Dhakshinamoorthy, A.; Alvaro, M.; Garcia, H., Catalytic activity of unsupported gold nanoparticles. *Catal. Sci. Tech.* **2013,** *3*, 58-69.

6. Kim, D.; Jon, S., Gold nanoparticles in image-guided cancer therapy. *Inorg. Chim. Acta* **2012,** *393*, 154-164.

7. Song, Y. J.; Wei, W. L.; Qu, X. G., Colorimetric Biosensing Using Smart Materials. *Adv. Mater.* **2011,** *23*, 4215-4236.

8. Liu, D. B.; Wang, Z.; Jiang, X. Y., Gold nanoparticles for the colorimetric and fluorescent detection of ions and small organic molecules. *Nanoscale* **2011,** *3*, 1421-1433.

9. Saha, K.; Agasti, S. S.; Kim, C.; Li, X. N.; Rotello, V. M., Gold Nanoparticles in Chemical and Biological Sensing. *Chem. Rev.* **2012,** *112*, 2739-2779.

10. Henz, B. J.; Hawa, T.; Zachariah, M. R., Mechano-chemical stability of gold nanoparticles coated with alkanethiolate SAMs. *Langmuir* **2008,** *24*, 773-783.

11. Jothibasu, S.; Kumar, A. A.; Alagar, M., Synthesis of maleimide substituted polystyrene-silica hybrid utilizing michael addition reaction. *J. Sol-Gel Sci. Technol.* **2007,** *43*, 337-345.

12. Liu, Y. L.; Lee, H. C., Preparation and properties of polyhedral oligosilsequioxane tethered aromatic polyamide nanocomposites through Michael addition between maleimide-containing polyamides and an amino-functionalized polyhedral oligosilsequioxane. *J. Polym. Sci. A Polym. Chem.* **2006,** *44*, 4632-4643.

13. Vretik, L.; Ritter, H., 1,3-dipolar cycloaddition in polymer synthesis. 1. Polyadducts with flexible spacers derived from Bis(N-methylnitrone)s and Bis(N-phenylmaleimide)s. *Macromolecules* **2003,** *36*, 6340-6345.

14. Gandini, A.; Coelho, D.; Silvestre, A. J. D., Reversible click chemistry at the service of macromolecular materials. Part 1: Kinetics of the Diels-Alder reaction applied to furan-maleimide model compounds and linear polymerizations. *Eur. Polym. J.* **2008,** *44*, 4029-4036.

15. Bergman, S. D.; Wudl, F., Mendable polymers. *J. Mater. Chem.* **2008,** *18*, 41-62.

16. Dispinar, T.; Sanyal, R.; Sanyal, A., A Diels-Alder/Retro diels-alder strategy to synthesize polymers bearing maleimide side chains. *J. Polym. Sci. A Polym. Chem.* **2007,** *45*, 4545-4551.

17. Dag, A.; Aydin, M.; Durmaz, H.; Hizal, G.; Tunca, U., Various polycarbonate graft copolymers via Diels-Alder click reaction. *J. Polym. Sci. A Polym. Chem.* **2012,** *50*, 4476-4483.

18. Szalai, M. L.; McGrath, D. V.; Wheeler, D. R.; Zifer, T.; McElhanon, J. R., Dendrimers based on thermally reversible furan-maleimide Diels-Alder adducts. *Macromolecules* **2007,** *40*, 818-823.

19. Polaske, N. W.; McGrath, D. V.; McElhanon, J. R., Thermally Reversible Dendronized Step-Polymers Based on Sequential Huisgen 1,3-Dipolar Cycloaddition and Diels-Alder "Click" Reactions. *Macromolecules* **2010,** *43*, 1270-1276.

20. Fu, Y.; Kao, W. J., In situ forming poly(ethylene glycol)-based hydrogels via thiol-maleimide Michael-type addition. *J. Biomed. Mater. Res. Part A* **2011,** *98*, 201-11.

21. Chen, Q.; Zhang, D.; Zhang, G.; Zhu, D., New cholesterol-based gelators with maleimide unit and the relevant Michael adducts: chemoresponsive organogels. *Langmuir* **2009,** *25*, 11436-41.

22. De, P.; Li, M.; Gondi, S. R.; Sumerlin, B. S., Temperature-regulated activity of responsive polymer-protein conjugates prepared by grafting-from via RAFT polymerization. *J. Am. Chem. Soc.* **2008,** *130*, 11288-9.

23. Harper, J. C.; Polsky, R.; Wheeler, D. R.; Brozik, S. M., Maleimide-activated aryl diazonium salts for electrode surface functionalization with biological and redox-active molecules. *Langmuir* **2008,** *24*, 2206-2211.

24. Bertin, P. A.; Ahrens, M. J.; Bhavsar, K.; Georganopoulou, D.; Wunder, M.; Blackburn, G. F.; Meade, T. J., Ferrocene and Maleimide-Functionalized Disulfide Scaffolds for Self-Assembled Monolayers on Gold. *Org. Lett.* **2010,** *12*, 3372-3375.

25. Wang, Y. F.; Yao, X.; Wang, J. X.; Zhou, F. M., Attachment of amine- and maleimide-containing ferrocene derivatives onto self-assembled alkanethiol and alkanedithiol monolayers: Voltammetric evaluation of cross-linking efficiencies and surface coverage of electroactive groups. *Electroanalysis* **2004,** *16*, 1755-1761.

26. Lee, J. K.; Chi, Y. S.; Lee, J. S.; Lim, Y. G.; Jung, Y. H.; Oh, E.; Ko, S. B.; Jung, H. J.; Kang, P. S.; Choi, I. S., In-plane enyne metathesis and subsequent Diels-Alder reactions on self-assembled monolayers. *Langmuir* **2005,** *21*, 10311-10315.

27. King, M. J.; Jepson, M. A.; Guest, A.; Mushens, R., Detection of hereditary pyropoikilocytosis by the eosin-5-maleimide (EMA)-binding test is attributable to a marked reduction in EMA-reactive transmembrane proteins. *Int. J. Hematol.* **2011,** *33*, 205-211.

28. Ni, J. H.; Singh, S.; Wang, L. X., Synthesis of maleimide-activated carbohydrates as chemoselective tags for site-specific glycosylation of peptides and proteins. *Bioconjugate Chem.* **2003,** *14*, 232-238.

29. Jose, J.; Handel, S., Monitoring the cellular surface display of recombinant proteins by cysteine labeling and flow cytometry. *Chembiochem* **2003,** *4*, 396-405.

30. Hill, K. W.; Taunton-Rigby, J.; Carter, J. D.; Kropp, E.; Vagle, K.; Pieken, W.; McGee, D. P. C.; Husar, G. M.; Leuck, M.; Anziano, D. J.; Sebesta, D. P., Diels-Alder bioconjugation of diene-modified oligonucleotides. *J. Org. Chem.* **2001,** *66*, 5352-5358.

31. Schweizer, E.; Hoffmann-Roder, A.; Olsen, J. A.; Seiler, P.; Obst-Sander, U.; Wagner, B.; Kansy, M.; Banner, D. W.; Diederich, F., Multipolar interactions in the D pocket of thrombin: large differences between tricyclic imide and lactam inhibitors. *Org. Biomol. Chem.* **2006,** *4*, 2364-2375.

32. Durust, Y.; Karakus, H.; Kaiser, M.; Tasdemir, D., Synthesis and anti-protozoal activity of novel dihydropyrrolo[3,4-d][1,2,3]triazoles. *Eur. J. Med. Chem.* **2012,** *48*, 296-304.

33. Ferrero, V. E. V.; Andolfi, L.; Di Nardo, G.; Sadeghi, S. J.; Fantuzzi, A.; Cannistraro, S.; Gilardi, G., Protein and Electrode Engineering for the Covalent Immobilization of P450 BMP on Gold. *Anal. Chem.* **2008,** *80*, 8438-8446.

34. Houseman, B. T.; Gawalt, E. S.; Mrksich, M., Maleimide-functionalized self-assembled monolayers for the preparation of peptide and carbohydrate biochips. *Langmuir* **2003,** *19*, 1522-1531.

35. Baldacchini, C.; Chamorro, M. A. H.; Prato, M.; Cannistraro, S., Highly Conductive Redox Protein-Carbon Nanotube Complex for Biosensing Applications. *Adv. Funct. Mater.* **2011,** *21*, 153-157.

36. de Araujo, A. D.; Palomo, J. M.; Cramer, J.; Seitz, O.; Alexandrov, K.; Waldmann, H., Diels-Alder ligation of peptides and proteins. *Chem. Eur. J.* **2006,** *12*, 6095-6109.

37. de Araujo, A. D.; Palomo, J. M.; Cramer, J.; Kohn, M.; Schroder, H.; Wacker, R.; Niemeyer, C.; Alexandrov, K.; Waldmann, H., Diels-Alder ligation and surface immobilization of proteins. *Angew. Chem. Int. Edit.* **2006,** *45*, 296-301.

38. Khan, M. N., Kinetics and Mechanism of the Alkaline-Hydrolysis of Maleimide. *J. Pharm. Sci.* **1984,** *73*, 1767-1771.

39. Matsui, S.; Aida, H., Hydrolysis of Some N-Alkylmaleimides. *Perkin Trans. 2* **1978**, 1277-1280.

40. Gobbo, P.; Workentin, M. S., Improved Methodology for the Preparation of Water-Soluble Maleimide-Functionalized Small Gold Nanoparticles. *Langmuir* **2012,** *28*, 12357-12363.

41. Baldwin, A. D.; Kiick, K. L., Tunable Degradation of Maleimide-Thiol Adducts in Reducing Environments. *Bioconjugate Chem.* **2011,** *22*, 1946-1953.

42. Shen, B. Q.; Xu, K. Y.; Liu, L. N.; Raab, H.; Bhakta, S.; Kenrick, M.; Parsons-Reponte, K. L.; Tien, J.; Yu, S. F.; Mai, E.; Li, D. W.; Tibbitts, J.; Baudys, J.; Saadi, O. M.; Scales, S. J.; McDonald, P. J.; Hass, P. E.; Eigenbrot, C.; Nguyen, T.; Solis, W. A.; Fuji, R. N.; Flagella, K. M.; Patel, D.; Spencer, S. D.; Khawlil, L. A.; Ebens, A.; Wong, W. L.; Vandlen, R.; Kaur, S.; Sliwkowski, M. X.; Scheller, R. H.; Polakis, P.; Junutula, J. R., Conjugation site modulates the in vivo stability and therapeutic activity of antibody-drug conjugates. *Nat. Biotechnol.* **2012,** *30*, 184-189.

43. Perrault, S. D.; Chan, W. C. W., Synthesis and Surface Modification of Highly Monodispersed, Spherical Gold Nanoparticles of 50-200 nm. *J. Am. Chem. Soc.* **2009,** *131*, 17042.

44. Zhu, J.; Kell, A. J.; Workentin, M. S., A retro-Diels-Alder reaction to uncover maleimide-modified surfaces on monolayer-protected nanoparticles for reversible covalent assembly. *Org. Lett.* **2006,** *8*, 4993-4996.

45. Hartlen, K. D.; Ismaili, H.; Zhu, J.; Workentin, M. S., Michael Addition Reactions for the Modification of Gold Nanoparticles Facilitated by Hyperbaric Conditions. *Langmuir* **2012,** *28*, 864-871.

46. Zhu, J.; Ganton, M. D.; Kerr, M. A.; Workentin, M. S., Chemical modification of monolayer-protected gold nanoparticles using hyperbaric conditions. *J. Am. Chem. Soc.* **2007,** *129*, 4904.

47. Asano, T.; Le Noble, W. J., *Chem. Rev.* **1978,** *78*.

48. Holzapfel, W. B.; Isaacs, N. S., In *High Pressure Techniques in Chemistry and Physics: a Practical Approach*, Oxford University Press1997.

49. Zhu, J.; Lines, B. M.; Ganton, M. D.; Kerr, M. A.; Workentin, M. S., Efficient synthesis of isoxazolidine-tethered monolayer-protected gold nanoparticles (MPGNs) via 1,3-dipolar cycloadditions under high-pressure conditions. *J. Org. Chem.* **2008,** *73*, 1099-1105.

50. Polo, V.; Domingo, L. R.; Andres, J., Toward an understanding of the catalytic role of hydrogen-bond donor solvents in the hetero-Diels-Alder reaction between acetone and butadiene derivative. *J. Phys. Chem. A* **2005,** *109*, 10438-10444.

51. Domingo, L. R.; Aurell, M. J.; Arno, M.; Saez, J. A., Toward an understanding of the 1,3-dipolar cycloaddition between diphenylnitrone and a maleimide : bisamide complex. A DFT analysis of the reactivity of symmetrically substituted dipolarophiles. *J. Mol. Struc. THEOCHEM* **2007,** *811*, 125-133.

52. Koehler, K. C.; Durackova, A.; Kloxin, C. J.; Bowman, C. N., Kinetic and thermodynamic measurements for the facile property prediction of diels-alder-conjugated material behavior. *AIChE J* **2012,** *58*, 3545-3552.

53. Domingo, L. R.; Andres, J., Enhancing reactivity of carbonyl compounds via hydrogen-bond formation. A DFT study of the hetero-Diels-Alder reaction between butadiene derivative and acetone in chloroform. *J. Org. Chem.* **2003,** *68*, 8662-8668.

54. Carey, F.; Sundberg, R. J., *Advanced Organic Chemistry*. Springer Ed.2004.

55. Lu, J.; Shi, M.; Shoichet, M. S., Click Chemistry Functionalized Polymeric Nanoparticles Target Corneal Epithelial Cells through RGD-Cell Surface Receptors. *Bioconjugate Chem.* **2009,** *20*, 87-94.

56. Sun, X. L.; Stabler, C. L.; Cazalis, C. S.; Chaikof, E. L., Carbohydrate and protein immobilization onto solid surfaces by sequential Diels-Alder and azide-alkyne cycloadditions. *Bioconjugate Chem.* **2006,** *17*, 52-57.

57. Taylor, A.; Wilson, K. M.; Murray, P.; Fernig, D. G.; Levy, R., Long-term tracking of cells using inorganic nanoparticles as contrast agents: are we there yet? *Chem. Soc. Rev.* **2012,** *41*, 2707-2717.

58. Milne, M.; Gobbo, P.; McVicar, N.; Bartha, R.; Workentin, M. S.; Hudson, R. H. E., Water-soluble gold nanoparticles (AuNP) functionalized with a gadolinium(III) chelate via Michael addition for use as a MRI contrast agent. *J. Mater. Chem. B* **2013,** *1*, 5628-5635.

59. Zhu, J.; Waengler, C.; Lennox, R. B.; Schirrmacher, R., Preparation of Water-Soluble Maleimide-Functionalized 3 nm Gold Nanoparticles: A New Bioconjugation Template. *Langmuir* **2012,** *28*, 5508-5512.

60. Ghiassian, S.; Gobbo, P.; Workentin, M. S., Water-Soluble Maleimide-Modified Gold Nanoparticles (AuNPs) as a Platform for Cycloaddition Reactions. *Eur. J. Org. Chem.* **2015**, 5438-5447.

61. Weissman, M.; Winger, K. T.; Ghiassian, S.; Gobbo, P.; Workentin, M. S., Insights on the Application of the Retro-Michael Addition on Maleimide-Functionalized Gold Nanoparticles in Biology and Nanomedicine. *Bioconjug Chem.* **2016**, DOI: 10.1021/acs.bioconjchem.5b00600.

62. Gobbo, P.; Biesinger, M. C.; Workentin, M. S., Facile synthesis of gold nanoparticle (AuNP)-carbon nanotube (CNT) hybrids through an interfacial Michael addition reaction. *Chem Commun.* **2013,** *49*, 2831-2833.

Chapter 2

2 Improved Methodology for the Preparation of Water-Soluble Maleimide-Functionalized Small Gold Nanoparticles

Chapter 2 has been published as a full paper, and it is reprinted (adapted) with permission from **P. Gobbo**, M. S. Workentin*, *Langmuir*, **2012**, *28*, 12357−12363.

I performed all the experimental work and I wrote the drafts of the manuscript, with input and final edit by my supervisor, Prof. M. S. Workentin.

The supporting information file referenced in the text can be downloaded from the web site of the publisher.

ABSTRACT: Improved methodology to prepare maleimide-functionalized, water-soluble, small (<3 nm) gold nanoparticles using a retro- Diels−Alder strategy that we developed for similar organic-soluble AuNP's is described. Importantly, our results suggest that a recent paper by Zhu, Waengler, Lennox, and Schirrmacher describing a similar strategy gave results inconsistent with the formation of the titled maleimide-modified AuNP (Zhu, J.; Waengler, C.; Lennox, R. B.; Schirrmacher, R. Langmuir 2012, 28, 5508) as the major product, but consistent with the major product being an adduct derived from the hydrolysis of maleimide formed under the conditions used for the required deprotection of the maleimide. Our methodology provides an efficient and accessible route to pure maleimide-modified small AuNP's that circumvents the formation of the hydrolysis product. The maleimide-modified small AuNP's are versatile because they are soluble in water and in a wide range of organic solvents and their reactivity can now be properly exploited as a reactive moiety in Michael addition for bioconjugation studies in aqueous solution.

2.1 Introduction

Maleimide functionalities at the interface of small hydrosoluble nanoparticles are of interest in biological applications because of the ability of the maleimide moiety to react through Michael addition with nucleophiles, especially amine and thiols. This general methodology is extensively exploited to label peptides, proteins, DNA strands, and cells.[1,2] Thus, having a maleimide group at the interface of a AuNP would allow for the exploitation of this type of reactivity in the use of the nanoparticle in applications such as drug or substrate delivery or as an optical marker for diagnostics in biological systems.[3,4] Such water-soluble AuNP's are a desirable platform because of their chemical stability, the biocompatibility of the gold core, and the ability to tune the functionality at the interface through the reactivity of the maleimide. Indeed, interfacial maleimide can react with amine or thiol functionalities present on liposomes or cell membranes, allowing the nanoparticle to be immobilized on the biosystem while preserving all of the optothermal properties of the original nanoparticle.[5] Despite the numerous potential biological applications that these water-soluble maleimide AuNPs can have, until recently the only hydrosoluble maleimide-functionalized nanoparticles synthesized were larger than 15 nm and their synthesis involved a difficult place-exchange reaction from citrate-protected or from CTAB-protected (cetyltrimethyl ammonium bromine) gold nanoparticles with very bulky and complex polyethylene glycol- based ligands.[5,6] Mono-maleimide-functionalized gold nanoparticles derived from phosphine-protected gold cores have been reported but are not very stable and thus are of limited utility.[7]

Recently, Zhu, Waengler, Lennox, and Schirrmacher described an approach to preparing stable water-soluble maleimide-tethered gold nanoparticles with an average core size of ca. 3 nm.[8] The goal was to synthesize small, stable maleimide water-soluble AuNPs through a route involving less-elaborate ligands that are easier and faster to synthesize and are based on tri- or tetra-ethylene glycol. Because of the smaller size of the Au core and the simplicity of the ligands, these nanoparticles were expected to be easier to make and characterize, allowing the effective number of functionalities present at the nanoparticle interface to be calculated to provide the ability for more careful control of the number of potential bioconjugation sites.

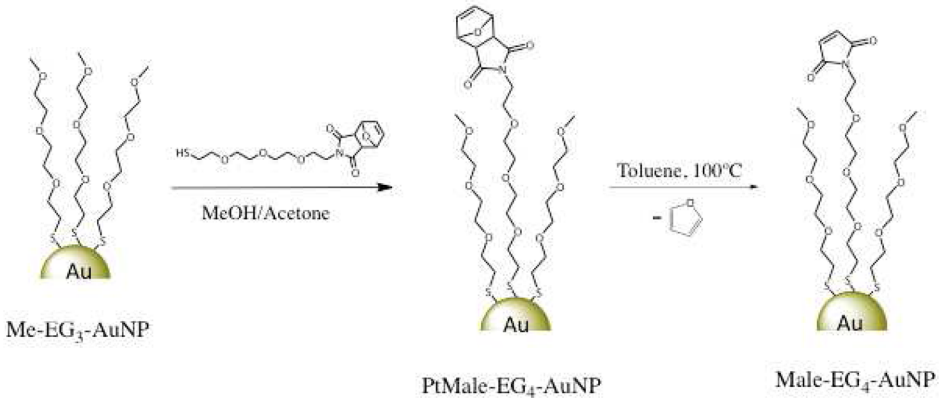

Scheme 2.1: Synthesis of Maleimide-Functionalized Gold Nanoparticles.

Their approach utilized a strategy that our group developed for the preparation of small organic-soluble maleimide AuNPs in the same size regime,[9] which itself was based on approaches used to install maleimide on other types of materials.[10−12] In fact, the strategy has long been used as a click-type reaction in macromolecular synthesis.[13] The strategy involves incorporating the maleimide moiety onto a AuNP as its furan Diels−Alder adduct and then liberating the free maleimide when desired by taking advantage of the propensity of this adduct to undergo an efficient retro-Diels-Alder reaction with the loss of furan at elevated temperatures (Scheme 2.1). This strategy must be employed because AuNPs of these types and sizes are prepared either by direct synthesis or by a place-exchange reaction that requires the thiol derivative of the functionality that you wish to install on the AuNP. In either method, a maleimide-functionalized thiol cannot be used directly because of its (desired) susceptibility to Michael additions and also because the ligand would simply react with itself. To avoid this and other complications, in our original report we prepared the dodecanethiol-derivatized maleimide-furan Diels-Alder adduct and introduced this ligand by a place exchange onto dodecane thiol-protected AuNPs ca. 2.2 nm in size. When desired, the free maleimide-AuNPs could be liberated by heating to 100 °C in toluene, which resulted in the loss of the furan that could then be removed to yield organic-soluble maleimide-modified AuNPs with only a small increase in the core size.[9] We subsequently utilized maleimide-AuNPs to prepare AuNP networks through a Diels-Alder strategy[9] and use it as a reaction template to prepare a wide variety

of organic-soluble AuNPs using Diels-Alder and 1,3-dipolar cycloaddition reactions and Michael additions.[14–16]

This strategy was utilized by Lennox and Schirrmacher to prepare water-soluble maleimide-AuNPs with the difference being that both the ligand in the starting (base) AuNP and the tether used for the furan-protected maleimide-thiol used in the place exchange were based on PEG ligands to make them water-soluble. This represents an important breakthrough because many applications using AuNP, especially those for biological systems, require water solubility and the ones we originally prepared were of limited utility because they were soluble only in organic solvents. Having a water-soluble maleimide-modified AuNP is especially relevant because of the wide use of Michael addition reactions of maleimide in bioconjugation-type studies. In this regard, the contribution of Lennox, Schirrmacher, and co-workers was important. However, because of our experience in this area, when their work appeared we were perplexed by aspects of the characterization of the maleimide-AuNP that differed from that previously published for the organic-soluble version and other derivatives. In particular, the maleimide-AuNP (after the removal of furan) was reported to have its olefinic protons 0.5 ppm upfield from the olefinic protons in the furan-maleimide adduct, whereas in all other studies and indeed for model maleimide compounds these protons are downfield from the olefinic protons of the furan-maleimide adduct. This is a dramatic solvent effect and perhaps suggests that what they prepared was not the maleimide-AuNP. We were surprised by the apparent low reactivity towards Michael addition given the high apparent loading of maleimide at the interface because unlike the Michael addition reactions we reported for maleimide-AuNP in organic solvents that require high pressure to proceed efficiently, this type of reaction should be rapid and efficient in aqueous and protic solvents.

Herein, we report an efficient method for preparing small, 2.5 nm core size water-soluble maleimide-AuNP using a different synthesis approach but still utilizing the furan-maleimide adduct to prepare the AuNPs and liberating the maleimide-AuNP through the retro-Diels-Alder reaction. Characterization confirms the formation of the target maleimide-AuNP, particularly the ^{1}H NMR spectroscopy that verifies the olefinic protons in the expected chemical shift region. Furthermore, we show that when the deprotection

of the furan-maleimide AuNP adduct is carried out in the presence of water the initially formed interfacial maleimide moieties are hydrolyzed at these temperatures to yield an interfacial polyammonium/maleic acid salt adduct. The method we describe outlines how to prepare small (<3 nm) maleimide-AuNPs that are soluble in both water and a host of other organic solvents. The latter allows for their preparation under conditions that avoid water and the resulting secondary hydrolysis reaction of the maleimide moiety. The versatile maleimide-AuNPs we describe are easy to prepare and suitable for bioconjugation studies.

2.2 Result and discussion

Our approach to preparing maleimide-AuNPs is shown in Scheme 2.1 and follows the strategy that we reported for organic-soluble maleimide-AuNPs of the same size, with the difference being that the thiolate ligands are PEGylated. This approach first involved the synthesis of methyl-terminated triethylene glycol thiol (Me-EG_3-SH) monolayer-protected AuNPs (Me- EG_3-AuNPs). The methyl-terminated EG_3 ligands were selected as the base ligand for the nanoparticles because unlike hydroxyl-terminated (HO-EG_3-AuNP) species they are soluble in both water and a wider selection of organic solvents, making the resulting maleimide gold nanoparticles more versatile. Me- EG_3-AuNP was then subjected to place-exchange reaction conditions in the presence of the Diels-Alder furan-protected maleimide tetraethylene glycol thiol (Pt-maleimide-EG_4-SH). This reaction was carried out in a mixture of dry methanol and acetone as the solvent. It is important to note that during this step the maleimide must be protected; otherwise, it will undergo a Michael addition with the thiols present in solution. The final step in the preparation of the desired maleimide-AuNP was the deprotection of the maleimide at the AuNP interface through the retro-Diels-Alder reaction at 100 °C in toluene (Scheme 2.1). The required Me-EG_3-SH and Pt-maleimide-EG_4-SH ligands were synthesized starting from readily available triethylene glycol monomethyl ether (Me-EG_3-OH) and tetraethylene glycol (HO-EG_4-OH), respectively (Scheme 2.2). The maleimide ligand was synthesized with one more ethylene glycol unit than in the base ligand to lower the steric hindrance on the maleimide functionality and make it easier to react through Michael addition or other cycloaddition reactions.[14–16]

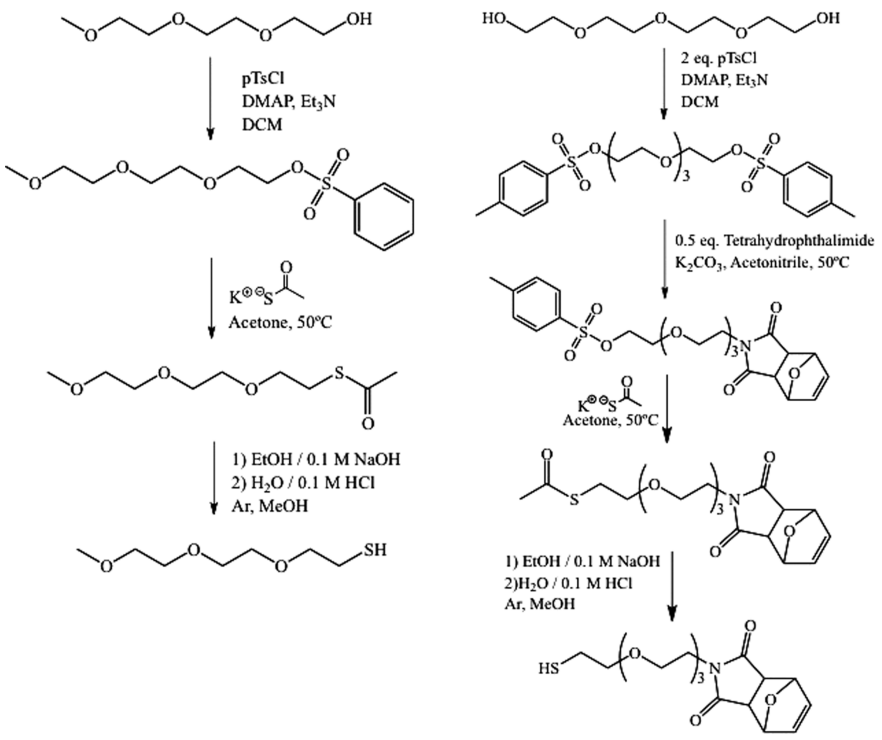

Scheme 2.2: Synthesis Paths for the Preparation of Me-EG$_3$- SH (Left) and Pt-maleimide-EG$_4$-SH (Right).

To synthesize Me-EG$_3$-SH, Me-EG$_3$-OH was tosylated to transform the hydroxyl group into a good leaving group. The tosylated Me-EG$_3$-OH was then converted to its corresponding thioacetate via an S_N2 reaction. The thiol was obtained through basic hydrolysis of the thioacetate functionality (Scheme 2.2). The same strategy was employed to synthesize Pt-maleimide-EG$_4$-SH. In this case, both hydroxyl groups of HO-EG$_4$-OH were tosylated, then one of the tosylated extremities of the molecule was reacted with furan-protected maleimide (3,6-endoxo-Δ4-tetrahydrophthalimide), and then the other tosylated extremity was converted to the thioacetate and subsequently hydrolyzed under basic conditions to generate the desired thiol, Pt-maleimide-EG$_4$-SH. A detailed synthesis procedure and a characterization of the ligands are reported in the Supporting Information. Me-EG$_3$-AuNP was synthesized using a modified one-phase synthesis method.[17] Briefly, the gold salt, $HAuCl_4 \cdot 3H_2O$, was dissolved in a mixture of methanol and glacial acetic acid. Me- EG$_3$-SH was dissolved in this solution, and finally a fresh solution of $NaBH_4$ was slowly added.

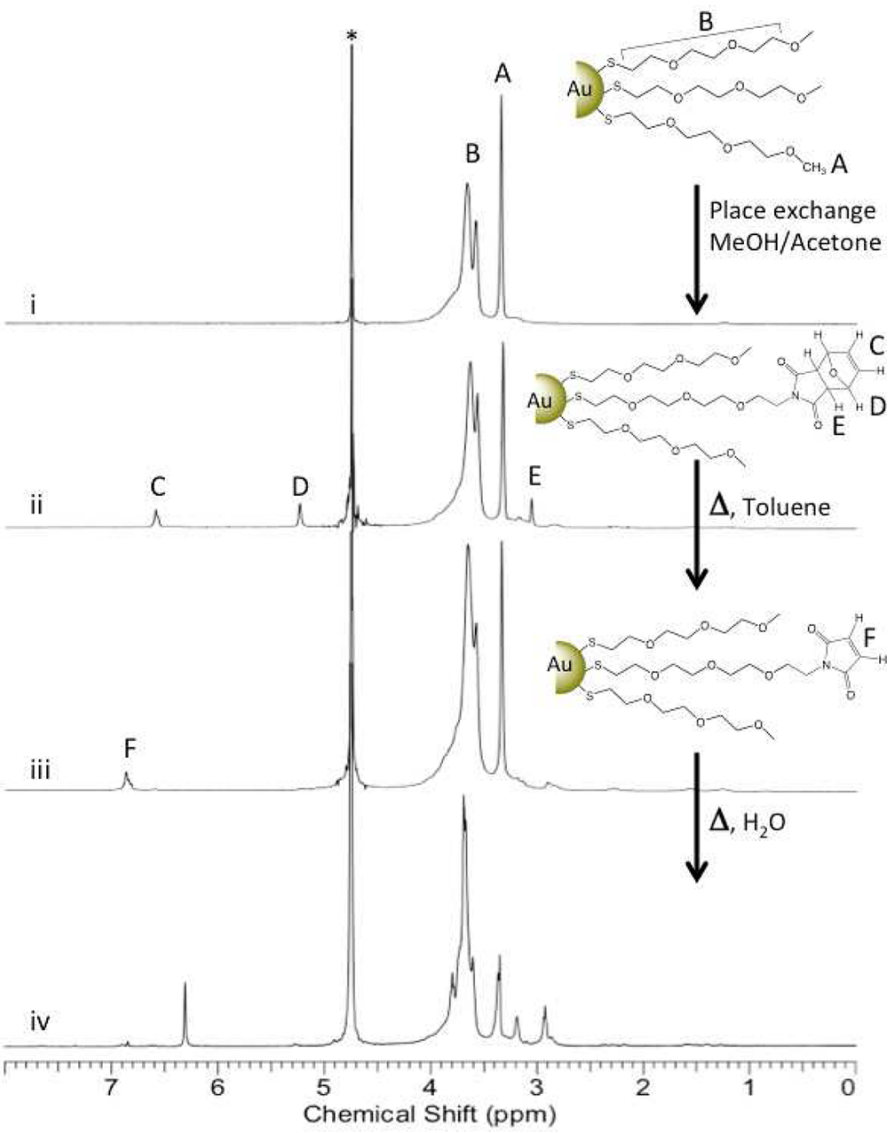

Figure 2.1: ^{1}H NMR spectra (recorded in D_2O) of (i) Me-EG_3-AuNP, (ii) Pt-maleimide-EG_4-AuNP, (iii) maleimide-EG_4-AuNP, and (iv) the hydrolysis product of maleimide-EG_4-AuNP. * indicates residual H_2O.

The mixture was stirred overnight at room temperature. Purification of the resulting nanoparticles involved extracting them from the aqueous phase using toluene. Successively, unreacted Me-EG_3-SH was washed away from a film of nanoparticles inside a round-bottomed flask using cyclohexane, in which the AuNPs are not soluble. Subsequently, the AuNPs were purified by dialysis. Through control of the gold-thiol ratio, it is possible to control the size of Me-EG_3-AuNP.

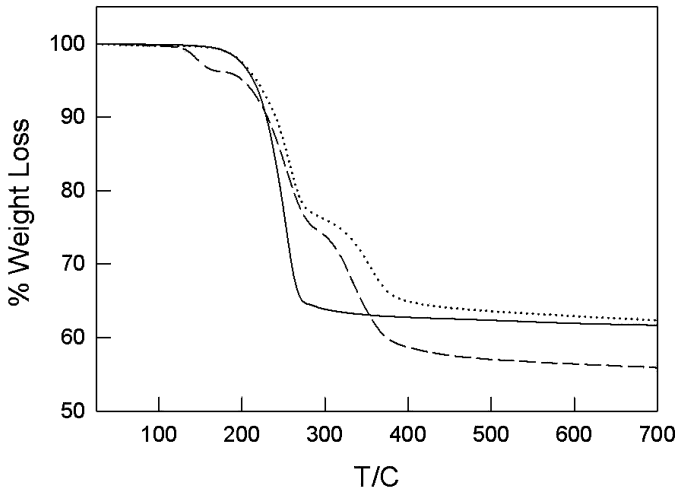

Figure 2.2: TGA of Me-EG$_3$-AuNP (−), Pt-maleimide-EG$_4$-AuNP (---), and maleimide-EG$_4$-AuNP (···).

In this work, a ratio of 1:3 gold/thiol was employed to yield 2.0 ± 0.3 nm Me-EG$_3$-AuNPs. These AuNPs were characterized by UV-vis spectroscopy and transmission electron microscopy (TEM) images (Supporting Information). ^{1}H NMR spectroscopy showed the expected broadened peaks at 3.34, 3.58, and 3.66 ppm, corresponding to the Me-EG$_3$-SH ligands (Figure 2.1, spectrum i). Thermogravimetric analysis (TGA) revealed that 38.3% of the AuNPs are composed of the PEGylated ligands, corresponding to 2.13 μmol of Me-EG$_3$-SH per milligram of AuNP (Figure 2.2). These nanoparticles, having PEG ligands with terminal methylether units at the solution interface, have the greater advantage of being soluble in both organic and water solutions. In particular, these Me-EG$_3$-AuNP's are soluble in water, methanol, ethanol, tetrahydrofuran, dichloromethane, chloroform, toluene, ethyl acetate, acetone, dimethylformamide, and acetonitrile. They can be repeatedly dried and redissolved in these solvents with little to no degradation or aggregation (none was apparent).

Pt-maleimide-EG$_4$-AuNP was synthesized using a place-exchange reaction. In a typical synthesis, 100 mg of Me-EG$_3$-AuNP is mixed with 37.1 mg of Pt-maleimide-EG$_4$-SH for 15 min in 20 mL of dry methanol and 2.5 mL of acetone. The solvent was then evaporated under vacuum, and the resulting film was washed with cyclohexane (in which it is not soluble) to get rid of excess Pt-maleimide-EG$_4$-SH and exchanged Me-EG$_3$-SH.

Pt-maleimide-EG_4-AuNPs were then purified further by dialysis to remove any unbound ligands. The furan-protected nanoparticles, Pt-maleimide-EG_4-AuNP's, were characterized by ^{1}H NMR and UV−vis spectroscopy, TGA, and TEM. The nanoparticles synthesized under these conditions are found to maintain their size of 2.0 ± 0.3 nm according to TEM images (Supporting Information). TGA confirmed the presence of the protected maleimide ligand (Figure 2.2). The first weight loss accounting for 3.9% takes place between 100 and 170 °C and is related to the loss of furan. This feature in the TGA is diagnostic of the incorporation of the protected maleimide, confirms the reversibility of the Diels-Alder reaction at around 100 °C, and can be used to determine the amount of maleimide ligand incorporated onto the AuNP's. Using the percentage mass loss of furan (3.9%) as an indication of the amount of furan-protected maleimide incorporated onto the AuNP's allows us to estimate that 30% of ligands on the Pt-maleimide-EG_4-AuNPs were the required furan-protected maleimide ligands. This loss of furan is then followed by the loss of triethylene glycol monomethyl ether ligands and the deprotected maleimide ligand. These data can be compared with previous work carried out in our laboratories on small maleimide organic-soluble nanoparticles.[9]

^{1}H NMR spectroscopy of the Pt-maleimide-EG_4-AuNPs (recorded in D_2O as the solvent, with the residual H_2O signal used as a reference) shows the appearance of the three broadened peaks related to the furan-protected maleimide functional group (Figure 2.1, spectrum ii). The peak at 6.60 ppm is related to the two alkene protons, the peak at 5.25 ppm is related to the protons adjacent to the bridging oxygen of the Diels-Alder adduct, and the peak at 3.07 ppm is related to the two protons closer to the carbonyl groups.[9] The relative integration of the $-CH_3$ peak due to the Me-EG_3S ligands with those of furan-protected maleimide confirms the 30% incorporation of the desired ligand onto the particle. Furthermore, the solubility of these nanoparticles is unchanged with respect to that of the Me-EG_3-AuNPs.

The choice of the solvent for the place-exchange reaction was found to be of crucial importance to the final synthesis of maleimide-AuNPs. Because the place-exchange reaction takes place on the time scale of minutes, a solvent with a low vapour pressure is required for the reaction. The use of the methanol-acetone mixture as the solvent for the

place-exchange reaction guarantees better control over the reaction time because it can be removed faster than water. Better control over the reaction time allows better control of the number of protected maleimide ligands that are introduced onto AuNPs. The quantity of the furan-protected maleimide ligand strongly influences the nanoparticle solubility. For example, when the percentage of furan-protected maleimide-thiol was over 40%, the resulting AuNPs were no longer soluble in toluene even though they are still readily redissolvable in water. The solubility in toluene is of crucial importance because toluene is a solvent suitable for the deprotection of maleimide without interference from competing reactions of maleimide (*vide infra*).

To carry out the retro-Diels-Alder reaction to liberate the desired maleimide moiety at the interface, Pt-maleimide-EG_4-AuNPs were dissolved in toluene and the solution was stirred overnight at 100 °C. The solvent was then evaporated under vacuum, and the AuNP film was washed with cyclohexane as described previously. Maleimide-EG_4-AuNP was characterized by ^{1}H NMR and UV-vis spectroscopy, TGA, and TEM. TEM images and UV-vis spectroscopy revealed a slight increase in the nanoparticle size to 2.5 ± 0.3 nm, similar to what we observed during the preparation of our original organic-soluble maleimide-AuNPs.[9] TGA (Figure 2.2) of the resulting maleimide-EG_4-AuNPs did not show the first weight loss between 100 and 170 °C present in the Pt-maleimide-EG_4-AuNPs, confirming that this was most likely due to the loss of furan in the latter. According to the mass loss measured, on 1 mg of maleimide-EG_4-AuNPs there are 1.30 μmol of Me-EG_3-SH and 0.50 μmol of Pt-maleimide-EG_4-SH, corresponding to a 28% maleimide ligand. TGA showed the presence of two ligands in essentially the same ratio as was obtained with the Pt-maleimide-EG_4-AuNPs.

^{1}H NMR spectroscopy of the product (Figure 2.1, spectrum iii) showed the disappearance (absence) of the peaks related to the furan Diels-Alder adduct (6.60, 5.25, and 3.07 ppm) and a new signal downfield at 6.86 ppm, as expected for olefin peaks of the maleimide moiety. This result completely agrees with our previous characterization of maleimide organic-soluble nanoparticles.[9] The simplified formula for the maleimide-EG_4-AuNPs can be calculated from the TGA and TEM measurements, assuming a spherical shape of

the gold core.[8] Maleimide-EG_4-AuNPs were found to have the simplified formula Au_{483}(Me-EG_3-S)$_{198}$(maleimide-EG_4-S)$_{77}$.

As stated above, the solubility of the Pt-maleimide-EG_4-AuNPs in toluene is a key component in the synthesis of maleimide-EG_4-AuNPs. Some attempts to deprotect the Pt-maleimide-EG_4-AuNPs were carried out by employing acetonitrile, acetone, and water as reaction solvents, and all of them resulted in a nanoparticle size growth characterized by a change in the solution color from dark brown (typical of a nanoparticle size between 2 and 3 nm) to ruby (typical of nanoparticles with diameter of between 4 and 5 nm).

Performing the retro-Diels-Alder deprotection in water gave very different results. After the reaction of Pt-maleimide-EG_4-AuNP in H_2O at 100 °C overnight, there was no peak due to the expected maleimide olefin protons at 6.86 ppm but a signal appeared at 6.23 ppm, upfield with respect to the peak at 6.60 ppm of the alkene protons of the protected maleimide ligand. The appearance of this upfield signal is also accompanied by significant changes in the region between 3 and 4 ppm. The peak at 3.07 ppm disappears, and three broad peaks (one at 3.15 ppm, one at 2.89 ppm, and one at 3.77 ppm) appear. This is also consistent with observation of Lennox and Schirrmacher.[8] Because the peak they assigned to maleimide was significantly upfield from where it was expected, we suspected that it was due to a reaction of the liberated maleimide with H_2O under the same reaction conditions.

To explore this possibility, we performed a number of control reactions. First, we took our fully characterized maleimide-EG_4-AuNP, prepared by deprotection in toluene, and heated this sample in water to 100 °C (similar to the deprotection conditions employed by Lennox, Schirrmacher, and co-workers). ^{1}H NMR spectroscopy shows the loss of the signal of the olefinic protons in maleimide from 6.86 ppm, a new peak growing in at 6.23 ppm, and the appearance of the same peaks in the region between 3 and 4 ppm as observed after the direct deprotection of Pt-maleimide-EG_4-AuNPs in water. The spectrum is shown in Figure 2.1(iv). This latter spectrum suggests that this product arises from the hydrolysis of maleimide by water under these conditions. But what could be the hydrolysis product that would give rise to such a simple singlet in the ^{1}H NMR spectrum

at ca. 6.2 ppm and still be associated with the AuNP? To address this issue, we carried out a number of model reactions. For simplicity, *N*-methylmaleimide was chosen as the first model compound. Its ^{1}H NMR spectrum was recorded in D_2O, and it revealed the expected signals at 2.94 ppm (CH_3−N) and 6.80 ppm (olefinic protons of the maleimide). This sample was then heated in nanopure water at 100 °C in a round-bottomed flask for 48 h. After reaction, the pH of the solution had changed from neutral to acidic. The solvent was then evaporated, and the reaction product was characterized by ^{1}H and ^{13}C NMR spectroscopy and mass spectrometry. As shown in Figure 2.3, ^{1}H NMR spectroscopy reveals the disappearance of the peaks of *N*-methylmaleimide at 2.94 and 6.80 ppm, related respectively to the methyl protons and to the olefinic protons. The main products of the reaction are represented by the peaks at 2.55 and 6.30 ppm, which are the same as those observed after heating the maleimide-EG_4-AuNPs in water. On the basis of the reactants (*N*-methylmaleimide and water) and the resulting ^{1}H NMR analysis, we suspected that the *N*-methylmaleimide was hydrolyzed to methylamine (as methylammonium, $CH_3NH_3^+$) and maleic acid (as hydrogen maleate, $HOC(O)=C(O)O^-$) under these conditions. Indeed, the large amount of water (the solvent) and the high temperature favor the hydrolysis of *N*-methylmaleimide. To validate the hypothesis of forming methylamine and maleic acid, small amounts of authentic *N*-methylamine and subsequently authentic maleic acid were added to the NMR tube containing the products of hydrolysis of the model compound. ^{1}H and ^{13}C NMR spectra recorded after every addition show an increase in the corresponding peak intensities upon addition of the pure reagent and, importantly, no new signals were recorded (Figures SI 12 and SI 13). Note that because of the pH change after the addition of excess base and then excess acid, the peaks, especially those corresponding to the maleic acid, shift slightly depending on the extent of salt formation but remain in the 6.2−6.35 ppm range. Mass spectrometry also revealed the presence of the molecular peaks of methylamine and maleic acid. Finally, the Kaiser test for the detection of primary amine was conducted for the reaction mixture and for a control solution of *N*-methylmaleimide in water.[18] The reaction mixture becomes dark blue (positive test), indicating the presence of a primary amine, and the *N*-methyl maleimide control solution becomes yellow (negative test) (Figure SI 11).

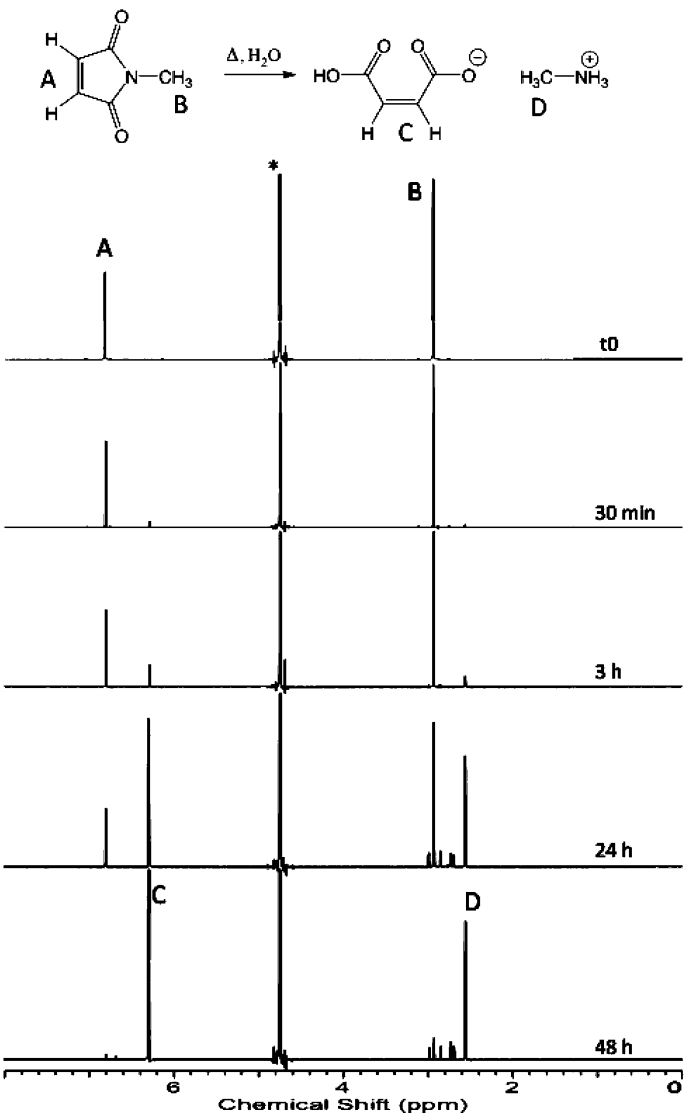

Figure 2.3: ^{1}H NMR spectrum recorded in D_2O showing the kinetics of hydrolysis of *N*-methylmaleimide. Peaks A and B are relative to the reactant, and peaks C and D are relative to the main products. * is the H_2O signal.

To understand better the process that leads to the hydrolysis reaction on the AuNPs and to explain what might have occurred in the earlier study, the protected maleimide tetraethylene glycol thioacetate (Pt-maleimide-EG_4-SAc) was employed as a second model compound. A few milligrams of Pt-maleimide-EG_4-SAc were inserted into a J. Young NMR tube and dissolved in D_2O, and the temperature was increased to 100 °C. ^{1}H NMR spectra were recorded after various time intervals (Figure SI 14 in the Supporting

Information). In addition to the expected hydrolysis of the thioacetate moiety (indicated by the signal due to acetic acid at 2.06 ppm), the signals due to the protected maleimide were also monitored as a function of time during heating in D_2O. This study shows the progressive deprotection of the maleimide functionality, indicated by the appearance of a signal at 6.85 ppm that is due to maleimide and then its progressive hydrolysis. After 8 h, the intensity of the peaks of protected maleimide (3.11, 5.29, and 6.60 ppm) markedly decreases, and this decrease is accompanied by the appearance of the furan peaks (6.47 ppm and 7.53 ppm), the peak related to the alkene protons of maleimide (6.85 ppm), the supposed maleic acid/maleate peak (6.31 ppm), and the peak of the protons alpha to the amine of the resulting amine(ammonium) tetraethylene glycol ($^{+}H_3N$-EG_4-S-D) (3.2 ppm). After 24 h, the amount of starting material is further decreased but the product of the hydrolysis of maleimide (indicated by the peak at 6.31 ppm) becomes the major product. After 48 h, the amounts of protected and deprotected maleimide are negligible and the major product is represented by maleic acid/maleate and $^{+}H_3N$-EG_4-SD.

The same experiment was performed using our maleimide-EG_4-AuNP, and it showed the same changes as described for model ligand Pt-maleimide-EG_4-SAc (Figure SI 15) with the loss of the maleimide signals at 6.86 ppm and the appearance of the signal at 6.23 ppm. At the end of this experiment and to confirm that the signal at 6.23 ppm was due to the maleic acid product from the hydrolysis of maleimide, a small amount of authentic maleic acid was added to the fully hydrolyzed AuNPs and an increase in the peak at 6.23 ppm was recorded (Figure SI 16). The addition of authentic *N*-methylmaleimide shows the expected olefinic signal at 6.86 ppm. In total, these experiments demonstrate that on heating in water to 100 °C the protected maleimide undergoes the expected retro-Diels-Alder reaction to form the desired maleimide, but this reacts under conditions that yield the corresponding R-NH_3^+ and maleate by the hydrolysis of maleimide.

These results highlight the importance of the choice of solvent for the maleimide deprotection reaction. Water, even though it is a green solvent and has a high boiling point, was found to react irreversibly at high temperatures with the maleimide functionalities present at the nanoparticle interface. Hydrolysis causes the release of maleic acid and the formation of amine functionalities at AuNPs, which can couple as

their salt. Our approach allows for the deprotection to be carried out in toluene, circumventing the hydrolysis of the desired maleimide functionality at the interface.

To demonstrate that maleimide-EG_4-AuNPs react via the Michael addition reaction for the possible application as a bioconjugation template, the maleimide-EG_4-AuNPs were functionalized with cysteine. In this experiment, 50 mg of maleimide-EG_4-AuNPs was mixed with 0.8 mg of L-cysteine for 1 h in nanopure water. The sample was then purified by dialysis to remove any unreacted nucleophile and to leave only the cysteine-functionalized AuNPs. The ^{1}H NMR spectrum showed the complete disappearance of the peak at 6.86 ppm due to maleimide and the appearance of broadened peaks at 3.17 and 3.25 ppm, expected for the Michael addition product, which partially overlapped with the peak at 3.32 (Figure SI 17).

2.3 Conclusions

In this article, we described the first synthesis method leading to stable maleimide, water-soluble, small (<3 nm) gold nanoparticles through a retro Diels-Alder strategy. The amount of protected maleimide ligand at the interface accounted for 30% of the total ligands. Attempts to incorporate more led to solubility issues, with the ligand becoming insoluble in toluene, and thus the maleimide deprotection reaction could not be carried out. Indeed, toluene was found to be the solvent suitable for conducting the retro-Diels-Alder reaction to lead to the desired water-soluble maleimide-AuNPs. The use of water in the deprotection reaction cannot lead to pure maleimide-functionalized AuNPs because under the conditions needed for deprotection the hydrolysis of maleimide occurs efficiently, giving a polyammonium-functionalized AuNP associated with the maleate anion. Maleimide-AuNPs derived from the improved method presented here are stable, soluble in aqueous solution as well as a selection of organic solvents, and reactive toward Michael addition, thus broadening the application and versatility of their use in biochemistry and biology. We are currently utilizing the water-soluble maleimide-EG_4-AuNPs prepared using our strategy for bioconjugation studies.

2.4 References

(1) Hermanson, G. T. *Bioconjugate Techniques*, 2nd ed.; Academic Press: San Diego, **2008**.

(2) Kim, Y.; Ho, S. O.; Gassman, N. R.; Korlann, Y.; Landorf, E. V; Collart, F. R.; Weiss, S. Efficient site-specific labeling of proteins via cysteines. *Bioconjugate Chem.* **2008**, *19*, 786−791.

(3) Jain, S.; Hirst, D. G.; O'Sullivan, J. M. Gold nanoparticles as novel agents for cancer therapy. *Br. J. Radiol.* **2012**, *85*, 101−113.

(4) Manju, S.; Sreenivasan, K. Gold nanoparticles generated and stabilized by water soluble curcumin−polymer conjugate: blood compatibility evaluation and targeted drug delivery onto cancer cells. *J. Colloid Interface Sci.* **2012**, *368*, 144−151.

(5)Ba,H.;Rodriguez-Fernańdez,J.;Stefani,F.D.;Feldman,J. Immobilization of gold nanoparticles on living cell membranes upon controlled lipid binding. *Nano Lett.* **2010**, *10*, 3006−3012.

(6) Oh, E.; Susumu, K.; Blanco-Canosa, J. B.; Medintz, I. L.; Dawson, P. E.; Mattoussi, H. Preparation of stable maleimide-functionalized Au nanoparticles and their use in counting surface ligands. *Small* **2010**, *6*, 1273−1278.

(7) Gregori, L.; Hainfeld, J. F.; Simon, M. N.; Goldgaber, D. Binding of amyloid beta protein to the 20 S proteasome. *J. Biol. Chem.* **1997**, *272*, 58−62.

(8) Zhu, J; Waengler, C.; Lennox, R. B.; Schirrmacher, R. Preparation of water-soluble maleimide-functionalized 3 nm gold nanoparticles: a new bioconjugation template. *Langmuir* **2012**, *28*, 5508−5512.

(9) Zhu, J.; Kell, A. J.; Workentin, M. S. A retro-Diels Alder reaction as an alternative route to uncovering maleimide-modified surfaces on monolayer protected nanoparticles. *Org. Lett.* **2006**, *8*, 4993−4996.

(10) Yousaf, M. N.; Mrksich, M. Diels Alder reaction for the selective immobilization of protein to electroactive self-assembled monolayers. *J. Am. Chem. Soc.* **1999**, *121*, 4286−4287.

(11) Mantovani, G.; Lecolley, F.; Tao, L.; Haddleton, D. M.; Clerx, J.; Cornelissen, J. J. L. M.; Velonia, K. Design and synthesis of N- maleimido-functionalized hydrophilic polymers via copper-mediated living radical polymerization: A suitable alternative to PEGylation chemistry. *J. Am. Chem. Soc.* **2005**, *127*, 2966−2973.

(12) Toncelli, C.; De Reus, D. C.; Picchioni, F.; Broekhuis, A. A. Properties of reversible Diels-Alder furan/maleimide polymer net- works as function of crosslink density. *Macromol. Chem. Phys.* **2012**, *213*, 157−165.

(13) Gandini A. The furan/maleimide Diels−Alder reaction: a versatile click−unclick tool in macromolecular synthesis. *Prog. Polym. Sci.*, published online April 28, **2012**, http://dx.doi.org/10.1016/j. progpolymsci.2012.04.002.

(14) Zhu, J; Ganton, M. D.; Kerr, M. A.; Workentin, M. S. Chemical modification of monolayer protected gold-nanoparticels using hyper- baric conditions. *J. Am. Chem. Soc.* **2007**, *129*, 4904−4905.

(15) Zhu, J.; Lines, B. M.; Ganton, M. D.; Kerr, M. A.; Workentin, M. S. Efficient synthesis of isoxazolidine-tethered monolayer-protected gold nanoparticles (MPGNs) via 1,3-dipolar cycloadditions under high-pressure conditions. *J. Org. Chem.* **2008**, *73*, 1099−1105.

(16) Hartlen, K. D.; Ismaili, H.; Zhu, J.; Workentin, M. S. Michael addition reactions for the modification of gold nanoparticles facilitated by hyperbaric conditions. *Langmuir* **2012**, *28*, 864−871.

(17) Zheng, M.; Li, Z.; Huang, X. Ethylene glycol monolayer protected nanoparticles: synthesis, characterization, and interactions with biological molecules. *Langmuir* **2004**, *20*, 4226−4235.

(18) Kaiser, E.; Colescott, R. L.; Bossinger, C. D.; Cook, P. I. Color test for detection of free terminal amino groups in the solid-phase synthesis of peptides. *Anal. Biochem.* **1970**, *34*, 595−598.

Chapter 3

3 Water-soluble gold nanoparticles (AuNP) functionalized with a gadolinium(III) chelate via Michael addition for use as a MRI contrast agent

Chapter 3 has been published as a full paper, and it is reproduced with permission from the Royal Society of Chemistry. The corresponding reference is: M. Milne†, **P. Gobbo†,** N. McVicar, R. Bartha, M. S. Workentin*, R. H. E. Hudson*, *J. Meter. Chem. B*, **2013**, *1*, 5628-5635.

Milne, supervised by Prof. Hudson, and I contributed equally to the work. Milne synthesized and characterized the DO3A contrast agent. McVicar, supervised by Prof. Bartha, performed the MRI experiments. I synthesized and characterized the Maleimide-AuNP and the Gd-AuNP. Milne and I wrote the draft of the manuscript with input and minor edits from the other co-authors and final edit by Prof. Hudson and Prof. M.S. Workentin.

The supporting information file referenced in the text can be downloaded from the web site of the publisher.

ABSTRACT: A contrast agent suitable for magnetic resonance imaging based on small, water soluble gold nanoparticles (AuNP) conjugated to over 50 Gd^{3+} chelators has been prepared by using an interfacial Michael addition in aqueous media. The resultant chelator-AuNP conjugates have been successfully characterized by ^{1}H NMR spectroscopy, IR spectroscopy, ICP-OES, ζ-potential analysis, TEM and MRI. T_1-weighted *in vivo* images of mouse kidney were obtained using the agent at 9.4 T. A preliminary *in vivo* experiment produced no ill effects and the clearance profile of the agent suggests it is suitable for animal testing at clinically relevant concentrations.

3.1 Introduction

Gadolinium (Gd^{3+}) based contrast agents (CA) for use in magnetic resonance imaging (MRI) have been employed because of their ability to enhance the T_1 relaxation of agent bound water protons *in vivo*.[1–7] This enhancement may highlight tissue involved in pathological processes following leakage of the agent from the vasculature into the tissue. The enhancement gained by Gd^{3+} based CAs is concentration dependent, such that a hyperintense region is observed as local CA concentrations increase. Ultimately, increased tissue contrast therefore depends on the bio-distribution of an agent, as a set molar amount is delivered per patient to limit the possible side effects associated with lanthanide-based CAs. To ensure that a site specific, effective concentration is achieved, there have been efforts to develop nano-sized carriers to aid in the delivery of clinically approved small molecule-based CAs. Covalent linkage of a small Gd^{3+} CA to a nano-carrier may increase its local concentration, potentially decreasing the concentration of nanoparticle needed to provide sufficient signal enhancement for MRI detection. Strategies in this field include the development of dendrimers,[8–12] liposomes,[3,13–15] micelles,[16–18] polymers[19–21] as well as silicon and gold-based nanoparticles.[22–27] Typically gadolinium labeled gold nanoparticles are synthesized through conventional one-pot synthesis where gold is reduced using sodium borohydrate in the presence of a thiol terminated organic ligand. This has yielded Gd^{3+}-AuNPs with a range of sizes 2.4 nm,[22] 12 nm,[23] 14 nm,[24] 13 nm[25] and relaxivities 4.1 mM^{-1} s^{-1} at 7T.[22] 12 mM^{-1} s^{-1} at 1T,[23] 18 mM^{-1} s^{-1} at 1.5T,[24] 5.1 mM^{-1} s^{-1} at 14.1 T.[25] While each of these systems have their benefits and drawbacks it is their size and the loading potential of gadolinium that will have the greatest impact on the MRI signal compared to a single Gd^{3+} CA. The size of the nano carrier is the limiting factor for a number of parameters, such as loading of the chelator, *in vivo* distribution, as well as the enhancement of relaxation gained by slower tumbling molecules.[2,28] The rotational benefit has the potential to increase the relaxivity of a given agent immensely; however, it is typically observed at lower magnetic field strengths (20–40 MHz) where the rotational frequency is closer to the larmor frequency of the ^1H, and is less pronounced at high fields (300–400 MHz). While loading of these nano carriers with 1000's of chelators generates agents with excellent sensitivity their synthesis still relies on the conventional one-pot synthesis method.[24] The drawback of the

one-pot nanoparticle synthesis is the difficulty in obtaining a reproducible AuNP size, lack of stability of the CA on the nanoparticle and the need to control a large number of reaction conditions. A change in one of these conditions, may result in an undesired product that would not be suitable for the development of clinically acceptable CAs where the control and characterization of the structure is strict. A better approach is to utilize a previously prepared water-soluble monolayer protected AuNP, where the size and solubility can be more carefully controlled and that contains a reactive functionality capable of undergoing a specific interfacial reaction to introduce the CA covalently onto the nanoparticle. To efficiently attach the Gd^{3+} chelator and enhance the prospect for *in vivo* studies, we utilize a small water-soluble gold nanoparticle with a core size of 3 nm ± 1 nm that is functionalized with approximately 80 maleimide moieties at the interface. Maleimide-modified AuNPs were chosen as they undergo efficient interfacial Michael addition when mixed with an appropriate nucleophile;[29,30] in the present case we utilize a Gd^{3+} CA, Gd^{3+}DO3A-amine chelator (Scheme 3.1).[20,31]

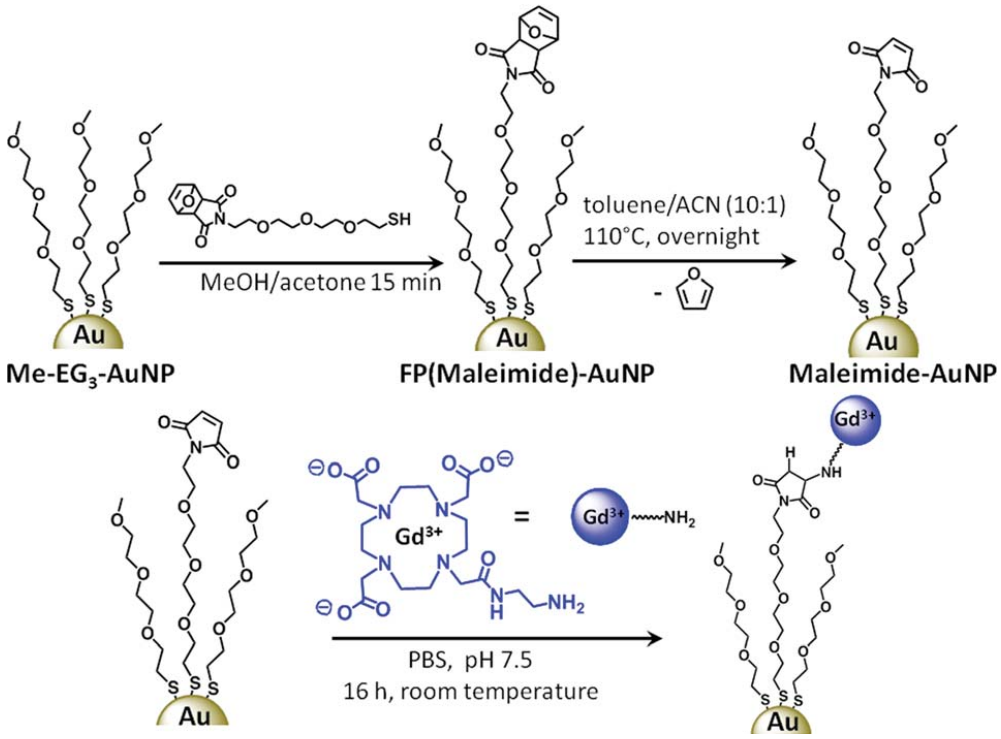

Scheme 3.1: Illustration of the synthetic strategy: the interfacial Michael addition between Gd^{3+}-DO3A-amine and maleimide-AuNP.

The benefit of using a post synthetic modification of the nano core is the possibility to fully characterize both molecular systems: the pre-derivatized gold core and the final product after modification of the corona. The interfacial Michael addition reaction is favoured over other synthetic methods as it has been shown to be quick, reliable and reproducible. To this end we describe the synthesis of Gd^{3+} modified water-soluble gold nanoparticles that have a reproducible and measurable number of chelators (Scheme 3.1). This innovative Gd-based contrast agent was characterized though ^{1}H NMR spectroscopy, IR spectroscopy, ICP-OES, ζ-potential measurements, TEM, and *in vitro* and *in vivo* MRI. The results show that ca. 70% of the 80 interfacial maleimide moieties were successfully functionalized with the gadolinium complex. For the first time it was possible to quantify the efficiency of the interfacial Michael addition reaction and this information is of important relevance for designing *in vivo* agents.

3.2 Material and Methods

General materials and methods

All chemicals and solvents were used as received unless specified. All solvents were HPLC grade, except water (18.2 MΩ cm). Organic extracts were dried with Na_2SO_4, and solvents were removed under reduced pressure by rotary evaporation. Flash column chromatography (FCC) was carried out using silica gel, mesh size 230–400 Å. Cellulose ester dialysis membranes with MWCO of 6–8 kDa were used. *In vivo* contrast-enhanced T_1-weighted MR images were acquired using a 400 MHz horizontal bore small animal MRI scanner equipped with a 30 mm millipede radio frequency coil (Agilent, Palo Alto, CA). Images were acquired before and immediately following intravenous (IV) injection in the tail vein. NMR measurements were made on an Agilent 400 MHz spectrometer. Relaxation measurements were made for 4 different concentrations of CA using an inversion recovery pulse sequence with 16 inversion times with a 2 second delay to ensure full relaxation.

Preparation of maleimide AuNP

Maleimide-AuNP was synthesized accordingly to our recently established procedure.[29–31] Briefly, triethylene glycol monomethyl ether AuNP (Me–EG_3–AuNP) was synthesized mixing 3 equivalents of triethylene glycol monomethyl ether thiol with 1 equivalent of $HAuCl_4 \cdot 3H_2O$ in a dry methanol-acetic acid solution (10 : 1), followed by slow addition of 10 equivalents of $NaBH_4$ in water. The purified Me-EG_3-AuNP underwent a place-exchange reaction with furan-protected-maleimide tetra-ethylene glycol–thiols ligands (FP(maleimide)-EG_4-SH). The resulting FP(maleimide)-AuNPs were deprotected by dissolving them in a toluene–acetonitrile (10 : 1) mixture and heating the system at 110 ºC overnight under vigorous stirring. This method leads to small water-soluble maleimide-AuNP with a gold core diameter of 3 ± 1 nm, as shown by the TEM images reported in the ESI (Figure S10). The maleimide-AuNP contains ca. 0.50 mmol mg^{-1} of maleimide moieties as determined by thermogravimetric analysis and ^1H NMR spectroscopy. These AuNP were dissolved in acetonitrile to obtain a concentration of 10 mg ml^{-1} and stored at -20 ºC. Maleimide-AuNPs stored in this way were found to be stable for months.

Synthesis of DO3A–amine

DO3A-amine was synthesized as previously reported.[32] In short, cyclen was alkylated with 3 eq. of ethyl bromoacetate in acetonitrile with potassium carbonate. After purification, the fourth alkylation was done with the previously reported boc-protected amino ethyl chloroacetamide. Complete deprotection was done with standard deprotection conditions. TFA/DCM 1 : 1 for 30 min to remove the boc group, followed by drying and hydrolysis under basic conditions using 3.3 eq. of NaOH at 60 ºC overnight.

Synthesis of Gd–DO3A–amine

The agent was prepared using to previously reported conditions.[20,33] After deprotection DO3A–amine was metallated with 1 eq. of $GdCl_3$ at pH 6. This reaction was monitored by ESI-MS until metallation was complete. Finally, the complex was dialyzed at a 500 Dalton cut-off to remove free Gd^{3+}.

Conjugation of CA onto maleimide AuNP via interfacial Michael addition reaction

The nucleophile (Gd–DO3A–amine or DO3A–amine, 6 eq.) was stirred overnight with AuNP–maleimide in a phosphate buffer at pH 7.5. The following day the pH of the solution was lowered to 3-4 and the reaction mixture was dialyzed at a cut-off of 6–8 kDa against water. The solution was then reduced in volume to achieve a concentration of 10 mM for *in vivo* testing. Gd^{3+}-DO3A-amine-AuNPs were stored at -20 ºC and were found to be stable for weeks. If stored in solution and at room temperature aggregation occurs after a week.

FT-IR measurements

Infrared spectra were collected using a Bruker Vector33 spectrometer. The blanks were collected first by purging the instrument with nitrogen gas for 5 minutes and averaging 128 scans from 600 cm^{-1} to 4000 cm^{-1}. Subsequently, the sample (~0.5 mg of AuNP) was dispersed in dry KBr and packed into a pellet using a press. The AuNP spectra were recorded in the same conditions of the blank, which was automatically subtracted.

Zeta potential measurements of DO3A-AuNP and Gd-AuNP

Zeta potential measurements were performed using a Zetasizer Nano-ZS (Malvern Instrument). A solution of AuNP in PBS pH 7.5 was prepared with a concentration of 0.5 mg ml^{-1}. A 1 ml solution was inserted in a latex folded capillary cell equipped with electrodes and the zeta potential was calculated by employing the Huckel approximation.

Relaxation measurements

The longitudinal relaxivity (r_1) for both the Gd^{3+}-DO3A-amine and the Gd^{3+}-AuNP were obtained by measuring the longitudinal relaxation rate ($R_1 = 1/T_1$) at 4 concentrations (Gd^{3+}-DO3A-amine = 1 mM, 2 mM, 4 mM, 8 mM and Gd^{3+}-AuNP = 1 mM, 2 mM, 4 mM, 8.26 mM [Gd^{3+}]). Measurements were performed at pH 6.8, 37 ºC, using an inversion recovery sequence with a 2 second delay to ensure full T_1 relaxation between measurements. The slope of the plotted R1 = $1/T_1$ *vs* concentration was measured and

reported as the relaxivity (r_1). The relaxivity was 2.3 mM-*1* s-*1* for Gd^{3+}-DO3A-amine and 2.2 mM^{-1} s^{-1} for Gd^{3+}-AuNP. All measurements were made at 9.4 T.

Gold and gadolinium concentration determination by ICP- OES

ICP-OES measurements were made on a series of concentrations to allow for an accurate measurement of both the concentration as well as the ratio of Au to Gd using 4 wave-lengths for each element. It was found that the ratio of Au to Gd was 14 : 1. Using the value of Au to maleimides calculated it is shown that 70% of the maleimides reacted with the Gd-DO3A-amine to afford ca. 56 Gd^{3+} chelators present per NP.

MRI studies on animals

To demonstrate MRI T_1 contrast *in vivo*, a C57BL/6 mouse (8 months of age, weighing ~20 g) was anaesthetized (induced using 4% isoflurane in oxygen and maintained using 1.5–2.5% isoflurane in oxygen). To reduce motion, the abdomen of the mouse was lightly taped to a MRI-compatible stage. The mouse was placed in a 30 mm Agilent millipede coil. Temperature was monitored with a rectal temperature probe, and respiration was monitored with a respiratory sensor pad that was connected to a pressure transducer placed over the thoracic/abdominal region (SA Instruments Inc., Stony Brook, NY). Body temperature was maintained at 37 ºC using a warm-air feedback system. A catheter was placed in the tail vein using a 27-guage needle. Three pre-injection T_1-weighted MR images were acquired. Then 200 mL of 10 mM Gd^{3+}-AuNP dissolved in water was injected directly into the tail vein at a constant rate of 40 mL min^{-1}, with the mouse secured to the MRI compatible stage. Post-injection MR image acquisition began within 2 min of injection. The animal procedure was performed according to a protocol approved by the Western University Animal Use Subcommittee. Same-slice pre- and post-injection images were continuously acquired for ~90 min through both kidneys using a T_1-weighted fast spin echo (FSE) pulse sequence (TR/echo time = 500/10 ms, echo-train length = 4, 128 x 128 linear readout, 30.0 mm2 field of view, 5 slices, 2 mm slice thickness, 2 pre-scans, 4 averages). All images were acquired at 9.4 T.

3.3 Results and Discussion

Synthesis and characterization of maleimide-AuNP

Our synthetic approach for preparing small water-soluble maleimide–AuNP is summarized in Scheme 3.1. This approach is based on a retro-Diels–Alder strategy where the maleimide is first protected, followed by its deprotection only once the ligand is attached to the gold core. The need for this protection is due the reactivity that thiols have for Michael addition onto unprotected maleimides. The AuNP template (Me–EG_3–AuNP) that is employed as starting material is based on using the ω-mercapto triethylene glycol monomethyl ether as the base ligand.[29] This ligand confers both water-solubility and organic solvent-solubility to the nanoparticle. This amphiphilic property permits the use of reactions in organic solvents, which is important in this case for the deprotection, yet confers water-solubility to the final maleimide-AuNP. The latter is the target because it can undergo the interfacial Michael addition reaction with the CA. In addition, the ethylene glycol based ligands are expected to hinder protein adsorption *in vivo* which should ensure prolongation of the AuNP circulation half-life and reduction of its immunogenicity.[34,35] The triethylene glycol monomethyl ether gold nanoparticle (Me-EG_3-AuNP) was then subjected to a place-exchange reaction in presence of the furan-protected maleimide-tetraethylene glycol-thiol (FP(maleimide)-EG_4-SH). This reaction was carried out by mixing 100 mg of Me-EG_3-AuNP with 37.1 mg of FP(maleimide)-EG_4-SH for 15 minutes in a 10 : 1 mixture of methanol and acetone. The (FP(maleimide))-EG_4-AuNP was then purified by repeatedly washing a film of the nanoparticles with hexanes, which removes the soluble, free thiols and leaves behind the insoluble AuNP. The AuNP were then further purified by dialysis to completely remove any trace of free thiol before the deprotection of the maleimide. The deprotection of the maleimide was accomplished using the retro-Diels-Alder reaction; this involved dissolving the particles in a mixture toluene-acetonitrile (10 : 1) and heating at 110 ºC overnight. Once the reaction was completed the solvent and liberated furan were removed under vacuum and the film of maleimide-AuNP was repeatedly washed with hexanes.

Characterization of the functionalized AuNPs was then performed by ^{1}H NMR spectroscopy in D_2O.[29] In particular, the appearance of the following signals after the place-exchange reaction were diagnostic: 6.60 ppm (alkene protons of the furan moiety), 5.25 ppm (protons adjacent to the bridged oxygen), and at 3.07 ppm (protons adjacent to maleimide carbonyl). After the retro-Diels-Alder reaction the olefinic signals at 6.60 and 5.25 ppm and the protons adjacent to maleimide carbonyl at 3.07 in the FP(maleimide)-EG_4-AuNP disappear concomitant with the appearance of the expected maleimide olefinic protons at 6.86 ppm. The ^{1}H NMR spectrum showed no indication of the double hydrolysis products that would have appeared as a signal at 6.23 ppm,[29] or the mono hydrolysis product that would have shown two broad doublets at 6.24 and 5.84 ppm. The target maleimide-AuNP was also characterized by thermogravimetric analysis (TGA) and transmission electron microscopy (TEM). TEM showed a gold core size of 3 ± 1 nm (see ESI Figure S10), while TGA showed the presence of 0.5 mmol of maleimide ligands per milligram of AuNP.

From the combination of the ^{1}H NMR, TGA and TEM data, and assuming that the AuNP are spherical and that their size is monodisperse (3 nm) it is possible to calculate an approximate molecular formula for the maleimide–AuNP. The number of gold atoms (N) can be calculated using the following formula:

$$N = \frac{\pi \, \rho \, d^3 \, N_A}{6 \, M_{Au}}$$

where ρ is the density of the face centered cubic (fcc) gold lattice (19.3 g cm^{-3}), d is the average diameter of the nanoparticles in centimeters found from the TEM images, M_{Au} is the mole atomic weight of gold (196.9665 g mol^{-1}), and N_A is Avogadro constant.

The number of thiol ligands surrounding the gold core (N_L) can be calculated using the following formula:

$$N_L = \frac{N \cdot M_{Au} \cdot W_{\%}}{(1 - W_{\%}) \cdot \{MW_{maleimide-S} \cdot M_{\%} + [MW_{Me-EG3-S}(1 - M_{\%})]\}}$$

where $W_{\%}$ is the percentage of mass loss due to the organic ligands found through TGA measurements, $MW_{Me–EG3–S}$ is the molecular weight of the base thiolate ligand, $MW_{Maleimide–S}$ is the molecular weight of the maleimide thiolates ligand, and $M_{\%}$ is the mole percentage of maleimide ligand.

Using these equations and determining the molar percentage of ligands from the ^{1}H NMR spectrum, we can calculate an approximate nanoparticle formula of Au_{800}(Me– EG_3–S)$_{370}$(Maleimide–EG_4–S)$_{80}$.

Interfacial Michael addition onto maleimide–AuNP

To optimize the synthetic conditions for preparing the Gd^{3+}-AuNP, a model reaction was performed using the un-metalated DO3A-amine to avoid NMR line broadening caused by Gd^{3+}, which would hinder characterization. Using the un-metalated DO3A-amine we could easily follow the course of the reaction using ^{1}H NMR spectroscopy observing the disappearance of the maleimide olefin protons signal at 6.86 ppm. The interfacial Michael addition reaction was performed by mixing DO3A-amine (181 mg) with maleimide-AuNP (60 mg) in a buffered solution at pH 7.5. This mixture was left overnight at room temperature. The amounts utilized correspond to ca. 6 equivalents of DO3A-amine to every one maleimide; the total number of maleimide moieties (80/AuNP) was estimated as outlined above. Although an alkaline pH is required to avoid protonation of the amine nucleophile, it cannot be higher than 7.5 due to the propensity of the maleimide to hydrolyze in water (time scale of hours).[29] Additionally, the solubility of Gd^{3+}-DO3A-amine decreases at basic pHs. The model reaction was monitored by ^{1}H NMR spectroscopy following the disappearance of the alkene protons signal at 6.86 ppm (see ESI). Once it was evident that the maleimide had reacted, the pH of the solution was lowered to 3-4 to re-dissolve the functionalized AuNP and the unreacted nucleophile. This acidic solution was then dialyzed against water using a membrane with a MWCO of 6–8 kDa to remove the excess nucleophile. The same reaction conditions and purification method were then employed to synthesize Gd^{3+}-AuNP. Importantly, the final Gd^{3+}-AuNP was found to be well soluble in water up to pH 7.4, while the Gd^{3+}-DO3A-amine was found to have a limited solubility at this pH.

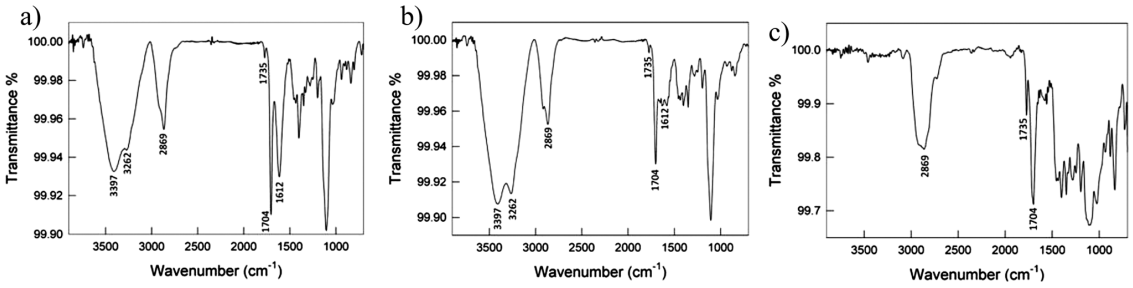

Figure 3.1: IR spectra of (a) Gd^{3+}-AuNP (b) DO3A-AuNP (c) maleimide–AuNP.

The success of the interfacial Michael addition reaction was shown by ^1H NMR spectroscopy, FT-IR spectroscopy and Zeta potential measurements. The ^1H NMR spectrum of the purified Gd^{3+}-AuNP showed the typical line broadening due to the presence of Gd^{3+}. Figure 3.1 shows the FT-IR spectra of maleimide-AuNP, DO3A-amine-AuNP and Gd^{3+}-AuNP, and confirms the success of our synthetic approach. The maleimide-AuNP spectrum (Figure 3.1a) shows the typical band at 2869 cm^{-1} due to the C–H stretching mode mainly due to the ethylene glycol units of the ligands, and maleimide's C=O stretching band at 1735 cm^{-1} (asymmetric) and at 1704 cm^{-1} (symmetric). The presence of the DO3A chelator is supported by the appearance of a broad band at 3600–3000 cm^{-1} that is due to the N–H stretching. In addition the increase in the intensity ratio of the C=O stretches (I_{1704}/I_{1735}) indicates presence of amide bonds on the Gd-modified nanoparticles that strengthen the maleimide signal at 1704 cm^{-1}. This along with the appearance of the stretch at 1612 cm^{-1} due to the amide II band of the DO3A-amine (especially visible for the Gd^{3+}-AuNP, Figure 3.1a) further supports the formation of Gd^{3+}-AuNP.

Zeta potential measurements were carried out at pH 7.5 on the maleimide–AuNP, on DO3A-amine–AuNP and on Gd^{3+}-AuNP, and were used to investigate the stability of the nanoparticle in aqueous solution and to measure the change in the surface charge after each interfacial reaction outlined in Scheme 3.1. The Zeta potential was found to shift from -36 ± 3 mV to -53 ± 3 mV from the maleimide-AuNP to the DO3A-amine-AuNP because of the presence of three deprotonated carboxylic groups per every interfacial Michael addition adduct. The presence of the cationic metal centre in Gd^{3+}-AuNP causes then the zeta potential to shift back to -30 ± 3 mV because Gd^{3+} compensates the negative

charges carried by the carboxylates. A potential of -30 ± 3 mV for the final product confirms the visual observation that the Gd^{3+}-AuNP form a stable solution even at a slightly basic pH.

Finally, the metal composition (Au and Gd) of the nanoparticle was investigated by ICP-OES. From these results, we determined the ratio of Au : Gd and this was used to calculate the number of Gd chelators that had successfully reacted with maleimide moieties. ICP analysis showed that a ratio of 14 : 1 Au : Gd atoms was present after the interfacial Michael addition which indicated that 56 of the possible 80 maleimide sites underwent Michael addition (70% yield of the interfacial reaction). The remaining 30% of the maleimides likely underwent the mono-hydrolysis prior to reaction as observed through ^{1}H NMR spectroscopy for the model reaction using DO3A-amine (ESI Figure S4). The incomplete reaction may also be related to the large size of the chelator compared and possible charge repulsion between the chelators limiting a higher loading. It should be noted that when an excessively large number of chelators are present there is the possibility that the exchange of bound water will not be efficient, resulting in a detrimental effects on the relaxation and performance as a CA.

Relaxation measurements

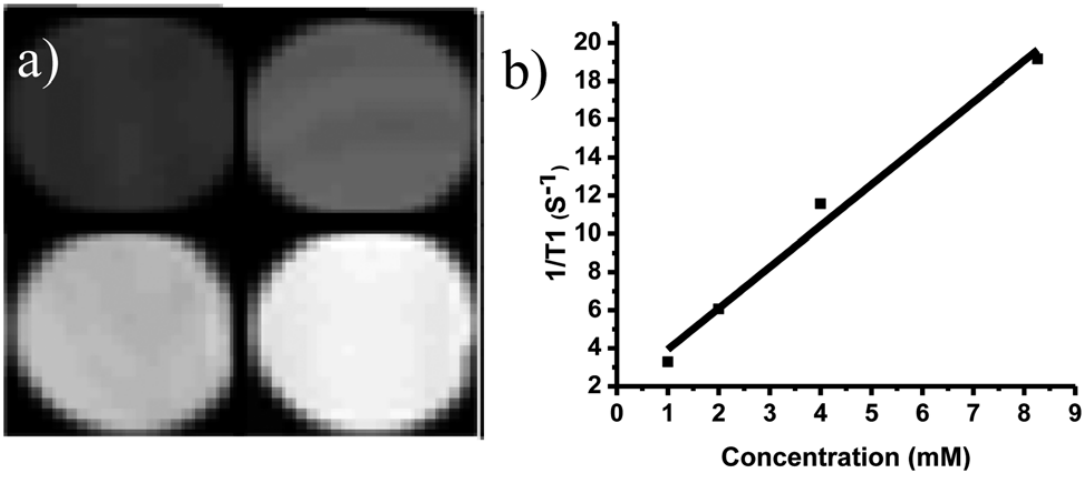

Figure 3.2: a) Images of phantoms of Gd–AuNP at concentrations 1 mM, 2 mM, 4 mM and 8.26 mM at pH 6.8 and 37 ºC. b) Calibration curve of a). The slope of the graph is the r_1 GdAuNP = 2.2 mM^{-1} s^{-1}.

Relaxation measurements were made on the individual Gd^{3+} chelator as well as the Gd^{3+}-AuNP at four concentrations (Gd^{3+}DO3A-amine = 1 mM, 2 mM, 4 mM, 8 mM; Gd^{3+}-AuNP = 1 mM, 2mM, 4mM, 8.26mM [Gd^{3+}]) at pH 6.8 at 37 ºC. The relaxation of Gd^{3+}-DO3A-amine as well as Gd^{3+} within the AuNP was the same within error. (r_1 Gd^{3+}-DO3A-amine = 2.3 mM^{-1} s^{-1}, r_1 Gd^{3+} within the AuNP = 2.2 mM^{-1} s^{-1}) (Figure 3.2).

These values are comparable to other small molecule CAs at 9.4 T.[36] While it has been shown that a large, slowly tumbling CA will have a more efficient relaxation compared to small fast tumbling molecules at lower field strengths (20–40 mHz),[2] that was not observed with these Gd^{3+}-AuNP at a field strength of 9.4 T. We did not evaluate our agent at lower field strengths as we did not acquire images at low field strengths. A second reason for not realizing a rotational enhancement is the free rotation of the chelator with respect to the AuNP which has been described previously.[5,28,37] While these results indicate that there is no enhancement to the single Gd^{3+} chelator at high field strengths (9.4 T) it is equally important to note that there is no decrease in relaxivity per chelator. This observation is important because scaffolding Gd^{3+} chelators in close proximity to each other on the surface of AuNPs has the potential to limit the access to the exchangeable proton source of the free water pool resulting in a decrease in the efficiency of relaxation. Since there was no decrease in the relaxivity per Gd^{3+} the overall r_1 of a single Gd^{3+}-AuNP is 56 times the r_1 of a single Gd^{3+} CA and is therefore expected to be 123 mM^{-1} s^{-1}.

In vivo evaluation

With the Gd^{3+}-AuNP in hand, we chose to investigate its ability to act as an *in vivo* contrast agent. Figure 3.3 shows *in vivo* MR images of the mouse kidneys pre injection (a), 5 min post injection of a 0.1 mmol kg^{-1} [Gd] dose (1.8 mmol kg^{-1} [NP]) (b) and the difference image (c). All *in vivo* images are from identical oblique slices and both kidneys are observed within the slice. Regions of interest containing the renal vasculature (solid line) and the medulla/cortex (dashed line) were identified using the 5 min post injection MR image as shown in Figure 3.3. Signal intensities collected from the regions of interest throughout the entire experiment are provided in Figure 3.4.

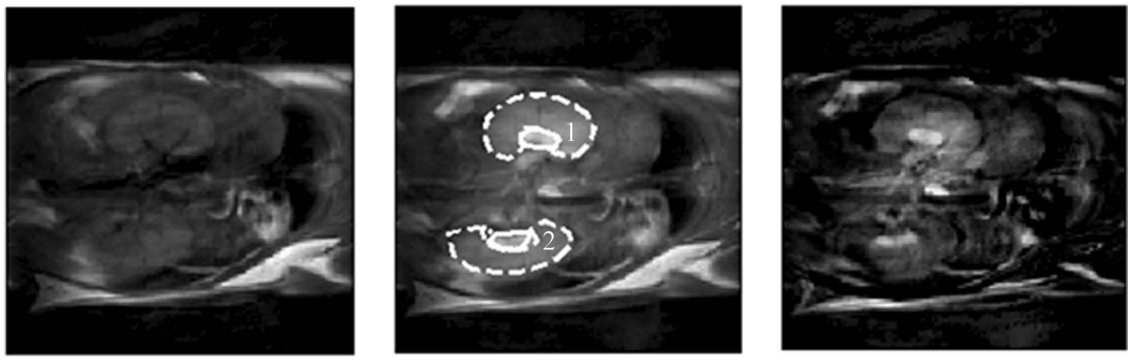

Figure 3.3: T_1 weighted images of kidneys 1 and 2. a) Pre-injection b) 5 min post injection of 0.1 mmol kg^{-1} of Gd^{3+}AuNP [Gd^{3+}] *via* tail injection. c) Subtracted image of a) and b).

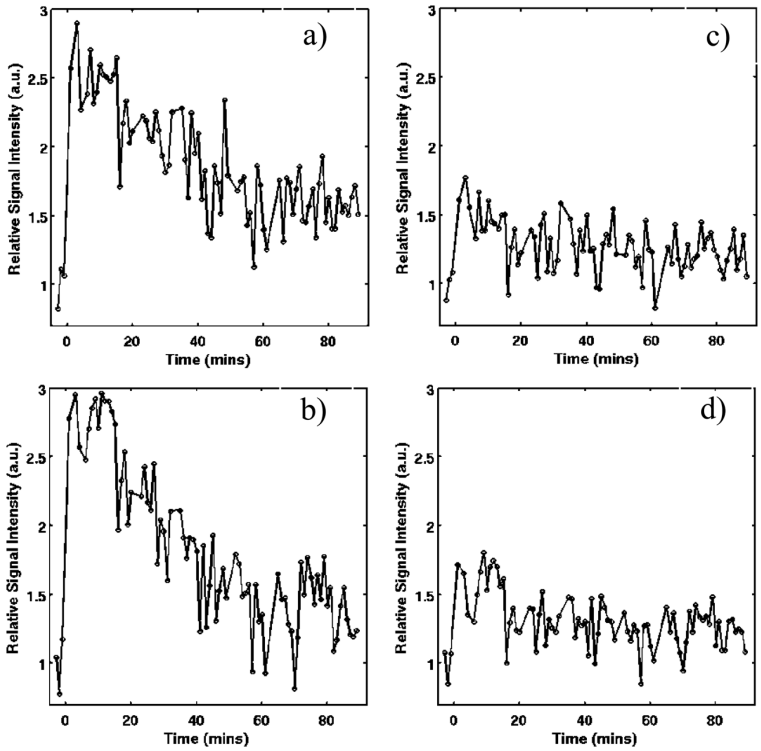

Figure 3.4: Signal enhancement of the vascular region of kidney 1 a) and kidney 2 b) showing a ~150–200% signal enhancement relative to baseline immediately after injection falling to ~40–60% enhancement by 60–90 minutes post injection. Signal enhancement of the medulla/cortex region of kidney 1 c) and kidney 2 d) showing an enhancement of ~20–30% consistently throughout the 90 min of imaging.

An increase in signal intensity of roughly 150–200% was observed in the vascular region of both kidneys along with an enhancement of 20–30% in the medulla/cortex of each kidney. The signal enhancement was observed throughout the entire monitoring period of 90 min as shown in the wash in and out profiles, Figure 3.4. This elongated period of filtration is significant as it indicates that the agent is circulating in the blood for an extended period of time, which in turn should allow a generous period for imaging. This value also compares favourably to Gd-DTPA which has a reported excretion half life of 20 min.[38] The small size and prolonged circulation of Gd^{3+}-AuNP contrast agent may allow for sufficient agent accumulation in tumours where the vasculature is permeable to circulating agents.[38] It should be noted that because of the small size of these nanoparticles, filtration would be primarily through renal excretion and as such is consistent with the observed enhancement in the kidneys. This is in contrast to larger nanoparticles which have been shown to be cleared through either liver or spleen.[39,40] The benefits of clearance of nanoparticles through the renal system allows for quick excretion post imaging as well as it indicates little to no degradation of the nanoparticles.[39,40] Although the contrast enhancement is an important property, equally so is the toxicity of the agent. In these preliminary studies, the Gd^{3+}-AuNP contrast agent produced no ill effects 24 h post scan.

3.4 Conclusion

We have demonstrated the ability to functionalize Au nanoparticles to nearly 70% under aqueous conditions to afford contrast agents that are suitable for MRI with over 50 Gd^{3+} chelators per AuNP. The Gd-AuNP are soluble at physiological pH and permit a higher concentration of CA to be delivered compared to the unbound CA that has a limited solubility at the same pH. We have developed a method to produce AuNPs of discrete size that maintain the relaxivity of the approved CA and produce no ill effects within 24 h. Moving forward we are expanding applications to other imaging modalities such as CT, which can take advantage of both Au and Gd to generate contrast.[22–25]

3.5 References

(1) S. Aime, C. Cabella, S. Colombatto, S. G. Crich, E. Gianolio and F. Maggioni, *J. Magn. Reson. Imaging,* 2002, **16**, 394– 406.

(2) S. Aime, M. Botta and E. Terreno, *Adv. Inorg. Chem.*, 2005, **57**, 173–237.

(3) D. D. Castelli, E. Gianolio, S. G. Crich, E. Terreno and S. Aime, *Coord. Chem. Rev.*, 2008, **252**, 2424–2443.

(4) A. D. Sherry, P. Caravan and R. E. Lenkinski, *J. Magn. Reson. Imaging*, 2009, **30**, 1240–1248.

(5) P. Caravan, *Chem. Soc. Rev.*, 2006, **35**, 512–523.

(6) P. Caravan, J. J. Ellison, T. J. McMurry and R. B. Lauffer, *Chem. Rev.*, 1999, **99**, 2293–2352.

(7) S. Laus, R. Ruloff, E. Toth and A. E. Merbach, *Chem.–Eur. J.*, 2003, **9**, 3555–3566.

(8) J. A. Pikkemaat, R. T. Wegh, R. Lamerichs, R. A. van de Molengraaf, S. Langereis, D. Burdinski, A. Y. F. Raymond, H. M. Janssen, B. F. M. de Waal, N. P. Willard, E. W. Meijer and H. Grull, *Contrast Media Mol. Imaging*, 2007, **2**, 229–239.

(9) M. Longmire, P. L. Choyke and H. Kobayashi, *Curr. Top. Med. Chem.*, 2008, **8**, 1180–1186.

(10) M. A. Mintzer and M. W. Grinstaff, *Chem. Soc. Rev.*, 2011, **40**, 173–190.

(11) E. Toth, D. Pubanz, S. Vauthey, L. Helm and A. E. Merbach, *Chem.–Eur. J.*, 1996, **2**, 1607–1615.

(12) G. M. Nicolle, E. Toth, H. Schmitt-Willich, B. Raduchel and A. E. Merbach, *Chem.–Eur. J.*, 2002, **8**, 1040–1048.

(13) V. Weissig, J. Babich and V. Torchilin, *Colloids Surf., B*, 2000, **18**, 293–299.

(14) E. Terreno, A. Sanino, C. Carrera, C. D. Delli, G. B. Giovenzana, A. Lombardi, R. Mazzon, L. Milone, M. Visigalli and S. Aime, *J. Inorg. Biochem.*, 2008, **102**, 1112–1119.

(15) E. Terreno, W. Dastru, D. D. Castelli, E. Gianolio, S. G. Crich, D. Longo and S. Aime, *Curr. Med. Chem.*, 2010, **17**, 3684– 3700.

(16) G. M. Nicolle, E. Toth, K. P. Eisenwiener, H. R. Macke and A. E. Merbach, JBIC, *J. Biol. Inorg. Chem.*, 2002, **7**, 757–769.

(17) J. P. Andre, E. Toth, H. Fischer, A. Seelig, H. R. Macke and A. E. Merbach, *Chem.–Eur. J.*, 1999, **5**, 2977–2983.

(18) M. Grogna, R. Cloots, A. Luxen, C. Jerome, C. Passirani, N. Lautram, J. F. Desreux and C. Detrembleur, *Polym. Chem.*, 2010, **1**, 1485–1490.

(19) A. Soleimani, F. Martinez, V. Economopoulos, P. J. Foster, T. J. Scholl and E. R. Gillies, *J. Mater. Chem. B*, 2013, **1**, 1027–1034.

(20) M. Grogna, R. Cloots, A. Luxen, C. Jerome, J.-F. Desreux and C. Detrembleur, *J. Mater. Chem.*, 2011, **21**, 12917– 12926.

(21) K. M. Atkins, F. M. Martinez, A. Nazemi, T. J. Scholl and E. R. Gillies, *Can. J. Chem.*, 2011, **89**, 47–56.

(22) C. Alric, J. Taleb, G. L. Duc, C. Mandon, C. Billotey, A. L. Meur-Herland, T. Brochard, F. Vocanson, M. Janier, P. Perriat, S. Roux and O. Tillement, *J. Am. Chem. Soc.*, 2008, **130**, 5908–5915.

(23) M. Beija, Y. Li, H. T. Duong, S. Laurent, L. Vander Elst, R. N. Muller, A. B. Lowe, T. P. Davis and C. Boyer, *J. Mater. Chem.*, 2012, **22**, 21382–21386.

(24) J.-A. Park, H.-K. Kim, J.-H. Kim, S.-W. Jeong, J.-C. Jung, G.-H. Lee, J. Lee, Y. Chang and T.-J. Kim, *Bioorg. Med. Chem. Lett.*, 2010, **20**, 2287–2291.

(25) Y. Song, X. Xu, K. W. MacRenaris, X.-Q. Zhang, C. A. Mirkin and T. J. Meade, *Angew. Chem., Int. Ed.*, 2009, **48**, 9143– 9147.

(26) J.-L. Bridot, A.-C. Faure, S. Laurent, C. Riviere, C. Billotey, B. Hiba, M. Janier, V. Josserand, J.-L. Coll, L. Vander Elst, R. Muller, S. Roux, P. Perriat and O. Tillement, *J. Am. Chem. Soc.*, 2007, **129**, 5076–5084.

(27) P.-J. Debouttiere, S. Roux, F. Vocanson, C. Billotey, O. Beuf, A. Favre-Reguillon, Y. Lin, S. Pellet-Rostaing, R. Lamartine, P. Perriat and O. Tillement, *Adv. Funct. Mater.*, 2006, **16**, 2330–2339.

(28) P. Caravan, *Acc. Chem. Res.*, 2009, **42**, 851–862.

(29) P. Gobbo and M. S. Workentin, *Langmuir*, 2012, **28**, 12357–12363.

(30) K. D. Hartlen, H. Ismaili, J. Zhu and M. S. Workentin, *Langmuir*, 2012, **28**, 864–871.

(31) P. Gobbo, M. C. Biesinger and M. S. Workentin, *Chem. Commun.*, 2013, **49**, 2831–2833.

(32) L. S. Natrajan, A. J. L. Villaraza, A. M. Kenwright and S. Faulkner, *Chem. Commun.*, 2009, 6020–6022.

(33) L. Tei, G. Gugliotta, Z. Baranyai and M. Botta, *Dalton Trans.*, 2009, **0**, 9712–9714.

(34) J. Lu, M. Shi and M. S. Shoichet, *Bioconjugate Chem.*, 2008, **20**, 87–94.

(35) A. Taylor, K. M. Wilson, P. Murray, D. G. Fernig and R. Levy, *Chem. Soc. Rev.*, 2012, **41**, 2707–2717.

(36) M. Milne, K. Chicas, A. Li, R. Bartha and R. H. E. Hudson, *Org. Biomol. Chem.*, 2012, **10**, 287–292.

(37) Z. Zhang, A. F. Kolodziej, M. T. Greenfield and 39 P. Caravan, *Angew. Chem., Int. Ed.*, 2011, **50**, 2621– 2624.

(38) H. F. Dvorak, J. A. Nagy, J. T. Dvorak and A. M. Dvorak, *Am. J. Pathol.*, 1988, **133**, 95–109.

(39) C. Alric, I. Miladi, D. Kryza, J. Taleb, F. Lux, R. Bazzi, C. Billotey, M. Janier, P. Perriat, S. Roux and O. Tillement, *Nanoscale*, 2013, **5**, 5930–5939.

(40) M. Longmire, P. L. Choyke and H. Kobayashi, *Nanomedicine*, 2008, **3**, 703–717.

Chapter 4

4 Insights on the Application of the Retro Michael-Type Addition on Maleimide-Functionalized Gold Nanoparticles in Biology and Nanomedicine

Chapter 4 has been published as a full paper, and it is reprinted (adapted) with permission from M. R. Weissman, K. T. Winger, S. Ghiassian, **P. Gobbo***, M. S. Workentin*, *Bioconjugate Chem*. DOI: 10.1021/acs.bioconjchem.5b00600. Copyright 2016 American Chemical Society.

Weissman and Winger were two undergraduate students under my direct co-supervision, along with my supervisor, Prof. M. S. Workentin. I mentored Weissman during the synthesis and characterization of the rhodamine B-MPA fluorophore and the performance and analysis of the fluorescence experiments. I mentored Winger during the performance and analysis of the ^{1}H NMR kinetic experiments. Ghiassian synthesized some Maleimide-AuNP starting material. I wrote the draft of the manuscript with final edit by my supervisor, Prof. M. S. Workentin.

The supporting information file referenced in the text can be downloaded from the web site of the publisher.

ABSTRACT: The glutathione-mediated retro Michael-type addition reaction is demonstrated to take place at the interface of small water-soluble maleimide-functionalized gold nanoparticles (Maleimide-AuNP). The retro Michael-type addition reaction can be blocked by hydrolyzing the Michael addition thioether adduct at the nanoparticle's interface under reaction conditions that do not cause AuNP decomposition. This procedure "locks" the molecule of interest onto the Maleimide-AuNP template for potential uses in medical imaging and bioconjugation, ensuring no loss of the molecular cargo from the nanocarrier. On the other hand, the glutathione-mediated retro Michael-type addition reaction can be exploited for delivering a molecular payload. As a proof of concept, a fluorogenic molecular cargo was

incorporated onto a Maleimide-AuNP and delivered via the glutathione-mediated retro Michael-type addition reaction.

4.1 Introduction

The maleimide moiety is an extremely versatile functional group that can undergo three click reactions with three different functionalities: Diels-Alder cycloaddition reactions with dienes,[1, 2] dipolar cycloaddition reactions with dipolar molecules[3, 4] and Michael addition reactions with appropriate nucleophiles.[5] Therefore interest in maleimide moieties attached to the interface of materials has grown as a result of their potential use for nanomedicine, biolabeling, and sensing. The Michael addition is probably the most employed of the three types of click reactions because of the large amount of potentially reactive thiols and amines in biological systems, the fast reaction kinetics, the mild reaction conditions required, the absence of byproducts, and the stability of the resulting thioether product.[6] All of these benefits have allowed the Michael addition reaction to find a variety of applications in the (bio)materials chemistry domain. For example, it has been used for the synthesis of polymers,[5, 7, 8] hydrogels,[9-11] fluorescent labels,[12, 13] regenerative biomaterials,[14] the functionalization of self-assembled monolayers,[15-17] and nanomaterial hybrids.[18]

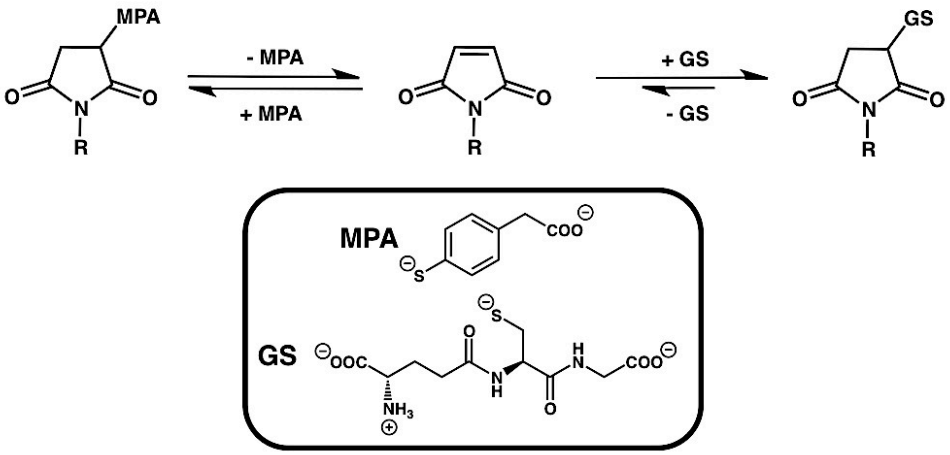

Scheme 4.1: Scheme representing the mechanism for the glutathione (GS)-mediated retro Michael-type addition reaction for a general MPA-*N*-substituted maleimide thioether adduct.

While the stability of the thioether adduct product of the Michael addition reaction between maleimide and thiols is always highlighted as a strength of this reaction, cases have been reported demonstrating that under certain conditions the Michael addition reaction is reversible.[19-21] K. L. Kiick and co-workers reported that the *N*-ethylmaleimide-thiol adduct can undergo retro Michael-type addition reaction in presence of biological amounts of glutathione (GS) at physiological pH and temperature.[22] The extent of the retro Michael-type addition reaction can be controlled by increasing or decreasing the nucleophilicity of the Michael donor. While aliphatic thiols have been found to yield completely stable thioether products, thiols with lower pK_a (such as 4-mercaptophenylacetic acid - MPA) can undergo a retro Michael-type addition reaction that regenerates the maleimide, which subsequently undergoes a Michael-type addition reaction with GS to yield a more stable thioether product (see Scheme 4.1). The conversion of the MPA adduct to the GS adduct reaches 90% in a few hours. They also reported that the retro Michael-type addition reaction was not triggered by other nucleophiles like amines (used in place of GS), and did not proceed with weaker Michael acceptors like acrylates. Most importantly, they showed that the retro reaction can be avoided by hydrolyzing the maleimide and "locking" the thioether adduct. The studies of Kiick and co-workers expanded the scope of maleimide chemistry and provided invaluable information on side reactions that can happen to a maleimide-thiol Michael adduct when exposed to biological environments for *in vivo* studies. There has been an increasing interest in the application of gold nanoparticles (AuNPs) for bioconjugation and *in vitro* and *in vivo* diagnosis and targeted therapy in recent years. This is due to the AuNPs' very low toxicity, their high stability, their availability in different sizes and shapes, and the relative ease of modifying their physical-chemical properties via surface modification. Our research group has been working on designing and synthesizing a toolbox of clickable and bioorthogonal AuNPs templates. These AuNPs are specifically designed to display interfacial clickable and bioorthogonal functional groups for the facile attachment of any molecular systems of interest, ranging from biomolecules and contrast agents to other nanomaterials. Recently, we reported a methodology for the synthesis of small ($\phi < 3$ nm) and water-soluble AuNPs displaying interfacial maleimide functionalities.[23] These Maleimide-AuNPs were shown to react through the Michael

addition reaction with thiols and amines, through the Diels-Alder reaction with dienes, and through the 1,3-dipolar cycloaddition with nitrones.[24] We showcased a number of potential applications for this clickable nanomaterial template. More specifically, we were able to click them onto single-walled carbon nanotubes that were modified with thiol functionalities,[18] and we were able to functionalize them with a Gd^{3+}-DO3A contrasting agent displaying a dangling primary amine. The resulting Gd-functionalized AuNPs were successfully employed for *in vivo* imaging.[25] Recently, J. Zhu and co-workers used the Maleimide-AuNP template to introduce, thanks to the Michael addition's fast reaction kinetics, a 4-(di-tert-butylfluorosilyl)benzenethiol group (where the fluorine is a ^{18}F) for positron emission tomography (PET) measurements *in vivo*.[26]

Considering the evident utility and versatility of the Maleimide-AuNP, it is of paramount importance that the occurrence of the retro Michael-type addition reaction at the interface of the Maleimide-AuNPs is understood in detail, especially in cases where the payload introduced onto the Maleimide-AuNP has a lower pK_a, like benzenethiols derivatives. It is also equally important to find a reaction condition that allows for the "locking" of the thioether adduct at the AuNP's interface in order to block the retro Michael-type addition reaction. This will ensure the efficiency of the nanotemplate as a drug and contrasting agent carrier, and as a bioconjugation platform. In this paper we show that the retro Michael-type addition reaction occurs at the interface of the Maleimide-AuNP under physiological conditions, and that the retro reaction can be blocked (or locked) by hydrolyzing the interfacial maleimide-thiol adducts under mild reaction conditions that do not cause AuNP decomposition. On the other hand, the retro Michael-type addition represents an attractive reaction for drug delivery and sensing that can be coupled to the high loading capacity of the Maleimide-AuNP template and its physical chemical properties. Herein, we also explore this possibility and show how the retro Michael-type addition can be exploited to deliver the maleimide's payload by taking advantage of the "unlocked" thioether adduct. We demonstrated this by preparing of a fluorogenic AuNP by exploiting the quenching property of the nanoparticle's gold core. The approach described in this work ensures a molecular-level control over the loading and release of a payload from a nanoparticle and represents an important advancement with respect to other "shotgun"-type methodologies for conjugation that rely on thiolated molecules and

uncontrolled ligand exchange reactions for the release of the payload.[27-32] In addition, through the controlled hydrolysis of the maleimide moieties we have the means to block the release of the cargo also in those media that are reach in thiolated molecules such as biological environments. This ensures the efficiency of our reactive nanomaterial template also for those applications that require the cargo to be irreversibly bound to the nanocarrier (*i.e.*, medical imaging).

4.2 Results and discussion

Synthesis of Maleimide-AuNPs:

Small and water-soluble Maleimide-AuNP were synthesized according to our previously established synthetic strategy.[23, 25] This procedure takes into account the high reactivity of the maleimide towards thiols, a functional group that is required for binding the maleimide ligand to the nanoparticle's gold surface. The maleimide must therefore be protected with furan through a Diels-Alder cycloaddition reaction. A furan-protected maleimide thiolated ligand is therefore a stable molecule and can be introduced onto the AuNP corona through a ligand exchange reaction, yielding furan-protected Maleimide-AuNPs. The maleimide is subsequently deprotected through an interfacial retro-Diels-Alder reaction carried out by dissolving the furan-protected Maleimide-AuNPs in dry toluene/10% acetonitrile and heating the solution at 110 ºC overnight. These reaction conditions ensure quantitative deprotection of the interfacial maleimides and no hydrolysis byproducts, as demonstrated in our seminal work.[23] This procedure yields Maleimide-AuNPs with a gold core size of 3 ± 1 nm. According to TGA (see Figure SI2) and TEM data (see Figure SI7), this nanoparticle template carries 0.5 μmol of maleimide per milligram of AuNPs and their simplified formula, assuming a spherical shape of the gold core and a monodispersed AuNP's size, is $Au_{500}(Me\text{-}EG_3\text{-}S)_{200}(Maleimide\text{-}EG_4\text{-}S)_{80}$.

Retro Michael-type addition investigation:

In order to investigate the retro Michael-type addition reaction at the interface of our nanomaterial, we clicked MPA onto the Maleimide-AuNP template (Scheme 4.2).

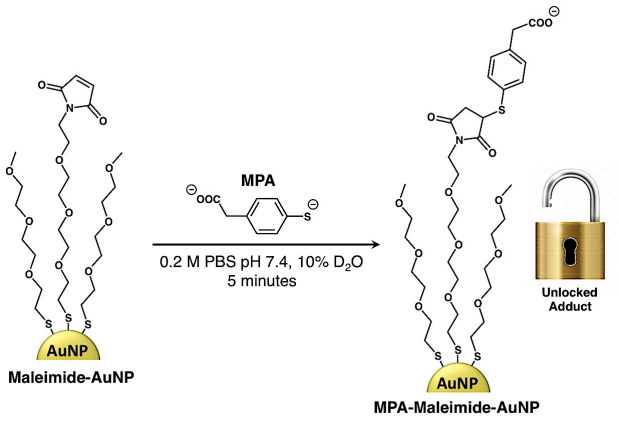

Scheme 4.2: Michael addition reaction between Maleimide-AuNP and MPA.

The reaction was performed by mixing 83.3 µL of a 72 mM solution of MPA in 0.2 M phosphate-buffer solution (PBS) (10% D_2O, pH 7.4) with a solution of 20 mg of Maleimide-AuNP in 444.7 µL of 0.2 M PBS (10% D_2O, pH 7.4). The reaction mixture was allowed to react for 5 minutes while being mixed using sonication. Thanks to our ability to quantitate the amount of interfacial maleimide moieties on our nanomaterial, we could perform this reaction using 1:1 equivalents of MPA to maleimide. If a large excess of MPA is used, this leads to undesired ligand exchange reaction, which eventually leads to nanoparticles aggregation. Nevertheless, it is noteworthy that MPA-Maleimide-AuNPs or fluorogenic Maleimide-AuNPs (*vide infra*) are remarkably stable in presence of the amount of GS employed for triggering the retro reaction, and little to no aggregation was observed during the time window of our experiments (5 or 7 days). The Michael addition adduct at the AuNP's interface was characterized by ^{1}H NMR spectroscopy. Figure 4.1A shows the ^{1}H NMR spectrum of the MPA-Maleimide-AuNPs dissolved in 0.2 M PBS solution (10% D_2O, pH 7.4) and referenced against CH_2Cl_2 as the internal standard (5.31 ppm). The broad signals centered at 7.31 ppm and 7.13 ppm belong to the aromatic protons of the MPA-maleimide adduct. The presence of the peak downfield at 7.42 ppm belongs to a small amount of MPA-MPA disulfide. Simultaneously, we sought to synthesize the MPA-NMM (*N*-methylmaleimide) adduct to be used for model experiments and for facilitating the characterization of the GS-mediated retro Michael-type addition at the AuNP's interface.

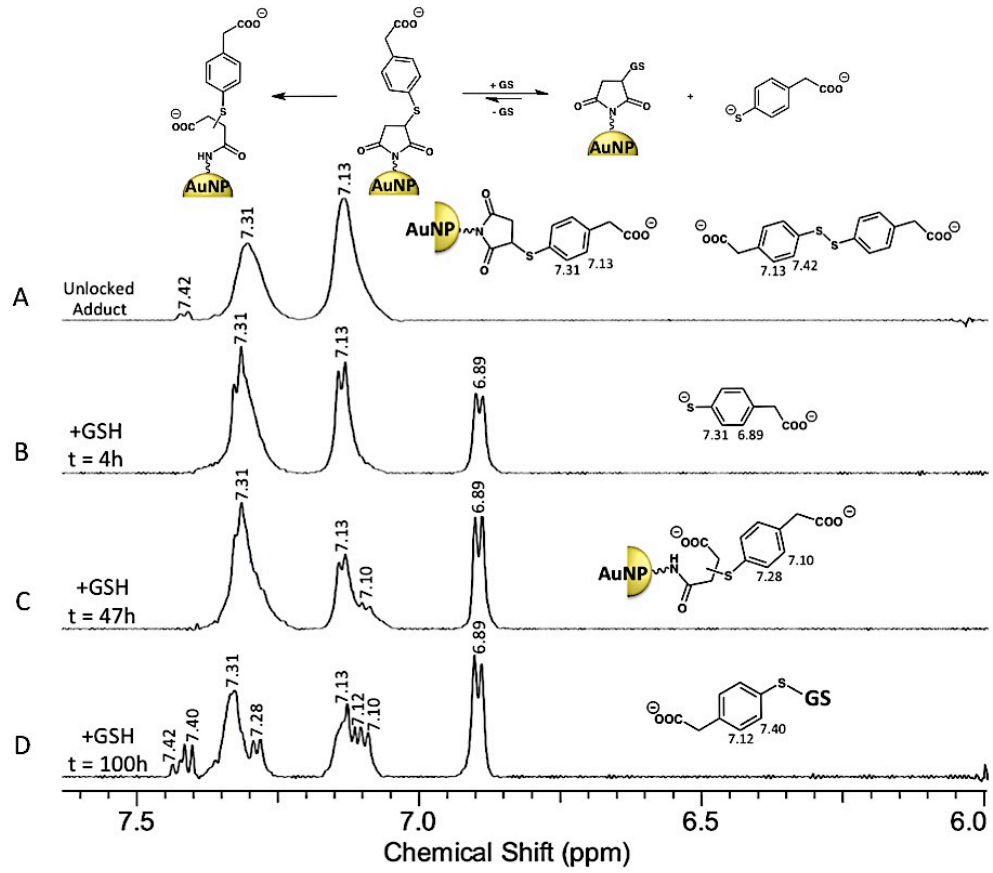

Figure 4.1: Typical retro Michael-type addition kinetic study on MPA-Maleimide-AuNPs. The ^{1}H NMR spectra highlight the changes over time of the aromatic region of (A) MPA-Maleimide-AuNPs, (B) after 4 hours, (C) 47 hours, and (D) 100 hours from the addition of glutathione (GS). Kinetic performed at 37 ºC. Spectra recorded with W5 water suppression in 0.2 M PBS (pH 7.4, 10% D_2O) and referenced against CH_2Cl_2 (5.31 ppm).

The detailed synthesis and characterization of the MPA-NMM adduct is reported in the supplementary information. Figure 4.2B shows the ^{1}H NMR of the MPA-NMM adduct dissolved in 0.2 M PBS (10% D_2O, pH 7.4) and referenced against CH_2Cl_2 as the internal standard (5.31 ppm). The spectrum shows perfect correspondence of the chemical shift of the aromatic peaks with those of the AuNP (Figure 4.1, spectrum A), validating that we had successfully clicked MPA onto the Maleimide-AuNP via the Michael addition reaction.

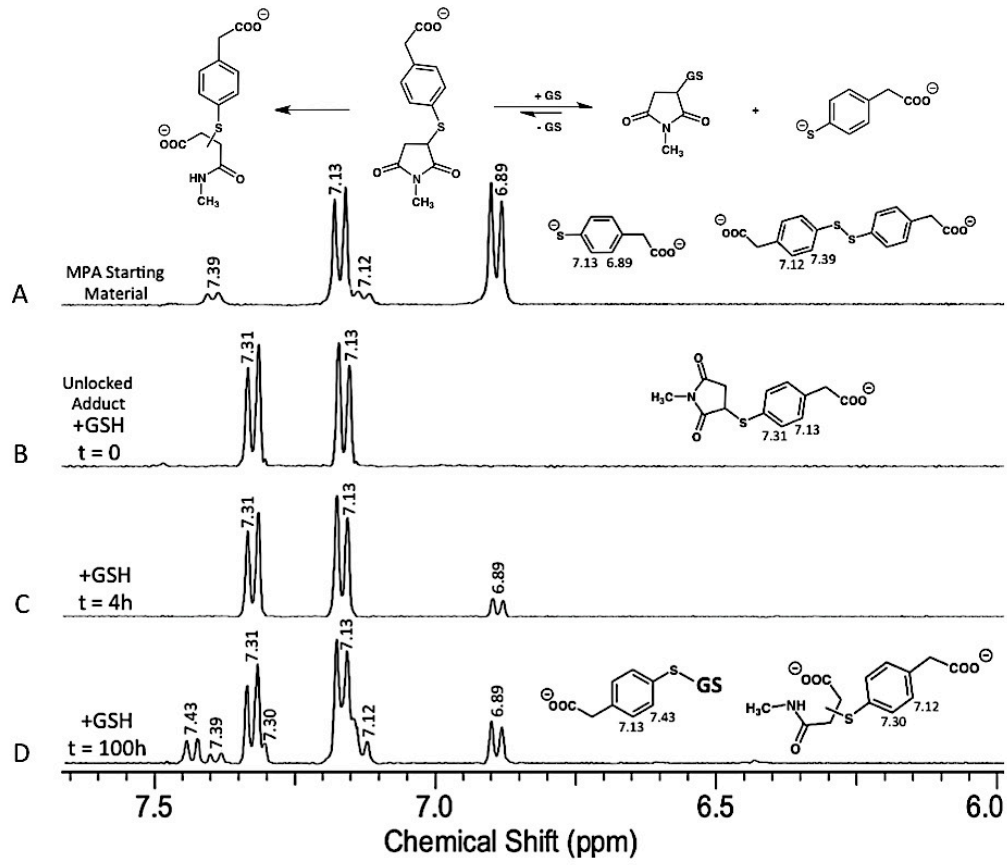

Figure 4.2: Typical retro Michael-type addition kinetic study on MPA-*N*-methylmaleimide adduct (model reaction). The ^{1}H NMR spectra highlight the changes over time of the aromatic region of (A) MPA starting material, (B) MPA-*N*-methylmaleimide adduct, (C) after 4 hours, and (D) 100 hours from the addition of glutathione (GS). Kinetic performed at 37 ºC. Spectra recorded with W5 water suppression in 0.2 M PBS (pH 7.4, 10% D_2O) and referenced against CH_2Cl_2 (5.31 ppm).

Next we tested both adducts (MPA-Maleimide-AuNP - interfacial reaction - and MPA-NMM - model reaction) towards the GS-mediated retro Michael-type addition reaction. Kinetic experiments were performed in an NMR tube by monitoring the aromatic region through ^{1}H NMR spectroscopy. A one molar equivalent of GS was introduced to both solutions of MPA-Maleimide-AuNPs adduct and MPA-NMM adduct in 0.2 M PBS (10% D_2O, pH 7.4). Upon addition of GS, in both model and AuNPs experiments, GS caused the immediate reduction of the MPA-MPA disulfides as can be seen by the disappearance

of the small downfield doublets in Figure 4.1A and Figure 4.2B. However, there was a striking difference between the two initial spectra right after the addition of GS (t = 0). Upon addition of GS to the MPA-Maleimide-AuNPs adduct, an immediate release of MPA was observed as a peak at 6.89 ppm appeared. This peak did not appear in the model reaction using the MPA-NMM adduct. We believe that this immediate release of MPA was not due to the retro Michael-type addition occurring, but it was caused by the release of a small amount of MPA that did not undergo the Michael addition reaction but instead attached to the gold core through a competing minor ligand exchange reaction. This amount of MPA was found to remain constant throughout the kinetic experiments when the same study was carried out on the hydrolyzed Michael addition adduct ("locked" adduct) that cannot undergo the GS-mediated retro Michael-type addition reaction (vide infra). Over a seven-day period, the reaction mixtures (interfacial and model) were incubated at 37 ^{o}C and periodically monitored by ^{1}H NMR spectroscopy. As time progressed, in both model reaction and Maleimide-AuNPs experiment the liberation of MPA was observed, as indicated by the increase in the intensity of the MPA aromatic protons at 6.89 ppm (Figure 4.1C and Figure 4.2D).

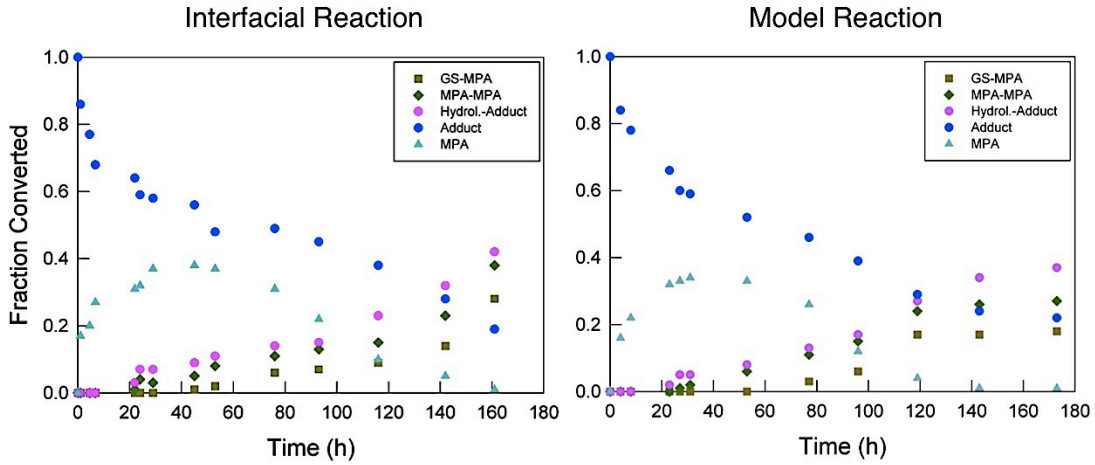

Figure 4.3: Variation over time of the relative concentrations of the different MPA species reported in Figure 4.1 and Figure 4.2, and monitored through ^{1}H NMR spectroscopy. Left: reaction at the AuNPs interface. Right: model reaction using *N*-methylmaleimide. The data report the average of measurements replicated in triplicate.

This showed that the retro Michael-type addition reaction can occur at the AuNP's surface and that, as expected, the MPA-Maleimide-AuNP adduct is "unlocked". During the seven-day period other side reactions could be observed to occur in parallel to the retro Michael-type addition. These are the formation of the disulfides (MPA-MPA and MPA-GS upon progressive release of MPA) and the slow ring opening (hydrolysis) of the MPA-maleimide adduct. These other products could be determined by comparison with the study of K. L. Kiick and co-workers.[22] The relative concentrations of all these species could be followed through the integration of the corresponding aromatic peaks of the MPA's aryl ring, and could be plotted versus time (refer to Figure 4.3). The resulting graphs show how during the first 8 hours the retro Michael-type addition is predominant with a fast release of MPA that reaches more than 20% for both model and AuNP experiments. After 24 hours at 37 ºC, hydrolyzed MPA-maleimides adducts start to be detected (doublets at 7.10 and 7.28 ppm), while after 30 hours MPA-MPA (7.13 and 7.42 ppm) and GS-MPA (7.12 and 7.40 ppm) disulfides start to form. The comparison between model reaction and interfacial reaction shows that the reaction kinetics are very similar, with a conversion of MPA that at the end of the monitoring period reaches a plateau at ~80%. These results are comparable to the kinetic studies performed by Baldwin and co-workers.[11] Of this 80%, 40% is MPA that has been released through the retro Michael-type addition reaction and 40% is hydrolyzed MPA-maleimide (locked) adduct. Minor differences can be noticed in the chemical shifts between the control and the experiment on the AuNPs. These are most likely due to the fact the AuNPs solution is nearly saturated. The concentration of the two solutions is identical but has been calculated in moles of maleimide, neglecting the molecular mass of the overall Maleimide-AuNP. 2D NMR spectroscopy was employed to correlate the doublets of the MPA aromatic protons for the different MPA species and ensure their proper integration (see Figure SI8-9).

These data demonstrate that the retro Michael-type addition occurs at the Maleimide-AuNP's interface. This is an important finding as it allows for the Maleimide-AuNPs to be potentially applied in biological applications such as drug release or biomolecule tagging, where the reversible linkage of the thiol to the maleimide is required. It also confirms that for those applications where the Michael adduct is required to remained

locked onto the nanomaterial surface, precautions (*i.e.*, hydrolysis of the adduct or selection of a thiol with a high pK_a) need to be taken (*vide infra*).

Locking the Michael addition thioether adducts at the nanomaterial's interface:

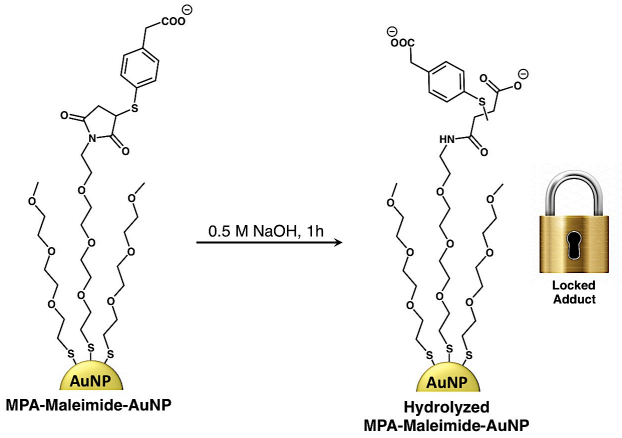

Scheme 4.3: Hydrolysis of the MPA-Maleimide-AuNP Michael addition adduct. The hydrolysis reaction yields two isomers in 1:4 ratio as determined from ^{1}H NMR spectroscopy.

With the confirmation that the retro Michael-type addition occurs at the Maleimide-AuNPs interface in the same extent as the model molecule NMM, we next sought to devise a procedure for locking the Michael addition adduct by the controlled hydrolysis of the maleimide moieties under reaction conditions compatible with the stability of the AuNPs. The locking of the thioether would allow the Maleimide-AuNPs to be used for applications that require the molecule of interest to be permanently attached to the nanocarrier (*e.g.*, as drug or contrast agent carrier). The locking of the MPA-maleimide adduct was performed by dissolving 20 mg of MPA-maleimide-AuNPs in a 0.5 M $NaOH_{(aq)}$ solution and allowing them to react for 1 hour (see Scheme 4.3). The "locked" MPA-Maleimide-AuNP were finally purified by dialysis. The AuNPs appeared to be stable to the strongly basic conditions, as their gold core diameter did not appear to change as verified by TEM analysis (see figure SI7). The hydrolyzed MPA-maleimide-AuNPs adduct was then characterized by ^{1}H NMR spectroscopy. Figure SI4 shows the ^{1}H NMR spectrum of the hydrolyzed MPA-Maleimide-AuNPs in 0.2 M PBS (10% D_2O, pH

7.4). The spectrum is referenced to CH_2Cl_2 as internal standard (5.31 ppm). The broad peaks centered at 7.29 ppm and 7.11 ppm belonged to the aromatic protons of the hydrolyzed MPA-maleimide adduct attached to the gold nanoparticles. This was confirmed by comparison with the ^{1}H NMR spectrum of the specifically hydrolyzed MPA-NMM model molecule recorded under the same conditions. The detailed synthesis and characterization of the hydrolyzed MPA-NMM adduct is reported in the supporting information. It is noteworthy that the hydrolyzed MPA-maleimide-AuNPs are not soluble in organic solvents, whereas the "unlocked" MPA-maleimide AuNPs adduct is. The absence of organic solvent solubility is a result of the ring-opened maleimide forming an extra interfacial carboxylate group, which creates a negatively charged capping ligand that only allow for the dissolution of these nanoparticles in water. This change in solubility also confirms that we successfully synthesized the hydrolyzed MPA-maleimide-AuNPs adduct.

Once both the hydrolyzed MPA-maleimide-AuNPs adduct and the hydrolyzed MPA-NMM adduct were synthesized, we proceeded to test if the retro Michael-type addition would occur upon exposure to GS. ^{1}H NMR spectroscopy was used to monitor the aromatic region, which would indicate, based on changes in the peaks' chemical shifts, whether or not the retro Michael-type addition occurred. For these experiments, in separate NMR tubes were introduced a solution of 20 mg of "locked" MPA-maleimide-AuNPs in 527 µL of 0.2 M PBS 10% D_2O, pH 7.4) and 500 µL of a solution 36.0 mM of hydrolyzed MPA-NMM model molecule in 0.2 M PBS (10% D_2O, pH 7.4). To these solutions, 1 equivalent of GS was then introduced and the interfacial and model reaction were monitored by ^{1}H NMR spectroscopy. Upon addition of GS, there was an immediate difference in the t = 0 spectra in both the control and the AuNPs experiment. When GS was added to the hydrolyzed MPA-maleimide-AuNPs adduct, an immediate release of MPA was observed as the peak at 6.89 ppm belonging to MPA's aromatic protons appeared. As previously explained, we believe that this immediate release of MPA is not due to the retro Michael-type addition occurring, but is most likely caused by the release of a small amount of MPA that attached directly to the gold core through a minor ligand exchange reaction. As the incubation at 37 ^{o}C progressed, this amount of MPA was found to be constant and no other peaks appeared indicating that the retro Michael-type addition

had not occurred. This confirms that the free MPA was the result of a ligand exchange reaction. In contrast, upon addition of GS to the hydrolyzed MPA-NMM adduct, no immediate release of MPA and no GS-mediated retro Michael-type addition reaction were observed.

This data proved that we had developed a method to hydrolyze the MPA-Maleimide-AuNPs adduct using reaction conditions where the AuNPs are stable. These findings provide a methodology to "lock" the thioether adduct and increase the efficiency of the Maleimide-AuNP template in bioconjugation and imaging.

Exploiting the retro Michael-type addition reaction: a fluorogenic AuNP sensor for GS

Finally, we wanted to demonstrate a potential application for the retro Michael-type addition reaction at the Maleimide-AuNP interface. AuNPs are well known to quench the fluorescence of a fluorophore that is in close proximity of their surface.[33] The general concept for this sensor is centered on the design and synthesis of a specific thiol-functionalized fluorophore characterized by a low thiol pK_a that will be conjugated through the Michael addition reaction to the Maleimide-AuNPs. Because the fluorophore is covalently bound to the AuNP corona and in close proximity to the gold core, its fluorescence will be quenched. However, when this fluorophore-Maleimide-AuNP conjugate is exposed to GS, this will trigger the retro Michael-type addition, and the thiolated fluorophore will be released with a consequent turn-on of its fluorescence, see Figure 4.4. The thiolated fluorophore that we synthesized is based on rhodamine B. This was selected because rhodamine B absorbs and emits at a wavelength where our small AuNP are not absorbing light, it has good photostability, and it is soluble in both organic solvents and water. The thiol functionality was introduced by coupling MPA to a rhodamine B-piperazine intermediate. This synthetic strategy has been recently reported by our research group and revealed to be very efficient, leading to high quantities of product with high purity.[34] The detailed synthesis and characterization of Rhodamine B-MPA is reported in the supporting information. To create the fluorogenic AuNP, Maleimide-AuNPs were mixed with a 50/50 solution of rhodamine B-MPA and pure MPA.

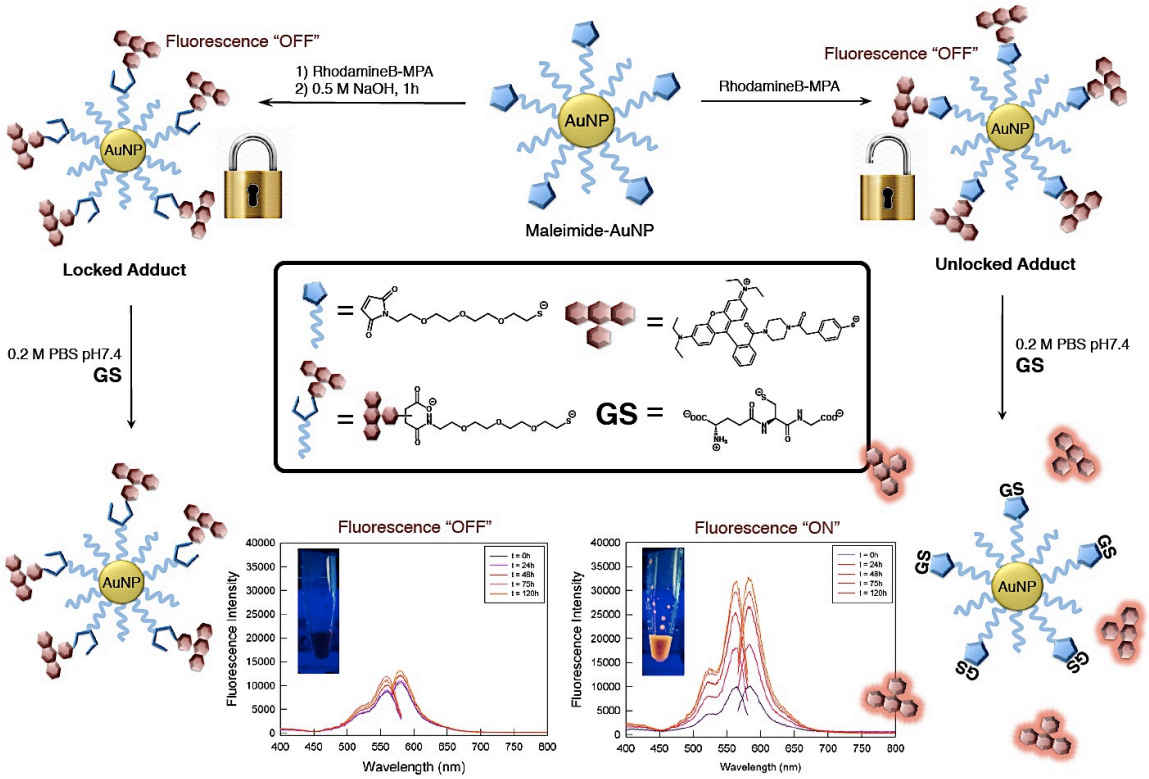

Figure 4.4: Cartoon representing the concept of "locked" or "unlocked" adduct on the fluorogenic AuNPs. When the fluorogenic AuNP are hydrolyzed and the rhodamine-maleimide adduct is "locked" (left path) there is no retro Michael-type addition reaction with glutathione (GS) and there is no turn-on of fluorescence. On the other hand, if the fluorogenic AuNP remains "unlocked" (right path), the retro Michael-type addition occurs and there is turn-on of fluorescence. Fluorescence data recorded over time in 0.2 M PBS pH 7.4, λ_{exc} = 556.6 nm, λ_{em} = 591.5 nm. The insets in the fluorescence data plots show pictures of the hydrolyzed fluorogenic AuNP (left) and fluorogenic AuNP (right) contained in an eppendorf tube and exposed to a long wave lamp.

The reaction was monitored through ^{1}H NMR spectroscopy by following the disappearance of the maleimide peak at 6.85 ppm (spectrum referenced *versus* residual methanol). When the reaction was completed, the fluorogenic particles were purified by dialysis. Details of the synthetic procedure for the fluorogenic AuNP are reported in the supporting information. A 50/50 mixture of rhodamine B-MPA and pure MPA was necessary because if only rhodamine B-MPA was used the final fluorogenic AuNP has

low solubility in water. The fluorogenic AuNP batch was then split in two fractions. One of the fractions was hydrolyzed under the same reaction conditions reported earlier for "locking" the Michael addition adduct. Upon hydrolysis reaction the AuNP sample was purified again by dialysis. This sample was employed as a control. In two separate and simultaneous experiments, the fluorogenic AuNP and the hydrolyzed fluorogenic AuNP were dissolved in 0.2 M PBS pH 7.4. To the two solutions 1 eq. of GS with respect to the maleimide was added, and the fluorescence of samples was monitored over 5 days. Figure 4.4 reports the excitation and emission spectra recorded over time for two samples and shows that while for the hydrolyzed fluorogenic AuNP sample there is not much variance in the fluorescence intensity, the fluorogenic AuNP sample display a clear turn-on of fluorescence signal that by the end of the experiment reaches more than 3 times its initial intensity. This is due to the GS-mediated retro Michael-type addition reaction that causes the release of rhodamine B-MPA from the AuNP's corona, which enters the bulk solution where its fluorescence is not quenched.

These experiments confirm our hypothesis that the GS-mediated retro Michael-type addition reaction with GS can occur at the Maleimide-AuNP interface if thiols with low pK_a are employed for conjugation. They also confirm the efficiency of our synthetic procedure for "locking" the Michael addition thioether product onto the nanomaterial's surface. Finally, they show how the retro Michael-type addition expands the scope of the Maleimide-AuNP template, which now can be used to deliver a molecular cargo. For this proof of concept fluorogenic nanomaterial the delivery of the payload takes place in the timescale of days. However, we anticipate that by modifying the electronic properties of the Michael acceptor and Michael donor it will be possible to tune the reaction kinetics in order to meet the requirements of any specific application.

4.3 Conclusion

In conclusion, we have shown that the GS-mediated retro Michael-type addition reaction has the potential to expand the versatility of the Maleimide-AuNPs in biological applications. We have confirmed that "unlocked" maleimide-MPA adducts at the interface of AuNPs undergo the retro Michael-type addition in solutions containing the biologically prevalent thiol GS. As demonstrated by Kiick and co-workers, by modifying

the pK_a of the Michael donor, the rate at which the retro Michael-type addition occurs can be tuned.[22] The higher the pK_a, the lower the extent of the retro Michael-type addition. In the light of these findings, it is evident that for those *in vivo* studies where the payload is required to be permanently attached to the nanocarrier, the selection of the right thiolated prosthetic group is of paramount importance. If a thiol with a low pK_a (structurally similar to MPA) is selected, then the probability that it undergoes the GS-mediated retro Michael-type addition *in vivo* is very high.

We were also able to develop a procedure for hydrolyzing the maleimide-MPA adducts at the AuNP's interface using reaction conditions that preserve the AuNPs' physical-chemical properties and do not cause aggregation. The resulting "locked" adduct prevents the retro Michael-type addition reaction and its consequent loss of nanoparticle's cargo into the surrounding environment. This "locking" protocol is useful for applications where the permanent linkage of the thiolated molecule to the AuNP is a requirement for the nanomaterial to be useful. Examples, as previously discussed, involve diagnostic imaging, where a contrast agent is linked to the gold core, or biolabeling.

4.4 References

(1) Boutelle, R. C., and Northrop, B. H. (2011) Substituent effects on the reversibility of furan-maleimide cycloadditions. *J. Org. Chem. 76*, 7994-8002.

(2) Tang, S. Y., Shi, J., and Guo, Q. X. (2012) Accurate prediction of rate constants of Diels-Alder reactions and application to design of Diels-Alder ligation. *Org. Biomol. Chem. 10*, 2673-2682.

(3) Domingo, L. R., Aurell, M. J., Arno, M., and Saez, J. A. (2007) Toward an understanding of the 1,3-dipolar cycloaddition between diphenylnitrone and a maleimide: bisamide complex. A DFT analysis of the reactivity of symmetrically substituted dipolarophiles. *Comp. Theor. Chem. 811*, 125-133.

(4) Sinclair, A. J., del Amo, V., and Philp, D. (2009) Structure-reactivity relationships in a recognition mediated [3+2] dipolar cycloaddition reaction. *Org. Biomol. Chem. 7*, 3308-3318.

(5) Nair, D. P., Podgorski, M., Chatani, S., Gong, T., Xi, W. X., Fenoli, C. R., and Bowman, C. N. (2014) The Thiol-Michael Addition Click Reaction: A Powerful and Widely Used Tool in Materials Chemistry. *Chem. Mater. 26*, 724-744.

(6) Hermanson, G. T. (2008) *Bioconjugate Techniques*, 2nd ed., Academic Press, San Diego, CA.

(7) Mather, B. D., Viswanathan, K., Miller, K. M., and Long, T. E. (2006) Michael addition reactions in macromolecular design for emerging technologies. *Prog. Polym. Sci. 31*, 487-531.

(8) Hall, D. J., Van den Berghe, H. M., and Dove, A. P. (2011) Synthesis and post-polymerization modification of maleimide-containing polymers by 'thiol-ene' click and Diels-Alder chemistries. *Polym. Int. 60*, 1149-1157.

(9) Nie, T., Baldwin, A., Yamaguchi, N., and Kiick, K. L. (2007) Production of heparin-functionalized hydrogels for the development of responsive and controlled growth factor delivery systems. *J. Control Release 122*, 287-296.

(10) Phelps, E. A., Enemchukwu, N. O., Fiore, V. F., Sy, J. C., Murthy, N., Sulchek, T. A., Barker, T. H., and Garcia, A. J. (2012) Maleimide Cross-Linked Bioactive PEG Hydrogel Exhibits Improved Reaction Kinetics and Cross-Linking for Cell Encapsulation and In Situ Delivery. *Adv. Mater. 24*, 64.

(11) Baldwin, A. D., and Kiick, K. L. (2013) Reversible maleimide-thiol adducts yield glutathione-sensitive poly(ethylene glycol)-heparin hydrogels. *Polym. Chem. 4*, 133-143.

(12) Peng, H. J., Chen, W. X., Cheng, Y. F., Hakuna, L., Strongin, R., and Wang, B. H. (2012) Thiol Reactive Probes and Chemosensors. *Sensors-Basel 12*, 15907-15946.

(13) Mabire, A. B., Robin, M. P., Quan, W. D., Willcock, H., Stavros, V. G., and O'Reilly, R. K. (2015) Aminomaleimide fluorophores: a simple functional group with bright, solvent dependent emission. *Chem. Commun. 51*, 9733-9736.

(14) Nimmo, C. M., and Shoichet, M. S. (2011) Regenerative Biomaterials that "Click": Simple, Aqueous-Based Protocols for Hydrogel Synthesis, Surface Immobilization, and 3D Patterning. *Bioconjugate Chem. 22*, 2199-2209.

(15) Houseman, B. T., Gawalt, E. S., and Mrksich, M. (2003) Maleimide-functionalized self-assembled monolayers for the preparation of peptide and carbohydrate biochips. *Langmuir 19*, 1522-1531.

(16) Harper, J. C., Polsky, R., Wheeler, D. R., and Brozik, S. M. (2008) Maleimide-activated aryl diazonium salts for electrode surface functionalization with biological and redox-active molecules. *Langmuir 24*, 2206-2211.

(17) Bertin, P. A., Ahrens, M. J., Bhavsar, K., Georganopoulou, D., Wunder, M., Blackburn, G. F., and Meade, T. J. (2010) Ferrocene and Maleimide-Functionalized Disulfide Scaffolds for Self-Assembled Monolayers on Gold. *Org. Lett. 12*, 3372-3375.

(18) Gobbo, P., Biesinger, M. C., and Workentin, M. S. (2013) Facile synthesis of gold nanoparticle (AuNP)-carbon nanotube (CNT) hybrids through an interfacial Michael addition reaction. *Chem. Commun. 49*, 2831-2833.

(19) Nampalli, S., McDougall, M. G., Lavrenov, K., Xiao, H. G., and Kumar, S. (2002) Utility of thiol-cross-linked fluorescent dye labeled terminators for DNA sequencing. *Bioconjugate Chem. 13*, 468-473.

(20) Alley, S. C., Benjamin, D. R., Jeffrey, S. C., Okeley, N. M., Meyer, D. L., Sanderson, R. J., and Senter, P. D. (2008) Contribution of linker stability to the activities of anticancer immunoconjugates. *Bioconjugate Chem. 19*, 759-765.

(21) Lin, D., Saleh, S., and Liebler, D. C. (2008) Reversibility of Covalent Electrophile - Protein Adducts and Chemical Toxicity. *Chem. Res. Toxicol. 21*, 2361-2369.

(22) Baldwin, A. D., and Kiick, K. L. (2011) Tunable Degradation of Maleimide-Thiol Adducts in Reducing Environments. *Bioconjugate Chem. 22*, 1946-1953.

(23) Gobbo, P., and Workentin, M. S. (2012) Improved Methodology for the Preparation of Water-Soluble Maleimide-Functionalized Small Gold Nanoparticles. *Langmuir 28*, 12357-12363.

(24) Ghiassian, S., Gobbo, P., and Workentin, M. S. (2015) Water-Soluble Maleimide-Modified Gold Nanoparticles (AuNPs) as a Platform for Cycloaddition Reactions. *Eur. J. Org. Chem.*, 5438-5447.

(25) Milne, M., Gobbo, P., McVicar, N., Bartha, R., Workentin, M. S., and Hudson, R. H. E. (2013) Water-soluble gold nanoparticles (AuNP) functionalized with a gadolinium(III) chelate via Michael addition for use as a MRI contrast agent. *J. Mater. Chem. B 1*, 5628-5635.

(26) Zhu, J., Chin, J., Wangler, C., Wangler, B., Lennox, R. B., and Schirrmacher, R. (2014) Rapid F-18-Labeling and Loading of PEGylated Gold Nanoparticles for in Vivo Applications. *Bioconjugate Chem. 25*, 1143-1150.

(27) Han, G., Chari, N. S., Verma, A., Hong, R., Martin, C. T., and Rotello, V. M. (2005) Controlled recovery of the transcription of nanoparticle-bound DNA by intracellular concentrations of glutathione. *Bioconjug Chem. 16*, 1356-9.

(28) Hong, R., Han, G., Fernandez, J. M., Kim, B. J., Forbes, N. S., and Rotello, V. M. (2006) Glutathione-mediated delivery and release using monolayer protected nanoparticle carriers. *J. Am. Chem. Soc. 128*, 1078-9.

(29) Chompoosor, A., Han, G., and Rotello, V. M. (2008) Charge dependence of ligand release and monolayer stability of gold nanoparticles by biogenic thiols. *Bioconjugate Chem. 19*, 1342-5.

(30) Ghosh, P. S., Kim, C. K., Han, G., Forbes, N. S., and Rotello, V. M. (2008) Efficient gene delivery vectors by tuning the surface charge density of amino acid-functionalized gold nanoparticles. *ACS nano 2*, 2213-8.

(31) Wang, X., Cai, X., Hu, J., Shao, N., Wang, F., Zhang, Q., Xiao, J., and Cheng, Y. (2013) Glutathione-triggered "off-on" release of anticancer drugs from dendrimer-encapsulated gold nanoparticles. *J. Am. Chem. Soc. 135*, 9805-10.

(32) Bao, Q. Y., Geng, D. D., Xue, J. W., Zhou, G., Gu, S. Y., Ding, Y., and Zhang, C. (2013) Glutathione-mediated drug release from Tiopronin-conjugated gold nanoparticles for acute liver injury therapy. *Int. J. Pharm. 446*, 112-8.

(33) Mayilo, S., Kloster, M. A., Wunderlich, M., Lutich, A., Klar, T. A., Nichtl, A., Kurzinger, K., Stefani, F. D., and Feldmann, J. (2009) Long-Range Fluorescence Quenching by Gold Nanoparticles in a Sandwich Immunoassay for Cardiac Troponin T. *Nano Lett. 9*, 4558-4563.

(34) Gobbo, P., Gunawardene, P., Luo, W., and Workentin, M. S. (2015) Synthesis of a Toolbox of Clickable Rhodamine B Derivatives. *Synlett 26*, 1169-1174.

Chapter 5

5 Facile synthesis of gold nanoparticle (AuNP)–carbon nanotube (CNT) hybrids through an interfacial Michael addition reaction

Chapter 5 has been published as a communication, and it is reproduced with permission from the Royal Society of Chemistry. The corresponding reference is: **P. Gobbo**, M. C. Biesinger, M. S. Workentin*, *Chem. Commun.*, **2013**, 49, 2831-2833.

Biesinger performed the XPS measurements and assisted in the discussion of the results. I performed the synthesis and characterization of the nanomaterial hybrid. I wrote the drafts of the manuscript, with input and minor edits from the other co-author and final edit by my supervisor, Prof. M. S. Workentin.

The supporting information file referenced in the text can be downloaded from the web site of the publisher.

ABSTRACT: A CNT–AuNP hybrid has been synthesized through the Michael addition reaction between thiol-functionalized single-wall CNT and small water-soluble Maleimide–AuNP. The resilience and stability of this hybrid nanosystem is ensured by a covalent bond linking the nanoparticle to the CNT and by the fact that the functionalization reaction involves the organic shell of the AuNP and not its metallic core.

5.1 Introduction, Results and Discussion

Since their discovery in 1991 carbon nanotubes (CNT) have been extensively studied for uses in emitting devices, energy storage, sensor field, and for biological and biomedical applications.[1–5] CNT combined with gold nanoparticles (AuNP) resulting in AuNP–CNT hybrid materials bring together the high conductivity of the CNT and combine it with the size-dependent optothermal properties of the AuNP with potential direct application as gas sensors, catalysts, and especially as structural components of electrochemical sensors.[6–11]

Different synthetic strategies have been explored to decorate CNT with AuNP. Generally all of these require the introduction of functionalities onto the CNT sidewalls that enable them to bind the nanoparticles. For this purpose electrostatic[12,13] or hydrophobic[14,15] interactions between the functionalized CNT and the AuNP, or the affinity of amines and thiols for gold[6,16–18] have been exploited. However, these methodologies generally lead to a non-robust nanohybrid material where the AuNP can be easily detached because of the lack of a covalent bond that links them to the CNT, or can rapidly coalesce, especially when solvent is removed, thereby destroying their size dependent properties.[14] Because of the high cost of these nanomaterials, it is desirable that the final product has a long life and is stable, and that the functionalization reaction works quickly and efficiently. To address these requirements we developed photochemical routes towards the synthesis of covalent AuNP– CNT hybrids exploiting interfacial carbene and nitrene reactions that involve the organic shell of the AuNP and not its gold core.[19,20] However, these systems utilize organic soluble AuNP and because CNT generally form stable dispersions in water and very polar organic solvents,[21,22] it is desirable that in these media the partner nanoparticles are soluble and stable, and that the functionalization reaction works efficiently. We synthesized small Maleimide–AuNP that addresses these two requirements. These AuNP can undergo a Michael addition reaction with thiols and amines, thanks to Maleimide functionalities present at their interface.[23] The Michael addition is one of the most used reactions for creating AuNP-bioconjugates and, as such, it is meant to be very fast and efficient, and to take place in water and at room temperature.[24,25]

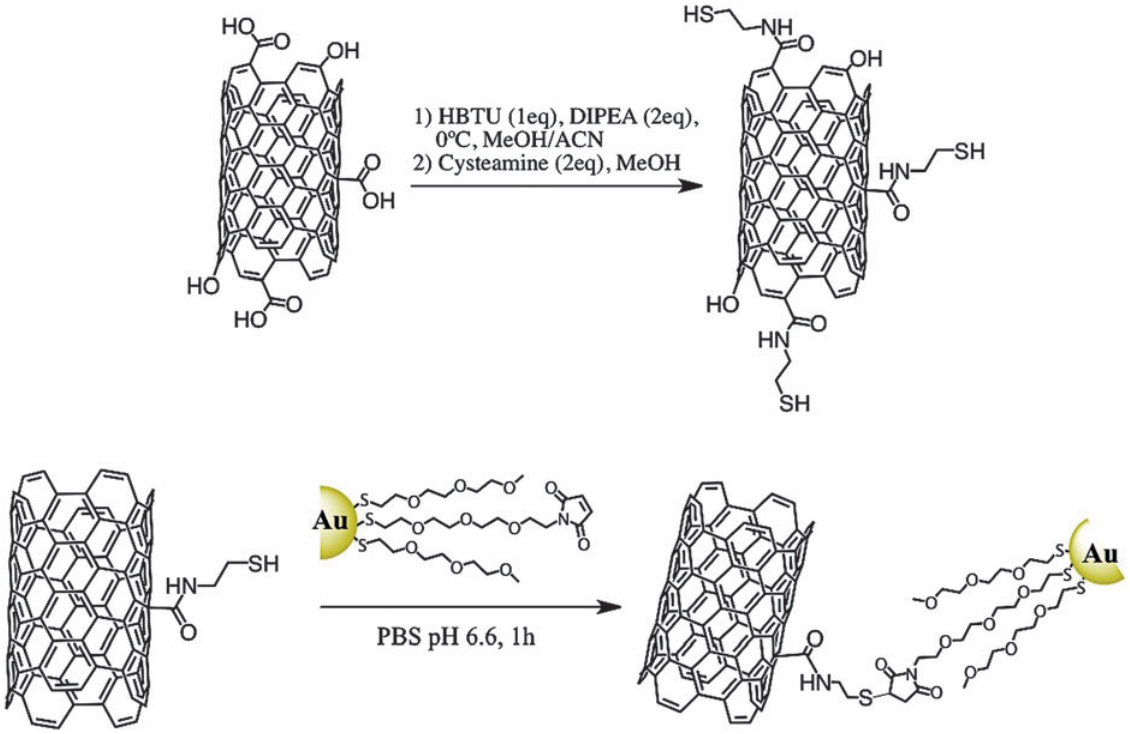

Scheme 5.1: Synthetic approach to the preparation of SWCNT–AuNP through Michael addition reaction at the Maleimide–AuNP interface.

Here we show for the first time the use of an interfacial Michael addition reaction towards a facile, convenient and efficient way for creating AuNP–CNT hybrids. These small water-soluble Maleimide–AuNP react readily with thiol-modified single-wall CNT (SWCNT–SH) under very mild conditions, leading to a robust AuNP-decorated SWCNT (SWCNT–AuNP).

Scheme 5.1 shows the synthetic strategy leading to the formation of gold nanoparticles-decorated single-wall carbon nanotubes (SWCNT–AuNP). The first step involves the introduction of thiol functionalities onto the CNT sidewalls through a coupling reaction between cysteamine and the carboxylic groups already present on the native SWCNT (see Scheme 5.1). This procedure is similar to the one reported by Z. Liu et al.21 However, it is noteworthy that it is not necessary to chemically oxidize the CNT before the coupling reaction. The protocol is simple. Briefly, 10 mg of SWCNT were dispersed in 5 ml of dry MeOH in a round bottom flask. The system was cooled down to 0 ºC, and

the solution was purged with argon for 10 minutes. 20 mg of HBTU (53 mmol) and 19 ml of DIPEA (106 mmol) were dissolved in a separate round bottom flask with 5 ml of a MeOH–Acetonitrile (2:1) mixture and they were purged with argon for 10 min. Once the two solutions were purged, HBTU and DIPEA were transferred using a glass syringe into the ice-cold solution of CNT. The reaction was left for 15 min at 0 ºC. In a clean round bottom flask a solution of cysteamine (8.2 mg, 106 mmol) in 2 ml of dry methanol was purged with argon. After 15 minutes the solution of cysteamine was injected into the ice-cold solution of CNT, HBTU and DIPEA, the ice-bath was removed and the reaction mixture was left overnight under vigorous stirring. The solution was then centrifuged (10 min, 6000 rpm) and the supernatant removed. The resulting thiol functionalized CNT (SWCNT–SH) were re-dispersed in acetonitrile, sonicated for 10 min, centrifuged again, and the solvent was decanted. This washing procedure was repeated once more, then acetonitrile was substituted with water and SWCNT–SH were washed and centrifuged twice. Finally, the solvent was evaporated and the SWCNT–SH was dispersed in a phosphate buffer solution (PBS) pH 6.6 to obtain a concentration of 2 mg ml^{-1}. This mother solution was stored in the freezer. SWCNT–SH was characterized by X-ray photoelectron spectroscopy (XPS) and infrared (IR) spectroscopy. The XPS survey of SWCNT–SH (Figure 5.1b) compared to that one of the starting material (Figure 5.1a) clearly shows the appearance of the peaks related to the sulphur at 160 eV (2p) and at 228 eV (2s) and to the nitrogen at 396 eV (1s). High-resolution scans of these regions indicate a successful coupling reaction. The N 1s core line (Figure S2, ESI) shows a single peak at 399.78 eV related to the amide nitrogens, while the S 2p core line clearly shows that the majority of the sulphur is present as thiol (S 2p3/2 at 163.65 eV, S 2p1/2 at 164.83 eV) (Figure 5.1d). It is noteworthy that XPS measurements carried out on samples two months old (Figure 5.1d) show that SWCNT–SH have a good stability to oxidation with only ~15% of the sulphur oxidized. The IR spectrum of SWCNT–SH also confirms this result showing the peaks related to the C–H stretching of the cysteamine at 2949, 2919, and 2848 cm^{-1}, and a band at 1580 cm^{-1} related to the stretching mode of the amide C=O (Figure S1, ESI).

In order to obtain the AuNP-decorated CNT, SWCNT–SH were reacted with the water-soluble Maleimide–AuNP through the Michael addition reaction in PBS pH 6.6.

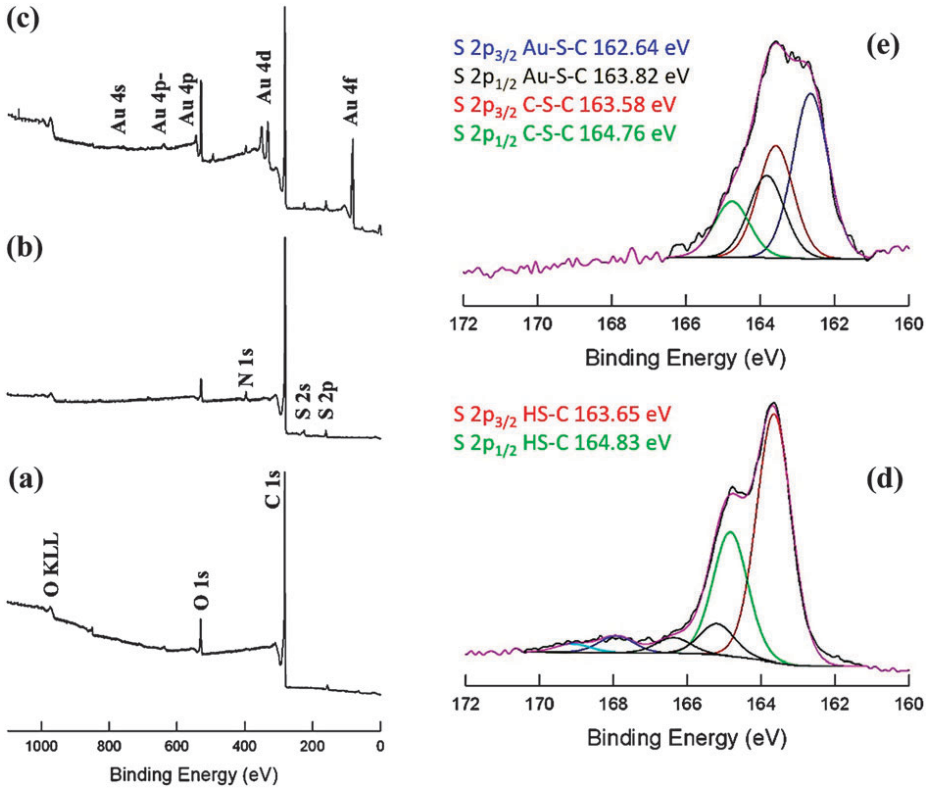

Figure 5.1: On the left XPS survey of a) SWCNT starting material; b) SWCNT-SH; c) SWCNT–MaleimideAuNP. On the right high-resolution S 2p spectra of d) SWCNT–SH; e) SWCNT–MaleimideAuNP.

Maleimide–AuNP was synthesized accordingly to our previously established procedure.[23] Briefly, Maleimide–AuNP was obtained through a retro Diels–Alder strategy because of the (desired) reactivity of the Maleimide functionality towards nucleophiles. The basic triethylene glycol monomethyl ether AuNP (Me-EG_3-AuNP) underwent a place exchange reaction with furan-protected-Maleimide tetraethylene glycol–thiols ligands (PtMaleimide-EG_4-SH). The resulting PtMaleimide–AuNP was deprotected from the furan using an improved methodology: the PtMaleimide–AuNP were dissolved in a toluene–acetonitrile (10 : 1) mixture and heated at 110 ºC overnight under vigorous stirring. The new mixture of solvents was found to readily redissolve all the PtMaleimide–AuNP (while before just the toluene-soluble fraction of PtMaleimide–AuNP could be deprotected) and still being suitable for the retro-Diels-Alder reaction

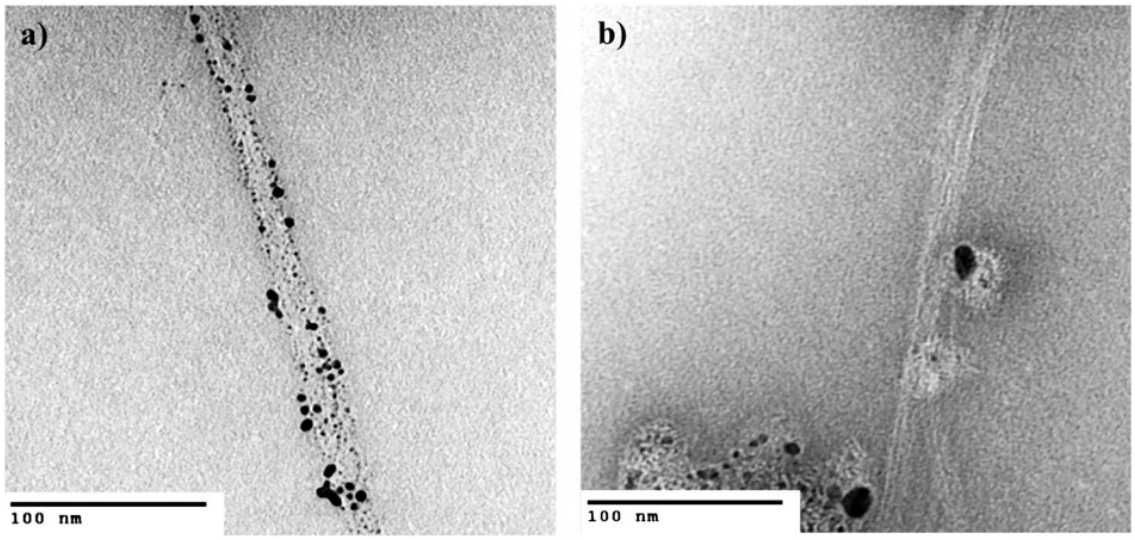

Figure 5.2: TEM images of a) SWCNT–AuNP; b) control experiment (SWCNT–SH + Me-EG$_3$-AuNP).

without forming any hydrolysis by-product[23] and leads to small water-soluble Maleimide–AuNP with a gold core diameter ranging from 2 to 4 nm. The Michael addition reaction was carried out adding 4 mg of Maleimide–AuNP dissolved in 1 ml of PBS pH 6.6 to a 1 ml of SWCNT–SH mother solution (see Scheme 5.1). The reaction was stirred for 1 hour at room temperature, and then the SWCNT– AuNP was centrifuged in a Pyrex centrifuge test tube. The supernatant was removed, and the decorated CNT bundles were dispersed in acetone, sonicated for 10 minutes and centrifuged. Subsequently, acetone was substituted with dichloromethane (DCM) and the washing procedure (sonication in DCM and centrifugation) was repeated twice more. The success of the interfacial Michael addition reaction between SWCNT–SH and Maleimide–AuNP was confirmed by XPS, IR spectroscopy, and by transmission electron microscopy (TEM) images. The XPS survey of SWCNT–AuNP (Figure 5.1c) clearly shows the appearance of the peaks related to gold at 83 eV (4f), 334–353 eV (4d), 547–643 eV (4p), and 762 eV (4s). The Au $4f_{7/2}$ core line is at 84.19 eV (Figure S3, ESI) and results shifted upwards from that of bulk gold (83.95 eV) due to the nanoparticle size effect.[26,27] The high resolution C 1s spectrum (Figure S3, ESI) shows a new component at 285.30 eV related to the C–O–C of the AuNP glycol units. Most notably, the S 2p core line now

shows the appearance of a new doublet related to the Au–S bonds with binding energies of 162.64 eV (S $2p_{3/2}$) and 163.82 eV (S $2p_{1/2}$), and the components related to the C–S–C bond (S $2p_{3/2}$ at 163.58 eV and S $2p_{1/2}$ at 164.76 eV) formed through the expected interfacial Michael addition reaction (Figure 5.1e). The IR spectrum of the hybrid nanomaterial (Figure S1, ESI) shows the appearance of the carbonyl stretching at 1704 cm^{-1} due to the presence of the AuNP's Maleimides. Transmission electron microscopy (TEM) images of the hybrid nanomaterial (Figure 5.2a) confirm that AuNP are linked to the surface of CNT bundles, that they kept their original size distribution, and that there are no unbound particles present, confirming the efficiency of our washing procedure. Indeed, the use of sonication favours the detachment of those AuNP that are physisorbed on the CNT leaving just those that are covalently bonded.[8]

To exclude the possibility of unspecific bonding of the AuNP to the SWCNT–SH, a control experiment was carried out under identical conditions and following the same experimental procedure but using the model Me-EG_3-AuNP. The Me-EG_3-AuNP, because of the absence of the Maleimide functionality, are not expected to react with the thiol-modified CNT because they cannot undergo the Michael addition reaction. Figure 5.2b is related to this control experiment and shows, as expected, completely clean CNT, confirming the successful synthesis of AuNP-decorated SWCNT through the Michael addition reaction between SWCNT–SH and Maleimide–AuNP.

Sonication was employed to test the stability and resilience of the final hybrid material. A fraction of SWCNT–AuNP was dispersed in water and sonicated for one hour. Its TEM images were then compared with those of the freshly prepared SWCNT–AuNP and they did not show any appreciable difference either in the density of chemisorbed AuNP or in the AuNP size distribution. This supports the efficiency of our synthetic approach and the resilience of the resulting AuNP–CNT hybrid.

In summary we have shown for the first time that water-soluble Maleimide–AuNP can be efficiently attached to thiol-modified CNT through a versatile interfacial Michael addition reaction. Because of the ability to run the chemistry in water, due to the solubility of the Maleimide–AuNP, the rate of the Michael addition is fast and results in a

hybrid material that is densely covered with AuNP. The robustness of this AuNP–CNT hybrid is due to the covalent bond linking the nanoparticle to the CNT and because the functionalization reaction involves the ligand of the organic shell of the nanoparticle and not due to s gold core. Our methodology presented here can be exploited to functionalize any carbonaceous material (*i.e.*, graphene, nano- diamonds, glassy carbon) with AuNP or any other functional molecular material as long as the appropriate PEG–Maleimide can be prepared. It is possible to take advantage of the intrinsic presence of carboxylic group on the surfaces of these materials to introduce thiol functionalities through the coupling reaction described here. These thiol-modified materials would then be able to bind Maleimide functionalities through the Michael addition reaction as shown in this work.

5.2 References

(1) S. Iijima, *Nature*, 1991, **354**, 56.

(2) D. Connolly, S. Currivan and B. Paull, *Proteomics*, 2012, **12**, 2904.

(3) W. R. Yang, P. Thordarson, J. J. Gooding, S. P. Ringer and F. Braet, *Nanotechnology*, 2007, **18**, 412001.

(4) E. Frackowiak and F. B´eguin, *Carbon*, 2002, **40**, 1775.

(5) I. Capek, *Adv. Colloid Interface Sci.*, 2009, **150**, 63.

(6) R. Zanella, E. V. Basiuk, P. Santiago, V. A. Basiuk, E. Mireles, I. Puente-Lee and J. M. Saniger, *J. Phys. Chem. B*, 2005, **109**, 16290.

(7) N. Chauhan, A. Singh, J. Narang, S. Dahiya and S. C. Pundir, *Analyst*, 2012, **137**, 5113.

(8) P. Gobbo, S. Ghiassian, M. Hesari, K. G. Stamplecoskie, N.Kazemi-Zanjani,F.Lagugn´e-LabarthetandM.S.Workentin, *J. Mater. Chem.*, 2012, **22**, 23971.

(9) J. Huang, X. Xing, X. Zhang, X. He, Q. Lin, W. Lian and H. Zhu, *Food Res. Int.*, 2011, **44**, 276.

(10) D. Cai, Y. Yu, Y. Lan, F. J. Dufort, G. Xiong, T. Paudel, Z. Ren, D. J. Wagner and T. C. Chiles, *BioFactors*, 2007, **30**, 271.

(11) Y. Guo, S. Guo, Y. Fang and S. Dong, *Electrochim. Acta*, 2010, **55**, 3927.

(12) L. Jiang and L. Gao, *Carbon*, 2003, **41**, 2923.

(13) K. Jiang, A. Eitan, L. S. Schadler, P. M. Ajayan, R. W. Siegel, N. Grobert, M. Reyes-Reyes, H. Terrones and M. Terrones, *Nano Lett.*, 2003, **3**, 275.

(14) A. V. Ellis, K. Vijayamohanan, R. Goswami, N. Chakrapani, L. S. Ramanathan, P. M. Ajayan and G. Ramanath, *Nano Lett.*, 2003, **3**, 279.

(15) L. Han, W. Wu, F. L. Kirk, J. Luo, M. M. Maye, N. N. Kariuki, Y. Lin, C. Wang and C.-J. Zhong, *Langmuir*, 2004, **20**, 6019.

(16) B. R. Azamian, K. S. Coleman, J. J. Davis, N. Hansonand, M. L. H. Green, *Chem. Commun.*, 2002, 366.

(17) J. Hu, J. Shi, S. Li, Y. Qin, Z. X. Guo, Y. Song and D. Zhu, *Chem. Phys. Lett.*, 2005, **401**, 352.

(18) X. Hou, L. Wang, X. Wang and Z. Li, *Diamond Relat. Mater.*, 2011, **20**, 1329.

(19) H. Ismaili, F. Lagugn´e-Labarthet and M. S. Workentin, *Chem. Mater.*, 2011, **23**, 1519.

(20) K. E. Snell, H. Ismaili and M. S. Workentin, *ChemPhysChem*, 2012, **13**, 3185.

(21) Z. Liu, Z. Shen, T. Zhu, S. Hou, L. Ying, Z. Shi and Z. Gu, *Langmuir*, 2000, **8**, 3569.

(22) L. Minati, G. Speranza, S. Torrengo, L. Toniutti, C. Migliaresi, D. Maniglio, M. Ferrari and A. Chiasera, *Surf. Sci.*, 2012, **604**, 1414.

(23) P. Gobbo and M. S. Workentin, *Langmuir*, 2012, **28**, 12357.

(24) M. D. Best, *Biochemistry*, 2009, **48**, 6571.

(25) W. R. Algar, D. E. Prasuhn, M. H. Stewart, T. L. Jennings, J. B. Blanco-Canosa, P. E. Dawson and I. L. Medintz, *Bioconjugate Chem.*, 2011, **22**, 825.

(26) H. Liu, B. S. Mun, G. Thornton, S. R. Isaacs, Y.-S. Shon, D. F. Ogletree and M. Salmeron, Phys. Rev. B: Condens. *Matter Mater. Phys.*, 2005, **72**, 155430.

(27) C. R. Henry, *Surf. Sci. Rep.*, 1998, **31**, 231.

Chapter 6

6 Bioorthogonal Chemistry: Development of an Effective Tool for the Functionalization of Gold Nanoparticles and Their Surfaces

Chapter 6 will be published as an account paper.

I wrote the drafts of the manuscript, with input and final edit by my supervisor, Prof. M. S. Workentin.

ABSTRACT: In recent years bioorthogonal chemistry has emerged as a tool for the investigation of biomolecular systems *in vivo* that are impossible to study using traditional methodologies. The great characteristics of these reactions and the continued expansion of the bioorthogonal toolkit furnishes invaluable opportunities not only in chemical biology, but also for the synthesis of functional nanomaterials. This account will cover our methodologies to 1) introduce bioorthogonally reactive functionalities onto the surface of AuNP and CNT substrates; 2) characterize the final reactive nanomaterial template and determine the number of bioorthogonal functionalities that have been introduced; 3) follow their interfacial reactivity and obtain proof of successful interfacial bioorthogonal chemistry. Within each of these sections there were challenges that had to be overcome, and we will describe the evolution and adaptation of our methods to the different bioorthogonal groups and nanomaterial substrates.

6.1 Introduction

In the past twenty years, materials chemistry research has started what can be called the nanomaterials revolution. The impact of nanomaterials extends from medicine, biology, and engineering, to social science and philosophy. Nanoscience, nanotechnology, nanoparticles, and nanotubes are words that have now become commonly used in our everyday life, and nanomaterial-based products are now commercially available and are changing our way of living. For example, silver nanoparticles are now applied to wall paint, floor coatings and clothes; titanium dioxide nanoparticles are used in toothpaste, chewing gum, sunscreen, and solar cells; carbon nanotubes (CNTs) are making sport equipment more elastic and resilient; gold nanoparticles (AuNPs) are commonly employed as transduction elements in pregnancy tests and to make conductive inks. All these applications are possible because of the intrinsic physical-chemical properties of nanomaterials. Silver nanoparticles have very high antibacterial properties and size and shape dependent optical properties.[1,2] Titanium oxide (TiO_2) nanoparticles have a high diffraction index, strong light scattering and incident-light reflection capability, and excellent photo-catalytical properties.[3,4] CNTs have very high strength, stiffness and tenacity, and excellent thermal and conductivity properties.[5-7] AuNPs are biocompatible, and have size and shape dependent optical properties due to surface plasmon resonance phenomena.[8-10]

In addition to the peculiar intrinsic physical-chemical properties of nanomaterials, the explosion of their applications has evolved due to development of techniques for their surface functionalization or their attachment to a substrate. To name a few examples, biomolecules (*e.g.*, enzymes, antibodies, DNA strands) need to be conjugated onto a nanomaterial's surface for the construction of biosensors;[8,11-13] contrast agents or drugs need to be bound to a nanocarrier in order to exploit its high surface to volume ratio and use it for drug delivery or biomedical imaging;[14-18] dye-sensitized solar cells can be more efficient if nanomaterial sensitizers are organized into a monolayer on a TiO_2 surface.[19] Because of these reasons, in the past decade different interfacial chemistries have been developed and tailored to each kind of nanomaterial.

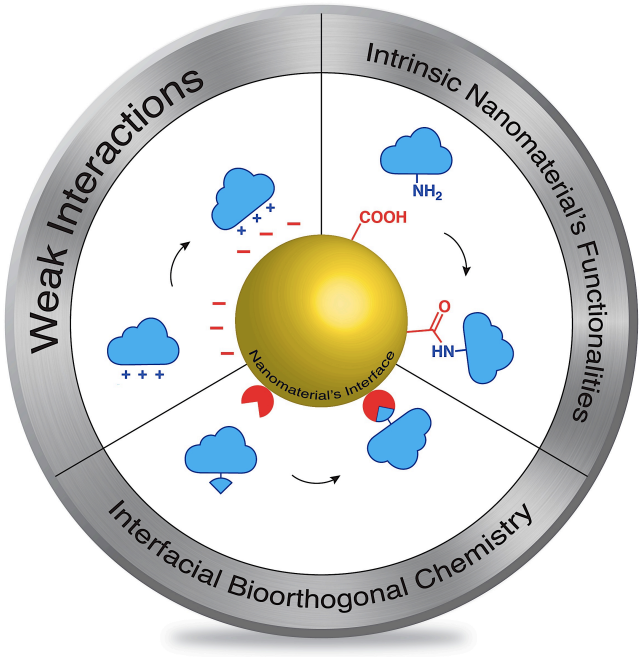

Figure 6.1: Cartoon representing the three strategies commonly employed for conjugation onto material surfaces. The cloud represents any molecular system or material of interest.

In general, there are three main strategies for the attachment of a molecular system of interest onto the nanomaterial's surface, or for the attachment of the nanomaterial to a substrate (see Figure 6.1). The first relies on weak interactions. For example, biomolecules can be electrostatically adsorbed onto a nanomaterial by exploiting the nanomaterial's surface charge;[20,21] hydrophobic molecular probes can be immobilized into a nanoparticle's organic corona by exploiting hydrophobic-hydrophilic types of interactions.[22-24] The second strategy exploits functional groups that are characteristic of the nanomaterial and are present on its surface. For example, biomolecules can be covalently bound to the CNT's surface exploiting carboxylic groups present on its defects sites.[25,26] The surface density of carboxylic groups can be also increased through preliminary chemical treatment of the nanomaterial, although this pre-treatment can lead to a modification of the CNT's physical-chemical properties.[27] The third method involves the introduction of exogenous reactive functional groups onto the nanomaterial surface. For example, biotin can be introduced onto AuNPs in order to impart on them the ability

to bind streptavidin-modified materials;[28] maleimide groups (a functional group able to undergo fast Michael addition-type of reactions and cycloaddition reactions with dienes and dipolar molecules) can be introduced onto nanotubes or nanoparticles for the facile conjugation of biomolecules onto the nanomaterial;[29-31] azides can be introduced onto quantum dots allowing them to react *in vivo* through a copper-catalyzed [3+2] Huisgen cycloaddition reaction.[32] This third strategy that relies on the creation of a reactive nanomaterial template allows for further expansion of the nanomaterial's application and utility beyond the nanomaterial's intrinsic physical-chemical properties. More specifically, it allows for 1) the formation of a resilient functionalization of the nanomaterial due to a covalent bond that forms between the nanomaterial and molecular system or substrate; 2) the expansion of the chemistry of the nanomaterial by making it reactive to diverse functional groups that would otherwise be inert towards the original nanomaterial, and 3) the exploitation of the virtually limitless potential of organic chemistry for the creation of nanomaterials that can perform specific functions.

While this third methodology is becoming more and more popular because of the reasons just explained, in order to further enhance the impact and utility of nanomaterials in science and technology, the reactive nanomaterial template must be selected so that ideally its interfacial reactivity:

1) *Is easy to perform*: that is, it does not require specific equipment and technical expertise (*e.g.*, the reaction must not be performed under inert atmosphere and must avoid the use of toxic and dangerous reagents).

2) *Has simple reaction conditions*: the reaction should go to completion at normal temperature and pressure and avoid the use of catalysts or reaction initiators.

3) *Is chemoselective*: that is, it can be performed *in vivo* and allow for the control over the orientation of the molecular system onto the nanomaterial.

4) *Has fast reaction kinetics*: so that side reactivity is minimized.

5) *Is high yielding*: that is, it leads to no byproducts or byproducts that are easy to remove, so that it makes it easy to characterize the final nanomaterial conjugate and determine the amount of introduced molecular system.

6) *Is biocompatible*: that is, it is based on reagents that are atoxic and not recognized by the metabolism of the organism under study.

The type of chemistry that best addresses all of these characteristics is bioorthogonal chemistry. Bioorthogonal chemistry is a subclass of the "click" class of reactions, and is mostly used in the field of chemical biology. In fact, bioorthogonal chemistry has been specifically designed to take place with high chemoselectivity in living organisms without interfering with the organism's biochemical processes. A bioorthogonal reaction relies on two exogenous functional groups, a *bioorthogonal functional group* and a *chemical reporter*,[33] that are not recognized by the metabolism of the organism under study. The *chemical reporter* is a small functional group (*e.g.*, azide, nitrones, ketones, aldehyde, terminal alkynes)[34] that is easy to introduce *in vivo* through metabolic or protein engineering, and is not reactive towards endogenous biological functionalities.[35]

The *bioorthogonal functional group* is instead more challenging to synthesize and too reactive to be introduced *in vivo*. It reacts with the chemical reporter quickly (rate constant $0.001 < k\ M^{-1}\ s^{-1} < 2.8 \cdot 10^{6}$), chemoselectively and at normal temperature and pressure. Examples of bioorthogonal functional groups include strained alkynes, methyl-2-(diphenylphosphino)benzoate groups, tetrazines, hydrazides, aminooxy groups, norbornenes, *trans* cyclooctenes, etc.[35] It is evident that bioorthogonal reactions give invaluable opportunities in engineering new nanomaterial templates and have the potential to amplify the impact of nanomaterials in our everyday life.

The goal of this review is to highlight the synthetic strategies and challenges behind the incorporation of *bioorthogonal functional groups* and *chemical reporters* onto nanomaterial surfaces. The synthetic strategy for the safe introduction of the desired *bioorthogonal functional group* onto the nanomaterial surface needs to exploit the nanomaterial's intrinsic surface chemistry and take into consideration the high reactivity of the bioorthogonal functional group.

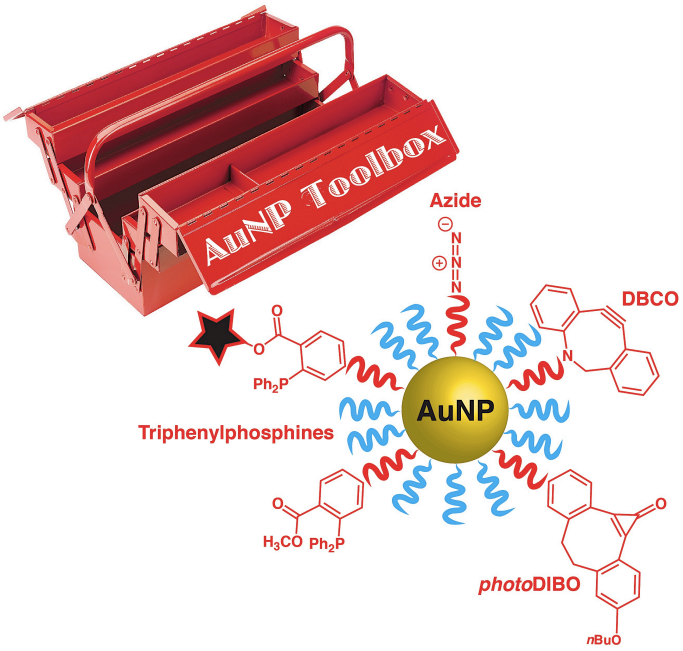

Figure 6.2: Toolbox of bioorthogonal nanomaterials successfully synthesized and that will be discussed in this account. The toolbox includes gold nanoparticles functionalized with an azide for both I-SPAAC and I-SBL reactions, a DBCO for I-SPAAC reactions, a *photo*-DIBO for the *shine n' click* I-SPAAC reaction (*vide infra*), and methyl-2-(diphenylphosphino)benzoate groups for I-SBL.

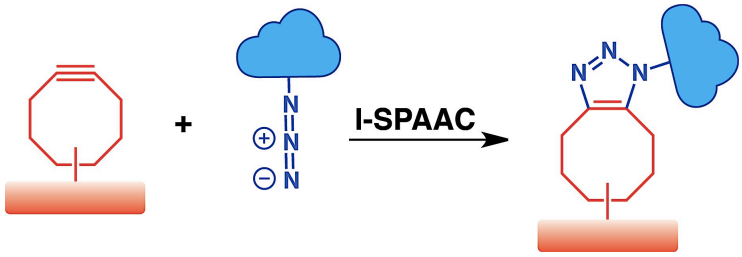

Scheme 6.1: Scheme representing the *interfacial* strain-promoted alkyne-azide cycloaddition (I-SPAAC) reaction. The red shape represents a general surface, which can be 1D (*e.g.*, CNT, nanowires etc.), 2D (*e.g.*, metal surface, graphene etc.), and 3D (*e.g.*, AuNP, quantum dots etc.); the blue cloud represent a general molecular system (or material) of interest that carries the azide chemical reporter.

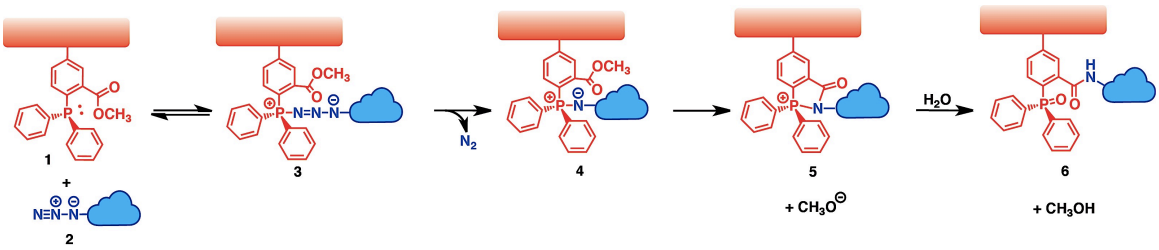

Scheme 6.2: Mechanism for the *interfacial* Staudinger-Bertozzi ligation (I-SBL). In the first reaction step triphenylphosphine (1) reacts with benzyl azide (2) to form the phosphazide complex (3). Phosphazide complex (3) undergoes unimolecular decomposition with loss of nitrogen gas to yield the aza-ylide complex (4). Subsequently, there is a cyclization step that yields complex (5) with loss of methoxide anion. The final step involves the hydrolysis of (5) by water and formation of complex (6) and methanol. The red shape represents a general surface, which can be 1D (*e.g.*, CNT, nanowires etc.), 2D (*e.g.*, metal surface, graphene etc.), and 3D (*e.g.*, AuNP, quantum dots etc.); the blue cloud represent a general molecular system (or material) of interest that carries the azide chemical reporter.

Another challenge relies on the creation of methodologies that allow for the precise quantification of the amount of introduced bioorthogonal functional groups and for the investigation of their proper interfacial reactivity. This review will discuss these challenges, bringing examples from the most recent research carried out in our research group. More specifically, we will discuss methodologies for the incorporation of bioorthogonal groups and chemical reporters onto a small water-soluble AuNP substrate for the preparation of a toolbox of bioorthogonally reactive AuNP templates (see Figure 6.2).

The first bioorthogonal groups that we successfully introduced onto the AuNP's organic corona were strained alkynes for *interfacial* strain-promoted alkyne-azide cycloaddition (I-SPAAC) reaction (see Scheme 6.1). This reaction is a version of the [3+2] Huisgen cycloaddition that takes place at room temperature without need of a copper catalyst (copper-free). Its driving force relies on a strained C-C triple bond that is embedded into an 8-member ring. We showcased the utility of the I-SPAAC for the synthesis of hybrid (bio)materials and photoreactive bioorthogonal nanomaterials.

We will also discuss strategies for the introduction of methyl-2-(diphenylphosphino)benzoate groups for *interfacial* Staudinger-Bertozzi ligation (I-SBL). The SBL is one of the first bioorthogonal reactions to be created, is historically the first to use an azide as the *chemical reporter*, and is the most chemoselective of the bioorthogonal family.[36] Originally, the Staudinger-Bertozzi ligation involved the reaction between a methyl-2-(diphenylphosphino)benzoate functional group with an azide to yield a stable amide bond (refer to Scheme 6.2). The reaction mechanism, fully investigated by F. L. Lin and coworkers in 2005,[37] involves methanol (from the methyl-ester trapping group) as a leaving group (see Scheme 6.2). This characteristic of the reaction mechanism allows for the exploitation of the I-SBL for drug delivery and makes it of extreme interest for the synthesis of functional nanomaterials. Finally, we were able to incorporate an azide onto the AuNP substrate. We used this azide-modified AuNP template in combination with its complementary bioorthogonal materials for the synthesis of nanomaterial hybrids.

Within each of these functional nanomaterial syntheses there were problems and issues that had to be overcome, and we will describe the evolution of the ideas so that readers can get a glimpse of our thinking and problem solving as we proceeded.

6.2 Small AuNP as a model substrate

In order to begin the development of bioorthogonal nanomaterial templates and methodologies for their detailed characterization, we had to select a nanomaterial substrate that would allow for easy characterization and investigation of its interfacial bioorthogonal chemistry. The choice fell on small (ϕ = 3 nm) gold nanoparticles (AuNPs) because of their approachable synthesis, the ability to synthesize them in gram scale, and the possibility of using spectroscopic techniques (*e.g.*, multinuclear magnetic resonance spectroscopy, UV-vis spectroscopy, FT-IR spectroscopy) for characterizing them and following their interfacial reactivity. The gold core of these small AuNPs is stabilized by a monolayer of triethylene glycol (TEG) mono-methyl ether thiolated ligands that makes them amphiphilic and extremely resilient.

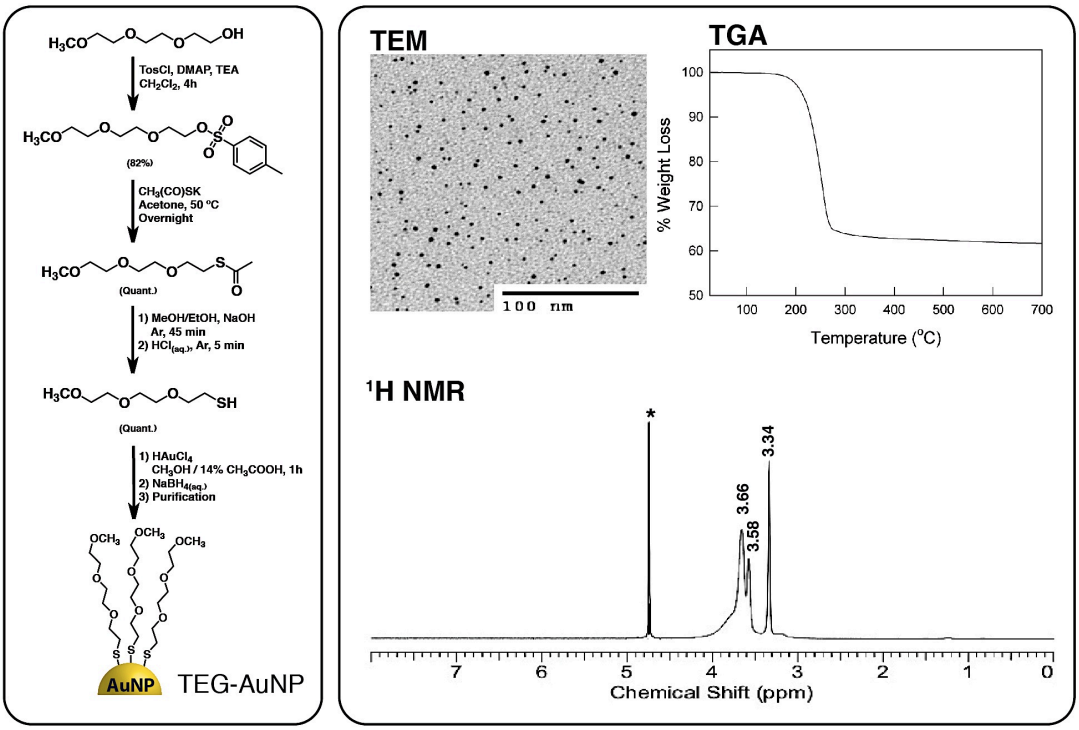

Figure 6.3: Synthesis and characterization data of TEG-AuNP substrate. Left: Synthetic approach for the synthesis of CH_3O-EG_3-SH ligands and TEG-AuNPs. The purification of the TEG-AuNP involves extraction of the AuNPs into toluene, followed by trituration using hexanes to remove excess thiols, dialysis against water, and finally centrifugation to remove residual precipitate. Right: Typical TEM, thermogravigram recorded under inert atmosphere, and ^{1}H NMR spectrum of TEG-AuNP (recorded in D_2O, * denotes residual solvent).

In fact, these TEG-AuNPs can be repeatedly dried and redissolved in water and different polar organic solvents, dissolved in strongly acidic[38] or basic solution[39], and heated at more than 100 ºC for prolonged periods[31] with little to no aggregation. The TEG-AuNPs were synthesized according to the procedure reported in Figure 6.3 and characterized by ^{1}H NMR spectroscopy, thermogravimetric analysis (TGA), and transmission electron microscopy (TEM).[31] ^{1}H NMR spectroscopy gives specific information on the nanoparticle's corona. A typical ^{1}H NMR spectrum of the TEG-AuNPs is reported in Figure 6.3 and shows typical broad peaks[40] that correspond to the protons of the ethylene glycol units and to the terminal methyl group (3.34 ppm in D_2O). The broadness of the

NMR spectrum peaks is also a good indication of the sample's purity: if sharp peaks are observed, then residual free thiolated molecules are most likely present and more care needs to be taken in performing the cleaning procedure especially before introducing electrophilic functional groups (*vide infra*).

TGA gives information on the nanoparticle's composition. A typical TGA plot is reported in Figure 6.3 and shows weight loss at ~260 ºC due to pyrolysis of the organic corona. From this data we can understand that ~62% of the weight of this size of TEG-AuNP is due to its gold core and ~38% of its weight is due to the methoxy-terminated thiolated ligands. TEM instead furnishes information specifically on the gold core shape and size distribution.

From the combination of the information obtained from these three analytical methods, and assuming that the AuNP are spherically shaped and monodispersed in size, a gold nanoparticle raw formula can be calculated using the following equations:

$$N = \frac{\pi \rho d^3 N_A}{6 M_{Au}} \qquad \textbf{(1)}$$

Where N is the number of gold atoms composing the gold core, ✗ is the density of the face centered cubic (fcc) gold lattice (19.3 g cm^{-3}), d is the average diameter of the nanoparticles in centimeters ($3 \cdot 10^{-7}$ cm) obtained from TEM images, M_{Au} is the mole atomic weight of gold (196.9665 g mol^{-1}), and N_A is the Avogadro constant. The number of thiol ligands that compose the gold core (N_L) is calculated form the following equation:

$$N_L = \frac{N \cdot M_{Au} \cdot W_{\%}}{(1-W_{\%}) \cdot MW_{MeO}} \qquad \textbf{(2)}$$

Where $W_{\%}$ is the percentage of mass loss due to the organic ligands found from the TGA measurements, and MW_{MeO} is the molecular weight of the methoxy-terminated thiolated ligand (179.3 g mol^{-1}). From these equations the calculated TEG-AuNPs raw formula is: $Au_{500}(MeO–EG_3–S)_{340}$.

These AuNPs represent an ideal substrate for developing bioorthogonal nanomaterial templates where NMR spectroscopy, TGA, and TEM allow for the determination of the amount of interfacial bioorthogonal functional groups with good precision and the monitoring of their interfacial reactivity.

6.3 Synthetic strategies

The incorporation of bioorthogonally reactive functionalities at the AuNP's interface requires the synthesis of the proper thiolated ligands carrying the desired bioorthogonal functional group. The reactive ligands that we use are based on a tetraethylene glycol spacer between the thiol head and the bioorthogonal group. This spacer preserves the AuNP amphiphilicity, ensures good packing of the monolayer around the gold core, and, because of the extra ethylene glycol unit, it allows the bioorthogonal group to extend out of the corona and be more prone to react, being less sterically hindered. There are three main synthetic strategies that we adopt for the introduction of a bioorthogonal functional group at the TEG-AuNP's interface (see Scheme 6.3). The first (and most simple) involves the use of a direct ligand exchange reaction. This reaction requires the mixing of an ethylene glycol-based thiolated ligand carrying the reactive functionality with the TEG-AuNPs in solution. The thiol head of the new ligand penetrates the monolayer that protects the gold core, attaches to the gold surface, and releases one of the triethylene glycol mono-methyl ether thiolated ligands of the TEG-AuNP starting material. The amount of bioorthogonal group to be introduced can be tuned to some extent by controlling the ratio between gold nanoparticle starting material and new thiolated ligand, and the time given for the ligand exchange reaction to occur. After ligand exchange, the nanoparticles are thoroughly washed to remove any unbound thiol. Despite its great simplicity and efficacy, this strategy can only work if the bioorthogonal group is stable in presence of thiols, which are strong nucleophiles.

To overcome this problem, the second strategy that we commonly employ relies on an interfacial coupling reaction. This method relies on the synthesis of carboxy- (or amine-) terminated thiolated ligands, which are remarkably stable, and can be introduced onto the AuNP's corona through a direct ligand exchange reaction.

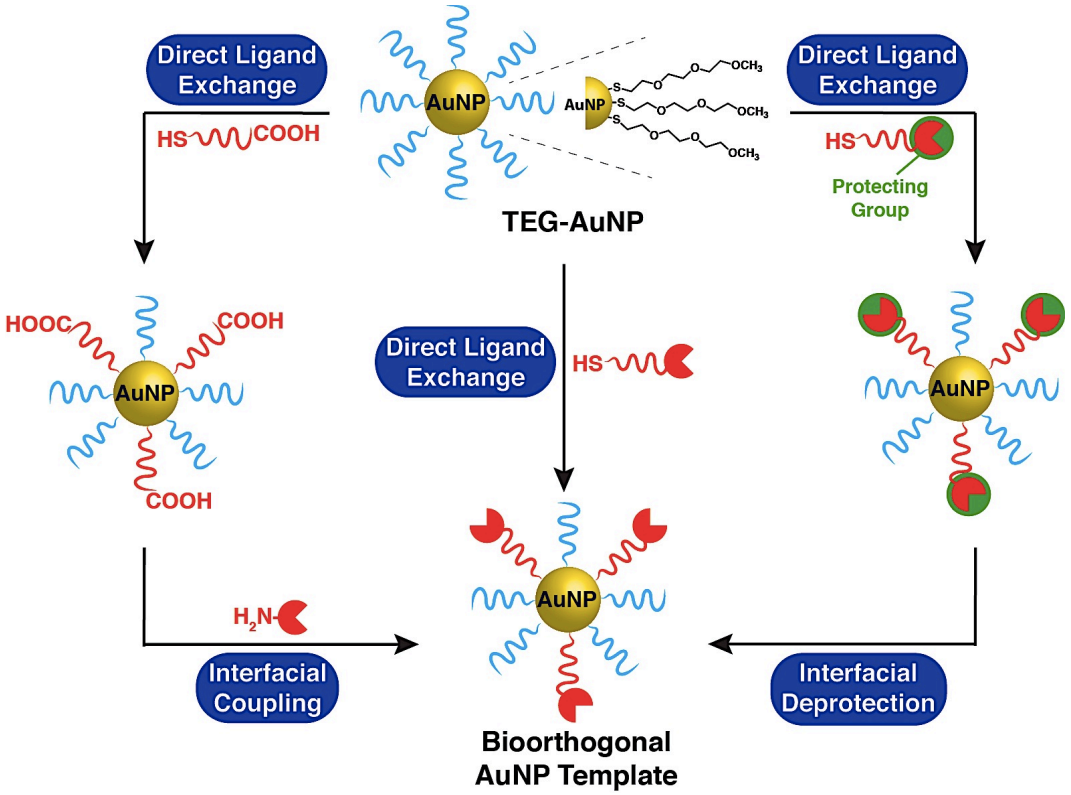

Scheme 6.3: Schematic representation of the three different methodologies that can be employed for the introduction of a bioorthogonal group onto the AuNP's corona. The red shape represents a general bioorthogonal group.

Once introduced onto the AuNPs, the carboxylic (or amine) groups can then react through a coupling reaction facilitated by a coupling agent (*e.g.*, HBTU, EDC, DCC, etc.) with the bioorthogonal moiety that carries an amine (or carboxylic) group. A similar approach based on an interfacial coupling reaction can be also employed for the introduction of reactive functional groups onto carbonaceous materials (*e.g.*, carbon nanotubes, graphene, glassy carbon, nanodiamonds), because they usually contain native carboxylic groups in their defect sites. While this second strategy is probably the most commonly used, it still relies on a highly trained user, whose skills have a high impact on the interfacial coupling yield. This method also leads to the formation of different byproducts that can get irreversibly (electrostatically or covalently) bound to the nanomaterial's surface, which, as a result, makes the determination of the amount of introduced bioorthogonal functionalities difficult or even impossible.

Finally, the third method relies on a protection-deprotection strategy (refer to Scheme 6.3). First, the bioorthogonal functionality is protected and synthetically incorporated to an ethylene glycol-based ligand containing a thiol precursor. Subsequently, the thiol is synthesized and the resulting thiolated ligand is introduced onto the AuNP's corona. The AuNPs are then thoroughly cleaned to remove any unbound thiol, and only then the protecting group is removed to regenerate the interfacial bioorthogonal functional group. This deprotection reaction must take place under conditions where the nanoparticle is stable, lead to quantitative removal of the protecting group, and to the formation of byproducts that are easy to remove. If these requirements are met, then the bioorthogonal AuNP template can be easily characterized and the amount of interfacial functionality can be determined with good precision.

The use of these strategies allowed us to introduce both bioorthogonal groups and chemical reporters onto the TEG-AuNP. In the next sections, we will discuss in detail bioorthogonal nanomaterial templates that carry strained alkynes for I-SPAAC reactions and substituted 2-(diphenylphosphino)benzoate groups for the I-SBL.

6.4 Interfacial Strain-Promoted Alkyne-Azide Cycloaddition (I-SPAAC)

The SPAAC reaction is the bioorthogonal reaction that achieved the most resounding success because of its applications for *in vivo* imaging and tracking of biomolecules. This is due to its fast reaction kinetics, clean reactivity, and good stability of the bioorthogonal group and chemical reporter. Because of these reasons the SPAAC reaction presents invaluable opportunities also for the preparation of functional nanomaterials.

The introduction of the azide chemical reporter onto the surface of AuNPs is fairly straightforward because of the great stability of this group. This allowed for the direct synthesis of the azide-terminated thiolated ligand that could be directly introduced onto the AuNP's corona through a direct ligand exchange reaction. The resulting Azide-AuNPs were characterized by ^{1}H NMR spectroscopy, FT-IR spectroscopy, TGA and TEM. The ^{1}H NMR spectrum recorded in CD_3CN showed the appearance of a new peak at 3.39 ppm related to the $–CH_2–$ alpha to the azide group. The FT-IR spectrum showed

the appearance of the asymmetrical stretching of the $-N_3$ at 2110 cm^{-1}. TGA data indicated that 35% of the organic corona is composed by the azide-terminated ligands. From the combination of the ^1H NMR, TGA and TEM data it was possible to calculate a AuNP raw formula, using a similar methodology to that used for the TEG-AuNPs. It is worth noting that for a mixed monolayer of two different thiolates ligands equation **(2)** becomes:

$$N_L = \frac{N \cdot M_{Au} \cdot W_{\%}}{(1-W_{\%}) \cdot \{MW_{MeO} \cdot M_{\%} + [MW_{N3}(1-M_{\%})]\}} \qquad \textbf{(3)}$$

where $W_{\%}$ is the percentage of mass loss due to the organic ligands found from the TGA measurements, $M_{\%}$ is the molar percentage of azide-terminated ligand obtained from the ^1H NMR spectrum, MW_{MeO} is the molecular weight of the methoxy-terminated thiolated ligand (179.3 g mol^{-1}), and MW_{N3} is the molecular weight of the azide-terminated thiolated ligand (234.3 g mol^{-1}). Under the assumptions earlier described, the average AuNP raw formula was calculated to be: $Au_{1000}(MeO–EG_3–S)_{455}(N_3–EG_4–S)_{245}$.[38,41]

The Azide-AuNPs were successfully employed for bioconjugation with strained alkyne-functionalized peptides through the I-SPAAC reaction. However, the conjugation of a strained alkyne, a dibenzocyclooctyne (DBCO), onto an RGD and a CRGDK peptide resulted to be challenging because the high reactivity of the strained C–C triple bond towards nucleophiles and the sensitivity of the DBCO to the acidic conditions required to cleave the peptide from the resin. To overcome these problems, a bioorthogonal cycloaddition/post-assembly deprotection (SPAAC-PAD) strategy was specifically designed (see Scheme 6.4). First, the desired DBCO-functionalized peptide having all the side chains protected is synthesized and conjugated onto the Azide-AuNPs through the I-SPAAC reaction, which occurs rapidly and efficiently. Finally, the peptide's side chains are deprotected by dissolving the AuNP bioconjugate in 90% TFA in CH_2Cl_2 where the AuNPs are stable.[38] If on one hand the SPAAC-PAD strategy was reliable and general, allowing the conjugation of peptides containing strongly nucleophilic residues onto AuNPs through the I-SPAAC, on the other hand the difficulty of conjugating a strained alkyne onto a biomolecule represents a drawback that needs to be overcome.

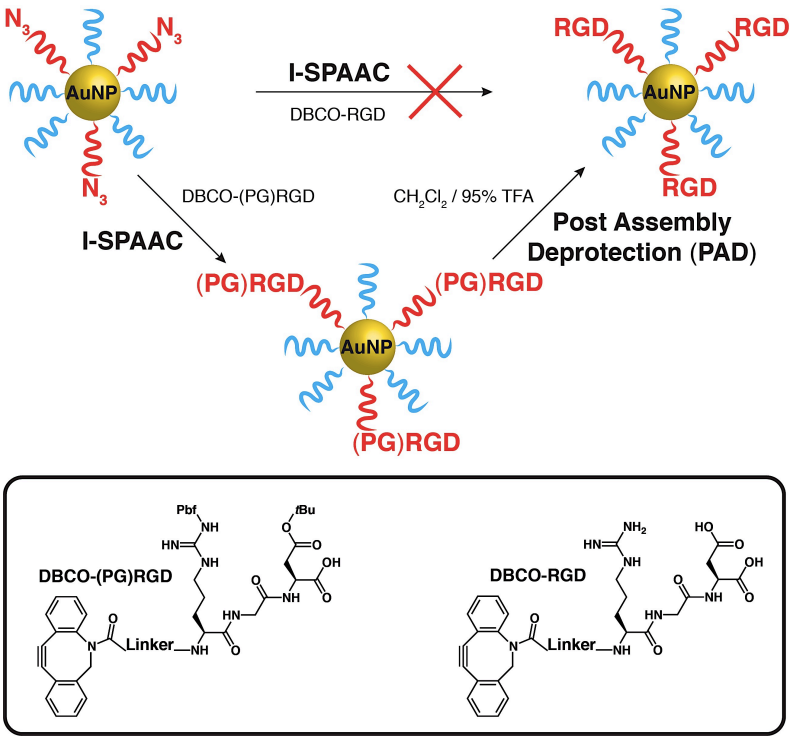

Scheme 6.4: Illustration of the I-SPAAC-PAD synthetic strategy, and structure of the peptides employed. "(PG)" stands for protecting group.

The most logical solution would be to reverse the system, that is to functionalize the biomolecule with an azide while having the strained alkyne on the AuNP. However, the synthesis and precise characterization of a strained alkyne-functionalized AuNP is just as challenging because of the impossibility of synthesizing the corresponding strained alkyne-thiol ligand. Nevertheless, we took on this challenge inspired by the idea of developing a desirable functional nanomaterial template that would be able to react with its chemical reporter through the I-SPAAC reaction even *in vivo*.

In our first work towards the synthesis of a strained alkyne-functionalized nanomaterial template, we employed the interfacial coupling approach and coupled carboxy-terminated gold nanoparticles with dibenzocyclooctyne-amine (DBCO-amine).[42] As mentioned earlier the carboxy-terminated ethylene glycol thiolated ligands are remarkably stable and could be easily introduced onto the nanoparticle's corona through a direct ligand exchange reaction.

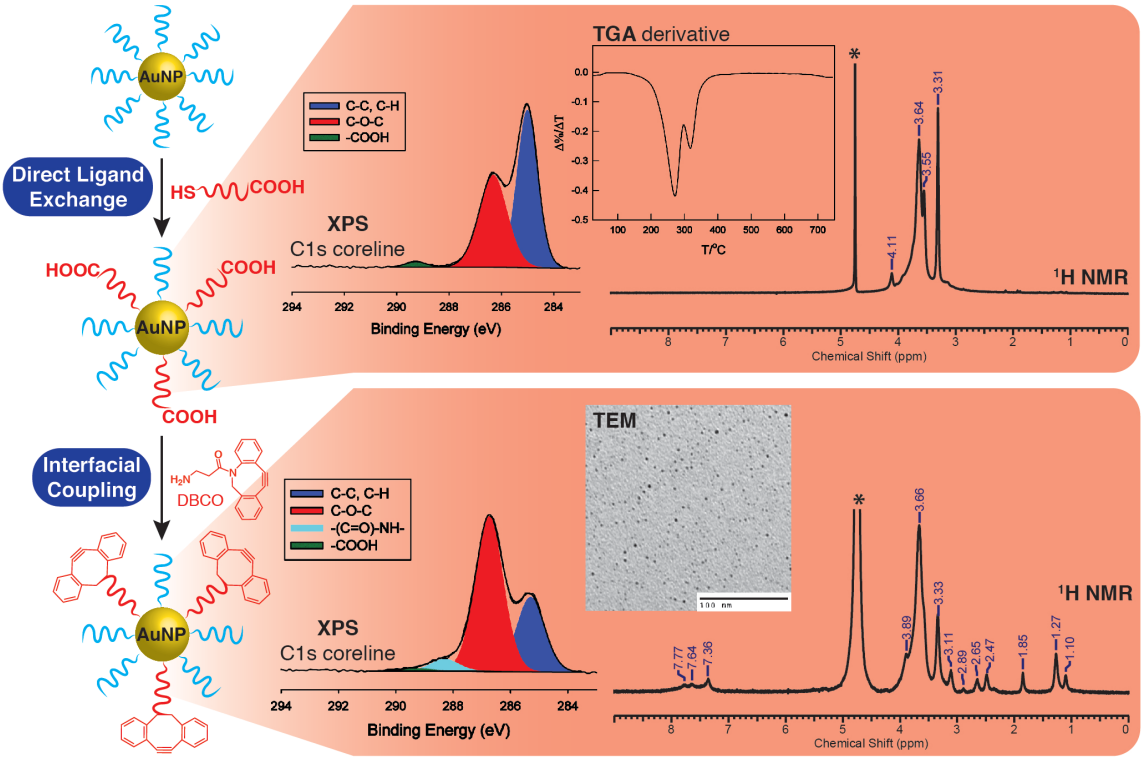

Figure 6.4: Scheme reporting the synthesis of DBCO-functionalized gold nanoparticles. The main characterization data of the carboxy-terminated AuNP and the DBCO-AuNP are also reported.

The carboxy-functionalized AuNP could be completely characterized using ^{1}H NMR spectroscopy, TGA, TEM and X-ray photoelectron spectroscopy (XPS) using a similar approach employed for the TEG-AuNP substrate. ^{1}H NMR of the carboxy-terminated AuNPs showed the appearance of a broad signal at 4.11 ppm in D_2O that is due to the CH_2 alpha to the carboxylic group (by comparison with the ^{1}H NMR of the carboxy-terminated thiolated ligand recorded in D_2O). TGA shows the decomposition of two distinct ligands: the methoxy-terminated ligand at ~260 ºC and the carboxy-terminated ligand that decomposes at ~320 ºC (compare TGA of TEG-AuNP starting material in Figure 6.3 and carboxy-terminated AuNPs in Figure 6.4). Deconvolution of the TGA derivative allows for quantification of the composition of the nanoparticles corona and a AuNP raw formula could be calculated using the same method employed for the Azide-AuNPs. Under the assumptions earlier described, the average AuNP raw formula was calculated to be: $Au_{500}(MeO–EG_3–S)_{280}(HOOC–EG_4–S)_{100}$. XPS allowed an independent

confirmation of the average amount of carboxylic groups per nanoparticles. The high-resolution spectrum of the C 1s core line clearly shows a component at 289.3 eV (see Figure 6.4) typical of carboxylic carbons that can be integrated for quantification.

Next we performed the interfacial coupling reaction for the introduction of DBCO-amine as the bioorthogonal functional group. Because DBCO-amine is exclusively organic solvent-soluble, extra care needs to be put into synthesizing carboxy-terminated AuNPs that retain amphiphilic solubility so that the interfacial coupling can be performed in polar organic solvent and be more efficient. The final strained alkyne-functionalized AuNP was fully characterized as well by employing the same set of characterization techniques, and the interfacial coupling reaction was found to have a 80% yield, as independently confirmed by ^{1}H NMR spectroscopy (by the integration of the DBCO's aromatic protons *vs* the peak at 3.32 ppm of the terminal methyl groups of the methoxy-terminated thiolated ligands) and XPS (by the integration of the N 1s peak, disappearance of the carboxylic component in the C 1s peak at 289.3 eV and appearance of a component related to the newly formed amide bond at 288.3 eV). This synthetic strategy led to the first example of a strained alkyne-modified AuNP template.

Finally, we showed their utility for the synthesis of a biohybrid material by making them react with azide-functionalized polymersomes (see Figure 6.5). This represented the first step towards the synthesis of multifunctional vesicles that can find potential use in a wide range of biomedical applications ranging from drug delivery and biomedical imaging. Most importantly, we showed that this bioorthogonal nanoparticle template represents an important technological advancement because it allows a nanomaterial to react through a [3+2] Huisgen cycloaddition in very high yield, through a simple pour and mix type of chemistry, and without the need of heat, copper catalysts or reducing agents, which can cause severe nanoparticles aggregation when used in combination with a colloidal gold solution.[43]

We were also successful in showing the generality of our synthetic approaches for the synthesis of bioorthogonal nanomaterials templates by synthesizing an alkyne-functionalized single-walled CNT (SWCNT) template.[41]

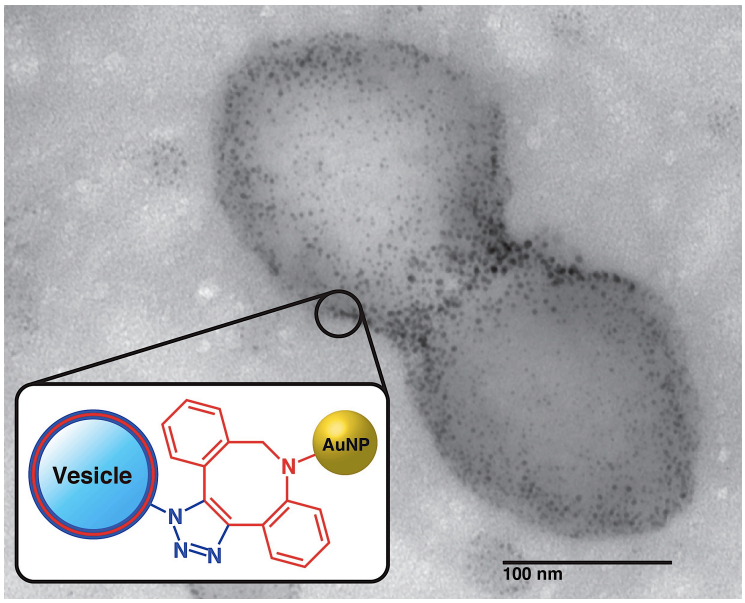

Figure 6.5: TEM image of the polymersome-AuNP biohybrid material synthesized through an I-SPAAC reaction. The DIBO-AuNPs were found to join together two different polymersomes.

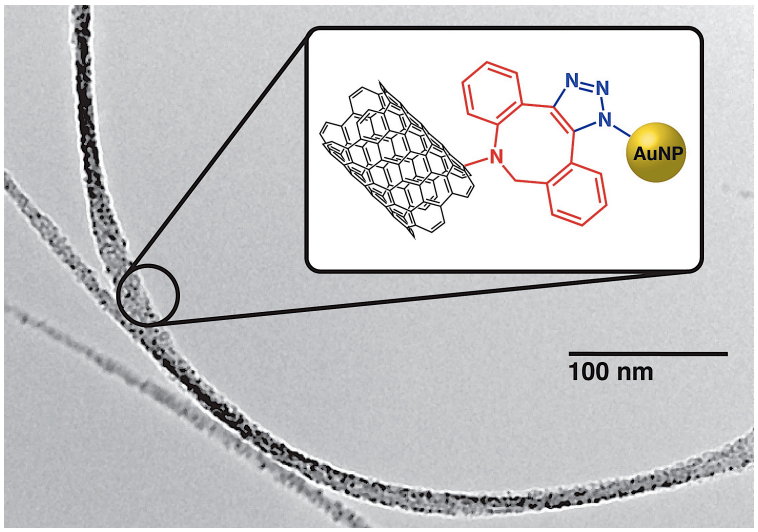

Figure 6.6: TEM image of the SWCNT-AuNP hybrid material synthesized through an I-SPAAC reaction.

For this particular synthesis we took advantage of the carboxylic functionalities present on the defects of SWCNT and performed a coupling reaction to covalently bind DBCO-amine onto the SWCNT's walls. Similarly to the DBCO-AuNPs, the bioorthogonal

SWCNT template was characterized by XPS and made to react with azide-functionalized AuNPs to showcase proof of its interfacial reactivity. The resulting AuNPs-decorated SWCNT was characterized by TEM and XPS. The recorded TEM images showed SWCNT fully and homogeneously covered by 3 nm AuNPs (see Figure 6.6). The AuNPs-SWCNT hybrid could be easily synthesized simply by mixing together the two bioorthogonal nanomaterial partners in phosphate buffer solution (pH 7), thus highlighting the ease of using the DBCO-functionalized SWCNT template for the creation nanostructured materials that can find applications as varied as catalysts, gas sensors, bioconjugation, transistors, and electrochemical sensors.

While on one side the interfacial coupling strategy for the introduction of strained alkynes on nanomaterials revealed to be very effective, its drawback lies in the formation of byproducts, which can irreversibly bind to the nanomaterial's surface, making its precise characterization difficult. This issue pushed us to explore other synthetic pathways, and in particular to design protection-deprotection strategies for strained C-C triple bonds. In the past year we were able to design two different strategies. The first relies on the reversible complexation of the C-C triple bond with dicobalt-octacarbonyl.[44] This method is commonly used in organic synthesis for the protection of linear alkynes, and the dicobalt protecting group can be removed by employing oxidizing or reducing agents. This method is generally less effective when applied to cyclic alkynes, leading to cycloalkenes, anhydrides, diiodocycloalkenes, cycloalkanones, etc.[45] However, we were successful in finding reaction conditions for the regeneration of the C–C triple bond in good yield by exposing the complex to triethylamine-*N*-oxide in dichloromethane. We then showcased the utility of this approach for the safe chemical modification of strained alkyne molecules. Unfortunately, this technology cannot be employed for the synthesis of strained alkyne AuNPs because the dicobalt-hexacarbonyl complex is unstable in the presence of thiols. However, we are currently developing uses of this strategy for the synthesis of other material templates with the goal of further expanding the scope of bioorthogonal chemistry in the materials chemistry domain.

The second protection-deprotection strategy instead relies on the use of a cyclopropenone as a precursor for a strained alkyne.

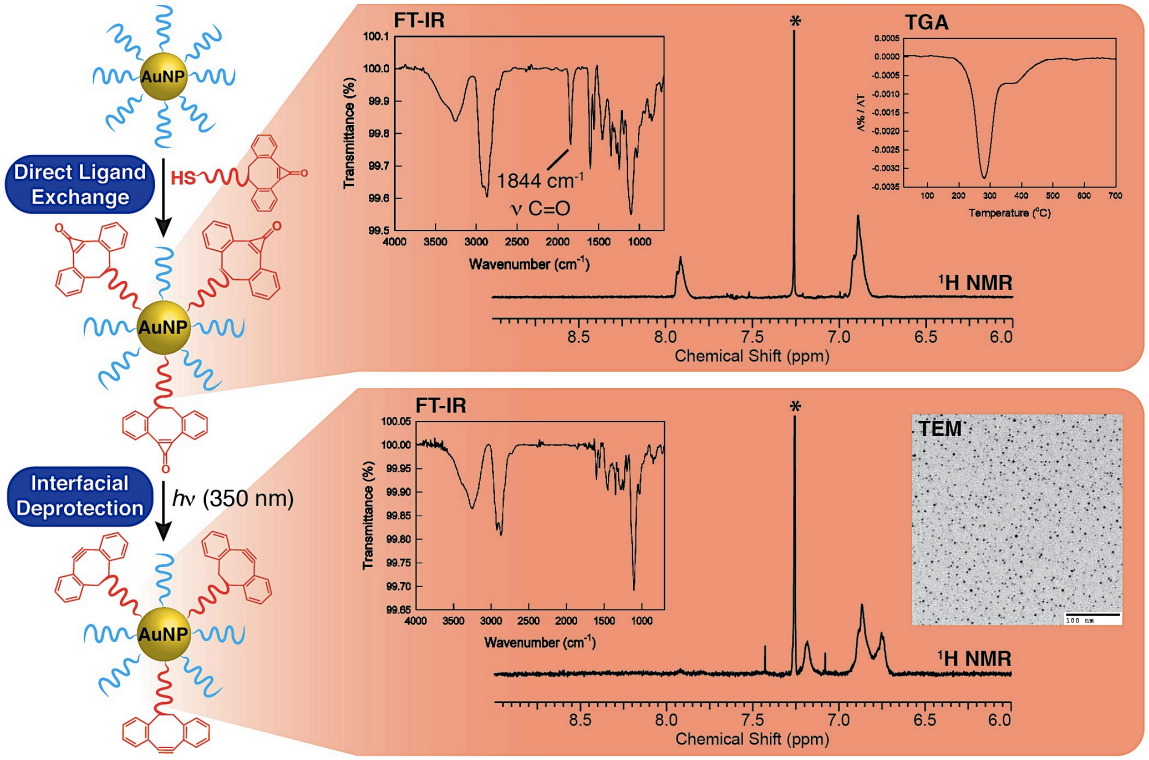

Figure 6.7: Scheme reporting the synthesis of DIBO-functionalized gold nanoparticles. The main characterization data of the *photo*DIBO-terminated AuNP and the DIBO-AuNP are also reported.

Prof. V. Popik and coworkers showed how a cyclopropenone-masked dibenzocyclooctyne (*photo*-DIBO) can undergo photo-decarbonylation under UV light to yield the parent strained alkyne in quantitative yield.[46] The characteristics of this reaction make it of extreme interest for the synthesis of a photo-switchable strained alkyne AuNP template. In collaboration with the Popik group we were recently successful in synthesizing a *photo*-DIBO-terminated thiolated ligand that is remarkably stable, and could be introduced onto the TEG-AuNP's corona through a direct ligand exchange reaction. The resulting *photo*-DIBO AuNPs were fully characterized using UV-Vis, IR, and ^{1}H NMR spectroscopy, TGA, and TEM, and the *photo*-DIBO AuNP raw formula, calculated using the methodology previously discussed, was $Au_{800}(MeO–EG_3–S)_{270}(photoDIBO–EG_4–S)_{30}$. The final DIBO-AuNP could be generated in quantitative yield (as confirmed by ^{1}H NMR and IR spectroscopy) through a photo-decarbonylation reaction by irradiating the *photo*-DIBO AuNPs at 350 nm in methanol or water.

This strategy revealed to be extremely reliable and has the potential to lead to the creation of a new class of materials that can react through a *shine and click* type of chemistry. We are currently exploring the possibility of synthesizing a family of *photo*-strained alkynes that can be photo-deprotected at different wavelengths for different applications.

6.5 Interfacial Staudinger-Bertozzi ligation (I-SBL)

As previously discussed, the SBL is a reaction that presents invaluable opportunities for the synthesis of functional nanomaterials. This is due to its high chemoselectivity and to the leaving group that is involved in its reaction mechanism.

The first step towards the synthesis of the Staudinger-AuNPs was always the synthesis of a thiolated ligand carrying the methyl-2-(diphenylphosphino)benzoate group. Our research group was able to synthesize a stable triphenylphosphine-terminated thiolated ligand, which revealed to be remarkably stable to both oxidation of the phosphorous center and of the thiol head, and could be introduced onto the TEG-AuNP's corona through a direct ligand exchange reaction (see Figure 6.5).[47] The resulting Staudinger-AuNPs were fully characterized using the same methodology employed for the other bioorthogonal AuNPs templates and their raw formula was calculated to be $Au_{1500}(MeO–EG_3–S)_{500}(Ph_3P–EG_4–S)_{200}(Ph_3P{=}O–EG_4–S)_{20}$.

Their interfacial reactivity was then investigated using benzyl azide as model azide partner molecule and the interfacial Staudinger-Bertozzi ligation was found to occur at the AuNPs interface with no changes in its mechanism. The only drawback of this reaction lies in its slow kinetics. The reaction proceeds in four days by using a 1:1 equivalents of triphenylphosphine and azide, while, by using a large excess of azide, the reaction goes to completion in 18 hours. It is noteworthy that the reactivity of the "Staudinger-AuNPs" could be monitored through ^{31}P NMR spectroscopy by the disappearance of the peak at 40.3 ppm (in $CDCl_3$) corresponding to the triphenylphosphine starting material and the appearance of the triphenylphosphine oxide product peak at 31.3 ppm (see Figure 6.8).

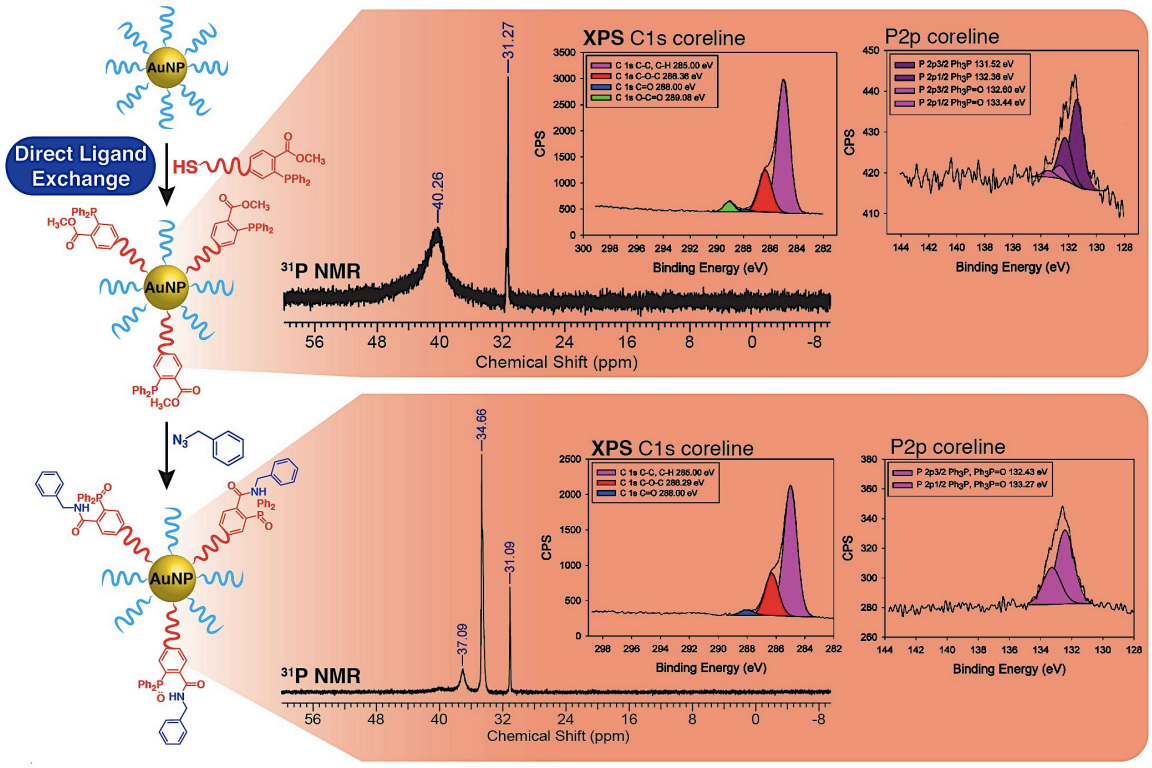

Figure 6.8: Scheme reporting the synthesis and reactivity of Staudinger-AuNPs. The main characterization data of the Staudinger-AuNPs and the Staudinger-AuNPs reacted with benzyl azide (model reaction) are also reported.

By using XPS and from the high-resolution scan of the P 2p coreline, it was also possible to obtain proof of interfacial reactivity and independently confirm the yield for the interfacial reaction (see Figure 6.8).

These two independent analytical methods showed to be very reliable for following the interfacial Staudinger-Bertozzi ligation and this represents another great advantage that derives from the use of this reaction for the preparation of functional nanomaterials. In particular, the use of XPS allows this type of reaction to be followed on solid macroscopic surfaces or if the chemical reporter is conjugated to a paramagnetic molecular systems. We showcased this by reacting the Staudinger-AuNP with an azide-functionalized nitronyl-nitroxide radical (see Scheme 6.5) and the interfacial reaction yield could be calculated by XPS from the amount of phosphine-oxide detected through

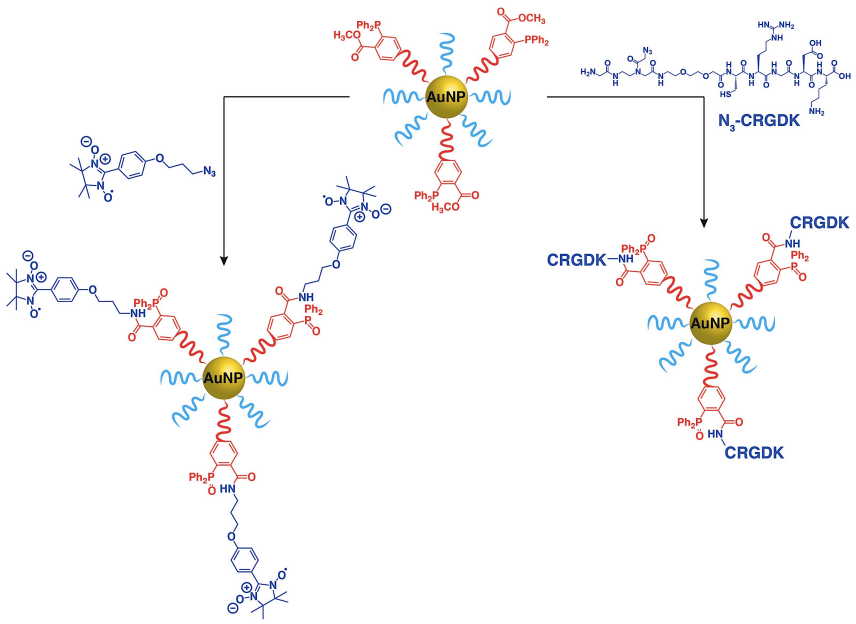

Scheme 6.5: Scheme representing the reaction of the Staudinger-AuNP with the azide-functionalized CRGDK peptide and nitronyl-nitroxide radical.

the high-resolution scans of the P 2p coreline. The data was then independently confirmed by quantitative EPR spectroscopy measurements.[48]

Because of the high chemoselectivity of the interfacial reaction, we decided to showcase its utility for bioconjugation. For this purpose, we employed an azide-functionalized CRGDK peptide containing a nucleophilic cysteine, lysine and arginine, which would have competed in the bioconjugation reaction if a strained alkyne-modified nanomaterial template was employed instead (see Scheme 6.5). Also in this case the yield for the I-SBL reaction could be easily calculated by ^{31}P NMR spectroscopy and it was independently confirmed by the analysis of the P 2p XPS peak. It is remarkable that even with such complicated molecular systems (*i.e.*, paramagnetic molecules and peptides), the extent of the I-SBL can be easily determined by using analytical techniques typical of organic chemistry and surface science.

As mentioned earlier, another advantage of the Staudinger-Bertozzi ligation relies on an alcohol leaving group (from the methyl-ester trapping group) that gets released upon chemoselective ligation.

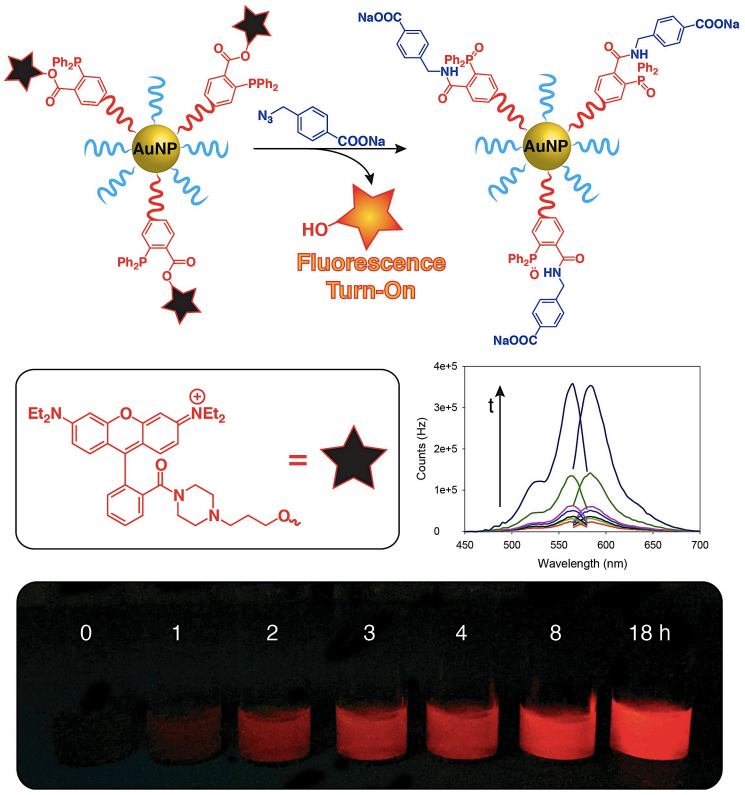

Figure 6.9: Scheme representing the fluorescence turn-on upon I-SBL reaction with benzyl azide. The star shape represents the rhodamine B fluorophore, whose fluorescence is quenched (black) when it is covalently bound to the AuNP, but it turns on (orange) upon it release into the bulk solution.

In order to exploit this characteristic of the reaction mechanism for the synthesis of a functional nanomaterial, we designed a new ligand that includes a fluorophore (a rhodamine B derivative) in place of a methyl group in the ester functionality (see Figure 6.9). This fluorescent and stable thiolated ligand was successfully introduced onto the AuNP's corona and the resulting functionalized nanoparticle was fully characterized. The fluorophore's fluorescence emission was quenched by the AuNP's core through a FRET type of mechanism,[49-51] but upon reaction of the modified triphenylphosphine with the azide partner, the fluorophore was released into the bulk solution where its fluorescence was not quenched (see Figure 6.9). This represented the first example of a nanomaterial sensor that is based on the SBL and the first step towards the creation of new

nanotechnology that can find application in drug delivery, biosensing, and biomedical imaging.

6.6 Conclusion and outlook

The continuous emergence of new nanomaterials and techniques for carefully controlling their size, shape and physical-chemical properties seems to represent a limitless source of new opportunities in science and technology. The creation of synthetic strategies for the modification of nanomaterial surfaces by the introduction of (bio)orthogonal moieties that allow the nanomaterial to react reliably, efficiently, and chemoselectively and perform specific functions has the potential to further enhance the impact of nanomaterials and lead to unprecedented directions in the field. Furthermore, the ease with which these bioorthogonal nanomaterial templates can be reacted with their *chemical reporter* allows them to be employed by users with very basic chemistry skills. This makes it possible to quickly develop new uses for them in the most diverse disciplines of science and technology.

However, the main challenge behind the realization of a toolbox of bioorthogonally reactive nanomaterial templates lies in the design of synthetic strategies that are tailored to each (bio)orthogonal group and nanomaterial. Furthermore, there is the need to develop methodologies for the characterization of the final template and to furnish proof of its proper interfacial reactivity, which must be tailored to each employed nanomaterial substrate as well. Our research group just started the first steps towards these long-term goals by developing synthetic strategies for the introduction of strained alkynes and substituted 2-(diphenylphosphino)benzoate functional groups onto AuNPs and CNTs as the nanomaterial substrates, and by developing the use of multinuclear magnetic resonance spectroscopy and XPS for characterizing their interfacial reactivity.

Finally, by merging nanomaterials chemistry and interfacial (bio)orthogonal chemistry, it is possible to pave the way towards the development of a new generation of nanomaterials able to simultaneously perform different functions. These multitasking nanodevices, or *nanobots* (as Asier Unciti-Broceta named them)[52] will lead to a new

phase of the nanomaterial revolution and will have a much deeper impact on our everyday life.

6.7 References

(1) Rycenga, M.; Cobley, C. M.; Zeng, J.; Li, W. Y.; Moran, C. H.; Zhang, Q.; Qin, D.; Xia, Y. N. *Chem. Rev.* **2011**, *111*, 3669.

(2) Rai, M.; Yadav, A.; Gade, A. *Biotechnol. Adv.* **2009**, *27*, 76.

(3) Sang, L. X.; Zhao, Y. X.; Burda, C. *Chem. Rev.* **2014**, *114*, 9283.

(4) Ren, R.; Wen, Z. H.; Cui, S. M.; Hou, Y.; Guo, X. R.; Chen, J. H. *Sci. Rep.* **2015**, *5*.

(5) Ajayan, P. M. *Chem. Rev.* **1999**, *99*, 1787.

(6) Dai, H. J. *Acc. Chem. Res.* **2002**, *35*, 1035.

(7) Sun, Y. P.; Fu, K. F.; Lin, Y.; Huang, W. J. *Acc. Chem. Res.* **2002**, *35*, 1096.

(8) Saha, K.; Agasti, S. S.; Kim, C.; Li, X. N.; Rotello, V. M. *Chem. Rev.* **2012**, *112*, 2739.

(9) Langille, M. R.; Personick, M. L.; Zhang, J.; Mirkin, C. A. *J. Am. Chem. Soc.* **2012**, *134*, 14542.

(10) Arvizo, R. R.; Bhattacharyya, S.; Kudgus, R. A.; Giri, K.; Bhattacharya, R.; Mukherjee, P. *Chem. Soc. Rev.* **2012**, *41*, 2943.

(11) Wang, J. *Electroanalysis* **2005**, *17*, 7.

(12) Jiang, Z. W.; Le, N. D. B.; Gupta, A.; Rotello, V. M. *Chem. Soc. Rev.* **2015**, *44*, 4264.

(13) Walcarius, A.; Minteer, S. D.; Wang, J.; Lin, Y. H.; Merkoci, A. *J. Mater. Chem. B* **2013**, *1*, 4878.

(14) Giljohann, D. A.; Seferos, D. S.; Daniel, W. L.; Massich, M. D.; Patel, P. C.; Mirkin, C. A. *Angew. Chem. Int. Edit.* **2010**, *49*, 3280.

(15) Yeh, Y. C.; Creran, B.; Rotello, V. M. *Nanoscale* **2012**, *4*, 1871.

(16) Luo, Z. T.; Zheng, K. Y.; Xie, J. P. *Chem. Commun.* **2014**, *50*, 5143.

(17) Mieszawska, A. J.; Mulder, W. J. M.; Fayad, Z. A.; Cormode, D. P. *Mol. Pharm.* **2013**, *10*, 831.

(18) Pissuwan, D.; Niidome, T.; Cortie, M. B. *J. Control. Release* **2011**, *149*, 65.

(19) Sambur, J. B.; Novet, T.; Parkinson, B. A. *Science* **2010**, *330*, 63.

(20) Fahmi, M. Z.; Chang, J. Y. *Rsc Adv.* **2014**, *4*, 56713.

(21) Narayan, S.; Rajagopalan, A.; Reddy, J. S.; Chadha, A. *Rsc Adv.* **2014**, *4*, 1412.

(22) Liu, Y.; Tu, D.; Zhu, H.; Ma, E.; Chen, X. *Nanoscale* **2013**, *5*, 1369.

(23) Tonga, G. Y.; Jeong, Y.; Duncan, B.; Mizuhara, T.; Mout, R.; Das, R.; Kim, S. T.; Yeh, Y. C.; Yan, B.; Hou, S.; Rotello, V. M. *Nat. Chem.* **2015**, *7*, 597.

(24) Stewart, A. F.; Lee, A.; Ahmed, A.; Ip, S.; Kumacheva, E.; Walker, G. C. *ACS nano* **2014**, *8*, 5462.

(25) Li, R.; Wang, X.; Ji, Z.; Sun, B.; Zhang, H.; Chang, C. H.; Lin, S.; Meng, H.; Liao, Y. P.; Wang, M.; Li, Z.; Hwang, A. A.; Song, T. B.; Xu, R.; Yang, Y.; Zink, J. I.; Nel, A. E.; Xia, T. *ACS nano* **2013**, *7*, 2352.

(26) Chen, Y.; Star, A.; Vidal, S. *Chem. Soc. Rev.* **2013**, *42*, 4532.

(27) Flavin, K.; Kopf, I.; Del Canto, E.; Navio, C.; Bittencourt, C.; Giordani, S. *J. Mater. Chem.* **2011**, *21*, 17881.

(28) Sonnichsen, C.; Reinhard, B. M.; Liphardt, J.; Alivisatos, A. P. *Nat. Biotechnol.* **2005**, *23*, 741.

(29) Liu, Z.; Tabakman, S. M.; Chen, Z.; Dai, H. *Nat. Protoc.* **2009**, *4*, 1372.

(30) Oh, E.; Susumu, K.; Blanco-Canosa, J. B.; Medintz, I. L.; Dawson, P. E.; Mattoussi, H. *Small* **2010**, *6*, 1273.

(31) Gobbo, P.; Workentin, M. S. *Langmuir* **2012**, *28*, 12357.

(32) Zhang, P.; Liu, S.; Gao, D.; Hu, D.; Gong, P.; Sheng, Z.; Deng, J.; Ma, Y.; Cai, L. *J. Am. Chem. Soc.* **2012**, *134*, 8388.

(33) Prescher, J. A.; Bertozzi, C. R. *Nat. Chem. Biol.* **2005**, *1*, 13.

(34) Patterson, D. M.; Nazarova, L. A.; Prescher, J. A. *ACS Chem. Biol.* **2014**, *9*, 592.

(35) Jewett, J. C.; Bertozzi, C. R. *Chem. Soc. Rev.* **2010**, *39*, 1272.

(36) Saxon, E.; Bertozzi, C. R. *Science* **2000**, *287*, 2007.

(37) Lin, F. L.; Hoyt, H. M.; van Halbeek, H.; Bergman, R. G.; Bertozzi, C. R. *J. Am. Chem. Soc.* **2005**, *127*, 2686.

(38) Wang, X. X.; Gobbo, P.; Suchy, M.; Workentin, M. S.; Hudson, R. H. E. *Rsc Adv.* **2014**, *4*, 43087.

(39) Weissman, M.; Winger, K. T.; Ghiassian, S.; Gobbo, P.; Workentin, M. S. *Bioconjugate Chem.* **2016**.

(40) Liu, X.; Yu, M.; Kim, H.; Mameli, M.; Stellacci, F. *Nat. Commun.* **2012**, *3*, 1182.

(41) Gobbo, P.; Novoa, S.; Biesinger, M. C.; Workentin, M. S. *Chem Commun (Camb)* **2013**, *49*, 3982.

(42) Gobbo, P.; Mossman, Z.; Nazemi, A.; Niaux, A.; Biesinger, M. C.; Gillies, E. R.; Workentin, M. S. *J. Mater. Chem. B* **2014**, *2*, 1764.

(43) Ismaili, H.; Alizadeh, A.; Snell, K. E.; Workentin, M. S. *Can. J. Chem.* **2009**, *87*, 1708.

(44) Gobbo, P.; Romagnoli, T.; Barbon, S. M.; Price, J. T.; Keir, J.; Gilroy, J. B.; Workentin, M. S. *Chem. Commun.* **2015**, *51*, 6647.

(45) Green, J. R. *Eur. J. Org. Chem.* **2008**, 6053.

(46) Poloukhtine, A. A.; Mbua, N. E.; Wolfert, M. A.; Boons, G. J.; Popik, V. V. *J. Am. Chem. Soc.* **2009**, *131*, 15769.

(47) Gobbo, P.; Luo, W.; Cho, S. J.; Wang, X.; Biesinger, M. C.; Hudson, R. H.; Workentin, M. S. *Org. Biomol. Chem.* **2015**, *13*, 4605.

(48) Stephanie M. Barbon; Pierangelo Gobbo; Wilson Luo; Jacquelyn T. Price; Mark C. Biesinger; Mark S. Workentin; Gilroy, J. B. *Synlett* **2016**, *27*, 304.

(49) Sapsford, K. E.; Berti, L.; Medintz, I. L. *Angew. Chem. Int. Ed.* **2006**, *45*, 4562.

(50) Mayilo, S.; Kloster, M. A.; Wunderlich, M.; Lutich, A.; Klar, T. A.; Nichtl, A.; Kurzinger, K.; Stefani, F. D.; Feldmann, J. *Nano Lett.* **2009**, *9*, 4558.

(51) Dulkeith, E.; Morteani, A. C.; Niedereichholz, T.; Klar, T. A.; Feldmann, J.; Levi, S. A.; van Veggel, F. C.; Reinhoudt, D. N.; Moller, M.; Gittins, D. I. *Phys. Rev. Lett.* **2002**, *89*, 203002.

(52) Unciti-Broceta, A. *Nat. Chem.* **2015**, *7*, 538.

Chapter 7

7 Peptide-decorated gold nanoparticles via strain-promoted azide–alkyne cycloaddition and post assembly deprotection

Chapter 7 has been published as a communication, and it is reproduced with permission from the Royal Society of Chemistry. The corresponding reference is: X. Wang†, **P. Gobbo**†, M. Suchy, M. S. Workentin*, R. H. E. Hudson*, *RSC Advances*, **2014**, *4*, 43087-43091.

Wang, supervised by Prof. Hudson, and I contributed equally to the work. Wang synthesized and characterized the peptides employed in this work. Suchy synthesized the DBCO linker. I synthesized and characterized the azide-AuNP and the peptide-AuNP. Wang and I wrote the drafts of the manuscript, with input and minor edits from the other co-author and final edit by Prof. R. H. E. Hudson and Prof. M. S. Workentin.

The supporting information file referenced in the text can be downloaded from the web site of the publisher.

ABSTRACT: A new method combining an interfacial strain-promoted azide–alkyne cycloaddition and post assembly deprotection (SPAAC-PAD) has been developed for the well-defined functionalization of small, water-soluble gold nanoparticles with oligopeptides.

7.1 Introduction, Results and Discussion

Due to their excellent biocompatibility, physical properties, and easily modified surfaces, gold nanoparticles (AuNPs) are being investigated for their use in medical applications such as imaging, clinical diagnosis and drug delivery systems.[1–3] The progress of AuNPs in these fields has led to the Food and Drug Administration (FDA) approval for AuNP-based in vitro diagnostic systems in clinical trials for cancer treatments.[4] To develop effective systems for targeted cancer diagnosis and therapies, it is necessary to functionalize AuNPs with biomolecules such as DNA, proteins and peptides. Peptide–AuNP conjugates have been exploited recently as contrast agents and nanocarriers in targeted imaging for early stage cancer diagnosis and in the pharmaceutical field for targeted intracellular drug/gene delivery, respectively.[2,5]

The main challenge of conjugation of peptides to AuNPs lies in understanding and controlling the interfacial chemistry between the peptide and the nanomaterial surface on the molecular scale. The reported strategies for bioconjugation of AuNPs with peptides include sulfur–gold bond formation by the direct reaction of cysteine-terminated peptides with the gold surface and electrostatic interactions between a particle and peptides that have been coupled to bovine serum albumin (BSA).[6] Although the first method is operationally easy to perform, it is difficult to achieve a high degree of substitution.

AuNP bioconjugation *via* electrostatic interactions has good stability in aqueous solution, but the layer-by-layer assembly results in large hydrodynamic radii of nanoparticles, which limits their application under certain conditions, and offers poor control over the degree of functionalization. Alternatively, a strategy via amide bonds formation involving a water-soluble carbodiimide, *N*-(3-dimethylaminopropyl)-*N*-ethylcarbodiimide hydrochloride (EDC), was developed for bioconjugation of AuNPs. Carboxylic groups can be activated by EDC and reacted with primary amines through a condensation reaction to yield amide bonds. Moreover, sulfo-NHS (*N*-hydroxy sulfosuccinimide) is used to increase the stability of active intermediates in coupling reactions via the formation of active ester functional groups with carboxylates. EDC/NHS coupling has been widely used in preparation of AuNP–peptide conjugates.[7] However, this method is still a challenge as quite often, the peptides do not couple efficiently to AuNPs.[8,9]

Additionally, EDC/NHS coupling method is not very selective as it involves the reaction between an amine and carboxylic acid groups, which widely exist in peptides.[10]

In order to overcome the aforementioned difficulties, recent effort has focused on the use of "click chemistry" for conjugation of AuNPs with biomolecules.[8] For example, the copper-catalyzed azide–alkyne cycloaddition has been utilized to conjugate large azido-containing AuNPs with alkyne functionalized horseradish peroxidase (HRP).[9] However, the requirement of using copper ion as catalyst complicates the reaction and could increase *in vivo* biological toxicity. The strain-promoted azide–alkyne cycloaddition (SPAAC), also known as Cu-free alkyne–azide cycloaddition, can be used to overcome these problems. The SPAAC reaction has been developed as a powerful bio-conjugation tool that displays outstanding chemoselectivity, excellent biocompatibility and takes place under very mild reaction conditions. Since its first development,[11] much effort has been directed toward the synthesis of cycloalkynes with increased ring strain (to accelerate the reaction) and higher hydrophilic character (for *in vivo* applications). The challenge behind the syntheses of these interesting molecules relies on finding the right balance between reactivity and chemoselectivity. Indeed, the greater the ring strain, the more susceptible the triple bond is to nucleophilic attack (*i.e.*, addition reactions or rearrangement of cyclooctynes) thus lowering the chemoselectivity towards the cycloaddition with an azide. For example, it has been reported that highly strained biarylazacyclooctynone and analogous bioconjugation reagents undergo rearrangement and addition reactions leading to tetracyclic products.[12] The rate of rearrangement was found to be accelerated as the concentration of acid increased. This is problematic because concentrated TFA, such as 95% TFA with scavengers, is the typical reagent for cleavage of peptides from solid supports like Wang resin, Rink Amide resin, etc. together with the removal of the side chain protecting groups. This limits the applications of strained alkynes for preparation of clickable peptides. Additionally, strained alkynes have been shown to undergo side reactions with cellular cysteines and other nucleophilic residues.[13,14] However, nucleophilic side chain functionalities, such as hydroxyl (Tyr, Ser, Thr), amino (Lys), guanidine (Arg) or sulfhydryl (Cys), widely exist in bioactive peptides and may react with highly reactive cyclooctynes through a nucleophilic attack.[15]

This also limits the application of SPAAC. Interestingly, the application of interfacial SPAAC for bioconjugation of AuNPs with peptides has not yet been disclosed.

Herein, we report a novel general method for the synthesis of AuNP-bioconjugates that takes into account the side reactivity of the strained alkynes and therefore combines an interfacial SPAAC with a post assembly deprotection (PAD) for the conjugation of dibenzocyclooctyne (DBCO)-oligopeptides to small, water-soluble azide–AuNPs. We show how this general approach overcomes the aforementioned drawbacks and extends the application of SPAAC to the bioconjugation of metallic nanoparticles in a quick, reliable and facile way. Importantly, we show that the undesired side reactions of the strained alkyne in the presence of concentrated TFA and with nucleophilic sites on peptides are avoided through mild cleavage condition and retention of side-chain protecting groups on the peptides during the SPAAC reaction. The protecting groups can then be easily removed, *i.e.* post assembly deprotection or PAD, under reaction conditions that preserve the integrity of the gold core, and the AuNP bioconjugate can be easily purified by dialysis. Finally, the amount of conjugated peptide can be easily calculated.

To showcase this SPAAC-PAD strategy we employed azide–AuNPs based on tri- and tetra-ethylene glycol ligands that impart both water- and organic solvent-solubility to final AuNPs. The amphiphilicity is useful for manipulating the AuNP in organic solvents to facilitate both the SPAAC reaction and the deprotection reaction, as well as maintaining solubility in water for further in vivo applications.

The azide–AuNPs were prepared and characterized following our previously reported procedure.[16] Briefly, triethylene glycol-monomethyl ether AuNP (Me-EG_3-AuNP) with a gold core diameter of 3 ± 0.5 nm were synthesized via a modified Brust-Schiffrin method. The azide ligand N_3-EG_4-SH was synthesized and introduced onto the surface of Me-EG_3-AuNP using a place-exchange reaction. In a typical synthesis 42.5 mmol of N_3-EG_4-SH were stirred for 20 min in acetone and in presence of 50 mg of Me-EG_3-AuNP. The free thiols were subsequently removed by trituration of the dried AuNP film first with hexanes and followed by isopropanol. Azide–AuNPs were characterized by

thermogravimetric analysis (TGA), transmission electron microscopy (TEM) and FT-IR spectroscopy. The IR spectrum of resulting AuNPs showed the appearance of asymmetrical stretching of the azide group at 2110 cm^{-1} (Figure S3a, ESI). TGA data indicated that the corona of the AuNP is composed of 35% of azide ligands (Figure S5, ESI) and thus these nanoparticles contain azide functionalities at a concentration of 0.745 mmol mg^{-1}. Based on ^{1}H NMR spectrum and TGA data, and assuming that the nanoparticles have a spherical shape and that their size is monodispersed, we can estimate a nanoparticle formula of $Au_{1000}(Me\text{-}EG_3\text{-}S)_{455}(N_3\text{-}EG_4\text{-}S)_{245}$ (calculation reported in ESI).

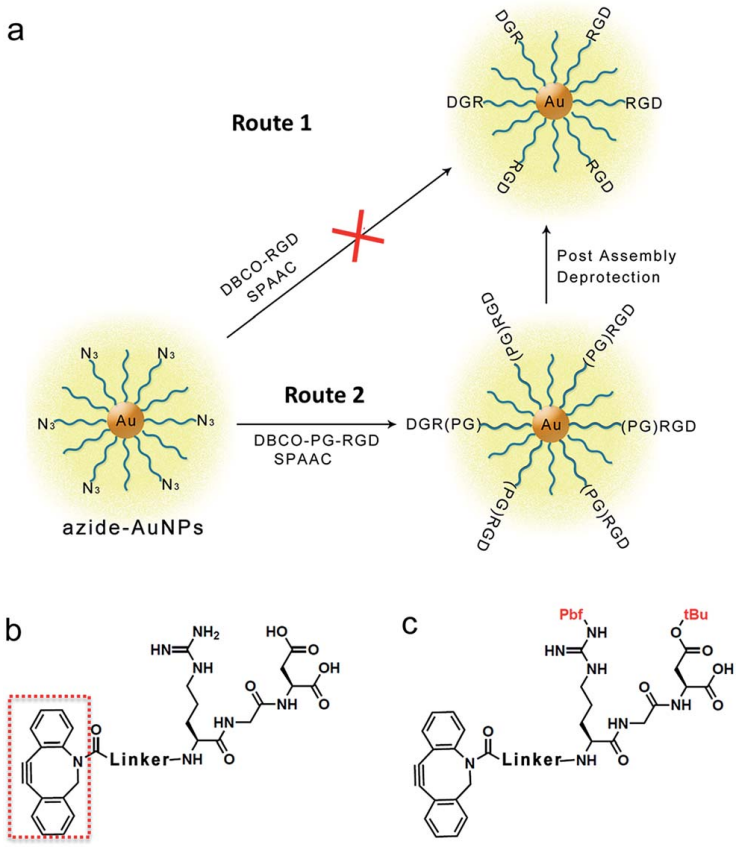

Scheme 7.1: Illustration of the attempted routes for the bioconjugation of azide–AuNPs with RGD peptide via SPAAC-PAD. a) Use of an unprotected peptide (Route 1) or use of a protected peptide (Route 2), b) and c) molecular structures of "DBCO"-RGD and DBCO-(PG)RGD. Protecting groups (PG) are Pbf and tBu.

The effectiveness of our SPAAC-PAD approach is shown through the example of bioconjugation of the arginylglycylaspartic acid (RGD) peptide. This peptide was chosen because it has targeting relevance- it is well-known to be specifically recognized by the integrin $\alpha_v\beta_3$ receptor and can act as tumour and angiogenesis marker.[17,18] In Scheme 7.1 two potential routes are illustrated for bioconjugation of the azide–AuNP with the RGD peptide. The first approach (Route 1, Scheme 7.1), involves preparing a "naked" peptide consisting of a dibenzocyclooctyl (DBCO) moiety connected *via* a polyethylglycol (PEG) linker to the RGD tripeptide (hereafter named "DBCO"-RGD). After preparation PEG-containing RGD, DBCO was constructed to the peptide via standard peptide coupling reaction. The resulting peptide, "DBCO"-RGD, was cleaved from the resin and deprotected by using 95/5 TFA/TES. After purification, it was then directly reacted with the azide–AuNP. The second approach (Route 2, Scheme 7.1) applies a construct possessing a side-chain protected peptide fragment (DBCO-(PG)RGD). It is noteworthy that dilute TFA (5/5/90 TFA/TES/DCM) was used as the reagent for cleavage of the peptide from the resin and for retention of protecting groups on peptide side chains. The peptide reacted with the azide–AuNPs *via* an I-SPAAC and all protecting groups were removed in a post-assembly deprotection step.

To undertake the approach described by Route 1, RGD peptide was synthesized via standard Fmoc solid-phase peptide synthesis (SPPS) procedure using rink amide resin as the solid support (Scheme S1, ESI) and DBCO acid was coupled to N- terminus of the peptide. Cleavage from the resin and protecting group removal was done in one step by treatment with 95/5 TFA/TES. The resulting native peptide was purified by HPLC and characterized by ESI-MS (Figure S1a and S2a, ESI). The observed molecular mass of 849.3472 was in agreement with the calculated mass (849.3657). In spite of this, close examination of the UV-spectrum of the peptide (Figure S2a, ESI) indicated that the chromophore was changed from DBCO (Figure S2d, ESI), thus implying decomposition of DBCO had occurred.

A control experiment was carried out to determine if the standard Fmoc-based oligomerization chemistry cleavage condition of concentrated TFA induced decomposition of DBCO. Starting with DBCO amine, we measured its purity by HPLC

before and after treatment with 95% TFA/DCM (rt, 1 h). HPLC analysis of the reaction mixture, along with subsequent ^{1}H NMR and high resolution mass spectral analysis, clearly showed the complete consumption of starting material and the production of several products (Figure S2d and e, ESI). The two major components of the mixture, *i.e.* the peaks with retention time of 20–20.5 min and of 26–26.5 min (Figure S2e) do not correspond to DBCO. On-line monitoring showed significant changes the UV spectrum indicating structural changes in the chromophore. The ^{1}H NMR spectra of the two isolated compounds (Figure S7b and c, ESI) confirmed neither was DBCO (Figure S7a, ESI). Mass spectral analysis showed that the earlier eluting peak retained the same mass as DBCO implying a molecular rearrangement had occurred,[12] while the later eluting peak possessed a greater mass. It is also noteworthy that the UV spectrum of the first peak in Figure S2e showed strong absorbance at 344 nm, which has also been detected in UV spectrum of "DBCO"-RGD (Figure S2a, ESI), indicating that DBCO on peptide RGD had decomposed under the standard cleavage condition of 95% TFA. To study the stability of the DBCO moiety toward TFA, DBCO was exposed to a series of solutions of 0–50% TFA/DCM for 1 h at room temperature. Under these conditions, DBCO was found to be stable when the TFA concentration was less than 30%.

Another control experiment was performed to model the interfacial SPAAC reaction by using "DBCO"-RGD peptide with an azide, namely ω-azido-triethylene glycol-monomethyl ether (Me-EG_3-N_3) as the reactive partner. The reactions were carried out in either water or acetonitrile solutions and the course of the reaction was monitored by UPLC/ESI-MS. Only the two starting materials were detected over 4 hours, indicating that the "DBCO"-RGD peptide and Me-EG_3-N_3 were not undergoing the SPAAC. Independently we determined that the Me-EG_3-N_3 was capable of participating in SPAAC with DBCO. Therefore, "DBCO"-RGD lost the ability of click and cannot be used as clickable peptide for bioconjugation of AuNPs. As a control for further study, the peptide "DBCO"-RGD was still added into azide–AuNPs (azide group : peptide, 1 : 1.2 ratio). The mixture was stirred in water at room temperature for 1 h. After removal of solvent, AuNPs were purified by centrifugal filtration (Millipore centrifugal filter units MWCO 10 kDa). As expected, characterization of these AuNPs by IR spectroscopy

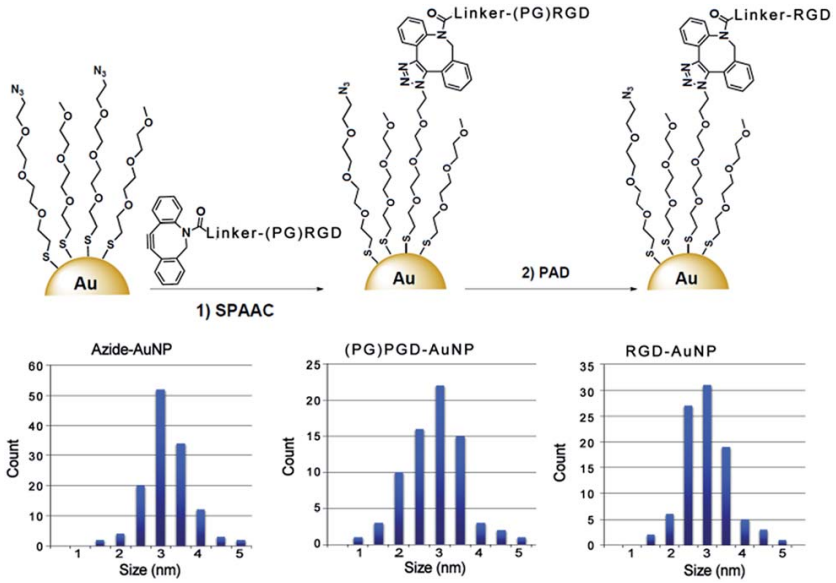

Figure 7.1: Bioconjugation of AuNPs with RGD peptide via SPAAC-PAD, 1) acetonitrile, room temperature, 1 h; 2) 90% TFA/DCM, room temperature, overnight; and AuNP size distributions obtained from the corresponding TEM image of RGD-functionalized AuNPs via SPAAC- PAD.

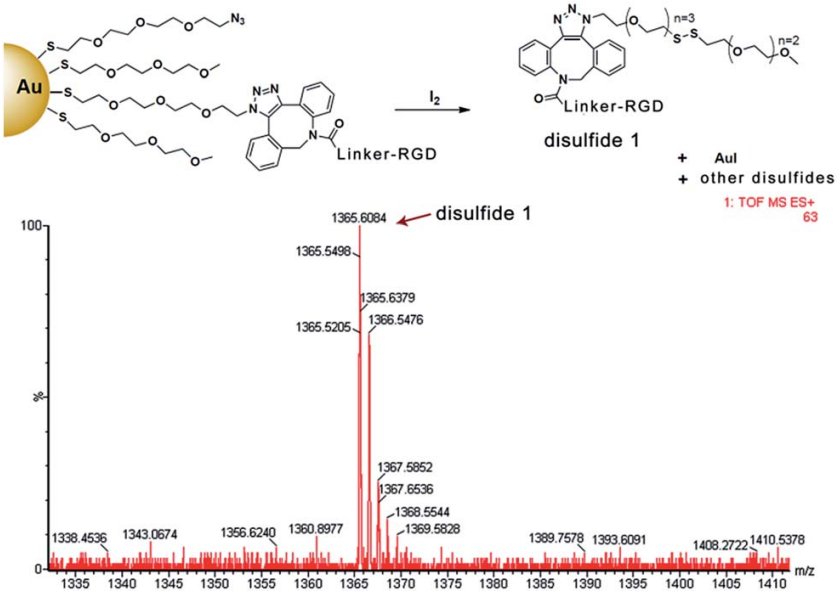

Figure 7.2: Re-oxidation of RGD–AuNPs by iodine. Disulfide 1 was characterized by ESI-MS. Calculated 1364.5992 and found 1365.6084 [1+] m/z.

showed the absorption of the azide group at 2110 cm^{-1} was still present with similar intensity to the starting material, which indicated lack of SPAAC reactivity, and showed no stretching at 1685 cm^{-1} corresponding to the amide functional groups. To circumvent the problem of decomposition of DBCO, Route 2 was devised. First we prepared DBCO-(PG)RGD by using a mild cleavage condition, it was then clicked to the azide–AuNP and subsequently the peptide was deprotected (Scheme 7.1). To synthesize the DBCO-(PG)RGD, the acid sensitive 2-chlorotritylchloride resin was used as solid support. The synthesis of DBCO-containing peptide followed the above procedure, except that the cleavage was performed with TFA/TES/DCM (5/5/90). This treatment effected the cleavage of the peptide from the resin but left the protecting groups intact and did not destroy DBCO (Scheme S2, ESI). The resulting protected peptide was purified by HPLC and characterized by ESI-MS (Figure S1b and S2b, ESI). The UV spectrum of DBCO-(PG)RGD showed the agreement with DBCO with absorbance at 290 nm and 308 nm. A model click was carried out with DBCO-(PG)RGD and Me-EG_3-N_3 in acetonitrile. Characterization of the reaction by UPLC/ESI-MS showed successful click, indicating that DBCO was not destroyed in the cleavage step. Then SPAAC between azide–AuNPs and DBCO-(PG)RGD was simply performed by adding them (azide : peptide, 1 : 1.2) in acetonitrile and stirring the resultant mixture at room temperature for 1 h (Figure 7.1). After reaction, the AuNPs were purified by using centrifugal filtration (Millipore centrifugal filter units MWCO 10 kDa) and washed with 60% MeOH/H_2O until no unreacted peptide was observed in the UPLC/ESI-MS analysis of the filtrate. The unreacted peptide was recovered from the filtrate and washings and the amount indicates that approximately 31% of the azide groups on AuNPs had reacted. Therefore, the approximate nanoparticle formula can be calculated as Au_{1000}((PG)RGD-linker-S)$_{75}$(N_3-EG_4-S)$_{170}$($MeEG_3S$)$_{450}$. The IR spectrum of the purified (PG) RGD–AuNPs showed that the azide stretching mode at 2110 cm^{-1} had markedly decreased while it had not changed in Route 1 (Figure S3c, ESI). Additionally, concomitant with the azide disappearance the appearance of stretching at 1685 cm^{-1} corresponding to the amide functional groups was observed, indicating that the protected peptide was covalently bonded to the AuNP via the Cu-free cycloaddition. To remove the protecting groups of the peptide, the AuNPs were then treated with 90% TFA/DCM at room temperature overnight to ensure complete

deprotection. It is important to note that these small oligo-ethylene glycol-based AuNP are perfectly stable under these acidic conditions. TEM images recorded before and after this acidic treatment confirmed that the relatively harsh condition for PAD did not adversely affect the AuNP size distribution (Figure 7.1). The obtained RGD–AuNPs were then purified by dialysis using cellulose ester dialysis membranes (6–8 KDa MWCO).

To further confirm that the interfacial SPAAC reaction had proceeded, the deprotected RGD–AuNPs were reacted with molecular iodine. Oxidation of AuNPs with iodine dissolved the gold into a mixture of Au(I) and Au(III) complexes and released the corona ligands as disulphides.[19] The structure of the most possible disulphide molecule produced by this reaction is shown in Figure 7.2. The mixture of disulphides was characterized by ESI-MS and the mass 1365.6084 [M + H]+ m/z agrees well with the calculated mass of 1364.5992 for the proposed disulphide 1. Importantly the mass for the corresponding disulphide with the protected peptide was not observed, indicating that the complete deprotection was achieved. This confirms the successful bioconjugation of AuNPs with a short oligopeptide via SPAAC-PAD without interference with side chains of the peptide. Moreover, efficient substitution was achieved on the surface of small size AuNPs with 31% of the azide groups reacting with the RGD peptide. This result is comparable with the reported conjugation of AuNPs with peptides via covalent bonding,[20] with the difference that this AuNP-bioconjugate was obtained through a simple and rapid pour-and-mix chemistry under ambient temperature and atmosphere while the purification only involved centrifugation and dialysis. The final calculated molecular raw formula of this AuNP is Au_{1000}(RGD- linker-S)$_{75}$(N_3-EG_4-S)$_{170}$($MeEG_3S$)$_{450}$.

To test the versatility of this method we employed a peptide with different nucleophilic residues. In particular because it has been reported that in presence of reduced peptidylcysteine residues, strained cyclooctynes mainly react via thiol-yne addition instead of SPAAC reaction,[15] we decided to synthesize a CRGDK peptide and conjugate it to the azide–AuNPs via our SPAAC-PAD strategy. This peptide has an additional interest because it is a neuropilin-1 (Nrp-1) receptor-targeted peptide for cancer treatment.[7,21,22]

For these experiments, we followed the same procedure as previously discussed with the noted exception. The CRGDK peptide was synthesized *via* standard Fmoc SPPS method and DBCO acid was coupled to the N-terminus. A change in the acid strength for resin cleavage (0.5% TFA/DCM) was made to preserve the trityl thioether protecting group of cysteine. After SPAAC-PAD, the CRGDK-functionalized AuNPs were characterized by IR (Figure S3e, ESI). The azide stretch in the IR spectrum became weaker compared to the azide–AuNPs before conjugation and the stretching at 1685 cm^{-1} corresponded to the functional groups of peptide bond appeared, suggesting successful conjugation through the I-SPAAC-PAD. Also, a new absorbance at 2692 cm^{-1} indicated the existence of the thiol group of cysteine and shows that the side chain of cysteine that would otherwise react with cyclootyne *via* thiol-yne addition did not interfere with the I-SPAAC reaction with the aid of PAD. Decomposition of the AuNPs by treatment with excess I_2 followed by ESI-MS analysis showed the two most possible disulfide molecules expected after a successful I-SPAAC-PAD (Figure S1e, ESI), and no trace of protected peptide was found. Therefore, our strategy showed to be also effective in creating small AuNP–oligopeptide bioconjugates in presence of nucleophilic residues that could otherwise attack the strained alkyne bond.

In summary, we have created a new, efficient, easy method to implement general approach to the synthesis of AuNP–peptide bioconjugates that combines the I-SPAAC reaction with post assembly deprotection. Using this strategy, peptides with protected side chains can be conjugated onto gold nanoparticles *via* I-SPAAC and all protecting groups can then be easily removed by PAD. The mild reaction conditions preserve the integrity of the alkyne so that it may perform the SPAAC reaction and the conjugated AuNPs are sufficiently robust to undergo peptide deprotection without deleterious effects. The approach presented herein usefully expands the repertoire of existing methods and presents an easy, reliable and quick way to functionalize AuNPs with short oligopeptides where the extent of incorporation of the interfacial biomolecule can be easily quantified. We anticipate that the demonstrated methodology for peptide–AuNP bioconjugation via the SPAAC-PAD will enable the fabrication of gold nanoparticles with a high degree of complexity with biomolecules for a variety of applications in

targeted cancer diagnosis and therapies. Targeted CT imaging studies of the functionalized AuNPs is currently underway.

7.2 References

(1) Z. Luo, K. Zheng and J. Xie, *Chem. Commun.*, 2014, **50**, 5143– 5155.

(2) H. Liu, Y. Xu, S. Wen, Q. Chen, L. Zheng, M. Shen, J. Zhao, G. Zhang and X. Shi, *Chem.–Eur. J.*, 2013, **19**, 6409–6416.

(3) B. Aydogan, J. Li, T. Rajh, A. Chaudhary, S. J. Chmura, C. Pelizzari, C. Wietholt, M. Kurtoglu and P. Redmond, *Mol. Imag. Biol.*, 2010, **12**, 463–467.

(4) S. K. Libutt, G. F. Paciotti, A. A. Byrnes, H. R. Alexander Jr, W. E. Gannon, M. Walker, G. D. Seidel, N. Yuldasheva and L. Tamarkin, *Clin. Cancer Res.*, 2010, **16**, 6139–6149.

(5) A. N. Shirazi, D. Mandal, R. K. Tiwari, L. Guo, W. Lu and K. Parang, *Mol. Pharm.*, 2013, **10**, 500–511.

(6) F. Porta, G. Speranza, Z. Krpeti, V. D. Santo, P. Francescato and G. Scari, *Mater. Sci. Eng.*, B, 2007, **140**, 187–194.

(7) A. Kumar, H. Ma, X. Zhang, K. Huang, S. Jin, J. Liu, T. Wei, W. Cao, G. Zou and X.-J. Liang, *Biomaterials*, 2012, **33**, 1180–1189.

(8) D. Bartczak and A. G. Kanaras, *Langmuir*, 2011, **27**, 10119– 10123.

(9) M.-X. Zhang, B.-H. Huang, X.-Y. Sun and D.-W. Pang, *Langmuir*, 2010, **26**, 10171–10176.

(10) C.-F. Wang, E. M. M ¨akil ¨a, M. H. Kaasalainen, D. Liu, M. P. Sarparanta, A. J. Airaksinen, J. J. Salonen, J. T. Hirvonen and H. A. Santos, *Biomaterials*, 2014, **35**, 1257.

(11) N. J. Agard, J. A. Prescher and C. R. Bertozzi, *J. Am. Chem. Soc.*, 2004, **126**, 15046–15047.

(12) M. Chigrinova, C. S. McKay, L.-P. B. Beaulieu, K. A. Udachin, A. M. Beauchemin and J. P. Pezacki, *Org. Biomol. Chem.*, 2013, **11**, 3436–3441.

(13) P. V. Chang, J. A. Prescher, E. M. Sletten, J. M. Baskin, I. A. Miller, N. J. Agard, A. Lo and C. R. Bertozzi, *Proc. Natl. Acad. Sci. U. S. A.*, 2010, **107**, 1821–1826.

(14) K. E. Beatty, J. D. Fisk, B. P. Smart, Y. Y. Lu, J. Szychowski, M. J. Hangauer, J. M. Baskin, C. R. Bertozzi and D. A. Tirrell, *ChemBioChem.*, 2010, **11**, 2092–2095.

(15) R. van Geel, G. J. M. Pruijn, F. L. van Del Delft and W. C. Boelens, *Bioconjugate Chem.*, 2012, **23**, 392–398.

(16) P. Gobbo, S. Novoa, M. C. Biesinger and M. S. Workentin, *Chem. Commun.*, 2013, **49**, 3982–3984.

(17) M. D. Pierschbacher and E. Ruoslahti, *Nature*, 1984, **81**, 5985–5988.

(18) M. D. Pierschbacher and E. Ruoslahti, *Proc. Natl. Acad. Sci. U. S. A.*, 1984, **81**, 5985–5988.

(19) L. Sun, R. M. Crooks and V. Chechik, *Chem. Commun.*, 2001, 359–360.

(20) Y.-H. Kim, J. Jeon, S. H. Hong, W.-K. Rhim, Y.-S. Lee, H. Youn, J.-K. Chung, M. C. Lee, D. S. Lee, K. W. Kang and J.-M. Nam, *Small*, 2011, **7**, 2052–2060.

(21) A. Kumar, S. Huo, X. Zhang, J. Liu, A. Tan, S. Li, S. Jin, X. Xue, Y. Zhao, T. Ji, L. Han, H. Liu, X. Zhang, J. Zhang, G. Zou, T. Wang, S. Tang and X. Liang, *ACS Nano*, 2014, 4205–4220.

(22) T. Wei, J. Liu, H. Ma, Q. Cheng, Y. Huang, J. Zhao, S. Huo, X. Xue, Z. Liang and X.-J. Liang, *Nano Lett.*, 2013, **13**, 2528– 2534.

Chapter 8

8 Versatile strained alkyne modified water-soluble AuNPs for interfacial strain promoted azide–alkyne cycloaddition (I-SPAAC)

Chapter 8 has been published as a communication, and it is reproduced with permission from the Royal Society of Chemistry. The corresponding reference is: **P. Gobbo**, Z. Mossman, A. Nazemi, A. Niaux, M. C. Biesinger, E. R. Gillies, M. S. Workentin*, *J. Mater. Chem. B*, **2014**, *2*, 1764-1769.

Mossman and Niaux were two undergraduate students under my direct co-supervision, along with my supervisor, Prof. M. S. Workentin. Mossman and Niaux helped with the synthesis and characterization of the compounds reported in this work. Nazemi, under the supervision of Prof. Gillies, prepared the azide-functionalized vesicles. I wrote the draft of the manuscript, with input and minor edits from the other co-authors and final edit by my supervisor, Prof. M. S. Workentin.

The supporting information file referenced in the text can be downloaded from the web site of the publisher.

ABSTRACT: Versatile water- and organic solvent-soluble AuNPs that incorporate an interfacial strained alkyne capable of efficient pour and mix strain promoted interfacial cycloadditions with azide partners have been synthesized and carefully characterized for the first time. The use of XPS to quantitate the loading of the strained alkyne on the AuNPs is noteworthy. The reactivity towards the interfacial strain promoted azide–alkyne cycloaddition reaction was demonstrated by using azide-decorated polymersomes as bioorthogonal reaction partners.

8.1 Introduction, Results and Discussion

The strain promoted alkyne–azide cycloaddition (SPAAC) is a bioorthogonal reaction designed as a tool for *in vivo* imaging and tracking of biomolecules. The power of this reaction relies on its rapid kinetics, chemoselectivity and biocompatibility. Therefore, it represents an important technological step that not only allows the spatial resolution of living organisms, but also furnishes unique temporal aspects of bioprocesses that happen in vivo.[1–8] Recent success in the application of the SPAAC reaction has been shown by C. R. Bertozzi and co-workers to follow *in vivo* the glycan evolution during the zebrafish development.[9,10] These characteristics not only make this reaction highly useful in biochemistry, but also provide invaluable opportunities in designing new materials. Surprisingly, given its broad application in biological applications, the use of the SPAAC reaction has been limited in the latter context so far. The SPAAC reaction has been used for the synthesis of dendrons and dendrimers.[11–13] Johnson and co-workers used the reaction to synthesize photodegradable star polymers.[14] Popik and co-workers prepared dibenzocyclooctyne (DBCO)-modified glass, silicon and quartz surfaces and showed their potential applications as platforms for the generation of multicomponent surfaces.[15,16] Bernardin and co-workers synthesized monosaccharide-functionalized quantum dots for *in vivo* metabolic imaging through the reaction between cyclooctyne-modified quantum dots and azide modified monosaccharides.[17] Recently we employed the SPAAC to create a carbon nanotube (CNT)–AuNP hybrid material by the interfacial reaction between a DBCO-modified CNT and an azide-modified AuNP.[18]

For the first time, we describe here a method for the synthesis of AuNPs that incorporate an interfacial strained alkyne moiety that can be used as a reactive template and undergo an interfacial SPAAC reaction (I-SPAAC) with azide modified reagents. A particular strength of this method is that it allows for a careful quantification of the amount of interfacial strained alkynes. This information is of particular relevance for potential application of these AuNPs in drug delivery and bioconjugation. The amount of interfacial strained alkynes was estimated through two independent methods: a combination of TGA and ^{1}H NMR data,[19] and through high-resolution XPS analysis. This novel bioorthogonal nanomaterial represents a desirable template for diverse applications

thanks to its biocompatibility (unlike quantum dots) and the size dependent properties of AuNPs combined with the reactivity properties of the SPAAC. In particular the rapid chemoselective reaction of these DBCO–nanoparticles is the main factor that distinguishes this novel nanomaterial from other clickable nanoparticles (*i.e.*, maleimide-functionalized nanoparticles) commonly used for bioconjugation and drug delivery.[20–23] Another important characteristic is that it displays both organic solvent solubility and water-solubility, despite the strong organic character of the interfacial DBCO moieties. The water-soluble AuNP based on tri- and tetra-ethylene glycol ligands that are used as the scaffold for our synthesis serves as a phase-transfer agent for overcoming one of the major drawbacks of the SPAAC reaction, which is the poor solubility of strained alkynes in water media.[1,24] For these reasons the DBCO–AuNPs represent an extremely versatile framework that can be functionalized with potentially any azide modified molecular systems in an easy and straightforward way. Herein, as proof of concept, we used azide-functionalized polymersomes as their reacting partners to show the potential of the DBCO–AuNPs in constructing covalent biohybrid materials, and furnishing the first example of an I-SPAAC reaction on the new strained alkyne-functionalized AuNPs. The resulting hybrid materials were prepared simply through a pour and mix chemistry in aqueous media, and the resulting vesicles were found to be functionalized with ~3 nm AuNPs.

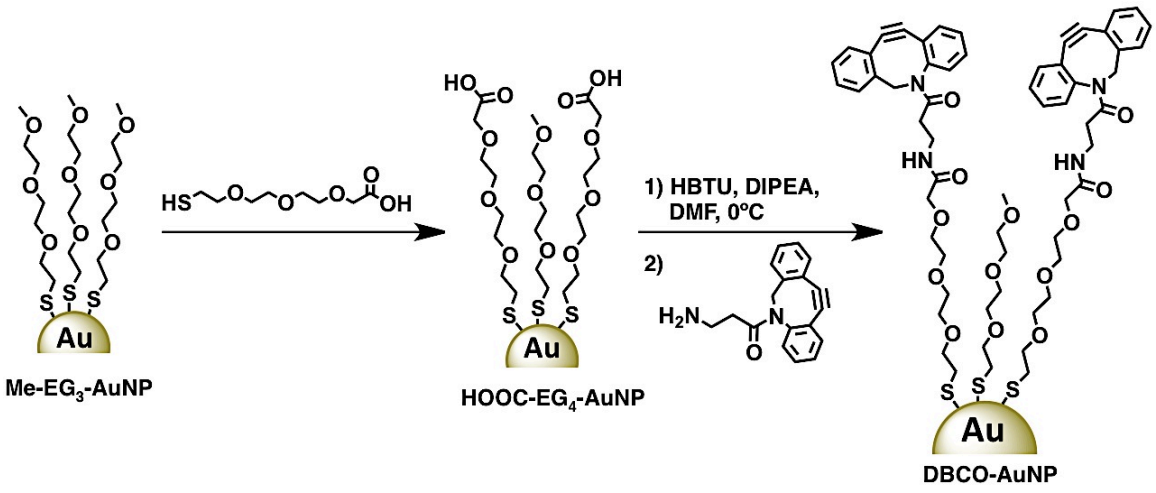

Scheme 8.1: Outline of the synthesis strategy employed to synthesize the DBCO–AuNP.

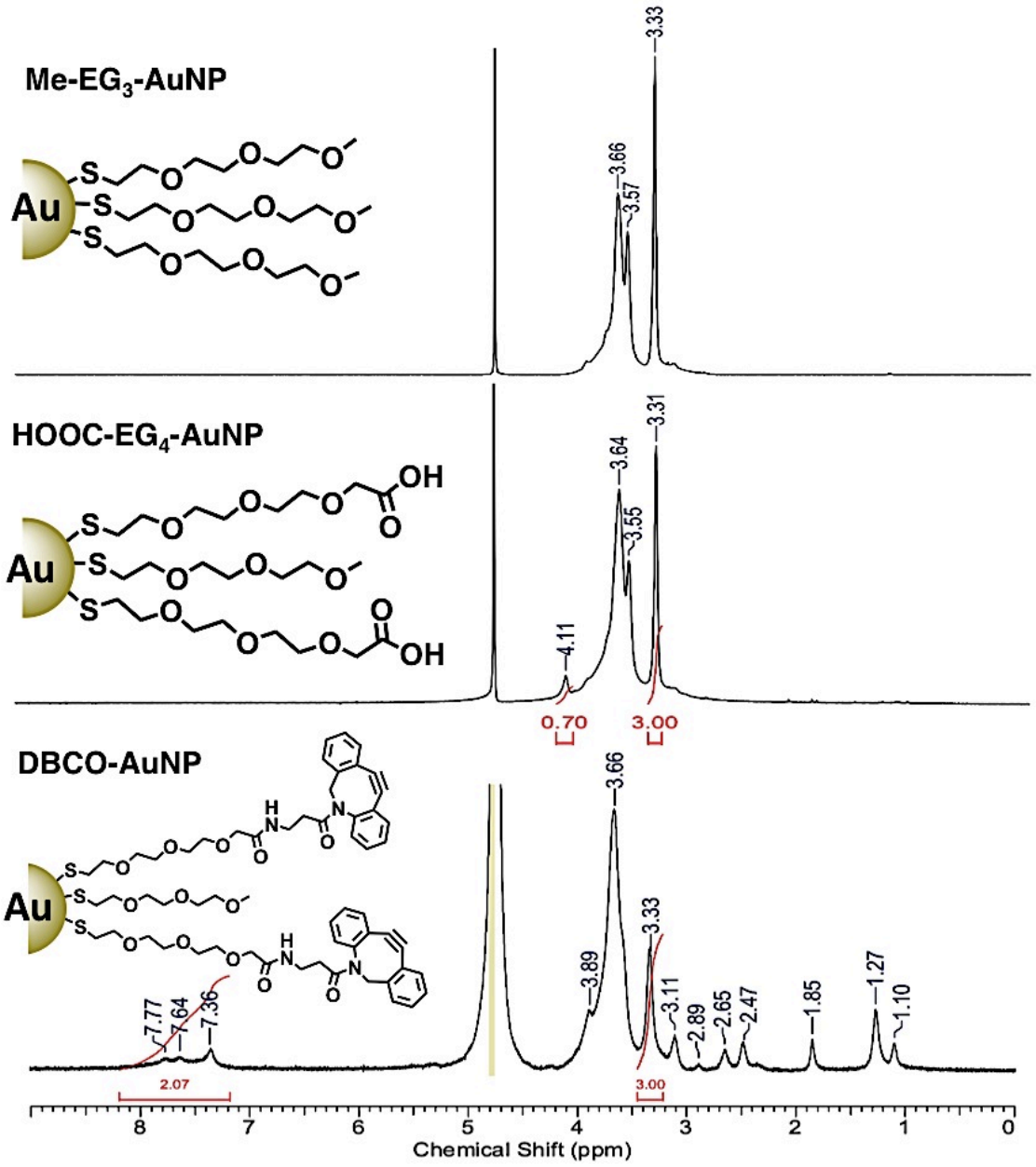

Figure 8.1: ^{1}H NMR spectra of the AuNPs after each synthesis step recorded in D_2O. Spectra calibrated against residual H_2O.

Scheme 8.1 shows our approach to the synthesis of DBCO–AuNPs. This approach must take into account the reactivity of the strained alkynes towards nucleophiles.[6,25–27] In fact, a thiol-functionalized strained alkyne ligand for rapid incorporation into the AuNPs *via* place-exchange reaction is unsuitable because it would rapidly self-react. For this reason we exploited an interfacial amide coupling reaction between a carboxy-terminated AuNP

ligand and a DBCO-amine, which could be run in organic solvents thanks to the amphiphilic properties of the prepared HOOC–AuNPs given by the ethylene glycol-based ligands. This reaction was selected because of its high yield, the product is resistant to hydrolysis allowing for applications in water media, and the formation of the new interfacial amide bond can be easily followed by IR spectroscopy and XPS, furnishing important quantitative data (*vide infra*). The first synthesis step was therefore the synthesis of methyl-terminated triethylene glycol monolayer-protected AuNPs (Me–EG_3–AuNPs) following our previously established procedure.[28] Briefly, $HAuCl_4 \cdot 3H_2O$ was mixed for 1 hour with 3 molar equivalents of Me–EG_3–SH using a methanol–acetic acid mixture as the solvent. To the resulting bright yellow solution a water solution of $NaBH_4$ was added resulting in a dark brown solution typical of the formation of 2.8 ± 0.6 nm AuNPs, as determined from TEM images. For further details refer to the ESI. Subsequently, the Me–EG_3–AuNP underwent the place-exchange reaction to introduce ω-carboxy tetra-ethylene glycol thiols (HOOC–EG_4–SH). The place-exchange reaction was carried out in CH_2Cl_2 for 30 min at room temperature. The free thiols (Me–EG_3–SH and HOOC–EG_4–SH) were removed by washing the nanoparticle film formed inside the reaction vessel after removing CH_2Cl_2, with hexanes and isopropanol, in which the carboxy-functionalized AuNPs (HOOC–EG_4–AuNPs) are not soluble. These carboxy-terminated AuNPs were found to be water-soluble and soluble in DMF and DMSO. HOOC–EG_4–AuNPs were characterized by ^{1}H NMR and IR spectroscopy, TEM, TGA and XPS. The ^{1}H NMR spectrum recorded in D_2O (Figure 8.1) shows the typical broad peaks of a AuNP sample, confirming the success of our washing procedure. The success of the place-exchange reaction was then confirmed by the appearance of a peak at 4.11 ppm corresponding to the two protons belonging to the carbon alpha of the carboxylic acid group in the carboxy-terminated ligands. Through the integration of the peak at 4.11 ppm and the integration of the peak at 3.32 ppm, which belongs to the three protons of the methyl group of the Me–EG_3–S^- ligands, it was possible to determine that 26 ± 5% of the ligands composing the monolayer that protects the gold core was composed of HOOC–EG_4–S^-, while 74 ± 5% was composed of Me–EG_3–S^-. This composition allows the amphiphilic property of the AuNPs to be maintained and therefore permits the subsequent coupling reaction in the organic solvent where it is more efficient. A higher

content of the HOOC–EG_4–S^- ligand would result in AuNPs that are exclusively water-soluble. The IR spectrum of the purified HOOC–EG_4–AuNP shows the appearance of the carbonyl stretching signal at 1740 cm^{-1}, confirming the presence of carboxylic moieties on the AuNP (see Figure S9). TEM images show that HOOC–EG_4–AuNPs maintain the same gold core diameter of 2.8 ± 0.6 nm of the starting material Me–EG_3–AuNPs (Figure S4). The derivative of the TGA curve (Figure S5) shows that the two ligands decompose at two different temperatures. The Me–EG_3–S^- decomposes at 265 ºC, while the HOOC–EG_4–S^- decomposes at 315 ºC. The assignment of the two peaks to the corresponding ligands was carried out by analyzing three different HOOC–EG_4–AuNP samples containing an increasing amount of carboxy-functionalized ligands, and comparing their TGA results with the corresponding ^{1}H NMR spectra. It was then possible to calculate that the HOOC–EG_4–AuNPs contain the carboxylic group in a concentration of 0.46 mmol mg^{-1}. From the combination of the ^{1}H NMR, TGA and TEM data, and assuming that the AuNPs are spherical and that their size is monodispersed (2.8 nm), it was possible to calculate an approximate molecular formula for the HOOC–AuNPs of $Au_{500}(Me–EG_3–S)_{280}(HOOC–EG_4–S)_{100}$.[19]

XPS analysis further confirmed the successful synthesis of HOOC–EG_4–AuNPs and the ratio between the two different ligands that surround the gold core. The Au $4f_{7/2}$ core line appears at 84.3 eV, which is shifted to a binding energy higher than that of the bulk gold (83.95 eV) due to particle size effects.[29] The S 2p core line shows the presence of two major components, S $2p_{3/2}$ at 162.8 eV and S $2p_{1/2}$ at 164.0 eV, in a 2:1 spin-orbit splitting ratio for the Au–S bonds, and just 11% of unbound thiol characterized by two components in a 2 : 1 ratio at 163.8 eV ($2p_{3/2}$) and 165.0 eV ($2p_{1/2}$), respectively.[30] Finally, the high-resolution scan of the C 1s peak and the O 1s peak (see Figure 8.2) confirmed the presence of carboxylic functionalities on the gold cores. The O 1s core line shows the appearance of a shoulder at 533.7 eV that corresponds to –(C=O)–OH, while the C 1s core line shows the appearance of an isolated component at 289.3 eV typical of the carboxylic functional group. From the molecular structure of the two ligands that surround the gold core and from the relative percentages of the C 1s component at 289.3 eV and that at 286.3 eV related to C–O of the ethylene glycol units of both the ligands, it

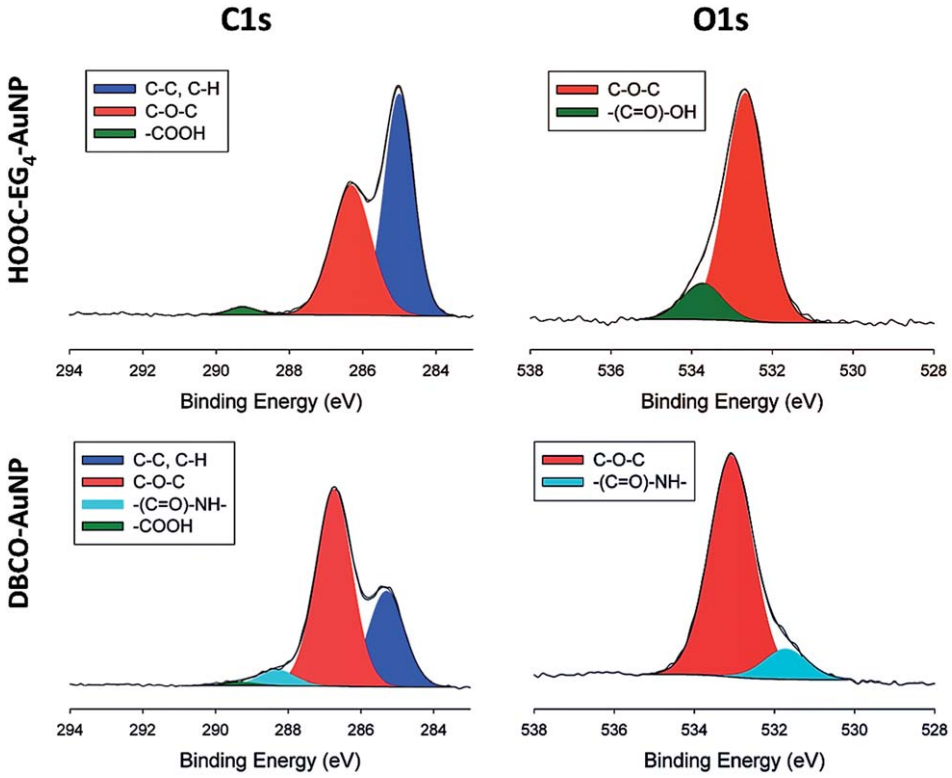

Figure 8.2: High-resolution C 1s and O 1s XPS spectra for HOOC–EG_4–AuNPs and DBCO–AuNPs.

was possible to estimate the composition of the organic layer protecting the gold core with good precision. Through this independent method we could confirm that 26 ± 2% of the ligands were HOOC–EG_4–S^-. Details of the calculation are reported in the ESI.

The DBCO-amine was then reacted with the HOOC–AuNPs using HBTU as a coupling agent. In a typical synthesis, HOOC–AuNPs (65 mg, 30 mmol of –COOH) and *N*,*N*-diisopropylethyl-amine (16 ml, 90 mmol) were dissolved in 10 ml of dry DMF in a round bottom flask. The solution was then cooled down to 0 ºC and purged with argon gas. To this solution was added HBTU (23 mg, 60 mmol) dissolved in 5 ml of dry DMF. The reaction mixture was stirred at 0 ºC for 15 min and then a solution of DBCO-amine (17 mg, 60 mmol) in 3 ml of dry DMF was added. The reaction was allowed to progress overnight in an inert atmosphere. The DBCO–AuNP was purified through dialysis using a 6–8 kDa MWCO membrane against DMF in order to remove the organic byproducts,

followed by dialysis against water in order to remove DMF. The DBCO–AuNP was characterized by ^{1}H NMR and IR spectroscopy, TEM and XPS. ^{1}H NMR spectroscopy recorded in D_2O (see Figure 8.1) showed the disappearance of the peak at 4.11 ppm, the concomitant appearance of aromatic protons between 7 and 8 ppm related to the aryl rings of DBCO and new peaks between 1 and 3 ppm. Through the integration of the aromatic protons and that of the reference peak at 3.32 ppm, corresponding to the Me–EG3–S^- ligands, it was possible to determine that 21 ± 5% of the ligands (0.10 mmol per mg of DBCO) were successfully modified with DBCO. XPS confirmed this result and furnished proof of interfacial reactivity, showing the appearance of the peak related to the amide nitrogens introduced with the DBCO-amine at 400.3 eV, a marked decrease of the carboxylic group components (O 1s at 533.7 eV and C 1s at 289.3 eV), and the concomitant appearance of the components of –(C=O)–NH– at 531.7 eV and that of –(C=O)–NH– at 288.3 eV (see Figure 8.2 and S8). Through the abundance of the nitrogen peak with respect to the initial abundance of –(C=O)–OH it was possible to calculate an 80% yield for the interfacial coupling reaction. This extent of interfacial reaction was confirmed by using the ratio between the percentage of the C 1s peaks from the residual carboxylic acid carbonyl carbon and that of the amide C=O at 288.3 eV and 289.3 eV, respectively. IR spectroscopy (see Figure S9) further confirmed the success of the interfacial coupling reaction showing the appearance of the typical amide stretching signal at 1658 cm^{-1} and the N–H stretching signal at 3420 cm^{-1}, and a marked decrease of the carbonyl signal at 1730 cm^{-1}. As expected, TEM images did not show any significant change in the size distribution of the nanoparticles after the interfacial coupling reaction because of the mild reaction conditions. Finally, the ζ-potential of the DBCO–AuNP in PBS of pH 7.0 was found to be -36.4 mV indicating good stability of the nanoparticles in water solution.

As a proof of concept and to highlight the reactivity of DBCO–AuNPs towards the I-SPAAC reaction, the nanoparticles were reacted with azide-decorated polymersomes.[31] These polymersomes were prepared from a PBD–PEO–N_3 block copolymer (see Figure 8.3) (for synthesis details please refer to the ESI) and were extruded 2 times through 1000 nm, 400 nm, 200 nm and 100 nm polycarbonate membranes (see ESI).

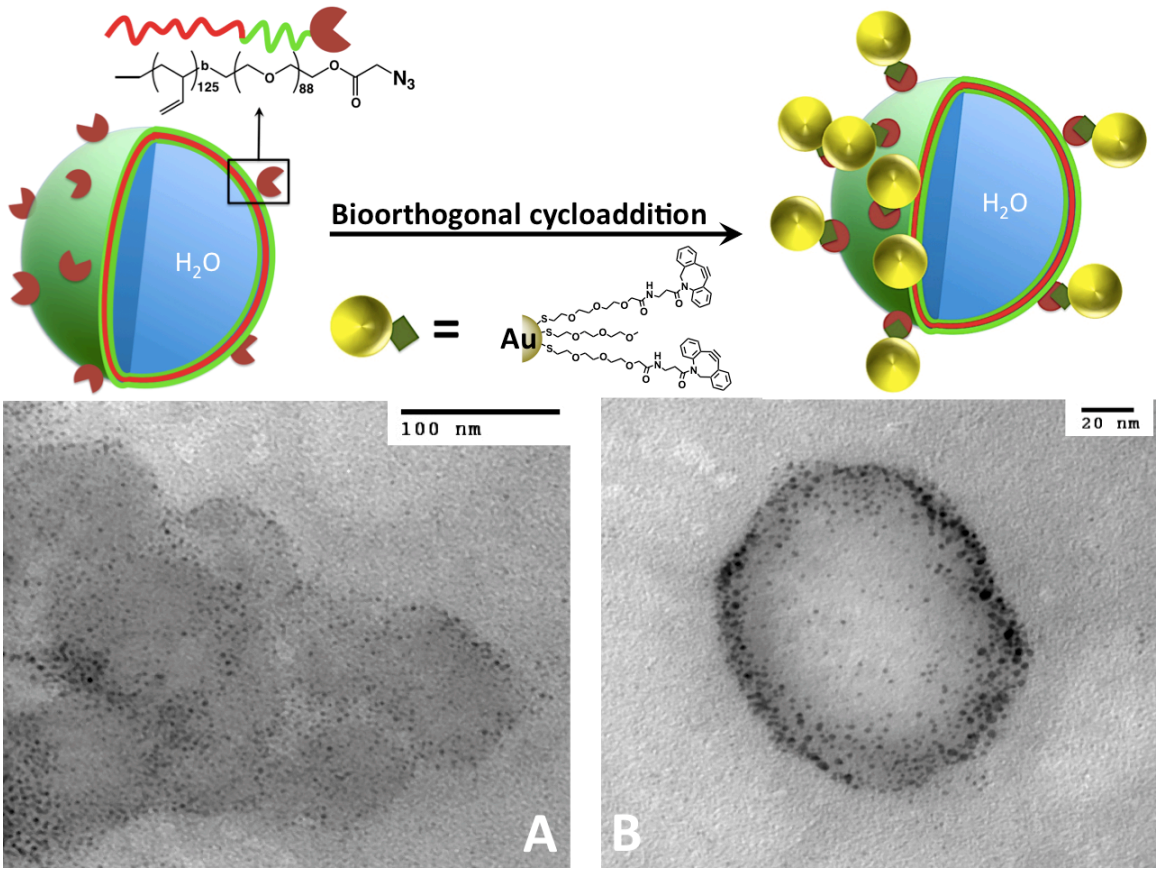

Figure 8.3: Top: a cartoon representing the I-SPAAC reaction between DBCO–AuNPs and azide-functionalized polymersomes. (A) TEM mage of the control experiment Me–EG$_3$–AuNP + azide-functionalized polymersomes. (B) TEM image of vesicles covered with AuNPs through the I-SPAAC reaction.

In a typical reaction 0.05 mg of DBCO–AuNPs were mixed with 0.5 mg of azide-decorated polymersomes in 1 ml of distilled water for 1 hour. A molar excess of 10 : 1 of azide with respect to the DBCO functional group was employed to ensure complete reactivity of the AuNPs with the polymeric vesicles. The success of the interfacial reaction was then verified through TEM. Figure 8.3 and S10 clearly show that the polymersome surfaces have been successfully functionalized with ~3 nm AuNPs, displaying well-defined and easy to image vesicles, thanks to the contrast given by the metallic nanoparticles. A control experiment was then carried out to verify that the presence of the nanoparticles was not due to unspecific interactions. This experiment was carried out under the same conditions as before but instead of using the DBCO–AuNPs,

Me–EG_3–AuNPs were employed. The TEM images of the control experiment (Figure 8.3a and S11) only show a limited number of AuNPs randomly scattered on the TEM grid and vesicles that are faint and difficult to distinguish because of the lack of specific interactions. The comparison between Figure 8.3A and B clearly shows that the AuNP-decorated vesicles can be obtained through the I-SPAAC reaction using the DBCO–AuNPs. The great impact of the DBCO–AuNPs relies on their ease of reaction with azide-functionalized molecular systems through a straightforward pour and mix chemistry under mild reaction conditions. This approach represents an important break-through in the AuNP interfacial click-chemistry because of the numerous problems related to the more well known copper catalyzed version of the azide–alkyne cycloaddition (also know as copper catalyzed [3 + 2] Huisgen cycloaddition), normally employed to create bioconjugates and other hybrid materials. In fact, the Cu-catalyzed azide–alkyne cycloaddition at the AuNP interface is known to give very low cycloaddition yields and cause severe AuNP aggregation/decomposition due to the reaction of Cu(I) salt with the gold surface and to the presence of reducing agents commonly employed to reduce in situ $CuSO_4$.[32] Different attempts have been reported in the literature to try improve the reaction efficiency at the AuNP interface, but they involve very harsh reaction conditions (*e.g.*, very long reaction times[33,34] or massive excess of reagents[34,35]) or the use of particular instrumentation (*e.g.*, microwave[36] or very high pressure[32]) that strongly limits its versatility. To show the improvement that our copper-free approach brings to this scenario, we compared the two different reactions (Cu-free vs. Cu-catalyzed) using small water-soluble azide modified AuNPs (azide-AuNPs). The azide-AuNPs were synthesized following our previously established procedure (see ESI) and were reacted with two different alkynes (2-propyn-1-amine hydrochloride and 1-ethynylpyrene) using standard procedures reported in the literature.[36] We made different attempts to carry out the copper catalyzed [3 + 2] Huisgen cycloaddition but all the experiments resulted in TEG– AuNP aggregation or, using lower reaction times, in negligible reactivity (see ESI). When instead the azide–AuNPs were exposed to DBCO-amine, the cycloaddition product was detected by ^{1}H NMR spectroscopy with only 1 hour of reaction time (see ESI) and with a 60% cycloaddition yield. The use of the I-SPAAC reaction in place of the copper catalyzed [3 + 2] Huisgen

cycloaddition not only allows preservation of the stability of the colloidal solution and makes the cycloaddition more efficient, but also allows the reaction to occur under physiological conditions, avoiding the use of the toxic copper catalyst.

For the first time we describe a simple synthesis and characterization of water-soluble AuNPs that incorporate an interfacial strained alkyne functionality, DBCO, able to efficiently undergo an I-SPAAC reaction in aqueous media with nanomaterials despite the exclusively organic solvent solubility of the DBCO moieties. The synthesis method presented takes into account the reactivity of the strained alkyne towards nucleophiles and involves an interfacial amide coupling reaction between carboxy-terminated AuNPs and a DBCO-amine. The same approach can also be used for coupling diverse amine-functionalized strained alkynes with different reaction kinetics toward the dipolar cycloaddition,[1] allowing the synthesis of strained-alkyne-functionalized AuNPs with tuneable reactivity towards the I-SPAAC reaction. The DBCO–AuNPs were characterized through ^{1}H NMR spectroscopy, IR spectroscopy, TGA, TEM, and XPS and the amount of DBCO on the corona was estimated with good precision through two independent methods. In particular we demonstrated that XPS is a powerful tool not only for qualitatively monitoring the interfacial reactivity, but also for quantifying with higher precision the newly introduced interfacial moieties. This quantification methodology can be transferrable also to larger particles. The precise quantification of the interfacial strained alkyne moieties is of great importance for the application of these nanoparticles in bioconjugation and drug delivery. To showcase the power of the interfacial reactivity of the DBCO–AuNPs, the nanoparticles were used to react with azide-decorated polymersomes. Polymersomes were selected because a visual proof of the I-SPAAC reaction can be easily obtained through electron microscopy, because they mimic the structures of cell membranes, and are emerging as highly promising, potentially multifunctional vehicles that have been used in a wide range of biomedical applications such as drug delivery and imaging.[37–40] The covalent attachment of inorganic nanoparticles into these structures is of significant interest in order to tune the chemical and physical properties of the materials and to obtain new properties that result from the synergistic combination of the organic and inorganic components.[41–43] Finally, by comparing the I-SPAAC reaction with its Cu-catalyzed version, we showed that our

strategy leads to a high yield for the interfacial reaction and preserves the stability of the AuNP. In addition it provides a copper-free environment necessary for potential applications of these DBCO–AuNPs *in vivo*.

Thanks to the intrinsic biocompatibility of these new AuNPs coupled with the chemoselectivity and the fast reaction kinetics towards the azide group conferred by the interfacial strained alkyne, the DBCO–AuNPs represent not only promising versatile scaffolds for the facile and efficient modification of material interfaces, but also represent a powerful tool exploitable in biochemistry, biology and nanomedicine. Indeed the *in vivo* labeling of azide modified biomolecules and tissues can be easily achieved through the methodology herein described, seeing the relative ease of introduction of azide functionalities in the biosystems compared to the introduction of strained alkynes. These possibilities are currently being explored.

8.2 References

(1) M. F. Debets, S. S. Van Berkel, J. Dommerholt, A. J. Dirks, F. P. J. T. Rutjes and F. L. Van Delft, *Acc. Chem. Res.*, 2011, **44**, 805–815.

(2) J. C. Jewett and C. R. Bertozzi, *Chem. Soc. Rev.*, 2010, **39**, 1272–1279.

(3) M. D. Best, *Biochemistry*, 2009, **48**, 6571–6584.

(4) H. L. Evans, R. L. Slade, L. Carroll, G. Smith, Q. D. Nguyen, L. Iddon, N. Kamaly, H. Stockmann, F. J. Leeper, E. O. Aboagye and A. C. Spivey, *Chem. Commun.*, 2012, **48**, 991–993.

(5) H. L. Evans, L. Carroll, Q. D. Nguyen, E. O. Aboagye and A. Spivey, J. *Labelled Compd. Radiopharm.*, 2013, **56**, S204.

(6) K. E. Beatty, J. D. Fisk, B. P. Smart, Y. Y. Lu, J. Szychowski, M. J. Hangauer, J. M. Baskin, C. R. Bertozzi and D. A. Tirrell, *ChemBioChem*, 2010, **11**, 2092–2095.

(7) J. Dommerholt, S. Schmidt, R. Temming, L. J. A. Hendriks, F. P. J. T. Rutjes, J. C. M. van Hest, D. J. Lefeber, P. Friedl and F. L. van Delft, *Angew. Chem., Int. Ed.*, 2010, **49**, 9422–9425.

(8) X. H. Ning, J. Guo, M. A. Wolfert and G. J. Boons, *Angew. Chem., Int. Ed.*, 2008, **47**, 2253–2255.

(9) K. W. Dehnert, J. M. Baskin, S. T. Laughlin, B. J. Beahm, N. N. Naidu, S. L. Amacher and C. R. Bertozzi, *ChemBioChem*, 2012, **13**, 353–357.

(10) S. T. Laughlin, J. M. Baskin, S. L. Amacher and C. R. Bertozzi, *Science*, 2008, **320**, 664–667.

(11) B. C. Sanders, F. Friscourt, P. A. Ledin, N. E. Mbua, S. Arumugam, J. Guo, T. J. Boltje, V. V. Popik and G. J. Boons, *J. Am. Chem. Soc.*, 2011, **133**, 949–957.

(12) P. A. Ledin, F. Friscourt, J. Guo and G. J. Boons, *Chem. – Eur. J.*, 2011, **17**, 839–846.

(13) C. Ornelas, J. Broichhagen and M. Weck, *J. Am. Chem. Soc.*, 2010, **132**, 3923–3931.

(14) J. A. Johnson, J. M. Baskin, C. R. Bertozzi, J. T. Koberstein and N. J. Turro, *Chem. Commun.*, 2008, 3064–3066.

(15) S. V. Orski, A. A. Poloukhtine, S. Arumugam, L. D. Mao, V. V. Popik and J. Locklin, *J. Am. Chem. Soc.*, 2010, **132**, 11024–11026.

(16) A. Kuzmin, A. Poloukhtine, M. A. Wolfert and V. V. Popik, *Bioconjugate Chem.*, 2010, **21**, 2076–2085.

(17) A. Bernardin, A. Cazet, L. Guyon, P. Delannoy, F. Vinet, D. Bonnaffe and I. Texier, *Bioconjugate Chem.*, 2010, **21**, 583–588.

(18) P. Gobbo, S. Novoa, M. C. Biesinger and M. S. Workentin, *Chem. Commun.*, 2013, **49**, 3982–3984.

(19) M. Milne, P. Gobbo, N. McVicar, R. Bartha, M. S. Workentin and R. H. E. Hudson, *J. Mater. Chem. B*, 2013, **1**, 5628–5635.

(20) Y. H. Kim, J. Jeon, S. H. Hong, W. K. Rhim, Y. S. Lee, H. Youn, J. K. Chung, M. C. Lee, D. S. Lee, K. W. Kang and J. M. Nam, *Small*, 2011, **7**, 2052–2060.

(21) J. C. Olivier, R. Huertas, H. J. Lee, F. Calon and W. M. Pardridge, *J. Pharm. Res.*, 2002, **19**, 1137–1143.

(22) F. Zhang, E. Lees, F. Amin, P. R. Gil, F. Yang, P. Mulvaney and W. J. Parak, *Small*, 2011, **7**, 3113–3127.

(23) W. Fritzsche and T. A. Taton, *Nanotechnology*, 2003, **14**, R63– R73.

(24) E. M. Sletten and C. R. Bertozzi, *Org. Lett.*, 2008, **10**, 3097– 3099.

(25) E. J. Kim, D. W. Kang, H. F. Leucke, M. R. Bond, S. Ghosh, D. C. Love, J. S. Ahn, D. O. Kang and J. A. Hanover, *Carbohydr. Res.*, 2013, **377**, 18–27.

(26) M. Golkowski and T. Ziegler, *Synthesis*, 2013, **45**, 1207–1214.

(27) R. van Geel, G. J. M. Pruijn, F. L. van Delftand W. C. Boelens, *Bioconjugate Chem.*, 2012, **23**, 392–398.

(28) P. Gobbo and M. S. Workentin, *Langmuir*, 2012, **28**, 12357– 12363.

(29) M. C. Bourg, A. Badia and R. B. Lennox, *J. Phys. Chem. B*, 2000, **104**, 6562–6567.

(30) D. G. Castner, K. Hinds and D. W. Grainger, *Langmuir*, 1996, **12**, 5083–5086.

(31) R. C. Amos, A. Nazemi, C. V. Bonduelle and E. R. Gillies, *Soft Matter*, 2012, **8**, 5947–5958.

(32) H. Ismaili, A. Alizadeh, K. E. Snell and M. S. Workentin, *Can. J. Chem.*, 2009, **87**, 1708–1715.

(33) W. Limapichat and A. Basu, *J. Colloid Interface Sci.*, 2008, **318**, 140–144.

(34) J. L. Brennan, N. S. Hatzakis, T. R. Tshikhudo, N. Dirvianskyte, V. Razumas, S. Patkar, J. Vind, A. Svendsen, R. J. M. Nolte, A. E. Rowan and M. Brust, *Bioconjugate Chem.*, 2006, **17**, 1373–1375.

(35) M. X. Zhang, B. H. Huang, X. Y. Sun and D. W. Pang, *Langmuir*, 2010, **26**, 10171–10176.

(36) W. J. Sommer and M. Weck, Coord. *Chem. Rev.*, 2007, **251**, 860–873.

(37) L. F. Zhang and A. Eisenberg, *Science*, 1995, **268**, 1728– 1731.

(38) B. M. Discher, Y. Y. Won, D. S. Ege, J. C. M. Lee, F. S. Bates, D. E. Discher and D. A. Hammer, *Science*, 1999, **284**, 1143– 1146.

(39) H. Kim, Y. J. Kang, S. Kang and K. T. Kim, *J. Am. Chem. Soc.*, 2012, **134**, 4030–4033.

(40) P. Tanner, P. Baumann, R. Enea, O. Onaca, C. Palivan and W. Meier, *Acc. Chem. Res.*, 2011, **44**, 1039–1049.

(41) R. Chen, D. J. G. Pearce, S. Fortuna, D. L. Cheung and S. A. F. Bon, *J. Am. Chem. Soc.*, 2011, **133**, 2151–2153.

(42) J. He, Z. J. Wei, L. Wang, Z. Tomova, T. Babu, C. Y. Wang, X. J. Han, J. T. Fourkas and Z. H. Nie, *Angew. Chem., Int. Ed.*, 2013, **52**, 2463–2468.

(43) Y. Ofir, B. Samanta and V. M. Rotello, *Chem. Soc. Rev.*, 2008, **37**, 1814–1823.

Chapter 9

9 Small gold nanoparticles for interfacial Staudinger–Bertozzi ligation

Chapter 9 has been published as a full paper, and it is reproduced with permission from the Royal Society of Chemistry. The corresponding reference is: **P. Gobbo***, W. Luo, S. J. Cho, X. Wang, M. C. Biesinger, R. H. E. Hudson, M. S. Workentin*, *Org. Biomol. Chem.*, **2015**, *13*, 4605 - 4612.

Luo and Cho helped with the synthesis and characterization of the thiolated ligand. Wang synthesized and characterized the peptide. Biesinger performed the XPS experiments and assisted in the discussion of the XPS results. I synthesized and characterized the Staudinger-AuNP and investigated their interfacial reactivity. I wrote the drafts of the manuscript, with input and minor edits from the other co-authors and final edit by my supervisor, Prof. M. S. Workentin. The supporting information file referenced in the text can be downloaded from the web site of the publisher.

ABSTRACT: Small gold nanoparticles (AuNPs) that possess interfacial methyl-2-(diphenylphosphino)benzoate moieties have been successfully synthesized (Staudinger-AuNPs) and characterized by multi-nuclear MR spectroscopy, transmission electron microscopy (TEM), UV-vis spectroscopy, thermogravimetric analysis, and X-ray photoelectron spectroscopy (XPS). In particular, XPS was remarkably sensitive for characterization of the novel nanomaterial, and in furnishing proof of its interfacial reactivity. These Staudinger-AuNPs were found to be stable to the oxidation of the phosphine center. The reaction with benzyl azide in a Staudinger–Bertozzi ligation, as a model system, was investigated using ^{31}P NMR spectroscopy. This demonstrated that the interfacial reaction was clean and quantitative. To showcase the potential utility of these Staudinger-AuNPs in bioorganic chemistry, a AuNP bioconjugate was prepared by reacting the Staudinger-AuNPs with a novel azide-labeled CRGDK peptide. The CRGDK peptide could be covalently attached to the AuNP efficiently, chemoselectively, and with a high loading.

9.1 Introduction

The conjugation of biomolecules to nanomaterials is of high interest because of the potential applications of the resulting bioconjugate in biological and medical diagnostics, therapeutics and drug vectors.[1–5] Among all nanomaterials, gold nanoparticles are often regarded as the most promising template because of their low toxicity and chemical stability. In addition, their optical properties can be easily tuned by varying the gold core diameter[6] and the chemical properties can be tuned by changing the ligand corona.[7] In the past decade, many different approaches have been developed to synthesize AuNP bioconjugates for different purposes. Generally these strategies rely on electrostatic interactions between the gold surface and the side chains of the biomolecule's residues, on hydrophobic–hydrophilic type of interactions, on direct place exchange exploiting the affinity of cysteine for gold, or on interfacial reactions (*e.g.*, interfacial EDC coupling, imine formation etc.).[8] These methods generally result in an uncontrolled "shotgun" type bioconjugation,[9] whereas for many applications it is desirable to have more precise control over the amount of biomolecule that is introduced. This can be achieved by designing a single stable AuNP that exhibits a chemoselective reactive moiety at its interface that serves as an anchoring group to incorporate a discrete number of biomolecules. This could result in the precise tuning of the final biophysical properties of the AuNP-bioconjugate. It is also desirable that the interfacial reactive group on the nanoparticle leads to a robust conjugate that relies on a strong bond between nanoparticle and biomolecule. In order for the interfacial reaction to be chemoselective, this nanoparticle template must undergo a reaction with a functional group that is not present in nature, atoxic, and small so that it does not affect the activity of the conjugated biomolecule. The functionality that addresses all these requirements is the azide group. The azide can undergo four different reactions. The [3 + 2] Huisgen cycloaddition and the copper catalyzed [3 + 2] Huisgen cycloaddition with dipolarophiles, the strained-promoted alkyne–azide cycloaddition (SPAAC) with strained alkynes and the Staudinger–Bertozzi ligation.[10,11] While the [3 + 2] Huisgen cycloaddition and its catalyzed version are not completely compatible with AuNPs chemistry because the high temperature or the Cu(I) required to push the reaction to completion cause severe nanoparticle aggregation,[12] the SPAAC reaction presents limited chemoselectivity due to

the possibility of nucleophilic attacks (especially from thiols and amines largely present in biomolecules) to the highly reactive strained triple bond.[13–15] A recent work of ours highlighted this issue showing how post assembly deprotection of peptides once "clicked" on the AuNP surface was necessary to efficiently synthesize a nanoparticle bioconjugate through the SPAAC reaction.[16] The Staudinger–Bertozzi ligation is a reaction that was specifically developed for investigating the metabolic engineering of cell surfaces[17] and takes place between the azide and a substituted triphenylphosphine. Whereas the cycloaddition reactions lead to a triazole ring, the Staudinger–Bertozzi ligation forms a stable amide bond. From its very first development the Staudinger–Bertozzi ligation has been successfully employed in biochemistry to immobilize peptides and proteins onto different materials,[18–22] for *in vivo* and *in vitro* imaging, and for protein detection.[23–25]

This reaction seems to be an ideal candidate for designing a new AuNP template that can react in a highly chemoselective and efficient way with any azide-modified (bio)molecule. For these reasons we report the synthesis of a thiol ligand that contains a methyl-2-(diphenylphosphino)benzoate moiety designed to undergo a Staudinger–Bertozzi ligation with azide functionalities. This ligand was introduced onto the surface of small water-soluble AuNPs through a place-exchange reaction and the reactivity of the resulting nanomaterial was investigated using benzyl azide as model clickable partner. Finally, to showcase the high chemoselectivity of these novel reactive AuNPs for bioconjugation, we react them with an azide-modified CRGDK peptide. CRGDK peptides are promising targeting biomolecules for diverse cancer cells lines and therefore the resulting AuNP-CRGDK bioconjugate would be a potential broad-spectrum targeting agent.[1] In addition, the presence of the cysteine in the CRGDK peptide represents a challenge for the chemoselective conjugation on nanoparticles. Herein, we present a facile, versatile, and straightforward protocol for the conjugation of biomolecules onto the AuNP surface through the Staudinger–Bertozzi ligation. Importantly, the study showcases the use of XPS as a method to easily characterize the interfacial reactivity of this new nanomaterial, and to quantify the amount of conjugated biomaterial, information that is very important for practical applications in biochemistry, medical diagnosis, therapies and drug delivery.

9.2 Results and discussion

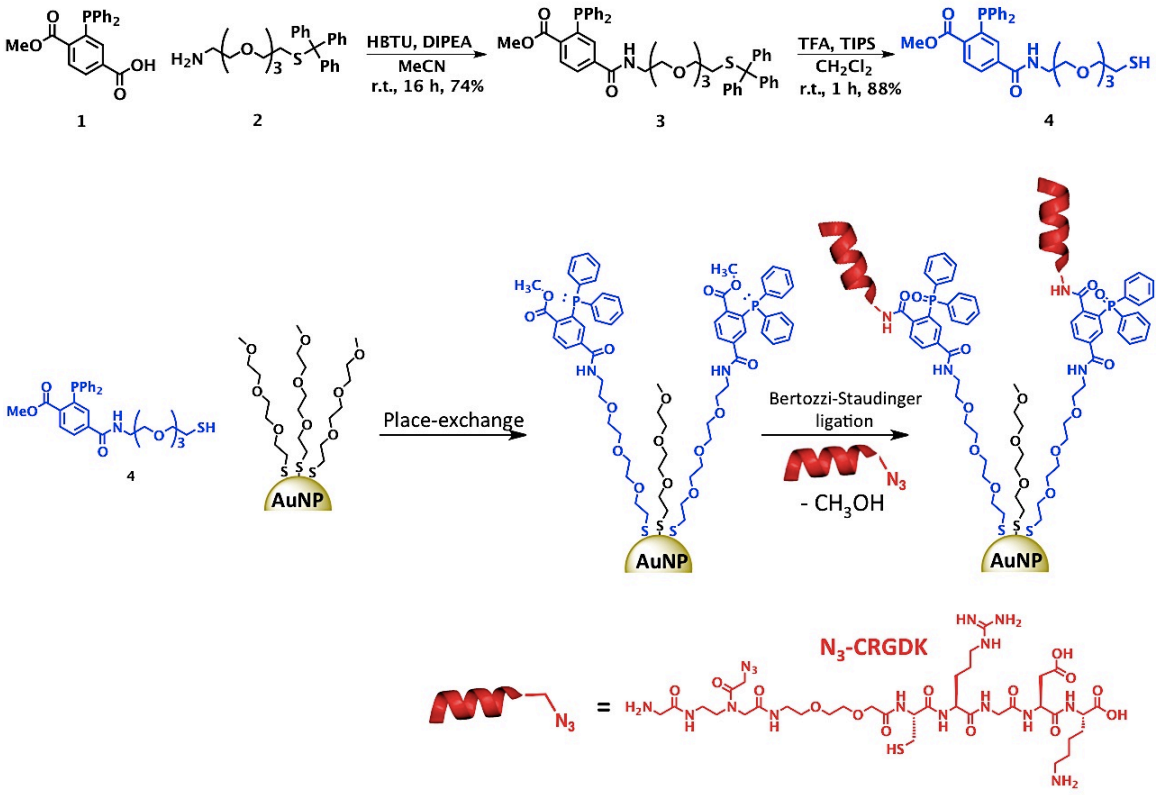

Scheme 9.1: Synthetic strategy for the synthesis of the Staudinger-AuNP.

The approach used to introduce the reactive triphenylphosphine moiety for the Staudinger–Bertozzi ligation onto the water-soluble AuNPs required the synthesis of the appropriate thiol containing ligand for a place-exchange reaction; see Scheme 9.1. The first step involved coupling 3-(diphenylphosphino)-4-(methoxycarbonyl)benzoic acid (1) to an amino-tetra- ethylene glycol-trityl-protected thiol (2). The deprotection of the thiol functionality in 5% trifluoroacetic acid/dichloromethane led to the desired phosphine-thiol ligand (4). Details of the ligand synthesis can be found in the ESI. Compound (4) was found to be remarkably stable to the oxidation of both phosphine and thiol ends. Attempts to oxidize the phosphine and the thiol by dissolving the molecule in wet solvents and by air bubbling failed. However, small amounts of phosphine oxide can form during the different stages of the ligand synthesis. It was possible to reduce the phosphine oxide back to the active phosphine using the synthetic procedure reported by

H.-C. Wu *et al.*[26] Before deprotecting the thiol end, the mixture of phosphine oxide and phosphine can be dissolved in a solution of triphenylphosphine and $HSiCl_3$ in dry toluene. Heating of this reaction mixture to 100 °C leads to the quantitative reduction of the phosphine oxide. It is noteworthy that this reaction fails in presence of free thiols and, if the phosphine-oxide reduction is carried out at the nanoparticles interface, $HSiCl_3$ causes a fast and total decomposition of the AuNP.

The Staudinger-AuNPs have been synthesized through a place-exchange reaction using triethylene glycol monomethyl ether AuNP (MeO-EG_3-AuNP) as the starting material, Scheme 9.1. Details of their synthesis of the latter can be found in the ESI. These nanoparticles have a gold core diameter of 3 ± 1 nm and are soluble in water and polar organic solvents.[27] MeO-EG_3-AuNPs represent a very resilient substrate for further modification and interfacial organic chemistry because they are resistant to acidic[16] and basic conditions,[12] they can be heated to over 100 °C,[27] and they can be repeatedly dried and re-dissolved in a solvent with little to no aggregation. The place-exchange reaction to introduce the phosphine-thiol (4) onto the nanoparticle's corona was carried out by dissolving 200 mg of MeO-EG_3-AuNP and 100 mg of phosphine-thiol (4) in dry and argon purged dichloromethane. The reaction was carried out for 15 minutes at room temperature, under inert atmosphere (to minimize potential oxidation of the reactive phosphine) and under vigorous stirring. The particles were then cleaned from the excess thiol by re-dissolving them in 6 ml of dichloromethane and by precipitating them by adding 33 ml of hexanes in which the nanoparticles are not soluble. This washing operation was repeated five times overall. The Staudinger-AuNPs were characterized by ^{1}H and ^{31}P NMR spectroscopy, transmission electron microscopy (TEM), UV-vis spectroscopy, thermogravimetric analysis, and X-ray photo- electron spectroscopy (XPS). The ^{1}H and ^{31}P NMR spectra showed presence of broad peaks typical of a AuNP sample indicating that the washing procedure was efficient and that the most of the free thiol ligands were successfully removed. Curiously the spectra did not show a perfect correspondence of the peaks with the free ligand (4). Usually the successful in-corporation of a second thiol ligand through the place-exchange reaction is easily determined by comparing the ^{1}H NMR spectra of the free ligand with that of the place-exchanged AuNPs sample.

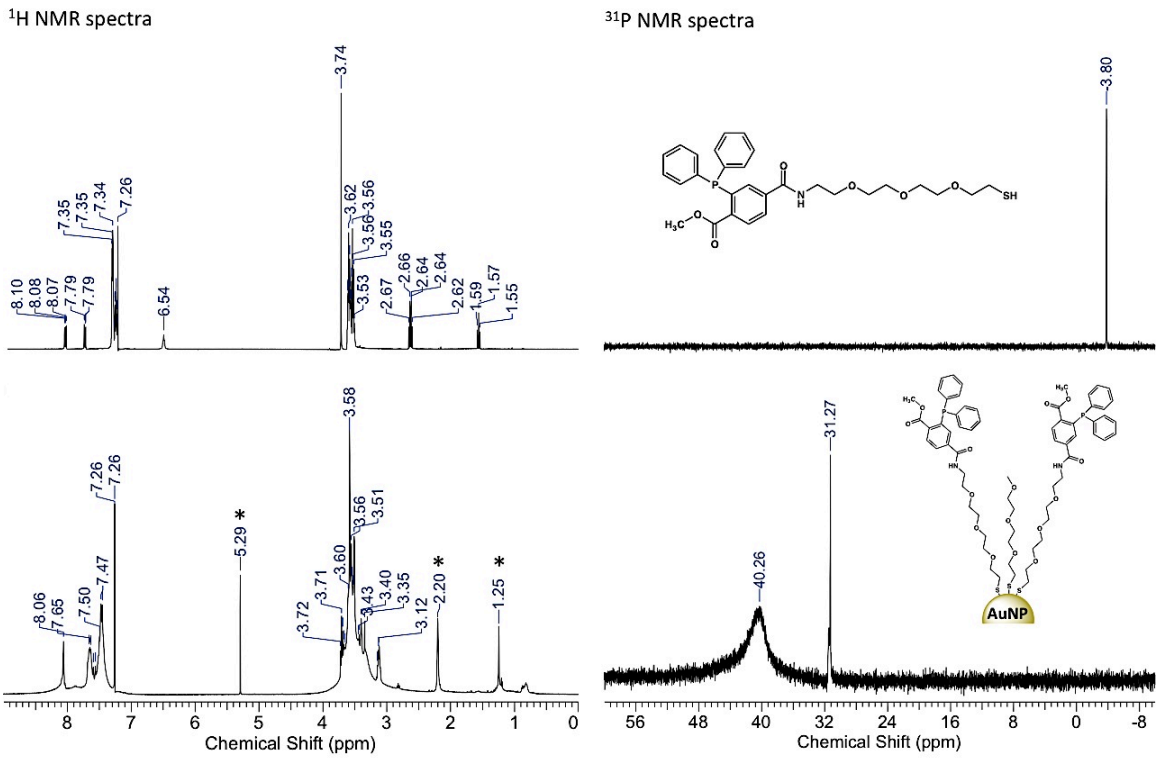

Figure 9.1: ^{1}H (left) and ^{31}P (right) NMR spectra of phosphine-thiol (4) (top) versus Staudinger-AuNP (bottom). *Denotes residual solvent peaks. Spectra calibrated against residual chloroform and H_3PO_4.

The chemical shifts typically match even though the peaks on the AuNPs spectrum are broader.[28,29] In this case ^{1}H NMR spectrum shows a substantial difference in the aromatic region as highlighted in Figure 9.1. An even more drastic difference is observed in the ^{31}P NMR spectrum of the Staudinger-AuNPs with respect to that of compound (4). The ^{31}P NMR spectrum of the Staudinger-AuNPs did not show a peak for the phosphine at −3.8 ppm, but two signals one broad and intense at 40.3 ppm and one at 31.3 ppm. By comparison with the data of the phosphine oxide formation gathered during the synthesis of compound (4), the signal at 31.3 ppm can be attributed to the oxidized methyl-2-(diphenylphosphino)benzoate. Integration of the ^{31}P NMR peaks shows that the AuNP sample has 9% of oxidized phosphine that is most likely generated during the washing procedure where it is exposed to air. The shift of the phosphine peak in the ^{31}P NMR and the difference in the aromatic region shown in the ^{1}H NMR seem to suggest that there is

an interaction at the phosphorous center that changes the electronic properties of the phosphine.

Transmission electron microscopy provided relevant insights on this issue. The TEM images reported in Figure 9.3A clearly show that 3.63 ± 1.4 nm Staudinger-AuNPs are interacting with each other forming AuNPs self-assemblies with an inter-particle distance of ~1 nm.[30,31] TEM images of similar ethylene glycol small AuNPs usually show well isolated and evenly distributed dark spots on the TEM grid, like after the interfacial Staudinger–Bertozzi ligation, see Figure 9.3B. This AuNPs self-assembly was also confirmed by UV-vis spectroscopy. Typically AuNPs of such a small size do not show any plasmon resonance band in the UV-vis spectrum. However, the UV-vis derivative reported in Figure 9.3C highlights the appearance of a weak plasmon band in the region 525–650 nm for the Staudinger-AuNP sample compared to the MeO-EG_3-AuNP starting material due to the very short distance between the gold cores involved in the AuNPs self-assemblies. The reason for this collective behaviour of the Staudinger-AuNPs is probably due to hydrophobic–hydrophilic-type of interactions between the hydrophilic ethylene glycol linker and the strongly hydrophobic character of the triphenylphosphine. As reported by K. J. M. Bishop and co-workers, ligands with different solubility properties introduced through a place-exchange reactions do not distribute homogenously on the particle's corona but rather tend to form patches or groups. These patches are responsible for the formation of inter-nanoparticles hydro- phobic "bonds" resulting in the self-assembly of nanoparticle islands (like in the present work) or chain-like structures.[31]

High-resolution XPS analysis, see Figure SI3, further confirms the presence of inter-nanoparticle interactions showing a peak for the Au 4f core line that displays two different components: a small component at 84.62 eV typical of isolated AuNPs and a larger component at 83.75 eV that is characteristic of bulk gold and is most likely related to the AuNP networks shown in the TEM images.[32] XPS analysis also shows a peak for the amide nitrogen at 399.75 eV. The high resolution scans of the P 2p peak, see Figure 9.4, shows a major component at 131.52 eV (P $2p_{3/2}$) related to the triphenylphosphine and a minor component (13%) at 132.60 eV (P $2p_{3/2}$) related to triphenylphosphine oxide,

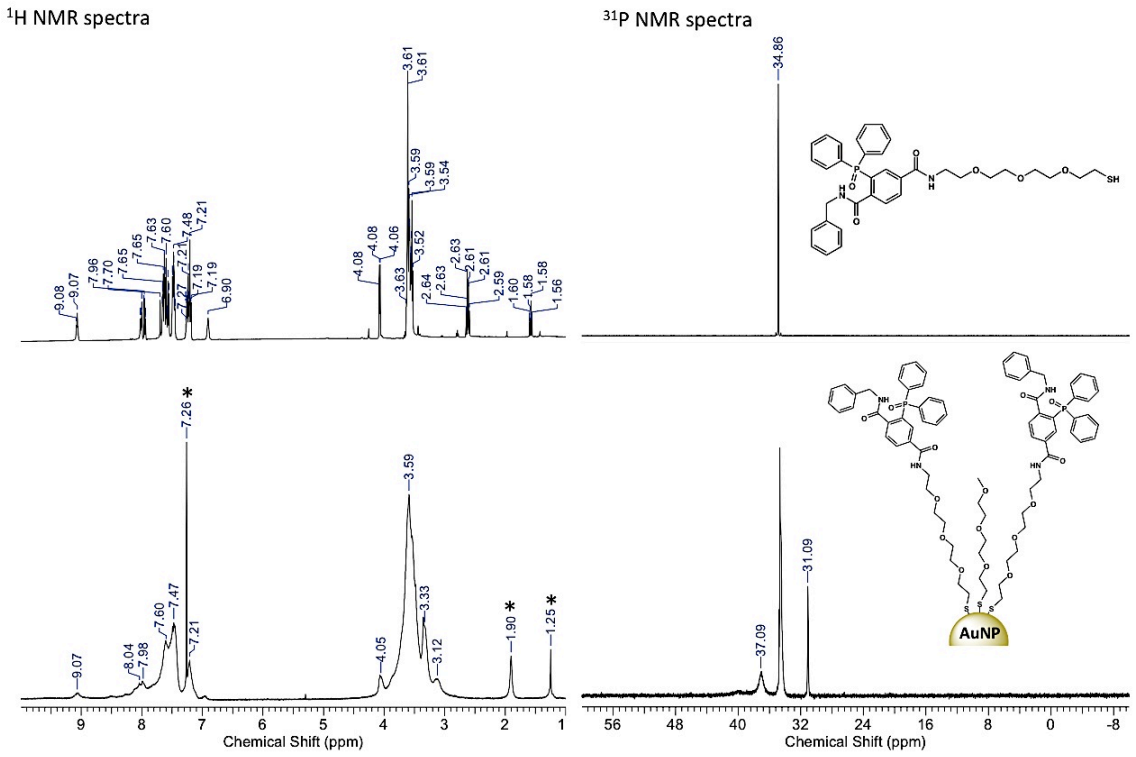

Figure 9.2: ^{1}H (left) and ^{31}P (right) NMR spectra of phosphine-thiol (4) after reaction with benzyl azide (top) versus Staudinger-AuNP after reaction with benzyl azide (bottom). * Denotes residual solvent peaks. Spectra calibrated against residual chloroform and H_3PO_4.

confirming independently and with higher precision the result obtained through ^{31}P NMR spectroscopy. The high resolution scans of the C 1s, see Figure 9.4, shows a distinct component at 289.08 eV that is related to the carbonyl of the ester functional group, a component at 288.00 eV that is related to the amide's carbonyl, and the typical components for the ethylene glycol ligands at 286.36 eV and 285.00 eV. Finally, the high-resolution scan of the S 2p peak, see Figure SI3, shows the typical components of the sulphur-gold bond and presence of a negligible amount of free thiol and sulfates.[33] The presence of free thiols and sulfates (generated by the slow oxidation of thiols over time) is due to the fact that they have been trapped in between the AuNPs self-assemblies and are difficult to wash away. Despite the peculiar behaviour of these AuNPs, exposure to benzyl azide provided clear evidence of the Staudinger–Bertozzi product. In fact the

peaks of the ^{1}H and ^{31}P NMR spectra returned to match those of the model Staudinger–Bertozzi product obtained using the phosphine-thiol (4) with benzyl-azide (*vide infra*).

Thermogravimetric analysis of the Staudinger-AuNP showed that the 43% of the total weight is due to the organic corona (see Figure SI5), of this the 60% is constituted by ligand (4), while the 40% is constituted by MeO-EG_3-S^-. Finally, from the deconvolution of the TGA curve, the ^{31}P NMR spectrum and the gold core diameter obtained from TEM images it was possible to calculate a raw formula for the Staudinger-AuNP: Au_{1500} $(MeO\text{-}EG_3\text{-}S)_{500}$ $(Ph_3P\text{-}EG_4\text{-}S)_{200}$ $(Ph_3P{=}O\text{-}EG_4\text{-}S)_{20}$. More specifically these Staudinger-AuNPs contain methyl-2-(diphenylphosphino)benzoate in concentration 0.432 μmol mg^{-1}. Details of these calculations are reported in the ESI.

Table 9.1: Second order rate constants of the Staudinger–Bertozzi ligation with benzyl azide obtained at 25 °C under different experimental conditions.

	[Phosphine] (M)	[Benzyl azide] (M)	[H_2O] (M)	Solvent	Second Order Rate Constant (10^{-3} M^{-1} s^{-1})
Staudinger-AuNP	0.026	0.518	5.56	$CDCl_3$	0.027 ± 0.002
Ligand **(4)**	0.026	0.518	5.56	$CDCl_3$	1.6 ± 0.1
Ligand **(4)**	0.026	0.518	5.56	DMSO-d_6	3.5 ± 0.1
Ligand **(4)**	0.044	0.830	5.56	DMSO-d_6	4.7 ± 0.1

The reactivity of the Staudinger-AuNP through the Staudinger–Bertozzi ligation was then investigated using benzyl azide and the reactions were monitored through ^{31}P NMR spectroscopy. In the ^{31}P NMR spectrum it was possible to follow the disappearance of the broad peak at 40.3 ppm corresponding to the active phosphine and the appearance of the peak of the ligation product at 34.9 ppm, refer to Figure 9.1 and 9.2. Kinetic experiments were carried out under pseudo-first-order reaction conditions at 25 °C and the reaction kinetics at the AuNP interface was compared with that in solution using ligand (4) as a model compound. For this investigation Staudinger-AuNP (0.026 M in phosphine, 30.0 mg of Staudinger AuNP) were reacted with benzyl azide (0.518 M) in wet $CDCl_3$. Chloroform was chosen due to the high solubility of the nanoparticles in this solvent that permitted the high AuNPs concentration required for the experiments. A reaction using the same conditions was carried out between model compound (4) and benzyl azide.

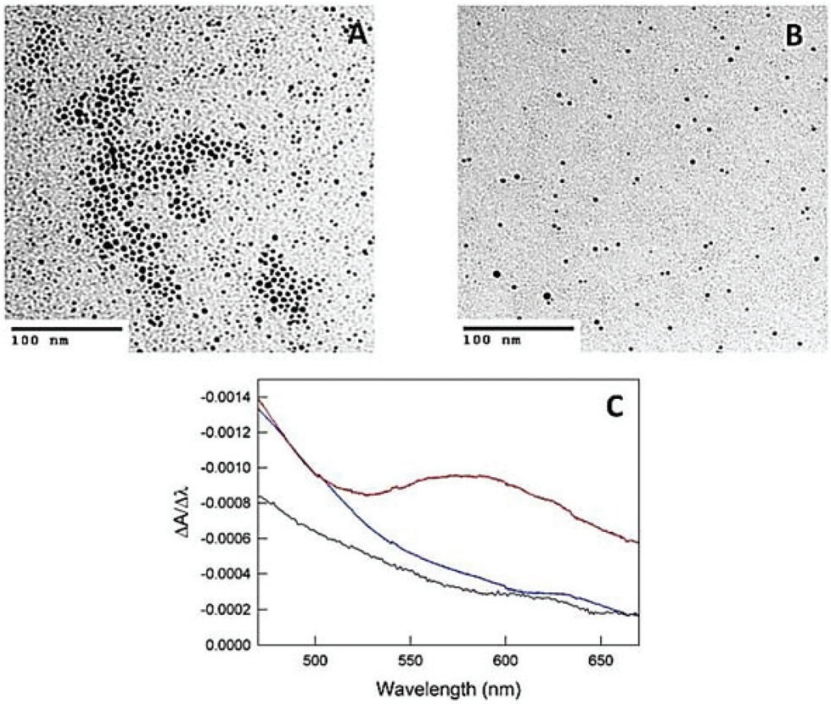

Figure 9.3: TEM images of (A) Staudinger-AuNP, and (B) Staudinger-AuNP after reaction with benzyl azide. (C) Derivative of UV-vis spectrum of MeO-EG$_3$-AuNP (blue), Staudinger-AuNP (red), and Staudinger-AuNP after reaction with benzyl azide. The derivative highlights the presence of the plasmon resonance band for the Staudinger-AuNP sample due to the AuNPs self-assemblies.

This same reaction was then carried out at higher concentration using $CDCl_3$ and DMSO-d_6 as the solvents to compare the results with those previously reported in the literature.[34] Table 9.1 summarizes the results of these kinetic experiments. During the course of all these reactions no intermediates were observed through ^{31}P NMR spectroscopy. This indicates that the reaction mechanism remains that proposed by F. L. Lin and co-workers with the rate-limiting step being the formation of the phosphazide.[34] While this is not surprising for the model reactions with ligand (4), it is remarkable that the Staudinger–Bertozzi ligation takes place at the AuNPs interface in a comparable manner despite the markedly different chemical environment represented by the nanoparticle structure and the networks that they form in solution. Our results show that the reaction of ligand (4) has second-order rate constants comparable to those reported by F. L. Lin and co-workers

and that they increase with an increase in solvent dielectric constant. The reaction at the AuNP interface instead results to be a hundred times slower. This is probably due to additional reaction parameters introduced with an interfacial reaction and because of the inter-nanoparticle interactions observed that need to be overcome before the ligation occurs. However, the interfacial phosphines are still reactive towards the Staudinger–Bertozzi ligation and the reaction yields the Staudinger–Bertozzi product quantitatively. The product of the interfacial Staudinger–Bertozzi ligation was then separated from the free benzyl azide by washing a film of nanoparticles made in a round-bottom flask and rinsing it with hexanes where the nanoparticles are insoluble. The purified sample was then characterized by ^{1}H and ^{31}P NMR spectroscopy, XPS, UV-vis spectroscopy and TEM. As anticipated, TEM images show the absence of AuNPs self-assemblies and only well isolated nanoparticles, see Figure 9.3B. The ^{1}H NMR spectrum of the reacted Staudinger-AuNPs sample now shows perfect correspondence with the chemical shift of the model reaction with compound (4), see Figure 9.2.

The UV-vis spectrum of the reacted nanoparticles sample now shows a spectrum similar to that of MeO-EG_3-AuNP starting material, characterized by the absence of a plasmon resonance band in the region 525–650 nm (see Figure 9.3C).

XPS proves to be a powerful technique to furnish proof of interfacial reactivity. Figure 9.4 shows that after the interfacial reaction with the azide, the C 1s core line no longer shows the component for the ester bond at 289.08 eV, and the component at higher binding energy is now that related to the newly formed amide at 288.00 eV. This is expected because of the generation of methanol that occurs during the reaction mechanism. In addition, the high-resolution scan of the P 2p core line now appears narrower and shows only the component for the triphenylphosphine-oxide.

These results together confirm that the interfacial reaction went to completion. The high-resolution scan of the S 2p core line now shows the absence of free thiols and disulfides as a result of efficient trituration once the nanoparticles self-assemblies has been abrogated.

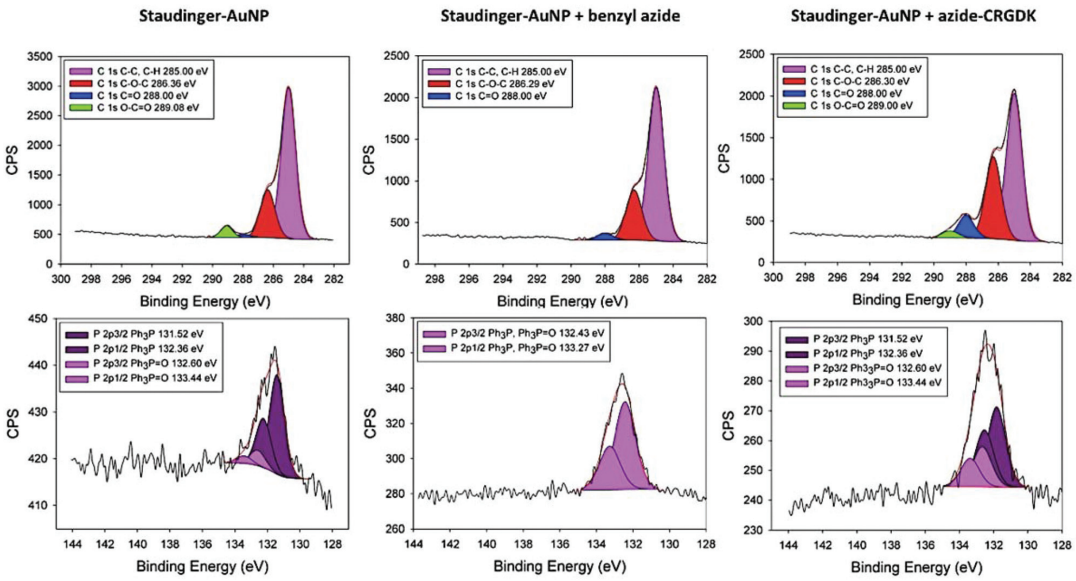

Figure 9.4: High-resolution XPS of C 1s and P 2p core lines of the Staudinger-AuNP (left) and Staudinger-AuNP after reaction with benzyl azide (middle) and azide-CRGDK peptide (right).

In summary, despite the peculiar inter-Staudinger-AuNPs interaction that leads to AuNPs self-assemblies and changes the electronic properties of the phosphine, the Staudinger-AuNP are still readily reactive towards the azide bioorthogonal partner as highlighted by the kinetic study using ^{31}P NMR spectroscopy and by the XPS analysis of the interfacial ligation product. More importantly, the reaction is quantitative as independently confirmed by ^{31}P NMR spectroscopy and XPS analysis, and the reacted Staudinger-AuNP could be recovered easily and quantitatively.

To showcase the high chemoselectivity of these Staudinger-AuNPs and their potential for bioconjugation, we reacted them with an azide functionalized CRGDK peptide. The CRGDK peptide was synthesized *via* standard Fmoc SPPS method and the azide functionality was coupled to the N-terminus. The AuNP bioconjugate was synthesized simply by mixing 20 mg of Staudinger AuNP (8.64 μmol of phosphine) with 30 μmol of azide-CRGDK in DMSO-*d*6 at 37 °C. The reaction was monitored through ^{31}P NMR spectroscopy following the progressive disappearance of the broad peak at 40.3 ppm and the appearance of the product peak at 33.2 ppm (see Figure SI11) indicating proper

interfacial reactivity with formation of the Staudinger–Bertozzi product. During the course of the reactivity we did not observe displacement of any of the AuNP ligands due to a place-exchange reaction by the peptide's cysteine. This would have resulted in the appearance of a peak at −3.80 ppm for the free phosphine ligand and easily identifiable disulphides peaks in the ^{1}H NMR spectrum. When reaction was completed the excess peptide was washed away with nanopure water using centrifugal filtration (Millipore centrifugal filter units MWCO 10 kDa). Interestingly the reaction stopped at ~30% (calculated from the ^{31}P NMR spectra), indicating that most likely the AuNPs reached saturation due to the larger size of the peptide compared to the smaller model molecule benzyl azide. The AuNP-bioconjugate was characterized by TEM and XPS. TEM images (see Figure SI10) show again isolated AuNPs of ~3 nm in diameter and no nanoparticles networks were observed. The high-resolution scans of the C 1s peak (see Figure 9.3) show still the presence of the ester component at 289.00 eV and a marked increase in the component related to amide's carbonyl at 288 eV due to the presence of the numerous peptide bonds. The high-resolution scans of the S 2p peak (see Figure SI12) now show a marked increase of the S–H component at 163.21 eV (S $2p_{3/2}$) and of the disulfide component at 168.45 eV (S $2p_{3/2}$)[33] due to the presence of the peptide's cysteines that do not interfere with the interfacial reactivity thanks to the high chemoselectivity of the Staudinger–Bertozzi ligation. Finally, the high-resolution scans of the P 2p peak confirms that the 30% of the phosphine reacted with the peptide to form the triphenylphosphine-oxide. Interestingly this 30% of interfacial reaction yield seems to be recurring when employing 3 nm AuNPs. The same result was indeed obtained when a DBCO-functionalized protected-peptide was clicked onto azide-functionalized AuNPs of the same size using the SPAAC-PAD strategy.[16] Because the smaller reactive partner (benzyl azide) reacted quantitatively, the lower extent of reaction with the peptide may simply be an issue of sterics with the peptide blocking additional reactive sites. These results together are consistent with successful conjugation of the peptide onto the Staudinger-AuNPs and the efficiency of the rinsing/trituration. Finally, the nanoparticle bioconjugate was found to be soluble in water and in polar organic solvents and could be repeatedly dried and redissolved in solvent with little to no aggregation.

9.3 Conclusion

In this paper we reported the first synthesis of small gold nanoparticles that present interfacial methyl-2-(diphenylphosphino)benzoate functionalities able to undergo Staudinger–Bertozzi ligation for the creation of nanoparticle bioconjugates. These small Staudinger-AuNPs were completely characterized and a nanoparticle raw formula could be estimated with good precision from the combination of the TGA data, NMR spectra and TEM images. This represents important information in the bioconjugation field because of the expense of both starting materials and consequent difficulty to work in excess of one or the other clickable partner.

The reactivity of the Staudinger-AuNP was then investigated through ^{31}P NMR spectroscopy using benzyl azide as the clickable partner. The possibility to easily monitor the reaction by ^{31}P NMR spectroscopy by following the disappearance of the phosphine peak at 40.3 ppm and the appearance of the phosphine oxide peak of the product at 34.9 ppm represents a great advantage of this novel nanomaterial, and makes their use easy and straightforward. The data obtained from the kinetic study showed that the reaction mechanism with which these AuNPs react appears to be identical to that of small methyl-2-(diphenylphosphino)benzoate molecules in solution. The only difference appears to be in the kinetic constant that resulted to be a hundred times slower, due to the interfacial character of the reaction. More importantly, these studies showed quantitative reactivity of the triphenylphosphine moieties with the azide partner small molecule and the reacted Staudinger-AuNPs could be quantitatively recovered.

XPS confirms to be a reliable and highly sensitive surface analysis technique for the study of interfacial organic chemistry. In fact, the Staudinger-AuNP and the successful formation of the interfacial ligation product could be effectively characterized through the high-resolution scans especially of the C 1s and the P 2p core lines. The former core line after the interfacial Staudinger–Bertozzi ligation clearly shows the disappearance of the component at 289.08 eV that corresponds to the methyl-ester functionality of the starting material; the latter distinctively show two components one for the triphenylphosphine at 131.52 eV and the other for the triphenylphosphine oxide at 132.43

eV, allowing for quantifying the amount of azide partner that has been clicked onto the nanoparticles.

Another great advantage of our Staudinger-AuNPs is the insensitivity of the Staudinger–Bertozzi ligation to nucleophiles such as thiols or amines that are largely present in bio-systems. The high chemoselectivity of the Staudinger-AuNPs makes them an attractive alternative to faster but less chemoselective bioconjugation techniques that for example involve the Michael addition to maleimide functionalities or the SPAAC reaction. In fact, the reactivity of the maleimide or the side-reactivity of cyclooctyne towards thiols and amines can lower the chemoselectivity of the corresponding nanomaterial representing a threat to the biomolecule's conformation and biochemistry. In contrast our Staudinger-AuNPs react exclusively with the azide, as highlighted by the successful conjugation of an azide-functionalized CRGDK peptide. This direct conjugation would have required additional precautions if the Michael addition or the strain-promoted cycloaddition techniques were employed. Instead, using the Staudinger–Bertozzi ligation the AuNP-CRGDK bioconjugate could be synthesized efficiently and with a high loading onto the nanomaterial.

Finally the Staudinger-AuNPs can be used also in material chemistry. Thanks to their clean way of reacting they can react easily with any azide modified surface or material for the creation of nanohybrid materials and sensors. We are currently exploring these possibilities.

9.4 References

(1) A. Kumar, H. L. Ma, X. Zhang, K. Y. Huang, S. B. Jin, J. Liu, T. Wei, W. P. Cao, G. Z. Zou and X. J. Liang, *Biomaterials*, 2012, **33**, 1180–1189.

(2) A. J. Mieszawska, W. J. M. Mulder, Z. A. Fayad and D. P. Cormode, *Mol. Pharmaceutics*, 2013, **10**, 831–847.

(3) D.Xi,S.Dong,X.X.Meng,Q.H.Lu,L.J.MengandJ.Ye, *RSC Adv.*, 2012, **2**, 12515–12524.

(4) Y. C. Yeh, B. Creran and V. M. Rotello, *Nanoscale*, 2012, **4**, 1871–1880.

(5) C. J. Murphy, A. M. Gole, J. W. Stone, P. N. Sisco, A. M. Alkilany, E. C. Goldsmith and S. C. Baxter, *Acc. Chem. Res.*, 2008, **41**, 1721–1730.

(6) S. Eustis and M. A. El-Sayed, *Chem. Soc. Rev.*, 2006, **35**, 209– 217.

(7) D. Pissuwan, T. Niidome and M. B. Cortie, *J. Controlled Release*, 2011, **149**, 65–71.

(8) J. B. Delehanty, K. Boeneman, C. E. Bradburne, R. Kelly, J. E. Bongard and I. L. Medintz, *Ther. Delivery*, 2010, **1**, 411–433.

(9) W. R. Algar, D. E. Prasuhn, M. H. Stewart, T. L. Jennings, J. B. Blanco-Canosa, P. E. Dawson and I. L. Medintz, *Bioconjugate Chem.*, 2011, **22**, 825–858.

(10) N. J. Agard, J. M. Baskin, J. A. Prescher, A. Lo and C. R. Bertozzi, *ACS Chem. Biol.*, 2006, **1**, 644–648.

(11) S. S. van Berkel, M. B. van Eldijk and J. C. M. van Hest, *Angew. Chem., Int. Ed.*, 2011, **50**, 8806–8827.

(12) P. Gobbo, Z. Mossman, A. Nazemi, A. Niaux, M. C. Biesinger, E. Gillies and M. S. Workentin, *J. Mater. Chem. B*, 2013, **2**, 1764–1769.

(13) K. E. Beatty, J. D. Fisk, B. P. Smart, Y. Y. Lu, J. Szychowski, M. J. Hangauer, J. M. Baskin, C. R. Bertozzi and D. A. Tirrell, *ChemBioChem*, 2010, **11**, 2092–2095.

(14) P. V. Chang, J. A. Prescher, E. M. Sletten, J. M. Baskin, I. A. Miller, N. J. Agard, A. Lo and C. R. Bertozzi, *Proc. Natl. Acad. Sci. U. S. A.*, 2010, **107**, 1821–1826.

(15) M. Chigrinova, C. S. McKay, L. P. B. Beaulieu, K. A. Udachin, A. M. Beauchemin and J. P. Pezacki, *Org. Biomol. Chem.*, 2013, **11**, 3436–3441.

(16) X. Wang, P. Gobbo, M. Suchy, M. S. Workentin and R. H. E. Hudson, *RSC Adv.*, 2014, **4**, 43087–43091.

(17) E. Saxon and C. R. Bertozzi, *Science*, 2000, **287**, 2007– 2010.

(18) S. H. Yoshimura, S. Khan, S. Ohno, T. Yokogawa, K. Nishikawa, T. Hosoya, H. Maruyama, Y. Nakayama and K. Takeyasu, *Bioconjugate Chem.*, 2012, **23**, 1488–1493.

(19) A. Watzke, M. Kohn, M. Gutierrez-Rodriguez, R. Wacker, H. Schroder, R. Breinbauer, J. Kuhlmann, K. Alexandrov, C. M. Niemeyer, R. S. Goody and H. Waldmann, *Angew. Chem., Int. Ed.*, 2006, **45**, 1408–1412.

(20) M. B. Soellner, K. A. Dickson, B. L. Nilsson and R. T. Raines, *J. Am. Chem. Soc.*, 2003, **125**, 11790–11791.

(21) D. E. Borchmann, N. T. Brummelhuis and M. Weck, *Macromolecules*, 2013, **46**, 4426–4431.

(22) C. I. Schilling, N. Jung, M. Biskup, U. Schepers and S. Brase, *Chem. Soc. Rev.*, 2011, **40**, 4840–4871.

(23) M. King and A. Wagner, *Bioconjugate Chem.*, 2014, **25**, 825–839.

(24) B. E. Ramakers, J. C. van Hest and D. W. Lowik, *Chem. Soc. Rev.*, 2014, **43**, 2743–2756.

(25) D. Grohmann, F. Werner and P. Tinnefeld, *Curr. Opin. Chem. Biol.*, 2013, **17**, 691–698.

(26) H. C. Wu, J. Q. Yu and J. B. Spencer, *Org. Lett.*, 2004, **6**, 4675–4678.

(27) P. Gobbo and M. S. Workentin, *Langmuir*, 2012, **28**, 12357– 12363.

(28) K. D. Hartlen, H. Ismaili, J. Zhu and M. S. Workentin, *Langmuir*, 2012, **28**, 864–871.

(29) J. Zhu, B. M. Lines, M. D. Ganton, M. A. Kerr and M. S. Workentin, *J. Org. Chem.*, 2008, **73**, 1099– 1105.

(30) J. He, X. L. Huang, Y. C. Li, Y. J. Liu, T. Babu, M. A. Aronova, S. J. Wang, Z. Y. Lu, X. Y. Chen and Z. H. Nie, *J. Am. Chem. Soc.*, 2013, **135**, 7974–7984.

(31) H. Y. Lee, S. H. R. Shin, A. M. Drews, A. M. Chirsan, S. A. Lewis and K. J. M. Bishop, *ACS Nano*, 2014, **8**, 9979– 9987.

(32) P. Gobbo, S. Novoa, M. C. Biesinger and M. S. Workentin, *Chem. Commun.*, 2013, **49**, 3982–3984.

(33) J. C. Azcarate, M. A. F. Addato, A. Rubert, G. Corthey, G. S. K. Moreno, G. Benitez, E. Zelaya, R. C. Salvarezza and M. H. Fonticelli, *Langmuir*, 2014, **30**, 1820–1826.

(34) F. L. Lin, H. M. Hoyt, H. van Halbeek, R. G. Bergman and C. R. Bertozzi, *J. Am. Chem. Soc.*, 2005, **127**, 2686– 2695.

Chapter 10

10 Interfacial strain-promoted alkyne–azide cycloaddition (I-SPAAC) for the synthesis of nanomaterial hybrids

Chapter 10 has been published as a communication, and it is reproduced with permission from the Royal Society of Chemistry. The corresponding reference is: **P. Gobbo**, S. Novoa, M. C. Biesinger, M. S. Workentin*, *Chem. Commun.*, **2013**, *49*, 3982-3984.

Novoa was an undergraduate summer student under my direct co-supervision, along with my supervisor, Prof. M. S. Workentin. Novoa helped with the synthesis and characterization of the azide-terminated thiolated ligand. Biesinger performed the XPS experiments and assisted in the discussion of the XPS results. I wrote the drafts of the manuscript, with input and minor edits from the other co-authors and final edit by my supervisor, Prof. M. S. Workentin.

The supporting information file referenced in the text can be downloaded from the web site of the publisher.

ABSTRACT: An interfacial strain promoted azide–alkyne cycloaddition (I-SPACC) is introduced as a method to prepare robust nanomaterial hybrids. This is demonstrated with a reaction between a novel dibenzocyclooctyne-modified single walled carbon nanotubes (DBCO-SWCNT) and a versatile water-soluble azide modified gold nanoparticle (N_3-EG_4-AuNP).

10.1 Introduction, Results and Discussion

Bioorthogonal reactions are a subclass of click reactions that address the strict requirements of biocompatibility. They represent a powerful tool in chemical biology for *in vivo* imaging and tracking of biomolecules, providing unique insights into spatial and temporal aspects of biological processes that cannot otherwise be achieved through traditional biochemical methodologies.[1–3] The most famous bioorthogonal reaction is the copper-free [3+2] Huisgen cycloaddition, also know as strain-promoted alkyne–azide cycloaddition (SPAAC), introduced by C. R. Bertozzi.[4] This reaction was designed to take place rapidly and selectively inside biosystems, solving the problems related to the use of copper in the Cu-catalyzed version of this reaction.[5–7] Thanks to the extremely fast kinetics, the high efficiency, and the biocompatibility coupled with the orthogonality conferred by the ring strain of the cyclooctyne moiety that is the centrepiece of this approach,[8] the SPAAC reaction has been exploited to label *in vivo* azide-modified proteins directly expressed in the cell's cytosol or metabolically functionalized on the cell's membrane.[9–13] The characteristics that make this bioorthogonal reaction desirable in the bioorganic chemistry field, are transferrable to materials chemistry. Indeed, such a fast, clean and orthogonal reaction has the potential to become an important tool for the synthesis of nanostructured systems that require expensive starting materials like nanoparticles and other nanomaterials to react efficiently together without the need for metal catalysts. Despite the great potential of this reaction in the material chemistry field, it has not been used interfacially to prepare hybrid nanomaterials. Indeed only a few applications in materials science have been described. Turro and co-workers used the SPAAC reaction to synthesize photodegradable star polymers,[14] Bernardin *et al.* synthesized monosaccharide-functionalized quantum dots for *in vivo* metabolic imaging through the reaction between cyclooctyne-modified quantum dots and azide-modified monosaccarides,[15] and Popik prepared dibenzocyclooctyne (DBCO)-modified glass, silicon and quartz surfaces, and showed their potential as platforms for the generation of multicomponent surfaces.[7,16]

Here we introduce the concept of an interfacial strain-promoted alkyne–azide cycloaddition (I-SPAAC) reaction in carbon based material chemistry, showing for the

first time that it can successfully take place at the interface between different nano-materials. To show this innovative application of the SPAAC reaction, as a proof of concept we prepared a gold nanoparticle (AuNP)–carbon nanotube (CNT) hybrid, which represent a desirable nanomaterial that is gaining always more importance in material chemistry because of its numerous applications in catalysis, sensing and nanomedicine, and its preparation still represents a challenge for material chemists.[17–20] In order to prepare the AuNP–CNT hybrid through the I-SPAAC reaction we synthesized two novel and versatile partner nanomaterials, namely a small (3 nm) water-soluble azide-modified AuNP (N_3-EG_4-AuNP) and a DBCO-modified single walled CNT (DBCO-SWCNT), that could give the final product by simply reacting at room temperature and in water media, where both form stable solutions. The final nanohybrid synthesized through the I-SPAAC reaction was easy to prepare, robust, and homogeneously covered with small AuNP as shown by transmission electron microscopy (TEM) and X-ray photoelectron spectroscopy (XPS).

The preparation of N_3-EG_4-AuNP, required first preparing the starting water-soluble gold nanoparticles (Me-EG_3-AuNP) using a modified Brust–Schiffrin method following the previously reported procedure.[21] The azide ligands N_3-EG_4-SH, whose synthetic details are reported in the ESI, were introduced onto the Me-EG_3-AuNP using a place-exchange reaction. In a typical synthesis 42.5 mmol of N_3-EG_4-SH were stirred for 20 min in acetone and in presence of the 50.0 mg of basic Me-EG_3-AuNP. The free thiols were subsequently removed by repeatedly washing the dried AuNP film with hexanes and isopropanol. These novel N_3-EG_4-AuNP exhibited the solubility properties of the Me-EG_3-AuNP, forming stable solutions and being readily re-dissolvable in H_2O, acetone, acetonitrile, methanol, ethanol, DMF, DMSO and DCM with no to little aggregation. The N_3-EG_4-AuNPs were characterized using ^{1}H NMR and IR spectroscopy, TGA, and TEM. The ^{1}H NMR spectrum recorded in D_2O exhibited the broad peaks typical of organic modified AuNP, and after place-exchange reaction it showed the appearance of a new resonance at 3.45 ppm related to the methylene protons alpha to the incorporated azide (Figure S4, ESI). The ^{1}H NMR spectrum was also recorded in d_3-acetonitrile showing the same characteristics but having better resolved peaks (Figure S5, ESI). Through the integration of the peak related to the protons alpha to the azide (3.39 ppm in d_3-

acetonitrile) and that of the peak related to the methyl unit of Me-EG_3-SH ligands (3.31 ppm in d_3-acetonitrile) it was possible to estimate the incorporation of 35% azide ligands on the AuNP surface. The IR spectrum of the purified N_3-EG_4-AuNP compared to that of the starting Me-EG_3-AuNP (Figure S8, ESI), showed the appearance of the expected asymmetrical stretching of the azide group at 2101 cm^{-1}, confirming the successful functionalization of the basic AuNP. From the analysis of the TGA data (Figure S9, ESI), and in particular from the increased percentage of the organic component related to the addition of [CHN_3] units (corresponding to 55.03 g mol^{-1}) through the place-exchange reaction, it was possible to calculate that the AuNP organic shell is composed of 65% of Me-EG_3-S^- ligands, and 35% of N_3-EG_4-S^- ligands, supporting the analysis of the ^1H NMR spectroscopy. From the TGA data and from the molecular weight of the two ligands, it was possible to calculate that per milligram of N_3-EG_4-AuNP there are 0.745 mmol of azide ligands. TEM images (Figure S6, ESI) showed that the average diameter of the N_3-EG_4-AuNP was 3.22 ± 0.50 nm. From the combination of ^1H NMR spectroscopy, TEM and the TGA data, and assuming that the nanoparticles have a spherical shape and that their size is mono-dispersed, it is possible to calculate a nanoparticle raw formula[21] of Au_{1000} $(Me\text{-}EG_3\text{-}S)_{455}$ $(N_3\text{-}EG_4\text{-}S)_{245}$.

The novel SWCNT-DBCO were synthesized through a coupling reaction between the carboxylic groups already present on the nanotube's sidewalls and the commercially available DBCO-amine (for details see ESI). It is noteworthy that it is not necessary to pre-treat or oxidize the CNT before the coupling reaction. The amount of carboxylic groups already present on the CNT sidewalls allows for an efficient functionalization of the carbonaceous material (*vide infra*). The DBCO-modified CNT was found to form stable dispersions in both water and polar organic solvents like DCM, ACN, acetone and ethanol. The SWCNT-DBCO was characterized by XPS and IR spectroscopy. The XPS spectrum of SWCNT-DBCO (Figure S10b, ESI) compared to that of the starting material (Figure S10a, ESI) clearly shows the appearance of the peak related to the amide nitrogen at 400.0 eV (1s). The high resolution scan of the carbon 1s (Figure 10.1a) and oxygen 1s peaks (Figure 10.1b) for the SWCNT-DBCO (centre) compared to that of the SWCNT starting material (left) confirms the successful synthesis of DBCO-modified CNT.

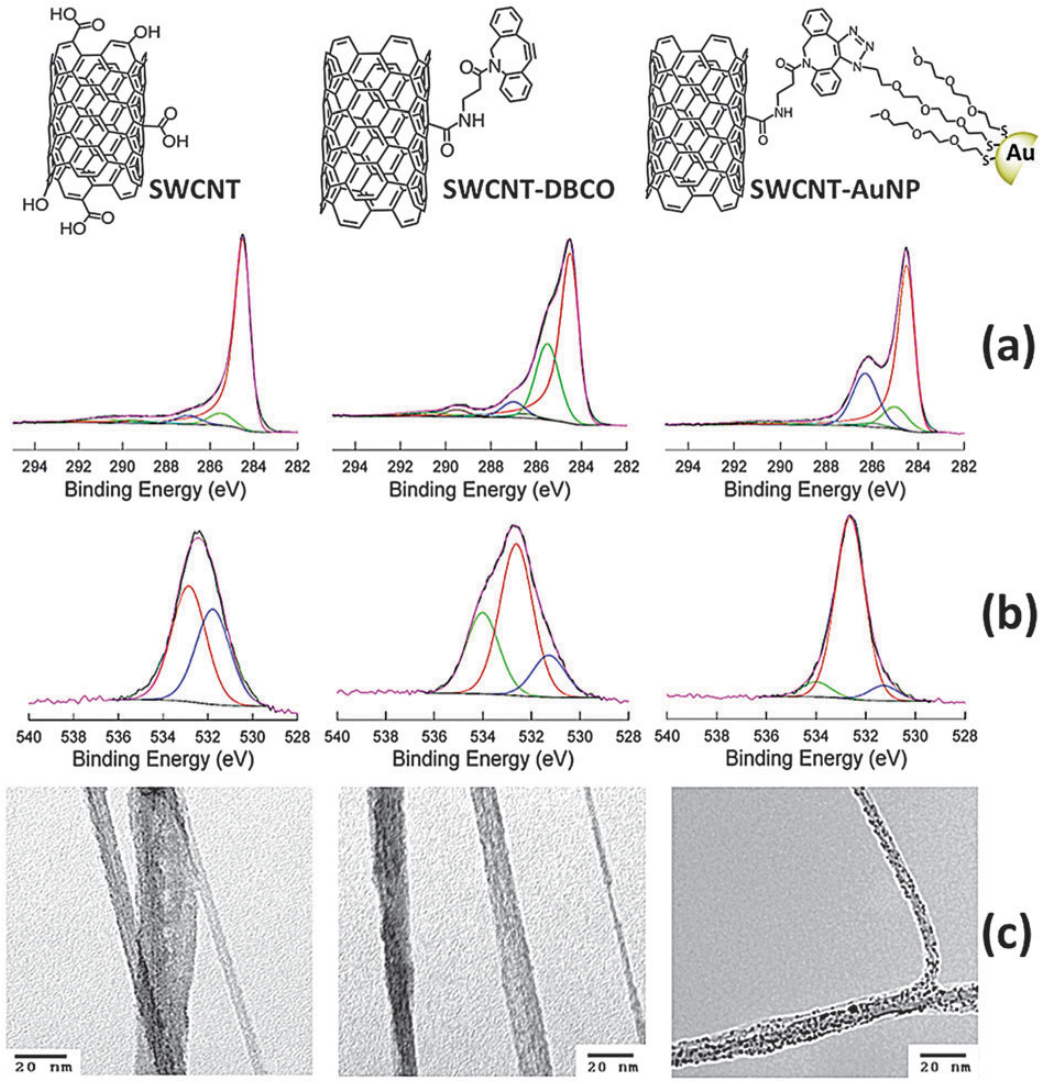

Figure 10.1: Top: schematic representation of the nanomaterials used/prepared; a) high-resolution C 1s XPS spectra, b) high resolution O 1s XPS spectra and c) TEM images (scale 20 nm) for SWCNT (left), SWCNT-DBCO (centre), SWCNT-AuNP hybrid (right), respectively.

The high-resolution scan of the carbon peak shows the appearance of a shoulder at 285.51 eV related to the sp^3-hybridized carbons introduced with the coupling reaction. This is also confirmed by the appearance of a shoulder at 534.01 eV on the high resolution scan of the oxygen peak related to the –(C=O*)–NH–, and by a marked decrease of the –(C=O*)–OH peak (531.28 eV), with respect to the steady component at

532.61 eV of the –C–OH. The IR spectrum of the purified SWCNT-DBCO further confirms this result showing the peaks related to the C–H stretching of the sp^3-hybridized carbons of the DBCO-amine at 2949, 2919, and 2848 cm^{-1}, and a band at 1580 cm^{-1} related to the stretching mode of the amide C=O.

The title SWCNT–AuNP hybrid nanomaterial was then easily prepared through the bioorthogonal I-SPAAC reaction between the two partners: SWCNT-DBCO and the N_3-EG_4-AuNP. The interfacial cycloaddition reaction was carried out simply by mixing the SWCNT-DBCO with the N_3-EG_4-AuNP in water media. In a typical synthesis, to a 1 ml of the SWCNT-DBCO mother solution was added 4 mg of N_3-EG_4-AuNP and the reaction volume was diluted to 4 ml with PBS pH 7 buffer. The system was stirred for 1 hour at room temperature and then the SWCNT–AuNPs were centrifuged in a Pyrex centrifuge test tube. The supernatant was removed, and the decorated CNT were dispersed in water, sonicated for 10 minutes and centrifuged. Subsequently, water was substituted first with acetone, then with dichloromethane (DCM), and the washing procedure (sonication in DCM and centrifugation) was repeated four more times. This protocol was to ensure removal of any non-covalently bound AuNP. The successful synthesis and purification of the covalent SWCNT–AuNP hybrid was confirmed by XPS and TEM. The XPS spectrum of SWCNT–AuNP (Figure S10c, ESI) shows the appearance of the peaks from Au at 84 eV (4f), 334–353 eV (4d), 547–643 eV (4p), and 762 eV (4s), and from S at 162.9 eV (2p) and 228 eV (2s). The high-resolution carbon 1s spectrum (Figure 10.1a, right) shows a marked increase of the component at 286.30 eV related to the C–O–C of the AuNP glycol units, while the high-resolution oxygen 1s spectrum (Figure 10.1b, right) shows an increase of the corresponding component at 532.63 eV. The Au 4f7/2 core line of AuNP is at 84.5 eV, this binding energy is shifted upwards from that of bulk Au (83.95 eV) due to particle size effects (Figure S13, ESI).[22,23] The N 1s core line after the interfacial I-SPAAC reaction shows a new component centered at 401.08 eV (Figure S13, ESI). While the major component at 399.98 eV is due to the DBCO-CNT amide nitrogens and to the nitrogen of the triazole rings; this new component is most likely related to the formation of $–NH^{3+}$ as a consequence of the photolysis of the unreacted $–N_3$ by the high energy incident radiation.[24] TEM images of the hybrid nanomaterial (Figure 10.1c, right) show that

AuNP are dispersed on the CNT surface, that they kept their original size and shape, and that there are no unbound particles present, confirming the efficiency of our purification procedure. Indeed, the use of sonication favours the detachment of the AuNP that are only physisorbed on the CNT leaving just those that are covalently bonded.

To further exclude the possibility of unspecific physisorption or bonding of the AuNP to the SWCNT-DBCO, a control experiment was carried out under identical conditions and following the same experimental procedure but using the model Me-EG_3-AuNP instead of the N_3-EG_4-AuNP. The Me-EG_3-AuNP, with the absence of the azide functionalities, is not expected to react with the DBCO-modified CNT because they cannot undergo the I-SPAAC reaction. Figure S14c (ESI) is from this control experiment and shows, as expected, clean SWCNT-DBCO comparable to those of Figure S14a (ESI). This confirms the successful synthesis of AuNP-decorated SWCNT through the new I-SPAAC reaction between SWCNT-DBCO and N_3-EG_4-AuNP.

Finally, sonication was employed to test the stability and resilience of the final hybrid material. A fraction of SWCNT–AuNP were dispersed in PBS pH 7.0 and ultra-sonicated for one hour. The TEM images obtained from these samples were compared with those of the freshly prepared SWCNT–AuNP and they did not show any appreciable difference either in the density of chemisorbed AuNP or in the AuNP size distribution. This supports the efficiency of our synthetic approach and the resilience of the resulting AuNP–CNT hybrid. The reaction of the N_3-EG_4-AuNP with DBCO as a model leads to efficient and total loading (complete reaction) on the AuNP. Because of this and the high effective concentration of the N_3 moiety on each AuNP we believe that every accessible DBCO on the DBCO- SWCNT reacts with N_3-EG_4-AuNP.

In summary, we introduce a simple and efficient copper-free interfacial strain-promoted alkyne–azide cycloaddition (I-SPAAC) reaction at the interface between different nanosystems: a new DBCO modified CNT and versatile water-soluble azide modified AuNP. This I-SPAAC reaction was fast and effective, leading to CNT homogeneously covered with small AuNP and to a robust and stable hybrid material thanks to the covalent bond that links the two nano-partners. Importantly, due to the nature of the

AuNP ligands these hybrid materials are easily dispersed in aqueous environment to aid in use for a variety of applications as varied as gas sensors, catalysts, and as structural components of electrochemical sensors. The coupling-based strategy introduced here can be exploited for exploring and creating a wide variety of bioorthogonal nanostructured materials for device applications. For example, it is possible to take advantage of the intrinsic presence of carboxylic acid groups on the surface of carbonaceous material (*i.e.*, graphene, nanodiamonds, glassy carbon) to introduce strained alkynes through the coupling reaction here described. These bioorthogonal materials would then be able to bind the azide-functionalized AuNP or other azide modified biomolecules through the I-SPAAC reaction.

10.2 References

(1) M. D. Best, *Biochemistry*, 2009, **48**, 6571.

(2) J. C. Jewett and C. R. Bertozzi, *Chem. Soc. Rev.*, 2010, **39**, 1272.

(3) M. F. Debets, S. S. Van Berkel, J. Dommerholt, A. J. Dirks, F. P. J. T. Rutjes and F. L. Van Delft, *Acc. Chem. Res.*, 2011, **44**, 805.

(4) N. J. Agard, J. A. Prescher and C. R. Bertozzi, *J. Am. Chem. Soc.*, 2004, **126**, 15046.

(5) E. Lallana, E. Fernandez-Megia and R. Riguera, *J. Am. Chem. Soc.*, 2009, **131**, 5748.

(6) J. M. Baskin, J. A. Prescher, S. T. Laughlin, N. J. Agard, P. V. Chang, I. A. Miller, A. Lo, J. A. Codelli and C. R. Bertozzi, *Proc. Natl. Acad. Sci. U. S. A.*, 2007, **104**, 16793.

(7) A. Kuzmin, A. Poloukhtine, M. A. Wolfert and V. V. Popik, Bioconjugate Chem., 2010, 21, 2076. 8 D. H. Ess, G. O. Jones and K. N. Houk, *Org. Lett.*, 2008, **10**, 1633.

(9) J. C. Jewett, E. M. Sletten and C. R. Bertozzi, *J. Am. Chem. Soc.*, 2010, **132**, 3688.

(10) J. Dommerholt, S. Schmidt, R. Temming, L. J. A. Hendriks, F. P. J. T. Rutjes, J. C. M. Van Hest, D. J. Lefeber, P. Friedl and F. L. Van Delft, *Angew. Chem., Int. Ed.*, 2010, **49**, 9422.

(11) K. E. Beatty, J. D. Fisk, B. P. Smart, Y. Y. Lu, J. Szychowski, M. J. Hangauer, J. M. Baskin, C. R. Bertozzi and D. A. Tirrell, *ChemBioChem*, 2010, **11**, 2092.

(12) N. E. Mbua, J. Guo, M. A. Wolfert, R. Steet and G.-J. Boons, *ChemBioChem*, 2011, **12**, 1911.

(13) H. Koo, S. Lee, J. H. Na, S. H. Kim, S. K. Hahn, K. Choi, I. C. Kwon, S. Y. Jeong and K. Kim, *Angew. Chem., Int. Ed.*, 2012, **51**, 11836.

(14) J. A. Johnson, J. M. Baskin, C. R. Bertozzi, J. T. Kobersteind and N. J. Turro, *Chem. Commun.*, 2008, 3064.

(15) A. Bernardin, A. Cazet, L. Guyon, P. Delannoy, F. Vinet, D. Bonnaffé and I. Texier, *Bioconjugate Chem.*, 2010, **21**, 583.

(16) S. V. Orski, A. A. Poloukhtine, S. Arumugam, L. Mao, V. V. Popik and J. Locklin, *J. Am. Chem. Soc.*, 2010, **132**, 11024.

(17) N. Chauhan, A. Singh, J. Narang, S. Dahiya and S. C. Pundir, *Analyst*, 2012, **137**, 5113.

(18) J. Huang, X. Xing, X. Zhang, X. He, Q. Lin, W. Lian and H. Zhu, *Food Res. Int.*, 2011, **44**, 276.

(19) D. Cai, Y. Yu, Y. Lan, F. J. Dufort, G. Xiong, T. Paudel, Z. Ren, D. J. Wagner and T. C. Chiles, *BioFactors*, 2007, **30**, 271.

(20) Y. Guo, S. Guo, Y. Fang and S. Dong, Electrochim. Acta, 2010, 55, 3927. 21 P. Gobbo and M. S. Workentin, *Langmuir*, 2012, **28**, 12357.

(22) H. Liu, B. S. Mun, G. Thornton, S. R. Isaacs, Y.-S. Shon, D. F. Ogletree and M. Salmeron, *Phys. Rev. B*, 2005, **72**, 155430.

(23) C. R. Henry, *Surf. Sci. Rep.*, 1998, **31**, 231.

(24) A. Devadoss and C. E. D. Chidsey, *J. Am. Chem. Soc.*, 2007, **129**, 5370.

Chapter 11

11 Conclusion and Outlook

In this thesis, the development of a new approach for the modification of materials based on what we define as *click and bioorthogonal nanomaterial templates* is reported. These are stable (*i.e.*, can be stored for indefinitely long periods of time under appropriate conditions) and biocompatible nanomaterials that display interfacial click or bioorthogonal moieties that are ready to react with any molecular system of interest that carries the complementary functional group or chemical reporter. The click and bioorthogonal nanomaterial template allows for the facile modification of the nanomaterial's surface with a reaction, which exhibit the following characteristics:

1) Is easy to perform.
2) Is chemoselective.
3) Has fast reaction kinetics.
4) Relies on biocompatible functional groups and does not generate toxic byproducts.
5) Leads to a robust nanomaterial functionalization due to the formation of covalent bonds.
6) Is orthogonal to native biological functionalities and processes in the bioorganism under study.
7) Is orthogonal to the surface chemistry of the nanomaterial.

This thesis describes the development of synthetic strategies for the safe introduction of click and bioorthogonal groups (namely azides, maleimides, strained alkynes, and methyl-2-(diphenylphosphino)benzoate functionalities) at the interface of small amphiphilic AuNPs. It also describes the development of methodologies for the detailed characterization of the resulting click or bioorthogonal AuNP templates and the determination of the number of reactive moieties that are present at their interface. This information is of paramount importance for potential applications of the click and bioorthogonal nanomaterial templates in drug delivery and bioconjugation. These methodologies involve the use of transmission electron microscopy, nuclear magnetic

resonance spectroscopy and thermogravimetric analysis to obtain an average AuNP raw formula. The calculation of the AuNP raw formula is performed under the assumption that the AuNPs are spherical and perfectly monodispersed in size. The same results were then independently confirmed by X-ray photoelectron spectroscopy.

Another important achievement of this work was the development of protocols to demonstrate that the click and bioorthogonal nanomaterial templates reacted as desired with the corresponding reaction partner and for tracking the nanomaterial's reactivity over time. These goals were achieved by using a number of techniques, but mostly NMR spectroscopy and X-ray photoelectron spectroscopy, which are techniques that can provide selective information on changes on the the AuNPs' organic corona. Through the development of these methodologies, we were able to achieve molecular level control over the reactivity of the click and bioorthogonal nanomaterial templates. This represents a major step forward in the functional nanomaterial field where the functionalization of a nanomaterial's surface was achieved so far only through "shotgun"-type approaches that have no control over the extent of incorporation of the desired molecular system or its quantification.

The future direction of this work will require the transposition of these methodologies to other nanomaterials substrates in order to extend the concept of click and bioorthogonal nanomaterial templates. A first step towards the achievement of this goal has already been made: single-walled carbon nanotubes (SWCNT) displaying interfacial functional groups able to undergo Michael-type addition reactions (see Chapter 5) and interfacial strain-promoted reactions (see Chapter 10) were synthesized. The reactive moieties were introduced through an interfacial coupling strategy that took advantage of the carboxylic groups present on the defect sites of the SWCNT. From this example it is evident that the challenges behind the realization of other click and bioorthogonal nanomaterial templates will require tailoring of the synthetic and analytical methodologies described in this thesis to the surface chemistry of each individual nanomaterial substrate and their specific physical-chemical properties.

This work also set the basis for the preparation of click and bioorthogonal multifunctional nanomaterial templates. These are nanomaterials that simultaneously display different click or bioorthogonal groups at their interface, where each reactive moiety is mutually orthogonal and will be responsible for a specific function, and the multifunctional nanomaterial template will still be able to react through a chemistry that will be controlled at the molecular level. This type of technology could be already realized using the small AuNPs and the synthetic approaches described in this thesis. For example, it would be interesting to introduce a maleimide and a strained alkyne onto a AuNP's corona. The maleimide could be used for conjugating a PET contrast agent for biomedical imaging onto the AuNPs through a fast and efficient Michael-type addition reaction, while the strained alkyne could be employed for targeting azide-functionalized antibodies *in vivo*. This would allow for the *in vivo* imaging of cancer cells or bacterial infections. While this represents a specific example, it is important to highlight that the scope of this multifunctional nanomaterial template would be much broader because it could be orthogonally modified with any molecular system of interest that displays azides, nitrones or nucleophiles. This high versatility would potentially further expand the number of potential applications for AuNPs in fields that would span from chemical biology, nanomedicine and sensing.

The continuous emergence of new nanomaterials and techniques for carefully controlling their size, shape and physical-chemical properties represents a limitless source of new opportunities for the creation of click and bioorthogonal nanomaterial templates. The creation of synthetic strategies for the modification of nanomaterial surfaces by the introduction of click and bioorthogonal functional groups that allow the nanomaterial to react reliably, efficiently, and chemoselectively and perform specific functions has the potential to further enhance the impact of nanomaterials and lead to unprecedented directions in the field. Furthermore, the ease with which these nanomaterial templates can be reacted with a molecular system of interest carrying the complementary functionality allows them to be employed by users with basic chemistry skills. This makes it possible to quickly develop new uses for them in the most diverse disciplines of science and technology, leading to a new phase of the nanomaterial revolution that will have a much deeper impact on our everyday life.

Appendices

Appendix A: The Supporting Information of Chapter 2 is available at:
http://pubs.acs.org/doi/suppl/10.1021/la302168g/suppl_file/la302168g_si_001.pdf

Appendix B: The Supporting Information of Chapter 3 is available at:
http://www.rsc.org/suppdata/tb/c3/c3tb20699h/c3tb20699h.pdf

Appendix C: The Supporting Information of Chapter 4 is available at:
http://pubs.acs.org/doi/suppl/10.1021/acs.bioconjchem.5b00600/suppl_file/bc5b00600_si_001.pdf

Appendix D: The Supporting Information of Chapter 5 is available at:
http://www.rsc.org/suppdata/cc/c3/c3cc00050h/c3cc00050h.pdf

Appendix E: The Supporting Information of Chapter 7 is available at:
http://www.rsc.org/suppdata/ra/c4/c4ra07574a/c4ra07574a1.pdf

Appendix F: The Supporting Information of Chapter 8 is available at:
http://www.rsc.org/suppdata/tb/c3/c3tb21799j/c3tb21799j.pdf

Appendix G: The Supporting Information of Chapter 9 is available at:
http://www.rsc.org/suppdata/c5/ob/c5ob00372e/c5ob00372e1.pdf

Appendix H: The Supporting Information of Chapter 10 is available at:
http://www.rsc.org/suppdata/cc/c3/c3cc41634h/c3cc41634h.pdf

Appendix I: Copyright Clearance

Water-soluble gold nanoparticles (AuNP) functionalized with a gadolinium(III) chelate *via* Michael addition for use as a MRI contrast agent

M. Milne, P. Gobbo, N. McVicar, R. Bartha, M. S. Workentin and R. H. E. Hudson, *J. Mater. Chem. B*, 2013, **1**, 5628
DOI: 10.1039/C3TB20699H

Facile synthesis of gold nanoparticle (AuNP)–carbon nanotube (CNT) hybrids through an interfacial Michael addition reaction

P. Gobbo, M. C. Biesinger and M. S. Workentin, *Chem. Commun.*, 2013, **49**, 2831
DOI: 10.1039/C3CC00050H

Versatile strained alkyne modified water-soluble AuNPs for *interfacial* strain promoted azide–alkyne cycloaddition (I-SPAAC)

P. Gobbo, Z. Mossman, A. Nazemi, A. Niaux, M. C. Biesinger, E. R. Gillies and M. S. Workentin, *J. Mater. Chem. B*, 2014, **2**, 1764
DOI: 10.1039/C3TB21799J

Small gold nanoparticles for interfacial Staudinger–Bertozzi ligation

P. Gobbo, W. Luo, S. J. Cho, X. Wang, M. C. Biesinger, R. H. E. Hudson and M. S. Workentin, *Org. Biomol. Chem.*, 2015, **13**, 4605
DOI: 10.1039/C5OB00372E

Interfacial strain-promoted alkyne–azide cycloaddition (I-SPAAC) for the synthesis of nanomaterial hybrids

P. Gobbo, S. Novoa, M. C. Biesinger and M. S. Workentin, *Chem. Commun.*, 2013, **49**, 3982
DOI: 10.1039/C3CC41634H

Curriculum Vitae

Name: Pierangelo Gobbo

Post-secondary Education and Degrees:
University of Padua
Padua, Italy
2005-2008 B.A.

University of Padua
Padua, Italy
2008-2010 M.A.

The University of Western Ontario
London, Ontario, Canada
2011-2016 Ph.D.

Scholarships, Fellowships, Research Grants and Awards:

i) Scholarships

1) *Marie Sklodowska-Curie International Incoming Fellowship (IIF)*, € 183,455.00, international. Awarded in Jan. **2016**. This award covers salary, research, travel, and administrative costs over 2 years. Score 90.80/100 Criteria: excellence, impact and implementation of the proposed research; excellence of the researcher and potential to transfer knowledge during the research program; capacity of the researcher to reach or re-enforce a position of professional maturity in research.
2) *NSERC Postdoctoral Fellowship*, $ 90,000.00 in two years, national. Awarded in Jan. **2016**. Fellowship awarded annually to less than 5% of Ph.D. students. Ranked 2 out of 82 applications by the Fellowship Selection Committee for Chemical, Biomedical and Materials Science Engineering. Overall score 94.20/100. Criteria: academic excellence, research achievement and potential, communication, interpersonal, and leadership abilities.
3) *NSERC Vanier Canada Graduate Scholarship (CGS)*, $ 150,000.00 for nine terms of tenure. Awarded in April **2013** with a total of 54 fellowships offered across Canada. Ranked 7 out of 139 by the NSERC Selection Committee with an overall average score of 7.53.
4) *Ontario Graduate Scholarship (OGS)*, $ 15,000.00 for three terms of tenure, 8 scholarships were available for international students at Western University in **2013**. Awarded in April 2013, scholarship declined due to the NSERC Vanier CGS.
5) *Caratterizzazione di monostrati autoassemblati (Characterization of self-assembled monolayers),* Euro 1,264.00. Scholarship founded by the research project CARIPARO, for the period of 1 month (March **2011**). Research activity carried out under the scientific supervision of Prof. Flavio Maran (University of Padua).

ii) Research Grants

1) Research Western Scholar Grant, $ 10,000.00 (Sept **2013**) in recognition of VCGS and in support of my scholarly activities.

iii) Awards and Honours

1) *CSC Young Emerging Materials Investigator* **2015**, conferred by the Canadian Society for Chemistry, Materials Chemistry Division.
2) *CSC Travel Award* **2014-2015** from the Department of Chemistry of Western University (Canada), for presenting my research at the *Materials Research Society* meeting in Boston (USA) ($ 900.00).
3) *XRCC Award.* 1st place in the oral presentations competition (Materials Division) at the *Canadian Society for Chemistry Conference* **2014** – Vancouver (BC), ($ 200.00).
4) *Thermo Fisher Scientific Award.* 1st place in the oral presentations competition (Materials Division) at the *Canadian Society for Chemistry Conference* **2014** – Vancouver (BC), ($ 200.00).
5) *Dr. N. Stewart McIntyre Award* **2013** from Surface Science Western for excellence in research ($ 1,000.00).
6) Nominated for the *Western Graduate Student Teaching Award* **2013** for excellence in graduate teaching (competition extended to all faculties of Western University).

Related Work Experience

Teaching Assistant
The University of Western Ontario
2011-2013

Research Assistant
University of Padua
2009-2010

Research Assistant
The University of Western Ontario
2011-2016

Publications:

i) Articles published or accepted in refereed journals

(denotes communicating author; † these authors contributed equally to the work; name of mentored students)*

1) M. R. Weissman, K. T. Winger, S. Ghiassian, **P. Gobbo***, M. S. Workentin*, *"Insights on the Application of the Retro Michael-Type Addition on Maleimide-Functionalized Gold Nanoparticles in Biology and Nanomedicine". Bioconjugate Chem.*, **2016**, DOI: 10.1021/acs.bioconjchem.5b00600. **Journal cover.**

2) **P. Gobbo,** T. Romagnoli, S. M. Barbon, J. T. Price, J. Keir, J. B. Gilroy*, M. S. Workentin*, *"Expanding the scope of strained-alkyne chemistry: a protection-deprotection strategy via the formation of a dicobalt-hexacarbonyl complex".*

Chem. Commun., **2015**, *51*, 6647-6650. **Highlighted on Organic-Chemistry.org in "Functional Group Protection".**

3) **P. Gobbo***, W. Luo, S. J. Cho, X. Wang, M. C. Biesinger, R. H. E. Hudson, M. S. Workentin*, *"Small Gold Nanoparticles for Interfacial Staudinger-Bertozzi Ligation"*. *Org. Biomol. Chem.*, **2015**, *13*, 4605 - 4612.
4) G. Q. Wallace, M. S. Zuin, M. Tabatabaei, **P. Gobbo**, F. Lagugné-Labarthet*, M. S. Workentin*, *"Gold nanosponges (AuNS): a versatile template for surface-enhanced Raman spectroscopy and biosensing applications". Analyst*, **2015**, *140*, 7278-7282.
5) **P. Gobbo***, P. Gunawardene, W. Luo, M. S. Workentin*, *"Synthesis of a Toolbox of Clickable Rhodamine B Derivatives". Synlett*, **2015**, *26*, 1169-1174.
6) S. M. Barbon†, **P. Gobbo**†, W. Luo, J. T. Price, M. C. Biesinger, M. S. Workentin*, J. B. Gilroy*, *"An azide-functionalized nitronyl nitroxide radical: synthesis, characterization, and Staudinger-Bertozzi ligation reactivity"*. *Synlett*, **2015**, *26*, 304-308.
7) S. Ghiassian, **P. Gobbo**, M. S. Workentin*, *"Water-soluble maleimide modified gold nanoparticles (AuNPs) as a platform for cycloaddition reactions". Eur. J. Org. Chem.*, **2015**, *24*, 5438-5447.
8) N. Kazemi-Zanjani, **P. Gobbo**, Z. Zhu, M. S. Workentin, F. Lagugné-Labarthet*, *"High resolution Raman imaging of bundles of single-walled carbon nanotubes by tip-enhanced Raman spectroscopy"*. *Can. J. Chem.*, **2015**, *93*, 51-59.
9) X. Wang†, **P. Gobbo**†, M. Suchy, M. S. Workentin*, R. H. E. Hudson*, *"Peptide-decorated gold nanoparticles via strain-promoted azide-alkyne cycloaddition and post assembly deprotection". RSC Advances*, **2014**, *4*, 43087-43091.
10) **P. Gobbo**, Z. Mossman, A. Nazemi, A. Niaux, M. C. Biesinger, E. R. Gillies, M. S. Workentin*, *"Versatile strained alkyne modified water-soluble AuNPs for interfacial strain promoted azide-alkyne cycloaddition (I-SPAAC)". J. Mater. Chem. B*, **2014**, *2*, 1764-1769.
11) **P. Gobbo**, S. Novoa, M. C. Biesinger, M. S. Workentin*, *"Interfacial strain-promoted alkyne-azide cycloaddition (I-SPAAC) for the synthesis of nanomaterial hybrids"*. *Chem. Commun.*, **2013**, *49*, 3982-3984.
12) **P. Gobbo**, M. C. Biesinger, M. S. Workentin*, *"Facile synthesis of gold nanoparticle (AuNP)–carbon nanotube (CNT) hybrids through an interfacial Michael addition reaction"*. *Chem. Commun.*, **2013**, 49, 2831-2833.
13) F. Pashaee, R. Hou, **P. Gobbo**, M. S. Workentin, F. Lagugné-Labarthet*, "*Tip-enhanced Raman spectroscopy of self-assembled thiolated monolayers on flat gold nanoplates using gaussian-transverse and radially polarized excitations". J. Phys. Chem. C.*, **2013**, *117*, 15639-15646.
14) E. Magdzinski, **P. Gobbo**, M. S. Workentin, P. J. Ragogna*, *"A novel diiminopyridine ligand containing redox active Co(III) mixed sandwich complexes"*. *Inorg. Chem.*, **2013**, *52*, 11311-11319.
15) J. M. Kaplan, J. Shang, **P. Gobbo**, S. Antonello, V. Chatare, D. M. Ratner, R. B. Andrade, F. Maran*, *"Conformationally constrained functional peptide monolayers for the controlled display of bioactive carbohydrate ligands*". *Langmuir*, **2013**, *29*, 8187-8192.

16) M. Milne†, **P. Gobbo**†, N. McVicar, R. Bartha, M. S. Workentin*, R. H. E. Hudson*, *"Water-soluble gold nanoparticles (AuNP) functionalized with gadolinium(III) chelate via Michael addition for use as a MRI contrast agent"*. *J. Meter. Chem. B*, **2013**, *1*, 5628-5635.
17) **P. Gobbo**†, M. J. Biondi†, J. J. Feld, M. S. Workentin*, "*Arresting the time-dependent H_2O_2 mediated synthesis of gold nanoparticles for analytical detection and preparative chemistry*". *J. Mater. Chem. B*, **2013**, *1*, 4048–4051.
18) **P. Gobbo**, S. Ghiassian, M. Hesari, N. Kazemi-Kanjani, K. G. Stamplecoskie, M. S. Workentin*, "*Electrochemistry of robust gold nanoparticle-glassy carbon hybrids generated using a patternable photochemical approach*". *J. Mater. Chem.*, **2012**, *22*, 23971-23980.
19) E. Magdzinski, **P. Gobbo**, C. D. Martin, M. S. Workentin, P. J. Ragogna*, "*The syntheses and electrochemical studies of a ferrocene substituted diiminopyridine ligand and its P, S, Se, and Te complexes*". *Inorg. Chem.*, **2012**, *51*, 8425-8432.
20) **P. Gobbo**, M. S. Workentin*, "*Improved methodology for the preparation of water-soluble maleimide-functionalized small gold nanoparticles*". *Langmuir*, **2012**, *28*, 12357−12363.
21) A. Biffis, L. Gazzola, **P. Gobbo**, G. Buscemi, C. Tubaro, M. Basato*, "*Alkyne hydroarylations with chelating dicarbene palladium(II) complex catalysts: improved and unexpected reactivity patterns disclosed upon additive screening*". *Eur. J. Org. Chem.*, **2009**, *19*, 3189-3198.

ii) Manuscripts submitted or in preparation

1) **P. Gobbo***, M. S. Workentin*, "*Maleimide-Modified Gold Nanoparticles (AuNPs): a Versatile Platform for Interfacial Click Reactions Leading to Chemically Modified AuNPs"*. Account paper in preparation for *Langmuir*.
2) **P. Gobbo***, W. Luo, M. S. Workentin*, *"Bioorthogonal Chemistry: A New Tool for the Functionalization of Nanomaterial Surfaces".* Account paper in preparation for *Langmuir*.
3) W. Luo, **P. Gobbo**, D. A. Sutton, C. D. McNitt, V. V. Popik, M. S. Workentin*, "*Photoinduced Interfacial Unmasking of Strained Alkynes on Small Water Soluble Gold Nanoparticles*". Manuscript in preparation for *Langmuir*.
4) W. Luo, **P. Gobbo**, P. Gunawardene, M. S. Workentin*, "*A Water Soluble Gold Nanoparticle Platform: A Model for the Controlled Release of Molecules from AuNP Nanocarriers via Staudinger-Bertozzi Ligation*". Manuscript in preparation for *Chem. Commun*.
5) S. Ghiassian, A. Nazemi, L. Yu, **P. Gobbo**, E. Gillies, L. G. Luyt, M. S. Workentin*, "*Novel Nitrone Modified Gold Nanoparticles: Synthesis, Characterization and Their Potential for the Development of ^{18}F-Labeled PET Probes*". Manuscript in preparation for *J. Am. Chem. Soc*.
6) E. Magdzinski, **P. Gobbo,** C. D. Martin, M. S. Workentin, P. J. Ragogna*, *"The synthesis and reactivity of metallocene-substituted diimine ligands"*. Manuscript in preparation for *Eur. J. Chem.*
7) **P. Gobbo**, M. W. Lui, P. J. Ragogna, M. S. Workentin*, *"Furan-modified highly fluorinated phosphonium salt (HFPS): a new template for smart hydrophobic materials"*. Manuscript in preparation for *Eur. J. Org. Chem*.

iii) Invited Speaker

1) "*Interfacial photochemistry for materials modification*". Pacifichem, Symposium: Reactive intermediates and unusual molecules, Honolulu (HI). **Dec. 16 2015**
2) "*Expanding the scope of nanomaterials: the development of new strategies for the chemical modification of nanomaterials*". Invited lecture at Dalhousie University, Halifax (NS). **Oct. 23 2015**
3) "*Chemistry at the interface of nanomaterials*". Invited lecture at the University of New Brunswick, Fredericton (NB). **Jul. 13 2015**
4) "*A clickable gold nanoparticles toolbox for bioconjugation, imaging and drug delivery*". 98th Canadian Chemistry Conference and Exhibition, Materials Chemistry Division, Ottawa (ON). **Jun. 14 2015**
5) *"A toolbox of clickable gold nanoparticles for bioconjugation, imaging and drug delivery"*. National Research Council of Canada, Sussex Laboratories, Ottawa (ON). **Jan. 20 2015**
6) "*Nanotechnology: from research to future*" (original title: *"Nanotecnologia: tra ricerca e futuro"*). High School Liceo Tito Lucrezio Caro (Cittadella, Padua, Italy). Because of my academic accomplishments and good communication skills, I was selected by Prof. Stefano Mammi (University of Padua), responsible for the student orientation for faculty of science, to hold this lecture on nanotechnology. **Apr. 12 2011**

iv) Non-refereed contributions

Personally presented:

1) P. Gobbo, W. Luo, P. Gunawardene, S. Ghiassian, M. S. Workentin*: *"Toolbox of clickable and bioorthogonal gold nanoparticles: From synthesis to application"*. Pacifichem, Symposium: Bioorthogonal chemistry - Tools and applications in chemical biology Honolulu (HI), Dec. 15-20 **2015**. Oral presentation.
2) P. Gobbo, M. S. Workentin*: *"Clickable gold nanoparticles (AuNP) for bioconjugation, imaging and drug delivery"*. Materials Research Society Fall Meeting & Exhibit, Boston (MA), Nov. 30-Dec. 5 **2014**. Oral presentation.
3) P. Gobbo, Z. Zhu, S. M. Barbon, A. Niaux, M. C. Biesinger, J. B. Gilroy, M. S. Workentin*: *"Synthesis of clickable single-walled carbon nanotubes"*. 97th Canadian Chemistry Conference and Exhibition, Vancouver (BC), Jun. 1-6 **2014**. Oral presentation.
4) P. Gobbo, R. Wang, E. Simpson, A. Nazemi, R. H. E. Hudson, L. Luyt, E. Gillies, M. S. Workentin*: *"Interfacial strain-promoted alkyne-azide cycloaddition for the creation of gold nanoparticles (AuNP) bioconjugates and hybrid nanomaterials".* 97th Canadian Chemistry Conference and Exhibition, Vancouver (BC), Jun. 1-6 **2014**. Oral presentation.

5) P. Gobbo, M. S. Workentin*: "Synthesis, characterization and application of clickable gold nanoparticles". CAMBR Distinguished Lecturer and Research Day, UWO London (ON) (Canada), Nov. 1, **2013**. Oral presentation.
6) P. Gobbo, M. C. Biesinger, M. S. Workentin*: "Covalent functionalization of carbon nanotubes (CNT) using click chemistry". 96th Canadian Chemistry Conference and Exhibition, Quebec (Quebec), May 26-30 **2013**. Oral presentation.
7) P. Gobbo, M. Milne, R. Wang, E. Simpson, L. Luyt, R. H. E. Hudson and M. S. Workentin*: "Clickable gold nanoparticles (AuNP) for drug delivery and bioconjugation". 96th Canadian Chemistry Conference and Exhibition, Quebec (Quebec), May 26-30 **2013**. Oral presentation.
8) P. Gobbo, M. Milne, R. Wang, R. H. E. Hudson, M. S. Workentin*: "Small bioorthogonal gold nanoparticles (AuNP) for in vivo labeling of biosystems". CAMBR Distinguished Lecturer and Research Day, UWO London (ON) (Canada), Nov. 13, **2012**. Poster.
9) P. Gobbo, S. Ghiassian, M. Hesari, N. Kazemi, K. G. Stamplecoskie, M. S. Workentin *: "Method to covalently functionalize glassy carbon electrode surfaces with gold nanoparticles through photolysis of interfacial diazirine functionalities". 95th Canadian Chemistry Conference and Exhibition, Calgary (Alberta), May 26-30 **2012**. Oral presentation.
10) P. Gobbo, S. Ghiassian, N. Kazemi, F. Lagugné-Labarthet, M. S. Workentin*: "Modification of glassy carbon (GC) electrode surfaces with Au nanoparticles via an interfacial carbene reaction". 39th Physical Organic MiniSimphosium (POMs), UWO London (ON) (Canada), Nov. 4-6 **2011**. Poster.
11) P. Gobbo, S. Antonello, I. Guryanov, M. Hesari, A. and F. Maran*: "Superefficient electron transfer through 3_{10}-helical peptides". CAMBR Distinguished Lecturer and Research Day, UWO London (ON) (Canada), Jun. 23, **2011**. Poster.

Presented by others:

1) G. Q. Wallace, M. S. Zuin, M. Tabatabaei, P. Gobbo, M. S. Workentin, F. Lagugné-Labarthet*: "Molecular and biomolecular detection by surface-enhanced Raman spectroscopy using a nanoaggregate-on-mirror plasmonic sensor". 98th Canadian Chemistry Conference and Exhibition, Materials Chemistry Division, Ottawa (ON), Jun. 13-17 **2015**.
2) W. Luo, P. Gobbo, S. J. Cho, X. Wang, M. C. Biesinger, R. H. E. Hudson, M. S. Workentin*: "Interfacial Staudinger-Bertozzi ligation in the synthesis of gold nanoparticles bioconjugates". 98th Canadian Chemistry Conference and Exhibition, Materials Chemistry Division, Ottawa (ON), Jun. 13-17 **2015**.
3) W. Luo, P. Gobbo, M. C. Biesinger, M. S. Workentin*: "Phototriggered interfacial unmasking of strained alkynes on gold nanoparticles". 98th Canadian Chemistry Conference and Exhibition, Materials Chemistry Division, Ottawa (ON), Jun. 13-17 **2015**.
4) W. Luo, P. Gobbo*, S. J. Cho, X. Wang, M. C. Biesinger, R. H. E. Hudson, M. S. Workentin*: "Small gold nanoparticles for interfacial Staudinger-Bertozzi ligation: from synthesis to bioconjugation". 42nd Physical Organic Mini-

Symposium (POMs), McMaster University, Hamilton (ON), Nov. 7-9 **2014**. Oral presentation.

5) S. Ghiassian, A. Nazemi, P. Gobbo, L. Yu, E. R. Gillies, L. G. Luyt, M. S. Workentin*: *"Rapid and efficient gold nanoparticle modification via interfacial strain-promoted alkyne-nitrone cycloaddition (I-SPANC) reaction"*. 42nd Physical Organic Mini-Symposium (POMs), McMaster University, Hamilton (ON), Nov. 7-9 **2014**. Oral presentation.
6) W. Luo, P. Gobbo, S. J. Cho, R. Wang, M. C. Biesinger, R. H. E. Hudson, M. S. Workentin*: *"Synthesis and characterization of small gold nanoparticles for interfacial Staudinger-Bertozzi ligation"*. 5th Annual Nano Ontario Conference; University of Windsor, Windsor, ON, Canada; Nov. 6-7 **2014**. Poster presentation.
7) S. Ghiassian, P. Gobbo, A. Nazemi, M. S. Workentin*: *"Thermal and photochemical modification of small water soluble gold nanoparticles"*. 97th Canadian Chemistry Conference and Exhibition, Vancouver (BC), Jun. 1-6 **2014**. Oral presentation.
8) E. J. Simpson, P. Gobbo, F. Bononi, M. S. Workentin, L. G. Kuyt*: *"Bombesin functionalized water-soluble gold nanoparticles for prostate cancer imaging".* 97th Canadian Chemistry Conference and Exhibition, Vancouver (BC), Jun. 1-6 **2014**. Oral presentation.
9) M. S. Zuin, G. Q. Wallace, M. Tabatabaei, P. Gobbo, F. Lagugne-Labarthet, and M. S. Workentin*: *"Controllable one pot synthesis of water-soluble gold nanosponges for surface enhanced Raman spectroscopy: towards biosensing"*. Graduate Students Symposium, Buffalo (US), May 19-21 **2014**. Oral presentation.
10) F. Pashaee, P. Gobbo, M. S. Workentin, F. Lagugne-Labarthet*: *"Tip-enhanced Raman spectroscopy of thiolated monolayers on flat gold nanoplates"*. CAMBR Distinguished Lecturer and Research Day, UWO London (ON) (Canada), Nov. 1 **2013**. Oral presentation.
11) X. Wang, P. Gobbo, M. S. Workentin, R. H. E. Hudson*: *"Bioconjugation of a receptor-avid peptide to gold nanoparticles for cancer imaging"*. CAMBR Distinguished Lecturer and Research Day, UWO London (ON) (Canada), Nov. 1 **2013**. Oral presentation.
12) J. M. Kaplan, J. Shang, P. Gobbo, S. Antonello, V. Chatare, D. M. Ratner, R. B. Andrade, and F. Maran*:*"Conformationally constrained functional peptide monolayers for the controlled display of bioactive carbohydrate ligands"*. 64th ISE Meeting, Santiago de Queretaro, Sep. 8-13 **2013**. Oral presentation.
13) X. Wang, P. Gobbo, M. Workentin*, R. H. E. Hudson*, *"Oligopeptide decorated gold nanoparticles via post assembly deprotection"*. Western Research Forum, UWO London (ON) (Canada), Mar. 26-27 **2013**. Oral presentation.
14) J. M. Kaplan, J. Shang, P. Gobbo, S. Antonello, V. Chatare, D. M. Ratner, R. B. Andrade, F. Maran*: *"Conformationally constrained functional peptide monolayers for the controlled display of bioactive carbohydrate ligands".* 223rd ECS Meeting, Toronto, May 12-17 **2013**. Oral presentation.
15) F. Pashaee, P. Gobbo, M. S. Worketntin, F. Lagugné-Labarthet*: *"Tip-enhanced Raman spectroscopy of self-assembled azobenzene thiol monolayers on gold nanoplates"*. CAMBR Distinguished Lecturer and Research Day, UWO London (ON) (Canada), Nov 13 **2012**. Poster.

16) E. Magdzinski, P. Gobbo, M. S. Workentin, P. J. Ragogna*: *"The synthesis, reactivity, and electrochemical study of metallocene-substituted-diimine ligands"*. 45th Annual Inorganic Discussion Weekend, Ottawa (ON, Canada), Nov. 3 **2012**. Oral presentation.
17) E. Magdzinski, P. Gobbo, M. S. Workentin, P. J. Ragogna*: *"The syntheses and electrochemical studies of a ferrocene substituted diiminopyridine ligand and its main group complexes"*. 45th Annual Inorganic Discussion Weekend, Ottawa (ON, Canada), Nov. 3 **2012**. Poster.
18) F. Pashaee, P. Gobbo, M. S. Workentin, F. Lagugné-Labarthet*: *"Tip enhanced Raman spectroscopy of self-assembled azobenzene thiol monolayers on gold nanoplates".* 24th Canadian Materials Science Conference, Western University (London ON), Jun. 5-8 **2012.**
19) E. Magdzinski, P. Gobbo, C.D. Martin, M. S. Workentin, P. J. Ragogna*: *"The synthesis, and reactivity of metallocene-substituted-diimine ligands"*. 95th Canadian Chemistry Conference and Exhibition, Calgay (Alberta), May 26-30 **2012**. Oral presentation.
20) P. Gobbo, S. Antonello, I. Guryanov, M. Hesari, and F. Maran*: *"Superefficient electron transfer through 3_{10}-helical peptides".* 221st ECS Meeting in Seattle, Washington (USA), May 6 -10 **2012**.
21) Gobbo, P.; Antonello, S.; Guryanov, I.; Hesari, M.; Soldà, A.; Maran, F.*: *"Superefficient electron transfer through 3_{10}-helical peptides".* Materials Research Society Boston (MA, USA), Nov. 25-30 **2011**.
22) S. Antonello, L. Armelao, P. Gobbo, M. Hesari, I. Guryanov, A. Soldà, F. Maran*: *"Spectroscopic and electrochemical characterization of Aib-peptide self-assembled monolayers on gold".* GEI-ERA 2010, Modena (Italy), Sep. 5 - 10 **2010**.
23) S. Antonello, P. Gobbo, I. Guryanov, M. Hesari, M. Zamuner, F. Maran*: *"Stability of and electron transfer through self-assembled monolayers of conformationally constrained peptides"*. 217th ECS Meeting, Vancouver (Canada), Apr. 25 - 30 **2010**.